AD NUMBER

AD367910

CLASSIFICATION CHANGES

TO: unclassified

FROM: confidential

LIMITATION CHANGES

TO:

Approved for public release, distribution unlimited

FROM:

Distribution: DoD only: others to Director, Naval Research Lab., Attn: Code 1221.1. Washington, DC 20375-5000.

AUTHORITY

Nov 1969, DoDD 5200.10, 26 Jul 1962; NRL ltr, 26 Feb 2001.

NRL Memorandum Report 754

DESIGN AND DEVELOPMENT PROGRAM FOR F4H-1 and F8U-3 WEAPON SYSTEMS

Peter Waterman

RADAR DIVISION

November 1957

NAVAL RESEARCH LABORATORY
Washington, D.C.

DESIGN AND DEVELOPMENT PROGRAM FOR F4H-1 and F8U-3 WEAPON SYSTEMS

by

Peter Waterman

Equipment Research Branch
Radar Division
Naval Research Laboratory

TABLE OF CONTENTS

INTRODUCTION

The development of any complex system should be based upon an orderly, clearly defined system approach. The end objective or problem to be solved should be the design goal for the system. If this objective cannot be reached, the problem to be solved should be modified to be consistent with the state of the art or time available for system development. The design of the system should be based upon parameters resulting from system analysis. This system approach will result in a product which has a predictable use capability and will be successful within this defined capability.

SYSTEM DEVELOPMENT

The block diagram of Fig. 1 shows the flow of events which take place in the development of a complex service equipment. The top left block of Fig. 1 is entitled Operational Requirements. The existence of a need for the system, its general description, and a statement of necessary performance to satisfactorily accomplish its mission is spelled out in the Operational Requirements. In its initial concept, the system can be described as being comprised of certain major elements having prescribed operational capabilities which are presented as design objectives. These objectives, as defined in the Operational Requirement, include system functions; features such as accuracy, countermeasures invulnerability, safety, servicing and operational flexibility, and acceptable limits of operational performance. The Operational Requirement generally describes the conceptual system and provides overall performance objectives to be met if the system is to accomplish its mission.

Initially, as illustrated by the figure, definition of the functional system (and its technical analysis) provides a basis for the detailing of technical requirements for the system and for its principal elements. Technical analysis may confirm the validity of, or the necessity to modify, the initial conceptual system. Where such modification is extensive, a reappraisal of resultant change in "mission accomplishment" potential will provide an early means for determining whether the project should justifiably be continued or whether a new system concept should be generated that can more predictably accomplish the desired mission. Presuming that technical analysis has confirmed feasibility of initial weapon system concept, the project has then reached a point where design studies can be initiated.

Each procedural step from this point, as indicated by the figure, is validated or appraised by an evaluation process. Moreover, evaluation is shown to be capable of effecting, through feedback to preceding steps,

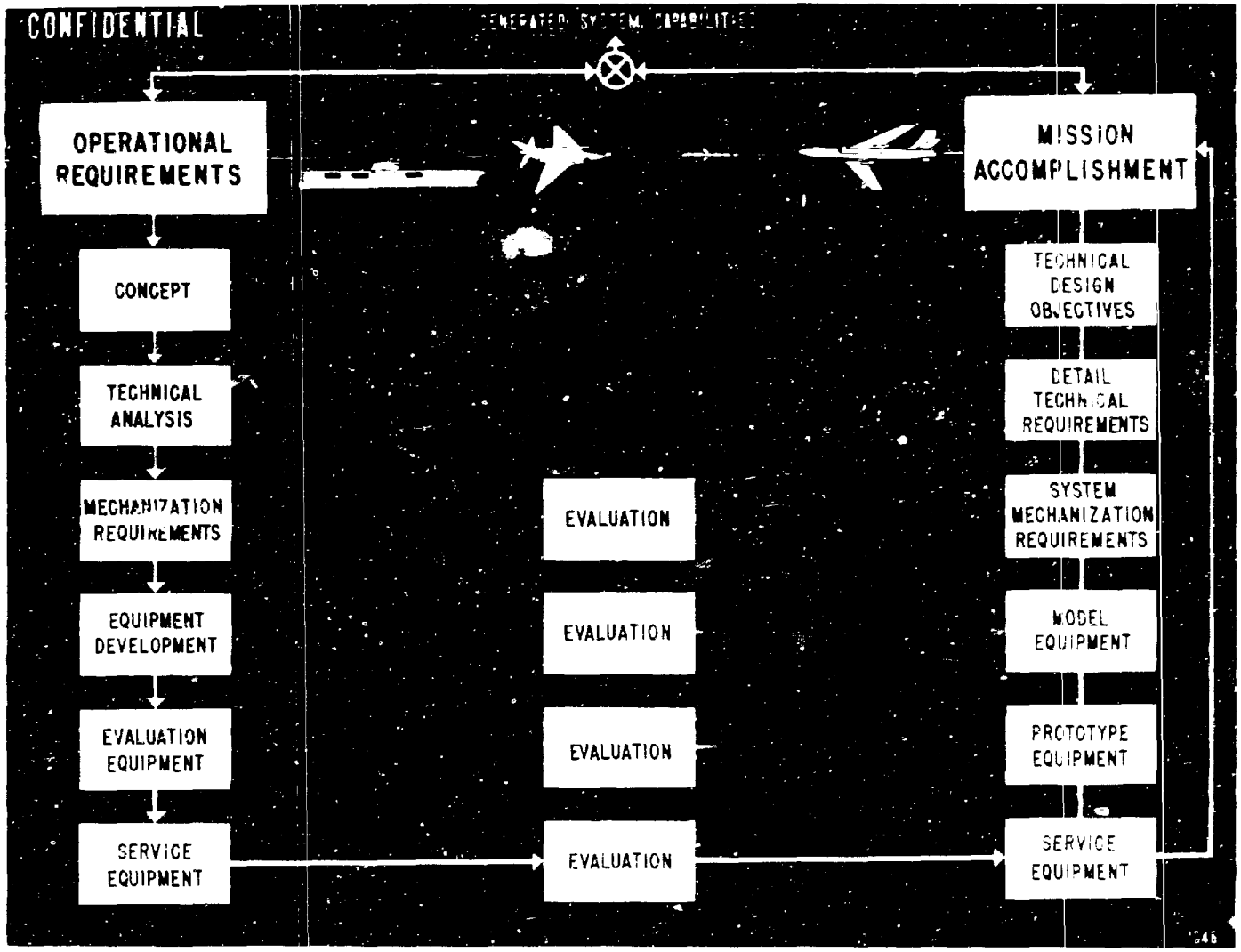

Figure 1 - Flow Diagram for System Development

theoretical as well as mechanical design parameter improvements.

System mechanization requirements have now been, in accordance with procedural steps, theoretically defined and evaluated. Where desired performance quantities, established by the technical analyses, must be degraded in the actual mechanization process by reason of technological or state of the art limititations, an appraisal of resultant effects upon mission accomplishment is indicated. Theoretical mechanization requirements are validated by the design, construction and evaluation of an experimental model. Feasibility, operability and adequacy for the application are assessed. Each illustrated procedural step should result in feedback to the preceding steps with modifications incorporated as indicated by new findings. When this thesis is followed, there will be no absolute technological freeze during system development of the weapons system concept, or of its design mechanization, before final OPDEVFOR service evaluation. The changes in concept which thus occur during the orderly program of developmental progress become more constrained as it progresses toward the delivery goal.

Figure 1 shows design and evaluation of developmental models following the determination and assessment of mechanization requirements. A written statement of mechanization requirements provides the premise for specification of the developmental model equipment. This equipment is ordinarily evaluated by the contractor with observation by the Navy. Evaluation and resultant modification of the model equipment permits specification and design of the prototype equipment. Evaluation of the prototype is specified by the Navy and may be conducted with contractor assistance. Evaluation objectives include demonstration of performance reproducibility, conformance with predetermined requirements and adequacy for service use. Firm, detailed specifications can now be written defining the final product (service equipment) which, when constructed, is delivered to the Navy for Operational Development Force type service evaluation.

The foregoing development and evaluation process is generally applicable to the development of service equipment. As presented, it is an obvious and simple method, rather easy to apply in the generation of subsystem equipment. Its application in developing a weapons system of the F4H-1-F8U-3 magnitude is appreciably more difficult, more important, and more rewarding. The program objectives can be met in a limited time only through an orderly procedure, such as that described above, with continuous evaluation, feedback, and re-evaluation of concept and design. It is emphasized that "evaluation" as illustrated by Fig. 1, is on a systems basis, in terms of the relationship of subsystem performance to mission accomplishment. Thus the contribution of the subsystem to the complete system is determined in a sensitive manner.

AIR-TO-AIR WEAPONS SYSTEM LINKS

The combination block diagram and pictorial diagram shown on Fig. 2 give the principal links essential in the tactical usage of any air-to-air weapons system. Basically, these links are as follows:

1. Target detection, assessment and fighter direction from surface or airborne CIC.
2. Communication of vectoring data to the interceptor aircraft either from surface or airborne CIC.
3. Detection and tracking of the target by the fire control equipment of the interceptor.
4. IFF from the interceptor aircraft and/or from a remote position such as surface CIC.
5. The links employed during missile guidance.
6. Fuzing link.
7. Target characteristics and objectives.

All of these links and associated equipments go to make up the overall complex system. Each of the links are dependent upon the other (except for the unlikely case of chance intercepts). For example, design of the fire control equipment in the aircraft is dependent upon the accuracy and reliability of vectoring data from CIC. The accuracy of airborne fire control equipment and missile guidance equipment are interdependent. Since all of these links depend upon one another, the system designer must follow a system approach if a successful design is to be achieved.

OPERATIONAL PROFILE

The pictorial diagram of Fig. 3 further illustrates the dependence of each of the links or steps in a typical intercept. Each of the funnels depict a decreasing probability as the engagement proceeds. Starting at the left center of the figure it is seen that not all of the aircraft in CAP are available, because of position, fuel and commitment problems, for attack of a specific target. From the fighter direction phase only part of the available aircraft will successfully arrive at AI radar detection because of CIC vectoring inaccuracy. Of the aircraft which arrive at AI radar detection, only part will arrive at missile launch because of fire

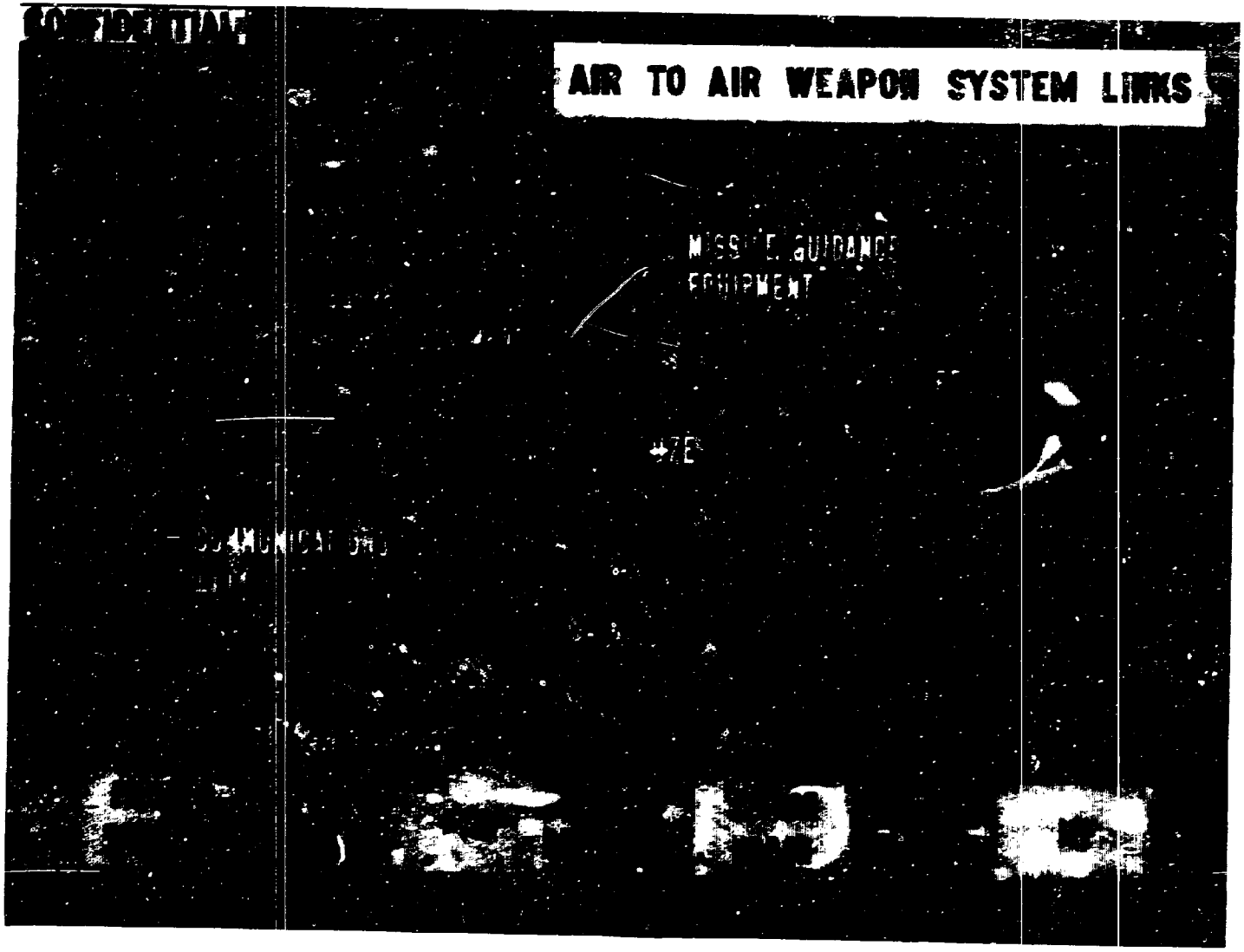

Figure 2 - Air-to-Air Weapon System Links

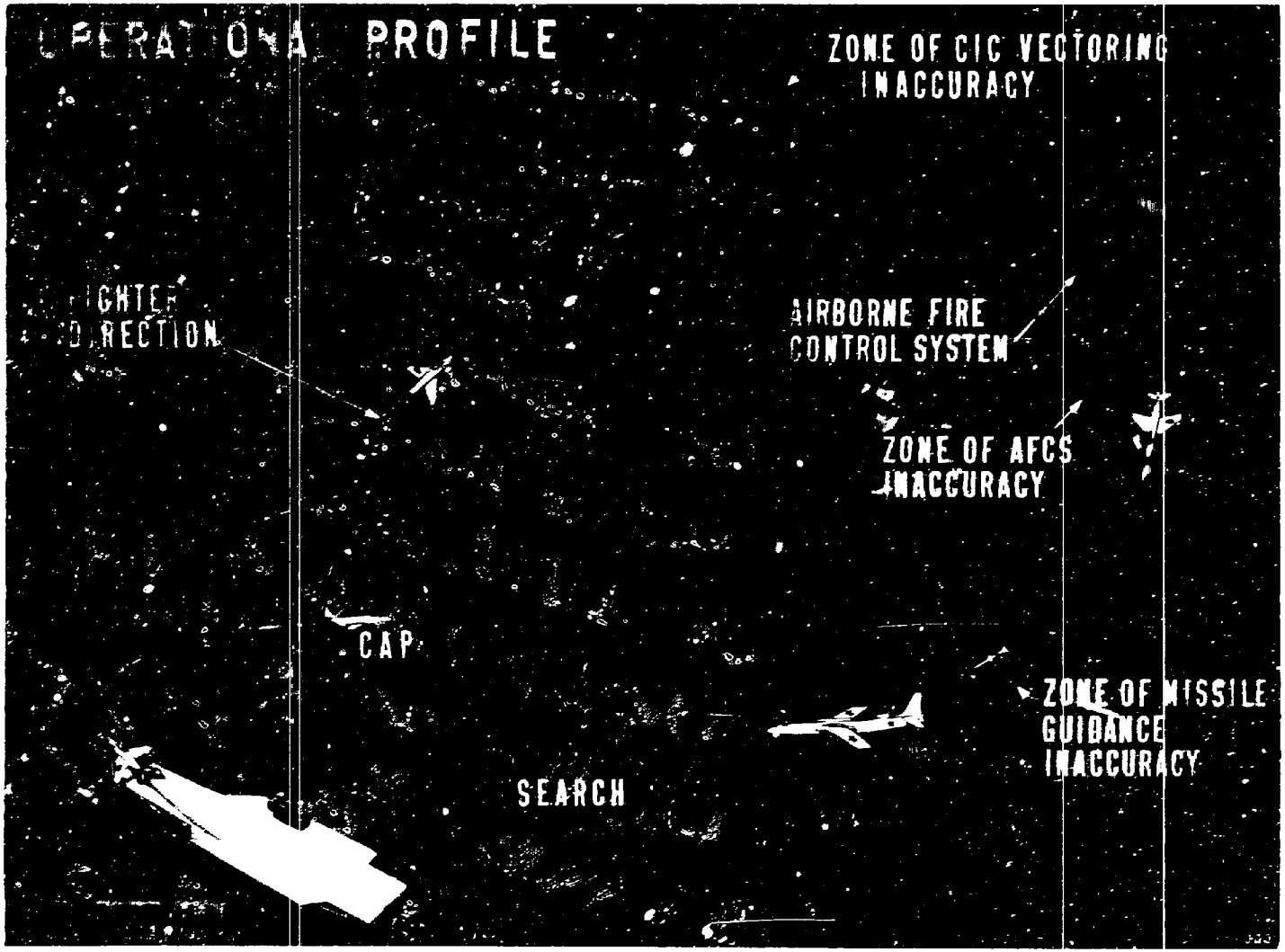

Figure 3 - Operational Profile

control inaccuracies, position difficulties and speed-maneuver capability. Associated with the missile guidance phase there are additional inaccuracies [illegible] that only part of the available missiles could be successfully employed against the target. From this figure it is obvious that the system designer must achieve a balance between system elements. For example, if each of the probabilities for the four phases given were 90%, the overall probability of success would be approximately 66%. However, if one of the phases had a 50% probability associated with it, the resultant probability of success would decrease to approximately 36%.

FUNCTIONAL SYSTEM

The block diagram of Fig. 4 shows the functional system for the F4H-1 and F8U-3. This block diagram in effect repeats the steps shown on Figs. 2 and 3. Principal system elements are shown as: an operational requirement for the generation of a weapons system, a tactical doctrine for its application and an operational system comprised of shipboard, aircraft, weapon and target subsystems. The overall system is illustrated as regenerative in that, for its generation, the maximizing of "Mission Accomplishment" will require establishment of the important interrelationships between system elements and mechanization of sensitive parameters so that system performance within respectable tolerance will result. This process is shown as likely to include modification of requirements and doctrine as dictated by system concept considerations.

JOINT ACTION TO MEET REQUIREMENTS

The preceding sections have described the procedure one follows in systematic development of an airborne weapons system. It is now important to establish the status of the two systems of interest (F4H-1 and F8U-3) and outline a procedure to be followed in the course of design and development. Present programming of study results from the contractor team call for a completion of technical analysis of the problem on 1 January 1958. Following that, a mechanization study employing the theoretical information is due to be completed 1 July 1958, which leads to a military specification approval of the principal parts of the system in September 1958.

At the present time preliminary results are available from the Navy air-to-air missile study program which should be useful in making decisions on important phases of the program planning and execution. These preliminary results are detailed in the study summary attached to this report. Even though the study is not complete it is possible to draw from it inferences which will at least allow the design and development of the long lead time

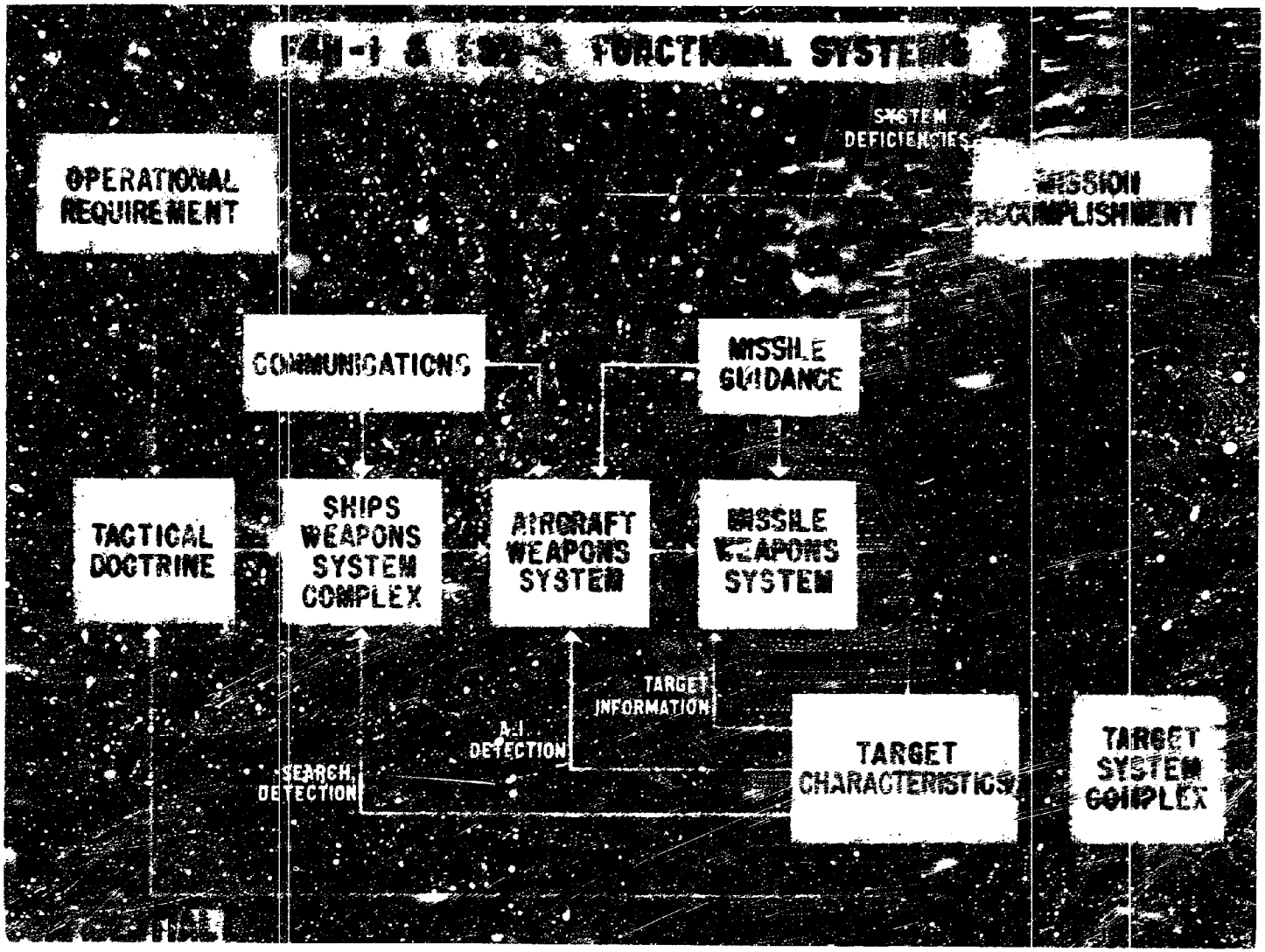

Figure 4 - F4H-1 and F8U-3 Functional Systems

items to be implemented. This action is strongly recommended. The fact that study outputs are available does not detract from the importance of increased emphasis on contractor conducted study of the problem. Instead, it is intended that the Navy's study results be used to expedite system development until such a time as the contractor study results in design information useful in defining the actual characteristics required in the various system elements.

Proceeding on the assumption that the data presented in the study summary will be used as recommended above, Fig. 5 lists a procedure whereby one could carry forward the systematic development program. As stated previously, important within these inferences is information which should be useful in establishing the guide lines for work on system elements wherein development time represents a critical factor when related to the programmed delivery dates for the operational system. Figure 5 lists such inferences as related to system development. The details of these items are as follows:

1. There is a need for the formulation of the basic system configuration so that an integrated design approach can be made to the following areas:

   a. Environmental suitability
   b. Maintainability
   c. Compatibility of elements
   d. Packaging concept (integrated effort by the participating contractors)

2. The results of the Navy's study confirm earlier estimates that a situation display will be vital to the extraction of useful capability from the system. The need for and possible type of situation display was described in an earlier NRL Memorandum C-5309-612/57 which is included as Enclosure 1 to this report.

3. There is a need for the formulation of tactical doctrine guide lines so that best use may be made of the otherwise very limited capability of the system to fulfill operational requirements. These guide lines should specify the operational interdependence placed upon external logistic areas such as:

   a. BUSHIPS cognizant areas - CIC operational procedure, ships environment, search radar, handling equipment, vacuum tube spares, etc.

TASKS

1. Formulate basic system configuration
2. Develop situation display
3. Formulate tactical doctrine guide lines
4. Revise operational concept for usage of secondary missile seekers
5. Establish applicability of secondary AI fire control systems, such as IR, to the deficient areas of the primary fire control system.
6. Establish lowest acceptable limits defining a useful Navy system
7. Actions on Items 1 thru 6 above cannot await the completion of all study effort, but must be actively pursued to insure that a useful system capability can result.

Fig. 5 - Joint Action to Meet Requirements

b. BUORD cognizant areas - interconnection with other weapon systems, avoidance of hazardous areas of other weapons systems, warhead, fuze, etc.

c. BUAER cognizant areas - aircraft airframe environment, power sources, spares (AFO), etc.

d. CNO cognizant areas - operational requirements.

e. Contractor cognizant areas - dependence upon contractor for maintenance.

4. A change in the operational concept is required if value is to be derived from the proposed weapon system flexibility to be achieved through the use of IR Sparrow III missiles or other mixed load capabilities when targets of interest approach those spelled out in the operational requirements. The preliminary study shows that for high speed targets $V_T/V_P = 1$, the rear hemisphere area (high probability area for IR seeker) is not attainable because of the inability of the interceptor system to attain a proper launch position. For cases where $V_T/V_P = 0.8$ or less marginal capability exists for the IR technique. Thus, reappraisal of the tactical use concept for IR capability is indicated.

5. There continues to be a need for the establishment of requirements for the basic system so that the applicability of IR (fire control) and other redundant systems may be examined. Concurrent with the application of redundant systems, the tactical doctrine must be re-established as it applies to the fulfillment of revised mission accomplishment capability for these systems. In support of this opinion, NRL has submitted memorandum C-5364-594/57 which is included as Enclosure 2 to the report.

6. There is a need to establish an early indication of the operational limitations imposed by development time limitations. From this indication the lowest acceptable limits which will provide the Navy with a useful operational capability must be established. During this process a balance between performance as related to sensitive parameters, among which are AI radar range; AI gimbal limits; preparation time; missile seeker range; etc., must be attained. This conclusion is supported by data in the Navy study summary and by NRL Memorandum 5364-748/57 which is included as Enclosure 3.

7. The Navy's study results to date, as interpreted by NRL, indicate that the limitations imposed by the present system approach, by equipment deficiencies, and by lack of adequate development time will severely limit the attainment of the operational requirement objectives. If the preceding six generally deficient areas can be remedied, useful attainment of operational requirement objectives can be achieved.

DETAILED RECOMMENDATIONS AND CONCLUSIONS FROM SUMMARY OF NAVY STUDY PROGRAM

1. The preliminary results of the study indicate that for co-altitude high-speed attacks under "ideal" conditions with $V_T/V_F = 1$ the interceptor must start its approach from forward of 70° off the target's nose if it is to get into a position to launch a missile.

2. It can be easily shown from the study results that when additional time is added for systems preparation (currently estimated as 27 seconds total) most of this forward 70° zone will be eliminated. In the case of $V_T/V_F = 1$ for attacks occurring at 30,000 and 50,000 feet, approximately a 10° zone (from 60° to 70° off the target's nose) would remain.

3. When V_T/V_F is reduced to 0.8, attacks can originate from around the clock for ideal conditions. However, when the total system settling time is considered, it can be shown that approximately the forward 60° is eliminated from the usable attack zone.

4. When the interceptor is slowed down to V_{cruise} additional time is available for forward hemisphere attack. However, when the target is a high speed one, the approach aspect is even more restricted. For example, when the target is flying at Mach 2.0 at 30,000 feet the interceptor must approach from forward of 40° off its nose.

5. When the target speed is Mach 2.0 and the interceptor speed is Mach 2.0 or V_{max} and pull-up attacks are employed under ideal conditions, successful engagements are restricted to 7,000 feet altitude differential for targets flying at 30,000 feet altitude and higher. No capability exists for targets flying at 65,000 feet altitude.

6. When the target speed is reduced to Mach 0.9 and the interceptor is flying at Mach 2.0 or V_{max}, successful engagements are restricted to altitude differentials of 17,000 feet or less for targets flying at 50,000 feet altitude or higher. When the target altitude is 30,000 feet or less, successful pull-up engagements can occur from sea level to co-altitude.

7. For the cases where the interceptor is slowed down to Mach 0.9 at the start of pull-up, no capability exists for pull-up attacks against either a Mach 2.0 or Mach 0.9 target at altitudes of 65,000 feet or higher.

8. For the pull-up attacks at 50,000 feet or less, a greater altitude differential capability exists when the interceptor is slowed down to Mach 0.9 than for the cases where V_F = Mach 2.0. With the target flying at 50,000 feet (V_T = Mach 2.0), this altitude differential is 10,000 feet.

9. The probability of successful attack when limited by some of the degrading factors such as gimbal angle and vectoring inaccuracies have been in part investigated. When the interceptor is flying at Mach 2.0 in a co-altitude attack and V_T/V_F = 1, the probability of successful arrival to missile launch for the nose-on case is 46% and for 30° off the target's nose is 52%. At 60° off the target's nose, the probability goes to zero because of the interceptor's inability to get into position and because of gimbal angle limits.

10. When V_T/V_F is reduced to 0.8 and the engagement occurs at co-altitude, the probability of successful arrival to missile launch is increased to 48% for nose-on, to 82% at 30° off the target's nose, and to 50% at 60° off the target's nose.

11. When the interceptor is slowed down to Mach 0.9 the head-on probability of success goes up but falls off rapidly as the aspect angle from which the engagement starts moves toward the beam. For the case of V_T/V_F = 1.7, the probability of successful arrival to missile launch is 71% for nose-on and zero at 30° off the target's nose.

12. Although many of the degrading factors which will be encountered under realistic tactical conditions have not been included in the study to date the results can be inferred. It is predictable that the indicated probability of success values given in Items 9 thru 11 will be reduced markedly.

13. Thus far in the study program the resulting improvement from the use of a bright display, bandwidth switching, and optimized search area have been investigated. The result is an increase in AI detection range from 12.7 n.mi. to 19 n.mi. for a Mach 2.0 interceptor attacking a Mach 2.0 target head-on.

14. The improvement factor given in this report for a bright display is an engineering estimate of that which could result by brightening the current presentation. There are many other "lost" db's which could be recovered through a program of system analysis having as its objective an optimization of the pilot's environment. This program would include

the possibility of such items as an NRL type bright display, situation display and general cockpit optimization.

15. When the improvement factors of Item 13 are included and when the antenna gimbal limits are increased to $\pm 57^{\circ}$ in azimuth and elevation there is a marked improvement in probability of successful arrival to missile launch. For example, when V_F = Mach 2.0 and V_T/V_F = 1.0 there is an improvement in probability of success of approximately 30% for head-on attacks resulting in a value of 75%.

16. It is believed that the improvements of Item 13 could be incorporated in the system during the time era of interest. The Laboratory would strongly recommend that the Bureau direct the contractors to proceed toward this end.

17. The results of the study program infer that a situation display is a necessity if a tactically useful system is to result. This situation display is important because it can provide data from which the pilot can start an intercept prior to AI radar detection, (Enclosure 1).

18. A preliminary study of the sensitivity of probability of success to AI radar range and gimbal angle limits has been made. The result is that in some areas, especially nose-on, the probability of success is very sensitive to range. In other areas, especially 60° off the nose of the target aft, the probability of success is very sensitive to gimbal angle limits. It is obvious that these features are interdependent. Thus a compromise in mechanization (for example large dish versus gimbal angle coverage) which can result in an approach to maximum overall use capability must be reached before design effort can be specified, (Enclosure 3).

19. The findings of this study could and should be applied in the system design effort being conducted by the various contractors. To this end, the study results and details should be made available to the principal contractors. The impact of this is directly related to the importance of defining the long lead time system elements.

20. The undefined developmental state of IR for the fire control system is such that no current system can be realistically analyzed in terms of its potential contribution to overall system performance. Test information taken under controlled conditions would provide information needed by this study program in order to investigate system deficiencies to determine the applicability of secondary systems, (Enclosure 2).

21. Analysis of system performance resulting from use of the Sparrow III IR Seeker will begin as soon as sufficient data is supplied by the contractor. To date the information available to NRL is not adequate to warrant an analysis.

22. Results of incorporation of the Sidewinder missile in the system will be investigated. Forthcoming study effort will initially be based upon estimates of missile performance, since design of the Sidewinder Ic will not be frozen during the remaining study interval.

23. In order to continue on an uninterrupted basis, it is important at this time for the Bureau of Aeronautics to program an extension to contract NOas 57-663d under the administrative cognizance of the Bureau of Aeronautics Av-3122 and under the technical direction of the Equipment Research Branch, Code 5360, NRL. As detailed in the report, there are important areas where timely coverage will not occur in the current study program. In addition there are problem areas which should be investigated but because of the limited scope of the current program will not be investigated.

24. The Laboratory will forward to the Bureau, under separate cover, a recommended extended study program.

C-5309-612/57 9 August 1957

MEMORANDUM

Subj: Indicators Configuration for F4H-1 Airplane and Aero X1A System

1. The F4H-1 airplane is a high performance two-place fighter which will be equipped with the Aero X1A fire control system and will use Sparrow III as its principal armament. The introduction of the data link, during the early fleet employment of this aircraft dictates that the fire control system operation be set up to utilize the information available as an output of such a system to optimize the utility of the overall weapons control system. The outputs from the data link must be displayed to present the airplane operators a usable tactical display and at the same time data from the airborne intercept radar must be displayed in a manner consistent with the tactical display. In this aircraft the problem is complicated by the fact that the phasing in of data link may lag the initial fleet deployment of the aircraft. Thus the tactical display must be usable with current voice communication. This memorandum will outline some of the requirements that are placed on the system by these conditions and outlines a recommended solution.

2. The aircraft has a pilot whose principal task is to fly the aircraft to intercept, utilizing first ground generated attack data, and after AI detection, the data generated from his AI radar and fire control computer. Without such a visual attack display the probability of intercept will be low. The radar operator has the primary task of radar detection and identification of the target, and subsequent to detection he acts as a monitor to assist the pilot where possible. He also serves as navigator and for this system will serve to put certain ground generated inputs into the system, prior to the time of introduction of the data link. The introduction of the data link will allow automation of this particular function.

3. With the advent of newer cathode ray tubes the use of two color presentation will be used to present primary and secondary information. The use of such a tube is assumed in this study, however, it is not mandatory.

4. The basic vectoring system to be used would be based on the triangle presentations. It is felt that the advantages of this system are principally the wide bandwidth of the usable information and the flexibility that the system allows in the establishment of intercept doctrine. The

triangle system has ground generated data inputs:

(a) X, the N-S displacement between target and interceptor.

(b) Y, the E-W displacement.

(c) Target altitude.

(d) Target speed.

(e) Target heading.

These quantities are then combined with data generated in the aircraft and operated on to generate range, bearing, elevation, and target heading in airplane coordinates. These are put on an indicator as shown in Fig. 1, in a PPI type presentation.

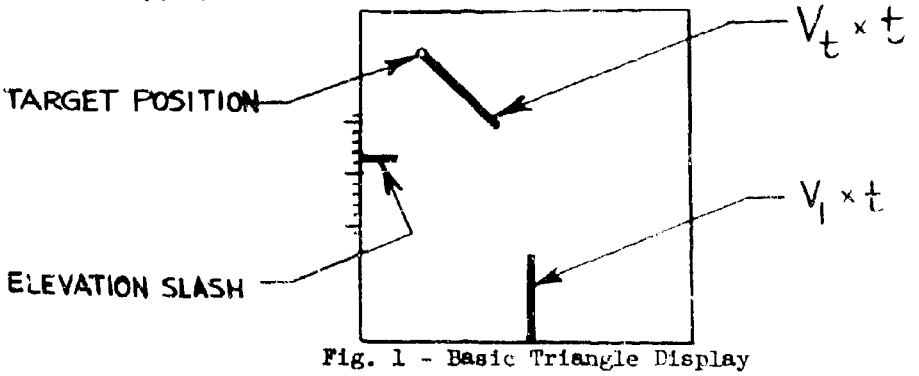

Fig. 1 - Basic Triangle Display

This shows two vectors, one emanating from the bottom of the indicator is the interceptor vector, and the other from the target is the target vector. The length of the vector is the velocity times a preset time. A pilot-operated time dial can be set so as to bring the ends of the two vectors to the same range as shown in Fig. 2. (The dial is time driven so that the time shown is always time to go). "a" shows the relationship of the two vectors when the time dial has been set to time to go.

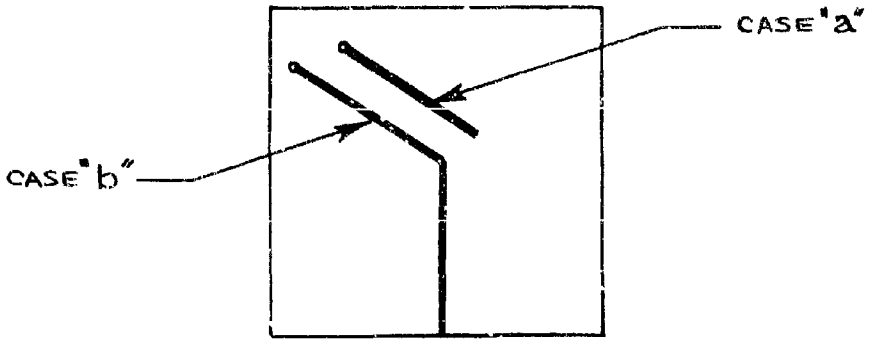

Fig. 2 - Establishing a Collision Vector

Condition "a" shows the pilot that his course is toward the left of a collision course, and by turning the aircraft right he can bring the ends of the vectors into coincidence as in "b." At this time the airplane is in a collision course.

It is such a maneuver that points up the first advantage or triangle. The maneuver shows up immediately on the vector display. Were the vectoring computation done on the ground the feedback of information regarding the turn would have to wait several sweeps of the search radar before the new track would be generated. The triangle results in a vastly increased vectoring system bandwidth. The second principal advantage foreseen for the system is in the flexibility of establishing doctrine for vectoring approaches. The pilot could, for example, readily fly a collision course toward a cut-off point which he could establish visually on the scope. If he wanted to start his attack run from a cut-off point 10 miles off to one side and 20 miles forward of the target, in order to assure a forward hemisphere approach, he could readily fly a collision course toward this point and then make a turn toward the ultimate attack course.

5. An additional computed quantity is to be added to the pilot's vectoring indicator. This is a line which indicates to the pilot the detection range required for a high probability of successful intercept. If the target is approaching this barrier and as yet detection has not been made he is warned that some delaying tactics are required. A slowdown in the forward hemisphere may be necessary or a course which would alter his approach would be suitable tactics for maintaining a high probability of kill. Such tactics can be experimentally derived using this vectoring

system. The addition of gimbal limits in this indicator appears necessary. The complete primary pilot display for vectored search operation vectoring mode is shown in Fig. 3. It includes an elevation slash which gives the elevation difference between him and the target.

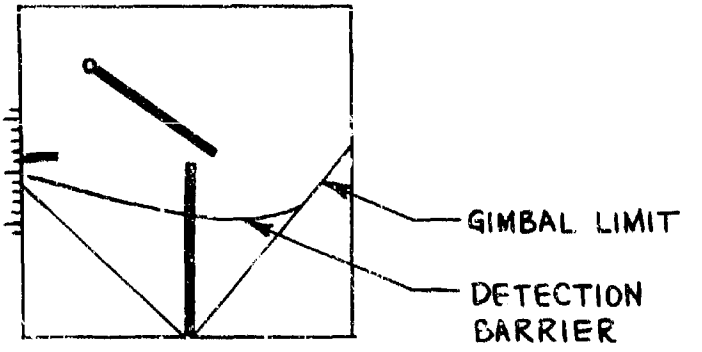

Fig. 3 - Complete Vector Display

6. The radar operator would normally require only the search display during the search period. Since outputs of the triangle computer are bearing, elevation angle and range it is possible to point the antenna toward the expected target position. Only the area which is likely to contain the target will be searched and will be displayed on the indicator. The expected target position will lie at the center of the tube and the center will therefore serve as a designation point. As the airplane turns the antenna would continue to search around the most probable target location. Thus the display would be stabilized about the line of sight to the expected target position.

Designation of the target would be accomplished by overriding the triangle designation and performing a lock-up. Designation would require insertion by the radar operator of the difference in range, bearing, and elevation between the actual detected target position and the position indicated by the output from the triangle system. They will be inserted using a conventional joystick. Also, on the presentation for the radar operator will be a minimum detection range curve comparable to the one on the pilot display. The principal display for the radar operator is shown in Fig. 4.

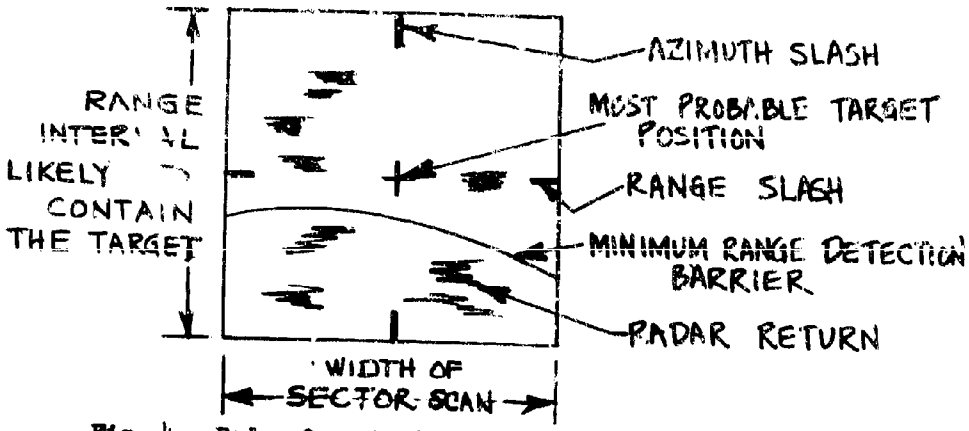

Fig. 4 - Radar Operator's Principal Search Display

7. During the time when the data link and the associated ground equipment is not available for the fleet the radio operator will function as a transducer of information. He will take data comparable to the normal data link outputs and manually feed them into the system. This will place an additional requirement on the systematic mechanization of the vectoring computer, in that it must be capable of functioning with either automatic or manual inputs.

8. Secondary or emergency modes and training operations require that the pilot and the radar operator be able to monitor each other's scope. For this reason, as an optional display, either man can choose to superimpose the other's display on his in a second color.

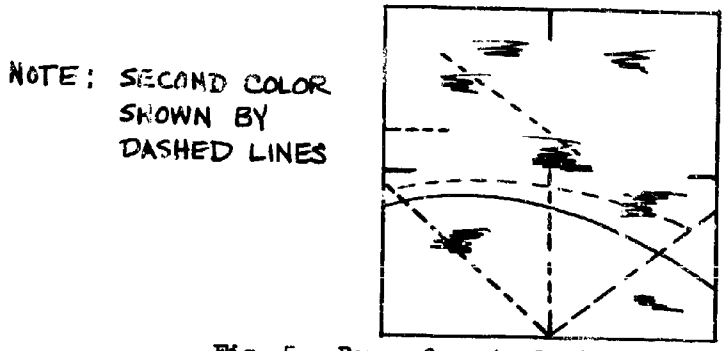

Fig. 5 - Range Operator's Optional Two-Color Display

The development of the two-color display using a transparent phosphor has advanced sufficiently far to plan for its use with this system. A two-color display is not essential but would offer great advantages. With this facility, the pilot can assist the radio operator in cases where the radio operator experiences difficulty in detection and also the radar operator could aid the pilot in determining cut-off distances and so forth. In the event of failure of either indicator, the mission could be completed with a reduced probability of success.

9. After detection, designation, and lock-up the pilot will get a display which once again will rely on a two-color display. This is shown in Fig. 6.

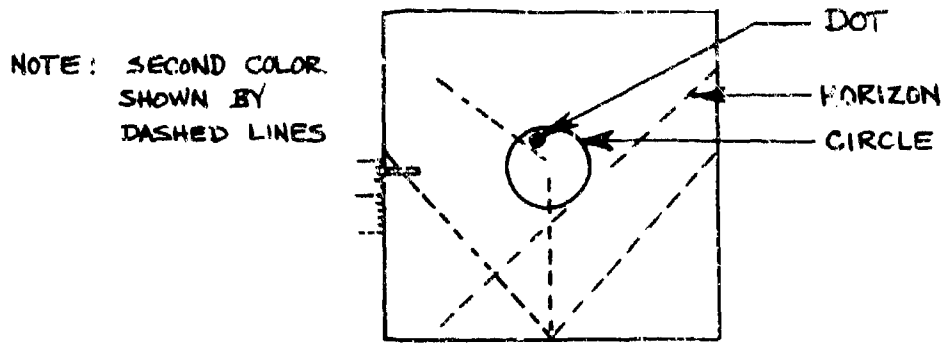

Fig. 6 - Pilot's Attack Display

The circle-dot display will consist of collapsing circle fixed at the center of the display. The size of the circle will be such that if the pilot keeps the dot within the circle he can be assured of completing the intercept. Thus, as the run nears its completion and the requirements of heading accuracy increase its reduced size will reflect this increase in required accuracy. The triangle situation display will display the range, time to go, range rate, approach angles, lead angle in a manner which should be superior to the current techniques. The data to generate this display will come from the AI radar, and not the ground. All the required quantities are now computed for the fire control solution.

10. The principal duties of the radar operator during the attack phase lie in monitoring the attack situation, in checking radar operation and in watching for counter measures. His primary display will be the collapsed B-scope. The triangle situation display will be added in the second

color as shown in Fig. 7.

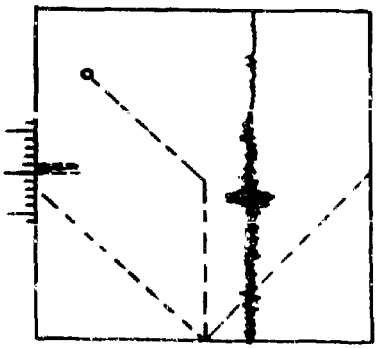

Fig. 7 - Radar Operator Display

11. The breakaway signal will be a computer generated oral tone.

12. Secondary modes of operation call for modification of these displays. When on patrol operations, the area to be searched may call for a wide azimuth angle search or for a possible sector scan. A selector switch should be set for either wide or sector scan for the patrol mode. In this case the radar operator's indicator could show all targets within some preset range, and over the azimuth angles which have been chosen. The pilot can use the triangle presentation as a navigation aid. If a preset point is put in the system as a target, the pilot can use this as a reference point in his patrol activity. If several planes are used in a routine patrol the use of preselected reference points can assure a thorough search of an area. Navigation back to the ship or base can be accomplished by setting in the base location as the reference or target point.

Charles H. Dodge

C-5364-594/57

2 August 1957

MEMORANDUM

Subj: IR Tie-in for Aero X1A and X1B

1. At the AMCS Aero X1A/B coordinating conference on 27 July 1957, NRL was verbally requested by the Bureau of Aeronautics (AV-33211) to render advice concerning the IR tie-in for this system. At present, under contract with the Aircraft Division of BuAer, McDonnel Aircraft Company has subcontracted to Avion the development of an IR search and track device for the F4H aircraft. Additionally, the Bureau (Avionics Division) has a contract with Aerojet for the development of IR equipment. This contract has been oriented to be applicable to the F8U-3 aircraft. There is a desire on the part of the Bureau to combine this IR development effort in the hands of only one contractor.

2. Because of statements made by the two IR contractors at the AMCS Aero X1A/B Coordinating Conference, namely that each is fully cognizant of the tie-in problems into the rest of the AMCS and that each could use any of several tie-in methods, it is not possible to make a selection of contractor on a technical basis. In other words, each contractor stated that he would solve the tie-in problem to the satisfaction of the Navy. It is therefore recommended that the contractor be selected on the basis of his experience and reputation in the development of IR devices.

3. There are several system aspects of an IR tie-in which appear to have been neglected in planning the IR tie-in effort.

a. The use of an IR equipment in the AMCS can only be justified on the basis that it "fills a hole" in the system capability caused by a deficiency of the other parts. Such a deficiency might, for example, be the lack of radar low altitude capability. Because the development and use of IR devices in this country is only in its infancy, the capability of IR to supply an otherwise lacking performance is seriously in doubt until proven. This is particularly true at low altitude where atmospheric absorption and ambient background levels are high. For example, recent NRL IR measurements of the F8U-1 and F11F at cruise velocity, without afterburner, and at altitudes between 2,000 and 4,000 feet, show that these aircraft are not detectable in the nose aspect at any range. The measurement equipment was state of the art laboratory equipment of known high sensitivity.

b. To prove or disprove claims of IR capability, it is necessary to proceed with the development of IR equipment at a rapid rate.

c. Until IR equipment capability can be proven and because of weight and complexity considerations, it is necessary to proceed with the development of the AMCS Aero X1A/B as though no IR tie-in would be made.

d. It is very important because of Items a, b, and c above to develop completely separate radar and IR systems so that a failure of either system will not impede progress in the other. At such a time as both radar and IR capabilities are evaluated and exist as proven techniques it will be possible to reconnect the separate systems as a single system in a suitable tie-in configuration of less weight and size than that possible with separate systems. This will be possible because a number of the parts may be made common to both systems. Interconnection at this later date should be relatively easy and not very time consuming. It is recommended that such a program be adopted.

4. A research program to make radiometric measurements of airborne targets in the IR spectrum already exists at NRL. Equipment for this purpose is in hand and operating. The NRL program calls for measurements at both high and low altitudes. A parallel program to conduct similar research in the radar field has been in existence for some time and will continue indefinitely. It is suggested that the selected IR contractor, in his development program, make use of this facility for comparative radar and IR measurements. Such a method of data collection is of interest to cognizant NRL scientists.

5. In summary it is recommended that:

a. A single IR contractor be selected on the basis of experience and reputation.

b. Both radar and IR systems be developed as separate self sufficient packages.

c. When both radar and IR performance contributions to the AMCS can be fully appreciated, the integration (tie-in) be accomplished.

d. Equipment contractors use existing NRL facilities to perform separate and comparative radar and IR measurements.

Laurence F. Gilchrist

Laurence F. Gilchrist

C-5364-748/57

17 October 1957

MEMORANDUM

Subj: Estimated Technical Requirements for AN/APQ-72 and AN/APQ-74 Radar Antenna

1. Design of fleet deliverable, production AN/APQ-72 & 74 radars is due to be frozen (along with the design of the rest of X1A-X1B systems) on about 1 September 1958. Several long lead time components of the systems such as antenna and indicator require an early start to insure delivery of satisfactory hardware. This report deals principally with the antenna. The important subject of indicator requirements has been, and is being dealt with separately.

2. Studies leading to the design requirements for system components, such as an antenna, are being conducted by both contractor and Navy activities. The contractor study which officially governs design requirements will have an initial output by about 1 January 1958. Because of the long lead time it is necessary to estimate the design requirements for the antenna now so that detailed design work may proceed on schedule. Preliminary results of the NRL-Westinghouse study are used as a background for the tentative specifications which follow.

3. Estimates of the limiting technical requirements for X1A-X1B antenna together with comments on each item as necessary were generated by NRL and Westinghouse engineers on 16 October 1957. The requirements are broken into six parts, namely search, conversion, tracking, structure, environment, and rf.

SEARCH

Usable gimbal limits: $\pm 60^{\circ}$
Antenna diameter : 30"

Comment: Studies indicate that the problem to be solved is sensitive to range improvement of up to 8 miles and to gimbal limits beyond $\pm 67^{\circ}$. Present improvement programs (not including antenna size) are designed to give such an improvement. However, there is no way, at present, to guarantee the outcome of these changes. It therefore becomes practical to consider specifying that approximately half of the desired improvement will occur due to a change in antenna size.

A number of diversive efforts are under way to change the design of the fire control system outside the structure of contracted for responsibility. Since a certain amount of planning has occurred to provide aircraft structures which may support a larger antenna, the fire control contractor should consider the use of such sizes as are appropriate to furnishing a four mile range improvement for a single antenna design which will fit in both aircraft. A 30-inch diameter appears to satisfy this requirement. If, during design, it appears that a further change in size will ease the difficult task of supplying the large gimbal limit requirement, such a change is recommended. The fire control problem solution is more sensitive to gimbal angle limit than to increased antenna diameter.

Scan area: $35^{\circ} \times 12^{\circ}$

Comment: Several independent studies support these figures as being optimum for DIRECTED ATTACKS.

Frame time: seconds

Comment: Optimum in lies between 1 and 4 seconds.

Slew velocity: 60°/sec

Comment: This figure is a direct result of the choice of frame time if a four bar scan is used.

Error in following a stabilized search program: less than 1°

Comment: This is a reasonable design criteria which results in limiting aircraft maneuvers during search to those of a load factor of 3 or less.

Maximum roll angle: $\pm 90^{\circ}$

No comment

Maximum roll rate: 15°/sec

Comment: This is difficult to estimate for the search phase. The figure quoted is from instrumented F4D attack phase runs.

Maximum pitch rate: as resulting from a load factor of 2 maneuver at cruise velocity.

Aircraft resonances which affect stabilization design:

pitch, 2-12 rad/sec
yaw , 2-5 rad/sec

CONVERSION (Weak signal tracking)

Stabilization design: as in SEARCH above. Additionally the effects of own ships motion must be reduced by a factor of 10 in the band below 10 radians per second.

Comment: This criteria has been satisfactory in the F4D in the past. Lack of such a criteria is the reason why conversion and lock-on must be delayed in the F3H system.

Design limits of rate of change of line of sight: rates between 0.1^{o}/sec and 10^{o}/sec must be resolvable from noise at point of use in the system.

No comment.

Usable gimbal limits: $\pm 60^{o}$

Comment: Until initial errors are corrected a large gimbal angle limit requirement still exists.

TRACK

Usable gimbal limits: $\pm 60^{o}$

Comment: No change in mechanical design is required from that used for SEARCH. However, it does not appear necessary to extract measured lead angle as a linear function beyond $\pm 45^{o}$ limits.

Stabilization: Design must reduce the effects of own ship's motion by a factor of 10 in the band below 10 radians per second.

Comment: Comments as before apply. Additionally, the antenna design bandwidth is controlled by the stabilization bandwidth. Tracking bandwidth requirements are less severe.

Post launch load factor: a design limit of 4 appears reasonable during which maneuver the line of sight error must be less than 3°.

Comment: This requirement appears to satisfy the need for post launch illumination for guidance.

STRUCTURE

No structural resonances which increase gain above the contour $\mu = (\frac{33+s}{s})^2$ should be allowed.

Comment: Primary resonances in the structure must be maintained at frequencies above 300 rad/sec under all environmental conditions to avoid instability from this cause. If the airframe supporting structure does not permit meeting this design requirement, mechanical filter networks in the form of vibration isolators should be used to mount the antenna.

ENVIRONMENT

Ships environment: no major fatigue failures in 5 years.

Aircraft environment: no major fatigue failures in 5 years.

Storage life: 5 years.

Comment: These specifications are the result of the 5 year life of the weapon system spelled out in the Operational Requirements. They result in the following detailed requirements.

Shock: Must withstand 60g to 80g repeated loads of 11 millisecond duration while operating.

Vibration: Must withstand .036 inch inputs in the band 10 to 100 cps while operating. Resonances in the band 10 to 1000 cps must be of amplification factor less than three to result in long fatigue life.

Temperature and humidity: MIL E-5400A

Altitude: 0 to 65,000 feet

Comment: Due consideration must be made of the fact that operation at extreme altitude limits is for very short times (perhaps 30 minutes total time at 65,000 feet in a five year period). A reasonable criteria must be established for failure at altitude.

Mission profile: The training profile is more severe than the combat profile and will involve 2 flights per day, 2 days out of 3. Each flight will involve 5 conversions from search to track including 2 hours of radar operation of which 5 minutes will be in the track mode. Little of the profile will be at either extreme of altitude, 35,000 feet being likely.

R.F.

Bandwidth: As specified by study of frequency separations required to avoid mutual interference. The study should be completed immediately. This approach automatically gives all the frequency diversity countermeasures protection needed.

Polarization: Primary mode, vertical; secondary mode, in weather, circular.

Comment: Serious doubt still exists that circular polarization will contribute anything unless the radome design is made to reduce depolarizing effects. Automatic circuitry must be designed into the rest of the system to make use of the secondary mode, otherwise benefits to be gained may be cancelled by losses attributable to pilot judgment and attention factors.

Boresight shift: 1.5 mils rms including radome. No destabilizing effects of boresight shift can be tolerated.

Harmonic distortion of scan frequency: A tolerance level must be set in view of various proposals for the use of noncircular dishes and aircraft structure interferences.

4. All of the above estimated requirements are to be viewed as combined specifications for aircraft, radome, and antenna.

Laurence F. Gilchrist

SUMMARY OF NAVY STUDY PROGRAM FOR F4H-1 and F8U-3 WEAPON SYSTEMS

by

Clair M. Loughmiller and John C. Ryon

VOLUME I

TABLE OF CONTENTS

INTRODUCTION

The Bureau of Aeronautics has contracted with Westinghouse, Air Arm Division, for analytical services to be used in a study to establish the tactical use capability of the F4H-1 and F8U-3 Weapon Systems. This study is conducted under the technical direction of the Naval Research Laboratory with all inputs derived from Navy sources. Westinghouse, using these inputs, will submit analytical results to the Navy. Recommendations and conclusions to be drawn from analytical results are assumed to be a Navy responsibility and in particular the responsibility of the technical directors (NRL). This report is the first in a series directed toward carrying out this responsibility.

The data presented herein is only partially complete. There are many areas where much work remains to be done. Nevertheless, it is important to present the study material at this time for several reasons. Among these are; (1) to indicate the scope of work accomplished and work remaining to be done, (2) to provide guide lines useful now to the Bureau of Aeronautics in their direction of contractor study efforts, (3) to provide timely information that will assist the Bureau in making decisions on hardware development.

This memorandum is intended primarily for Bureau information. It is realized that the material presented, in some cases, is incomplete (work still underway in many areas) and probably should not be released to contractors at the present time. Except for government activities, all distribution will be handled through the Bureau channels.

STUDY PROCEDURE

Table I is an outline of the Navy's Air-to-Air Missile Study Program. As originally planned the outline was intended to be a general guide having flexible elements in order that additionally needed study areas, which developed as the study progressed, could be included if desired. A second investigation, considered separate for contractual reasons, was planned to be essentially a repeat of Phases I to V of the basic study but for the Sparrow II missile. Postponement of the Sparrow II study and of Phase VIII of Table I is presently planned in order that more pressing problems, which have come up as a result of study to date, can be investigated.

For purposes of pursuing this study on a working basis, a framework of six parts has been constructed against which the performance of each system combination is to be analyzed. This framework is as follows.

Part 1: Development of effective theoretical co-altitude attack zones under ideal conditions.

Part 2: Development of effective theoretical non co-altitude attack zones under ideal conditions.

Part 3: Development of effective theoretical attack zones in the presence of the degradation of expected tactical conditions.

Part 4: Repeat Part 3 for possible improvements to the system which are being considered by the Navy.

Part 5: Study to determine and assess realizable improvements.

Part 6: Study of infrared (IR) tie-in for AI fire control systems.

The material presented in this report is grouped to fit this framework.

F4H-1 and F8U-3 WEAPON SYSTEMS PERFORMANCE UNDER IDEAL CONDITIONS - INPUT DATA

The performance of the system under "ideal" conditions will indicate a tactical capability representative of the best that can be achieved with high probability. As is evident from the outline of Table I, several parameters are assumed to be without error. Perfect vectoring against a non-maneuvering target is assumed for example. In addition the effects of weather, clutter, and CM are not considered. However, the word "ideal" as used here should be read in a limited sense since the performance of the weapons system sub-elements is defined by realizable rather than "infinite" quantities.

Radar Analyses

All detection ranges given for the AI radar in this study were obtained by scaling test results from NATC, Patuxent. Figure 1 gives probability of detection versus range curves for the AN/APQ-50 radar against an F2H-2 target at an altitude of 30,000 feet. The first models of the AN/APQ-72 and AN/APQ-74 radars will have essentially the same performance as the AN/APQ-50 (if not degraded by added complexity of extraneous system functions found in the original concept of the weapon system. This curve was originally obtained from Reference (1) and was taken from Reference (2) for inclusion in this report. The probability of detection

TABLE I

OUTLINE OF NAVY AIR-TO-AIR MISSILE SYSTEM STUDY PROGRAM

PHASE I System Performance Under Ideal Conditions

A. Aircraft Characteristics

1. F4H-1
2. F8U-3

B. Altitudes (co-altitude case)

1. 1000 feet or less
2. 30,000 feet
3. 50,000 feet

C. Interceptor Velocity -

1. F4H at altitude (V_{max} & V_{cruise})
2. F8U-3 at altitude (V_{max} & V_{cruise})

D. Target to interceptor speed ratio for interceptor at V_{max}

1. 0.45
2. 0.8 } Some cases may be trivial and will not be used
3. 1.0

Target speed resulting from above will be used for interceptor at V_{cruise}

E. Conditions -

1. Perfect vectoring
2. Straight line flight path
3. Current AI detection capability
4. B-47 size target
5. Preparation time - Two cases determined by study
6. Sparrow III - Capability of current seeker is to be used.
7. Sparrow III - Aerodynamic capability of current missile is to be used.
8. Gimbal angle limits in F4H and F8U-3 aircraft -
   a. APQ-72
   b. Seeker

9. Illumination consideration - Geometry of keeping both target and missile illuminated. Illumination requirements to be determined by study.

PHASE II System Snap-up Performance Under Ideal Conditions

A. A, C, D, and E - same as Phase I

B. Altitudes (snap-up case)

1. Target

a. 30,000 feet
b. 50,000 feet
c. 65,000 feet

2. Interceptor Altitude - To be determined by study of system capability.

PHASE III System Performance Under Expected Tactical Conditions

A. Target maneuver

B. Vectoring accuracy

C. Weather

D. Limits imposed by interceptor tactics

1. Climb capability
2. Endurance
3. Dead time

E. Countermeasures

1. Airborne weapons system

PHASE IV System Performance Under Expected Tactical Conditions With Addition of Currently Proposed Improvements

A. Improvements proposed:

1. Search volume optimization

2. Triangle system vectoring
3. Automatic alarm
4. Improved receiver noise figure
5. Back-biased range and display IF amplifier with broadband switching
6. Gated narrowband angle track IF amplifier (home on jam)
7. Bright display
8. Provision for switching polarization (circular and vertical)
9. Broad banding of the plumbing
10. Jittered PRF
11. Antenna with high altitude feed
12. Improved two-speed AFC
13. Relocation of CW injection plumbing to increase gimbal angle in elevation
14. Non-saturating AGC

PHASE V Study to determine and assess realizable system improvements -

A. AI Radar

B. Missile

C. Vectoring

D. Tactics

PHASE VI Study of IR tie-in with the fire-control system

PHASE VII Performance capability of Sparrow III with an IR seeker

PHASE VIII Sparrow III X performance capability

PHASE IX Repeat study Phases I through Phase VI for the Sidewinder 1-B and 1-C

curve for the combined head-on and tail-on runs was used. This contour was then scaled to a B-47 size target for the speed and altitude conditions of interest using the method detailed in Reference 3.

Figure 2 gives a normalized radar reflective area curve. The scaling ratio used in going from Patuxent data to the B-47 size target was 5.3/1. The resulting detection range contours used are for 85% cumulative probability of detection against the B-47 size target. All contours were obtained using a 10 db field degradation (expected degradation between Patuxent usage and fleet usage). To date this degradation factor appears to be optimistic. However, it is believed that 10 db can be approached during the use period of this equipment.

In developing the detection range contours the following parameters for the AN/APQ-72 and AN/APQ-74 radars were used.

Peak Power	200 kw
Dish Size	24"
Noise Figure	10.5 db
Receiver Bandwidth	4 mcps
Search Area	90°x8.5° (spec value - to antenna beam center - as not restricted by CW injection)
Frame Time	2 seconds
Scanning Rate	100 deg/sec
Pulsewidth	1.75 µsec
PRF	550 pps

In addition to the above parameters, the following radar parameters were used in development of attack zones which will be described later.

Time from detection to lock-on: 10 seconds

Gimbal angle limits of current APQ-72 & 74: $\pm 41^{\circ}$ az.

$+ 47^{\circ}$
$- 38^{\circ}$ el.

Figures 3-6 give the 85% cumulative probability of detection ranges versus aspect angle for a B-47 size target for the altitude and speed conditions listed in Table 2. These curves were obtained from Reference 2. In addition, Fig. 7 gives 85% cumulative probability of detection ranges versus aspect angle for a B-47 target at low altitude. These latter curves are based upon theoretical calculations and will be modified when

NATC, Patuxent test data is made available. For this reason, work on the 1000 ft. altitude cases of Table 2 has not yet been initiated.

Aircraft Analyses

To date only the F4H-1 aircraft has been included in the analysis. Performance data on the F8U-3 have become available recently and will be included in future analyses. The memoranda of Appendices I, II, III, IV of Volume II of this report describe the model aircraft (F4H-1) used throughout the work detailed in the remainder of this report. The material of these memoranda was obtained from voluminous McDonnell Aircraft Company data, has been reviewed by McDonnell, and is stated by them to be representative of the aircraft to be used in the weapon system.

Missile Analyses

The lateral and longitudinal equations describing the Sparrow III missile trajectory in space during a coplanar attack are given in Appendix V of Volume II of this report. Much additional data describing the performance of Sparrow III has been obtained from Raytheon. Some of this is included and given by Figs. 8 to 14.

The interlock equations describing maximum and minimum aerodynamic ranges used in this study are as follows:

$$R_{max} = R_{1(h)} + T_1 (V_c - V_f) \text{ - Limited to 6.5 n.mi.}$$

$$T_1 = 11 \text{ sec} \quad \text{when } V_c > V_f$$

$$T_1 = f_{(h)} \quad \text{when } V_c < V_f$$

$$R_1 = f_{(h)}$$

$$R_{min} = R_{2(h)} + T_2 V_c$$

$$R_2 = f_{(h)}$$

$$T_2 = 3.3 \text{ sec}$$

T_1, R_1, and R_2 as a function of altitude are given in Fig. 15.

Figure 16 gives the lock-on range performance of the current Sparrow III seeker. This curve was obtained by scaling from data received from NAMTC, Pt. Mugu to a B-47 size target. This scaling was done strictly on a reflective area basis; no velocity effects were considered. The basic range quantity from which the curve was obtained was a measured 90% probability of lock-on at 3.3 n.mi. in the head-on aspect against an F2H target. The contour given by Fig. 16 represents the computed 90% probability of lock-on for the seeker against the B-47 size target.

The preceding sections list some of the pertinent input data to this study program. Additional data may be found in Reference 4.

PHASE I - SYSTEM PERFORMANCE UNDER IDEAL CONDITIONS - HORIZONTAL ATTACKS

Following the format previously described, the first case to be investigated is that of the horizontal attack under "ideal" conditions. Figure 17 gives a pictorial representation of this ideal situation. The target is assumed to be nonmaneuvering under attack during fair weather. The interceptor is assumed to start on a perfectly vectored lead pursuit course. Using the preceding input data, the effective attack zones for the F4H-1 Weapon System have been developed.

Attack Zones

The conditions listed on Table I describe the speed and altitude cases of interest. Figure 18 shows the courses flown by the interceptor during a particular situation. Along these courses the interceptor heading is shown by vectors. The curve overlays of the figures to follow are only partially complete. The remaining work to be done will be described in a later section.

Figures 19-24 give polar plots of the effective attack zones for the F4H-1 Weapon System under "ideal" conditions. For these examples the interceptor was assumed to be flying at V_{max} at altitudes of 30,000 and 50,000 feet with target to interceptor speed ratios of 1.0, 0.8, and 0.45. The interceptor is placed on a perfectly vectored lead pursuit course. The target is flying a straight line course as indicated by the arrow on the base line of the plots. For this phase of the study, the characteristics of the F4H-1 aircraft were programmed on an IBM 704 computer. The courses shown on the overlays actually represent the performance capability of this aircraft.

The contours describing the effective attack zones are curve A (85% probability of AI detection range), curve B (AI lock-on range), curve C (Sparrow III maximum aerodynamic range), curve D (Sparrow III minimum aerodynamic range), curve E (constant load factor loci N_Z = 2,3), curve F (90% probability of Sparrow III seeker lock-on range), and curve G (6.5 n.mi. range). It is assumed that 10 seconds is consumed between AI detection and lock-on. It is believed that even for the "ideal" case, 10 seconds elapsed time is required for high probability of lock-on. The maximum and minimum aerodynamic contours are those resulting from the interlock equations as defined by Raytheon.

The effective attack zones as given on these polar plots are those bounded by the heavy line. The resulting complex contour is one made up of segments of the other curve overlays. For example, in Fig. 19 the attack zone is bounded by seeker lock-on capability from nose-on around to approximately 70° off the nose. From this point around to tail-on the limiting parameter is the maximum aerodynamic range of the Sparrow III. The inner boundary curve is that generated by the minimum aerodynamic range from nose on to approximately 40° off the nose; load factor loci 3 from 40° off the nose to 10° off the tail, and minimum aerodynamic range around to tail-on. It is important to note that even for the perfect situation, time plays a major role in the use of this system in a forward hemisphere attack. In these overlays only 10 seconds elapses between AI detection and lock-on. Since this is an idealized case, the missile could be launched at this time. It is obvious that when additional time is added because of system errors that exist at AI lock-on, the reduction in forward hemisphere capability can be great. For example, if 10 seconds is required to settle out errors at AI lock-on a large portion of the forward hemisphere attack zone will be wiped out. This will be discussed in more detail in later phases of the study.

In one sense this type of curve overlay can be misleading. For example, Fig. 19 implies around-the-clock capability. This is true or not depending upon one's definition. If by around-the-clock capability it is meant that attacks may terminate successfully at any clock aspect then Fig. 19 indicates around-the-clock capability. However, it is important to note that the limiting approach aspect is approximately 67° off the target's nose. For this 67° case the interceptor is just barely able to come into the maximum interlock range for the missile. For aspect angles greater than 67° the interceptor would fall behind due to lack of a speed advantage.

Figure 20 gives a polar plot of the case of an attack occurring at 30,000 feet altitude. The interceptor is flying at V_{max} and has a speed advantage ($V_T/V_F = 0.8$). For this case (under the assumed "ideal" conditions) the system does have around-the-clock capability. Attacks initiated at any aspect angle with respect to the target can be converted into a successful run. However, for attacks occurring aft of the beam, target penetration distance will be an important consideration. Due to the low speed advantage, considerable time can elapse between initiation of an attack and conversion to a successful launch. This is especially true if the attack is started at long range. For example, attacks started at the AI detection range, and 60° off the tail, approximately 28 n.mi. penetration distance results. An obvious indication is that CIC, for attacks aft of the beam, should attempt to vector the interceptor to a point as close to the maximum interlock range as possible.

The attack zone of Fig. 20 is that bounded by the same limits as those of Fig. 19. It is important to note that preparation time (assumed to be only 10 seconds for this case) plays a less important role in determining the effective attack zone as the relative closure rate is reduced. Also, the limit imposed by maximum load factor is reduced as closure rate is reduced.

Figure 21 is a polar plot of an attack case occurring at 30,000 feet. Again the interceptor is flying at V_{max} but has an increased speed advantage ($V_T/V_F = 0.45$). As for the case of Fig. 18, around-the-clock capability exists for this situation. The effective attack zone is no longer limited by the maximum load factor contour. The inner limit is now solely that imposed by the minimum aerodynamic range of the missile.

Comparison of the three polar plots illustrate several very important factors.

(1) Even under "ideal" conditions, high speed engagements result in marginal forward hemisphere capability. As additional time is added to account for event that must occur under tactical conditions this marginal forward hemisphere capability is wiped out.

(2) As the relative closure rate is reduced the effects of time on forward hemisphere attacks is reduced. This results from increased AI detection range and the lesser distance traversed during the 10 seconds from AI detection to AI lock-on.

The polar plots of Figs. 22, 23, and 24 are similar to the previously described three figures. However, the attack now occurs at 50,000 feet. The interceptor is flying at V_{max} (1940 fps) and the three figures show the resulting attack zones for V_T/V_F = 1.0, 0.8, and 0.45. The resulting limiting parameters are essentially the same as those previously described. There is one major difference in the attack zones. In the forward hemisphere the minimum aerodynamic range of the missile has been pushed out resulting in a very narrow use zone. This results from the interlock mechanization employed and the reduced response of the missile at high altitudes. The interlock equation for minimum aerodynamic range is

$$R_{min} = R_{2(h)} + T_2 V_c$$

$$R_2 = f_{(h)}$$

From Fig. 15 it is seen that going from 30,000 feet altitude to 50,000 feet changes R_2 from 4000 feet to 8000 feet. Since $T_2 V_c$ remains approximately the same for the cases shown in Figs. 19 and 22, there should be an increase of approximately 4000 feet in the minimum range. Comparing these figures it is seen that this is the case.

In addition to the attack zones described above, much additional valuable information relating to parameter variation can be obtained from the computer generated courses. For example, the variation in gimbal angle as the attack progresses is of extreme importance to the fire control designer. Knowledge of the antenna tracking rates is also very important. Figures 19a through 24k are plots of some of the more important parameters. On these plots the parameters are defined as follows.

λ_a = lead angle in azimuth

λ_e = lead angle in elevation

λ = total lead angle in the plane of action

Υ = angle between target velocity vector and the line of sight measured from the nose of the target

ψ = angle between the target velocity vector and the interceptor velocity vector measured from the nose of the target

ω_j = angular rate of the line of sight in the elevation plane of the antenna system

$\dot{\alpha}/k$ = angular rate of the line of sight in the azimuth plane of the antenna system

L/W = load factor

ϕ = roll angle

V_f = speed of the interceptor

α = angle of attack

The parameter plots in Fig. 19a through 19k come from the 30,000 feet altitude case shown in polar form on Fig. 19. The plots on these figures correspond to the approach courses of the polar plot and are designated by τ_o . On these courses A, B. C, and D correspond to the maximum aerodynamic range of the missile (R_{max}), the minimum aerodynamic range of the missile (R_{min}), load factor L/W = 3, and impact point for missile fired at R_{min} respectively. Figure 19a gives plots of λ_e versus range. For the cases of $\tau_o = 90^o$ and 120^o the points A and B never appear on the curve . Referring back to Fig. 19, it is seen that this is as it should be since the interceptor was never able to close to the maximum aerodynamic range of the missile. For the case of $\tau_o = 60^o$ the interceptor was able to convert to a successful attack. However, as shown on this plot he was never able to close to R_{min}. The 3g load factor boundary was passed through twice. For this case the azimuth lead angle varies from -27^o at detection to -13^o at the point where the 3g boundary was first encountered. For the case of $\tau_o = 30^o$, the 3g boundary was encountered before R_{min} was reached. For this case the azimuth lead angle varied from -16^o at detection to -8.5^o at the point where the 3g boundary was encountered.

Figure 19b gives plots of elevation lead angle (λ_e) versus range. As shown in Fig. 19, the cases for $\tau_o = 30^o$ and 60^o were the only ones examined which could be converted. For the case of $\tau_o = 30^o$ the elevation gimbal angle varied from -6^o at AI detection to -23^o at R_{min}. For the case of $\tau_o = 60^o$ the elevation gimbal angle varied from -15^o at detection to -35^o at the point where the 3g contour was encountered. It is extremely important to note that for this case and succeeding high speed cases (under "ideal" conditions) the elevation lead angle required approaches the gimbal angle limits of the current system ($+47^o$, -38^o elevation). This situation will get worse as one deviates from the perfectly vectored situation to one representative of the tactical situation.

Total lead angle (λ) versus range is plotted on Fig. 19c. These curves show the combined effects of Fig. 19a and 19b. Figure 19d gives the angle off the target's nose (Υ) as a function of range for the various approach courses. Figure 19e shows the heading angle (ψ) versus range.

Of particular interest to the AI radar and fire control system designers are the antenna rates involved in the solution of the tactical problem. The azimuth antenna rate (ω_k) versus range is shown on Fig. 19f for the courses generated on the polar plot of Fig. 19. For the case of $\Upsilon_o = 30^o$ the azimuth antenna rate varies from 0.27 deg/sec at AI detection to 0.7 deg/sec at the point where the 3g contour is encountered. For the case of $\Upsilon_o = 60^o$ the azimuth antenna rate varies from 0.43 deg/sec at AI detection to 1.38 deg/sec at the point where the 3g contour is first encountered. On Fig. 19g the elevation antenna rate (ω_j) versus range is plotted. As would be expected from examination of the preceding figures, the elevation antenna rate is in general higher than the azimuth antenna rate. For the case of $\Upsilon_o = 30^o$ the elevation antenna rate varies from 0.1 deg/sec at detection to 1.7 deg/sec at the point where the 3g contour is encountered.

Figure 19h gives load factor (L/W) versus range. These curves illustrate the "g" build-up as the attack progresses. As was stated previously one of the limiting parameters in the overlays depicting the effective attack zones is the locus of points described by L/W = 3g's.

Figure 19i gives the variation in roll angle (ϕ) with range. As can be seen from these plots, even for the perfect situation, roll angles as high as 70^o can be expected during the approach course. Figure 19j gives plots of interceptor velocity (V_f) as a function of time. These curves illustrate the slow-down of the interceptor while on the approach course. Figure 19k gives plots of angle of attack (α) as a function of time. As can be seen from these curves the angle of attack builds up quite rapidly.

The curves of Figs. 20a through 24k give the same parameter plots for the polar plots of Figs. 20 through 24.

Figures 25 through 30 give additional polar plots of the effective attack zones under "ideal" conditions. These attack zones are similar to those described previously. The basic difference is that the interceptor is assumed to be at V_{cruise} at time of detection. The altitudes and target speeds investigated are the same as those of Figs. 19 through

24. The lower interceptor speeds were chosen to study the possible system improvement as a result of lower closing velocity. This results in greater detection ranges and in reduced effects of preparation time (especially in the forward hemishpere). This is illustrated by Fig. 25. Comparing this to Fig. 19 shows that the AI radar 85% probability of detection has increased from 12.75 n.mi. head-on to 13.75 n.mi. and the 10 second lock-on point has moved out in range from 6.5 n.mi. to 9.1 n.mi. For the conditions of Figs. 25 through 30, AI lock-on range is no longer a limiting parameter.

The study of the cases illustrated in Figs. 25 through 30 is not completed. The work to date has assumed that the interceptor starts the attack at V_{cruise} and continues at V_{cruise} throughout the engagement. Examination of the overlays shows that only for one case does the interceptor have a speed advantage (see Fig. 27). The next step in the analysis will be to investigate the improvements realized by accelerating the interceptor toward V_{max} after AI lock-on occurs. The overlays of this group of figures have indicated the regions where this would result in improved capability. For example, Fig. 25 shows that the limiting approach course is approximately 36° off the nose of the target. It is thus of interest to investigate the improvement realizable at greater angles by accelerating the interceptor.

Remaining Study

The 1000 feet altitude case has not been studied to date. Analysis of this situation is awaiting low altitude radar detection performance data from NATC, Patuxent, to augment theoretical detection range calculations.

A study of the limits imposed by hydraulic oil to the wing servos as a function of system noise and control is being performed by NAMTC, Pt. Mugu. The results of this study will supply an additional boundary to place on the tactical polar plots.

It is noted that in the tactical polar plots for interceptor operation at V_{cruise}, considerable attack area is denied due to the speed disadvantage. An investigation will be made of the effects of interceptor acceleration toward V_{max} in these areas where attack is denied.

PHASE II - SYSTEM CAPABILITIES FOR SNAP-UP ATTACK UNDER IDEAL CONDITIONS

The preceding sections have described, in part, the ideal situation for horizontal attacks. Because of the relatively short ranges of the search radar from which vectoring information is derived (CIC or AEW)

because of vectoring inaccuracies and because of the high speed and altitude capability of expected targets, it will not always be possible to get the interceptor into a position for horizontal attack before the target aircraft has reached the release range of its own weapons. For this reason it is of importance to investigate the feasibility of launching Sparrow III from altitudes lower than that of the target (pull-up attacks). The following sections will describe the results of the analysis conducted to date.

Conditions

The following conditions are used in Phase II of the study program.

(a) Aircraft characteristics - F4H, F8U-3

(b) Target altitudes - 30,000, 50,000, and 65,000 feet

(c) Interceptor altitudes - as capable from below

(d) Reflective area - B-47 size target, assumed the same as for co-altitude case

(e) Velocities - interceptor velocity at altitude, V_{max} and V_{cruise}

(f) Target to interceptor speed ratios for interceptor at V_{max} - 0.45, 0.8, 1.0. Resulting target speeds from above also used for interceptor at V_{cruise}

(g) Perfect vectoring

(h) Straight line flight path (target)

(i) Current AI detection capability - 85% probability

(j) Time from detection to lock-on - 10 seconds

(k) Seeker capability - current Sparrow III

(l) Missile aerodynamics - current Sparrow III

(m) Gimbal angle limitations of current AN/APQ-72 radar - $\pm 41^{\circ}$ azimuth, $+47^{\circ}$, -38° elevation

(n) Interceptor restricted to 3g pullup or C_{Lmax}

In addition to the foregoing conditions, a limiting criteria for success was that it is necessary to reduce the heading error of the interceptor to within $\pm$ 10° of a lead pursuit course within the missile R_{max} to R_{min} zone. This 10° limitation is not based upon firm data, but rather on estimates made by the prime contractor. Currently, Pt. Mugu is conducting analyses to determine the validity of this number. The results of the analyses will be used in this study program as soon as they become available. Another limiting criteria used in the pull-up study phase and throughout the remaining study program is that L/W must be greater than 0.5 g's. This figure is based upon stability requirement data obtained from the aircraft contractors.

Figure 31 gives a pictorial representation of the "ideal" snap-up attack. As stated previously and shown on this drawing, the target is nonmaneuvering. All attacks occur about a vertical plane through the target and interceptor with no vectoring inaccuracy superimposed. The study to date has only considered the head-on attack case.

Attack Zones

Figure 32 shows an actual space plot of one of the courses generated during the snap-up investigation. For this course the target was flying at 50,000 feet. The interceptor's initial altitude from which the pull-up is started is 20,000 feet. The target's velocity is V_T = 874 ft/sec and the interceptor is initially flying at V_F = 874 ft/sec which corresponds to V_{cruise}. The cases for V_{cruise} in the pull-up study differ from the preceding analysis of the V_{cruise} for horizontal attack in that the interceptor has maximum re-heat applied at detection and accelerates toward V_{max}. For this space plot the interceptor starts his pull-up at 30 seconds after detection of the target. It is interesting to note the extreme flight path angles that occur during the run.

Figures 33 through 38 give, in effect, tally sheets for the results of the snap-up studies to date. These figures give plots of fighter altitude from which the attack initiated versus pull-up delay after detection and indicates for each run whether it was a success or failure along with the reasons for failure when this occurs. Two plots are given on each sheet. One of these is for the interceptor at V_{max} at the time of AI detection and the other is for V_{cruise} against a target at the speed and altitude conditions given at the top of each page. The symbols on each of the tally sheets are:

◊ - Unsuccessful attack

X - Launch error = 0

⊙ - Launch error $\leq 10^{o}$

Figure 33 gives the results of pull-up attacks against a Mach 2.0 target flying at 65,000 feet. The left hand side of this figure shows the results for the case where the interceptor is flying at V_{max} at the time of AI radar detection. Referring to this figure it is seen that with the interceptor flying at 45,000 feet and the pull-up starting at zero time (instant of AI detection), the run was a failure because the minimum error ($\epsilon_{min} = 16^{o}$) exceeded the maximum assumed launching error. When the attack was started from 55,000 feet and the pull-up initiated at time = 0, the run was a success (launch error = 0). When the pull-up was initiated at 5 seconds after detection, the run was a marginal success ($\epsilon_{min} = 9^{o}$). When the pull-up was initiated at 10 seconds the run was a failure because the minimum launch error was too large ($\epsilon_{min} = 23^{o}$). From these results, the usable launch zone can be approximated as shown by the dotted line on this figure. However, if the same criteria is applied as was applied to the co-altitude attack; namely that 10 seconds is required between AI radar detection and lock-on and if it is assumed that pull-up could not be initiated before lock-on (this is a valid assumption for the current state of the art in vectoring) there is no usable attack zone. This can be shown by drawing a vertical line through the altitude region of interest at time = 10 seconds.

The right half of Fig. 33 shows the result of starting the same problem with the interceptor flying at V_P = Mach 0.9 at the time of AI radar detection and then accelerating toward V_{max}. For these conditions we have no capability because for all of the cases examined the launch error was greater than 10^{o}.

The plots of Fig. 34 give the results of snap-up attacks against a Mach 0.9 target flying at 65,000 feet. The left hand side of this figure again gives the results of runs for the interceptor flying at V_{max} at the time of AI radar detection. For the cases of pull-up starting at time zero at 35,000, 45,000, and 55,000 feet, the runs were successful because the launch error was zero. When the pull-up started at 5 seconds the 35,000 ft. run was marginally successful since the launch error reached a minimum of 9.8^{o}. For the case of the run starting at 45,000 feet and the pull-up beginning at 5 seconds, a success occurred with the launch error reaching zero degrees. When the pull-ups started at 10 seconds, failures occurred at 35,000 and 45,000 feet with minimum launch errors

of 35° and 14° respectively. A successful run occurred for time equal to 10 seconds and 55,000 feet altitude with the launch error reaching zero. For the case of an attack starting with the interceptor at 55,000 feet and pull-up beginning at 15 seconds aft r AI radar detection, the run was a failure because the minimum launch error was 12°. The effective attack zone for this ideal condition can then be drawn in as shown by the solid lines. The inner boundary is determined by the 10 second requirement from AI radar detection to lock-on, the upper boundary by the altitude limit of the interceptor for stable flight (59,000 feet) and the outer limit by the runs described above. Thus it is seen that even for a relatively slow target (Mach 0.9), the effective attack zone resulting from the ideal situation is essentially nil.

The plot on the right side of Fig. 34 gives the results of starting the interceptor at Mach 0.9 against the same target (Mach 0.9 at 65,000 feet). As shown, all runs were failures. For the case of intercepts initiated at 35,000 feet, four failures resulted. When the pull-up was initiated at 10 and 20 seconds after AI radar detection, the minimum launch errors were below the maximum allowable but an unstable condition on the part of the interceptor was reached ($L/W \ll 0.5$ g's). For the case of pull-up starting at time = 25 seconds, the run was a failure because the minimum launch error (18°) exceeded the maximum allowable (10°). Looking next at intercepts starting from 45,000 feet it is seen that all runs were failures. When the pull-up started at zero time the run was a failure because the minimum launch error (18°) was excessive. For a pull-up attack starting at 10 seconds the minimum launch error (9°) was marginal but the elevation gimbal limit was exceeded ($\lambda_e \gg 47$). When the pull-up was initiated at 20 seconds, the run failed because of excessive launch errors ($\epsilon_{min} = 18^{\circ}$).

The plots of Fig. 35 give the results of pull-up attacks against a Mach 2.0 target at 50,000 feet. Beginning with this figure, the remaining cases will be under conditions where the interceptor could make a co-altitude attack if properly placed. Thus the upper boundary in each case will be that of a co-altitude attack with the outermost point on the usable zones representing the minimum aerodynamic range of the missile. The group of points plotted on the left of Fig. 35 give the results of pull-up attacks against a Mach 2.0 target flying at 50,000 feet with the interceptor flying at Mach 2.0. When the pull-ups were initiated at zero time a failure occurred at 30,000 feet because the minimum error ($\epsilon_{min} = 21^{\circ}$) exceeded the maximum allowable. A success occurred at 40,000 feet with the minimum launch error reaching zero. When the pull-up was

initiated at 5 seconds, a marginal success resulted with the error being reduced to 9°. Thus the usable zone can be drawn as shown by the solid lines. To make a successful pull-up attack, the interceptor must be at 45,000 feet or higher against a Mach 2.0 target at 50,000 feet. The right hand plot of Fig. 35 is for the same target condition but the interceptor has been slowed down to Mach 0.9 at AI radar detection. When the attack was initiated from 30,000 feet a failure occurred for a pull-up started at zero time because the gimbal angle was exceeded ($\lambda_e = -38^{\circ}$) and a failure occurred at 10 seconds because the maximum allowable launch error was exceeded ($\epsilon_{min} = 17^{\circ}$). When the attack was initiated from 40,000 feet a successful run occurred at zero time, a marginally successful run occurred for pull-up starting at 10 seconds ($\epsilon_{min} = 9^{\circ}$), and a failure occurred when the pull-up started at 15 seconds ($\epsilon_{min} = 21^{\circ}$). Thus the usable zone can be drawn as shown by the solid lines. The inner boundary is a vertical line drawn at 10 seconds. The upper boundary is that of a co-altitude attack with the outer limiting point being R_{min} (23.5 seconds) and the outer limiting curve resulting from the pull-up runs.

It is next of interest to investigate the results of pull-up attacks against a slower target (Mach 0.9) at the same altitude as that of the preceding figure (50,000 ft.). These results are shown on Fig. 36. The left hand plot shows the results of a Mach 2.0 interceptor attacking this target. Successful runs occurred at 20,000, 30,000, and 40,000 ft. altitude for pull-ups initiated at zero time. Successful runs also occurred at 20,000 and 30,000 feet altitude for attacks initiated at 5 seconds. When the pull-up was started at 10 seconds after AI detection, failures occurred for runs initiated at 20,000, and 30,000 feet with the minimum launch errors being excessive ($\epsilon_{min} = 23^{\circ}$ and 13°). A successful run occurred at 40,000 feet when the pull-up was initiated at 10 seconds, but a failure occurred when the pull-up was delayed to 15 seconds ($\epsilon_{min} = 11^{\circ}$). The usable zone that results is that given by the solid lines with the inner boundary being the vertical 10 seconds line the upper boundary being that of a co-altitude attack limited by R_{min} (2. 5 seconds) and the outer limiting line resulting from the pull-up courses. It is interesting to compare this plot with the right hand plot of Fig. 35. The horizontal span of the usable zones are essentially the same since the closure rates are the same. However, the vertical spans are quite different. This illustrates the penalty paid by reducing interceptor speed and then trying to accelerate during the pull-up attack.

When both the interceptor and target are slowed and the target is in a region from which a co-altitude attack can result, the improvement

in usable zone for the "ideal' situation is quite marked. This is shown by the right hand plot of Fig. 36. Here the fighter has been slowed to Mach 0.9 and is attacking a Mach 0.9 target flying at 50,000 feet. The successful runs are all shown by X's. Failures occurred as follows:

Pull-up at zero time from 10,000 feet - $L/W < 0.5g$

Pull-up at 10 seconds from 10,000 feet - $L/W < 0.5g$

Pull-up at 30 seconds from 30,000 feet - $L/W < 0.5g$

Pull-up at 30 seconds from 30,000 feet - $\epsilon_{mi} = 18^{\circ}$

Pull-up at 35 seconds from 40,000 feet - $\epsilon_{min} = 20^{\circ}$

As shown, a relatively large usable zone results for these speed cases under "ideal" conditions. The zone is bound again by the vertical 10 second line, horizontal co-altitude line extending to R_{min} at 44 seconds and the lower curve resulting from the actual pull-up runs. The remaining cases studied to date are those of a target at 30,000 feet. Figure 37 shows the results of runs against a Mach 2.0 target at this altitude. The left hand plot shows the results of runs made by the fighter at V_{max} or Mach 2.0 at time of AI detection. Unsuccessful runs occurred for attacks started at zero time and sea level ($\lambda_e = -67^{\circ}$), at 10,000 feet altitude and 5 seconds ($\epsilon_{min} = 24.5^{\circ}$) and at 20,000 feet altitude and 5 seconds ($\epsilon_{min} = 22^{\circ}$). The useful attack zone is bound by the solid line. The right hand plot shows the results of runs against this target with the interceptor flying at Mach 0.9. For this case, successful runs occurred at zero time and 10 seconds for runs initiated from 20,000 feet. Failures occurred at zero time and 10 seconds for runs initiated from 10,000 feet ($\lambda_e = -42^{\circ}$ at zero time and $\epsilon_{min} = 29^{\circ}$ at 10 seconds). A failure also occurred at 15 seconds for runs initiated from 20,000 feet ($\epsilon_{min} = 27^{\circ}$). The resulting usable zone is shown by the solid line and is bound by the vertical line at 10 seconds, the horizontal line for co-altitude attacks extending to R_{min} (24.5 seconds) and the line resulting from the pull-up attacks.

The left hand plot of Fig. 38 gives the results of pull-up attacks against a Mach 0.9 target at 30,000 feet. The interceptor is flying at V_{max} or Mach 2.0. Failures occurred at 10,000 feet and 20,000 feet because the launch errors were too large (34° and 20°). A failure also occurred for a run started at 25 seconds and at sea level (-L/W). The solid line gives the usable attack zone. The right hand plot shows the results of pull-up attacks against a Mach 0.9 target at 30,000 feet with the interceptor's initial velocity at Mach 0.9. The solid curve gives

the resulting usable zone. This is bound by the vertical 10 second line, the horizontal co-altitude line extending to R_{min} (42 seconds), a horizontal line at sea level, and the outer boundary resulting from the pull-up attacks. As seen, failures occurred at 30 seconds for 0 and 10,000 feet because an unstable condition on the part of the interceptor was encountered (-L/W). Also a failure occurred at 20,000 feet ($\epsilon_{min} = 33^{o}$).

The pictorial space plot of Fig. 32 shows the actual flight condition of the interceptor during one of the pull-up runs. This displays the actual run from which the point shown at 30 seconds and 20,000 feet altitude on the right hand plot of Fig. 36 was obtained. Figures 39 through 49 give additional polar plots of runs from which other of the preceding described points were obtained in the snap-up study. On each of the curves the following code is used.

+	Start of pull-up
➧	Start of lead pursuit
⊙	R_{max}
⊗	R_{min}
X	Impact
··	$C_L = C_{Lmax}$

Some of the more pertinent points from these figures are as follows. Figure 39 shows two successful runs; one starting at zero time and the other at 10 seconds. It is seen from these curves and from the pertinent data of the table that the criteria of being within the R_{max} to R_{min} zone without having excessive error was satisfied, that the maximum gimbal angle was not exceeded, that no unstable condition on the part of the interceptor was encountered, and that excessive flight path angle was not encountered. These two curves are represented as two points on Fig. 34. The curves of Fig. 40 correspond to two points on the right hand plot of Fig. 34. As described previously these two runs were failures because the interceptor encountered an unstable condition.

The curve of Fig. 41 corresponds to a point on Fig. 35. This curve represents a successful run. However, it is included as an example here to show another problem that the interceptor encounters; namely the C_{Lmax} boundary. Referring to the curve, it is seen that between zero

time and the beginning of the lead pursuit course and between R_{max} and R_{min} the interceptor is riding the C_{Lmax} boundary. Figure 42 gives successful runs which corresponds to points on Fig. 36 and further illustrates riding the C_{Lmax} boundary.

On Fig. 43, pull-up courses from an initial fighter altitude of 20,000 feet and starting at 10, 20, 25, and 30 seconds are shown. These correspond to points on Fig. 36. Of primary importance are the courses starting at 25 and 30 seconds. Note the flight path angles (104.3° and 157.8° respectively, interceptor on its back).

Figure 44 gives curves which correspond to additional points on Fig. 36. The important points brought out by these are: for the curve starting at zero time and at 10 seconds, $L/W < 0.5g$ is encountered; for the curve starting at 25 seconds, the flight path angle is getting very large (128.7°). For the curve that starts at zero time note the interceptor slow down that is encountered (from 873 ft/sec at detection to 323 ft/sec at missile impact). Figure 45 shows two successful runs which correspond to points in Fig. 37.

On Fig. 46 courses are generated which correspond to points on Fig. 38. The course starting at 30 seconds illustrates one of the boundaries that was encountered ($L/W < 0.5g$). In addition it is important to note the extreme flight path angle encountered (178°). These two factors are again illustrated on Fig. 47 where the curves correspond to additional points on Fig. 38. For the course starting at 30 seconds, $L/W < 0.5g$ was encountered and excessive flight path angles occurred (162°).

Figure 48 and 49 give additional curves which correspond to failures. The curve of Fig. 48 corresponds to a point on Fig. 37. As seen from the Table, the gimbal angle (-67.3°) exceeded that available (-38°). The curve of Fig. 49 corresponds to a point on Fig. 36. On this course an unstable condition was encountered ($L/W < 0.5g$) and the gimbal angle (-139.3°) exceeded the available (-38°).

Remaining Study

The preceding section described the results of the pull-up studies for the "ideal" situation. This study is not complete. Remaining items that will be included in the program are:

1. Extension of the analysis to include the F8U-3 aircraft.

2. Consideration of the limits imposed by wing servo hydraulic supply.

Investigation of Item 1 above is currently underway and will be included in the results in the near future. Item 2 is under study at Pt. Mugu. As soon as data are available, curve overlays will be added to the existing zones. Noise data supplied by NRL (Fig. 50) and agreeable to Raytheon are being used.

PHASE III - F4H-F8U WEAPON CONTROL SYSTEMS PERFORMANCE UNDER EXPECTED TACTICAL CONDITIONS

The preceding sections have described the study program to date for an "ideal" situation. The results given represent the best that one would hope to achieve, with a high probability of success, when certain sources of error are neglected. It is now of interest to look at the degradation resulting from a more realistic tactical situation. The degrading factors to be considered in the current study program are:

1. Vectoring inaccuracy
2. Target maneuver
3. Weather
4. Countermeasures against the airborne weapons system
5. Limits imposed by interceptor tactics
   - (a) climb capability
   - (b) endurance
   - (c) dead time

Degradation Caused by Vectoring Inaccuracy

One of the primary degrading factors that has to be investigated is that of vectoring inaccuracy. This inaccuracy is currently estimated as 1 Sigma = $\pm$ 3 n.mi. in azimuth, $\pm$ 3 n.mi. in range and $\pm$ 1 n.mi. in altitude. This estimate is a composite figure based upon many conferences with personnel of Navy CIC, Air Force GCI, Training Centers, and the designers of vectoring data gathering and information transfer equipments. It is hoped that during the time history of this system that the azimuth and range inaccuracies will be reduced to $\pm$ 2 n.mi.

Perhaps the principal effect of vectoring inaccuracy is in its contribution to system settling time. In the preceding "ideal" situations

10 seconds were allotted as the time required to go from detection to lock-on. In the co-altitude attacks for the "ideal" situation, no additional time was charged to settling out errors after lock-on, since it was assumed that the interceptor was on a correct course. If vectoring inaccuracies are added, however, additional time will be required after lock-on to settle out errors. It is true that in the pull-up attacks under ideal conditions errors did exist at detection and the interceptor has to settle these out during the run. However, in this case everything occurred in one plane. As vectoring inaccuracies are added, additional time will also be required to solve the pull-up attack problem.

To date, the analysis of effects of vectoring inaccuracy on system settling time is only partially complete. For the purposes of this study the work has been broken into two parts; (1) events occurring after lock-on, and (2) conversion from vectoring inaccuracy at detection to angular heading inaccuracy at lock-on. The work to date consists of a partial analysis of the effects of vectoring inaccuracy during a co-altitude attack.

For purposes of the current study program, an approximation of actual system settling time is sufficient. Thus several simplifying assumptions have been made. Referring back to the co-altitude attack polar plots (example Fig. 19) the regions of interest and assumptions made for investigation of these regions can be explained. For example, analysis based upon the assumption that lock-on occurs at constant ranges of 5, 10, and 15 n.mi. would yield results from which the actual lock-on curve could be approximated. As the speed conditions change and as the improvements, which are described later, are added the regions over which each of these constant lock-on ranges apply will also change. Thus it is very important that all of these cases be studied. With this in mind, the following conditions will be studied in the settling time analysis.

(1) Lock-on occurring at constant ranges - R_o = 5,10,15 n.mi.

(2) Target to interceptor speed ratios - V_T/V_F = 1.0 and 0.8 ($V_F = V_{max}$)

(3) Altitudes of interest - 30,000 feet and 50,000 feet

(4) F4H and F8U-3 characteristics

Appendix VI of Volume II of this report describes the work accomplished to date (very preliminary). The basic assumptions used are included in this report. The investigation is being conducted using a cockpit simulator tied into a REAC. In this simulation the actual performance is that of the F4H-1 aircraft. The presentation to the pilot is that of the currently proposed AN/APQ-72 radar. The major item of difference from actual conditions (aside from psychological factors) is that of "g" forces on the pilot. Pilots using the simulator were in fact jet pilots and they were instructed not to pull more than 3 g's. Those cases where 3 g's were exceeded will be deleted from the final analysis.

Examination of Appendix VI will clearly illustrate that the analysis is not complete. The results obtained are, in general, better than one would expect under tactical conditions. For example, Page 18 of Appendix VI shows that on most runs 3 g's were exceeded, thus reducing the settling time which would actually be realized under tactical conditions. In addition, the case of lock-on occurring at 5 n.mi. has not been examined. Only the cases of R_O = 10 and 15 n.mi. have received preliminary examination. Again optimistic settling times result. This in effect reduces the difficulty of the problem to be solved by the pilot-interceptor combination and is inconsistent with the performance of current AI radars, especially in attacks forward of 60° off the nose of the target (where R_O = 5 n.mi. would apply). Under Part 1 of the settling time study only one speed condition has been examined to date ($V_F = V_T$ = Mach 1.91). This corresponds to V_{max} for the F4H at 30,000 feet. AI lock-on was assumed to occur, as stated previously, at 10 and 15 n.mi. Under Part 2 of the settling time study only one speed condition has been considered to date, namely $V_F = V_{max}$ at 50,000 feet altitude. Unfortunately the speed and altitude conditions of Parts 1 and 2 differ. However, the speeds involved are very nearly equal (1897 ft/sec and 1940 ft/sec). Thus preliminary conclusions can be drawn.

From the above discussion it is obvious that much additional work is required to firmly establish system settling time. As stated previously the results are very optimistic as far as the performance of the current system is concerned. Even with these optimistic results the situation is extremely poor and should therefore be reported on at this time. As more complete results are obtained, the data on system performance will be modified.

Figure 51 gives a pictorial representation of Part 1 of the settling time study. At lock-on the interceptor is assumed to have an angular error (ϵ_{AO}) of 10, 20, or 30° at various angles off the nose of the

target (γ_o). These angles epresent the angle at which the interceptor reached the lock-on range. The cases studied were for γ_o equal to 20, 40, 60 and 90 degrees (initial starting angles).

Figure 52 shows a sample of the settling time courses plotted in Appendix VI. This figure shows the results of runs started at a lock-on range of 10 n.mi. and at an initial angle of $\gamma_o = 60^\circ$. These runs do represent a completed phase of the study since the lock-on range assumed is consistent with current AI radar performance and the pilot (Somerville) did stay within the 3g criteria (approximately). On each of the four graphs presented, radial error versus settling time is plotted. The upper left hand plot represents the case when it is assumed that the interceptor has to stay within a certain error for 3 seconds before the pilot-computer combination is able to tell that the error has been reduced to a point where the missile could be launched. All curves on this plot are for 85% settling time which means that the pilot was able to stay within a certain error for 3 seconds on 85% of the runs. Referring to the plot it is seen that if the initial error at lock-on is 30° then 14 seconds is required to settle the error to 10° (assumed required) and hold it for 3 seconds on 85% of the runs. If the initial error is 20° then 8 seconds is required to reduce the error to 10°. The lower left hand plot gives the results if the 3 seconds criteria is changed to 6 seconds. The two plots on the right hand side of Fig. 52 are for median settling times.

As stated previously the investigation of Part 2 of the settling time study (conversion from vectoring inaccuracy at detection to angular heading inaccuracy at lock-on) has only considered one speed condition - $V_F = V_{max}$ for 50,000 feet. Figure 53 gives a pictorial representation of this part of the settling time study. It is assumed that the interceptor is vectored on a pure collision course and continues on this pure collision course to lock-on (believed to be realistic for present operational conditions). The vectoring errors are normally distributed about this pure collision course (constant relative bearing line) with a 1 Sigma value of $\pm$ 3 n.mi. Courses are generated from this normal distribution and straight lines are flown to lock-on.

Some of the results under Part 2 of the settling time study are shown on Fig. 54. The initial angle off the targets nose (γ_o) is 60°. The coordinates of this figure are cumulative percentage of interceptions versus heading error in degrees at lock-on. The lock-on range is assumed to be 15 n.mi. While this lock-on range is optimistic, the results will serve to indicate the magnitude of heading errors expected. One point

is plotted on the $V_T/V_F = 1.0$ curve for purposes of illustration. For this point, 30% of the runs had heading errors of 23° or less. For the case of $V_T/V_F = 1$, a heading error of 30° or greater occurred on 47% of the runs. For the case of $V_T/V_F = 0.8$, 24% of the runs had heading errors in excess of 30°. To be consistent with the study requirements these curves will be extended to include 85%-90% region.

When the settling time study is completed (all appropriate values of Ro, heading errors, altitudes and speeds of interest and sufficient samples of each are included) it will be possible to combine the results of the two parts of the study program and predict settling times which are representative of the times one will encounter under tactical conditions. However, it will still be necessary to relate these settling times to realistic values of allowable launch errors. This is being supported by analysis at NAMTC, Pt. Mugu where miss distance simulations are underway to determine the launch errors which can be tolerated and still achieve and allowable miss. These two study efforts will be tied together so that realistic values representative of the total system settling time can be placed on the attack zone overlays.

Probability of Successful Arrival to Missile Launch

While the settling time study is not sufficiently complete to include results in the overall analysis, it is of importance to proceed, using approximations, in the computation of probability of success under tactical conditions. These computations will be modified at a later date when firm data is available.

Figure 55 gives a pictorial representation of the model used to determine probability of successful conversion to missile launch. In this model the interceptor is assumed to have been directed on a pure collision course. A normal distribution of AI radar lock-on probability is assumed with the 85% probability point consistent with the calculated values given previously. A normal distribution of vectoring inaccuracy (1 Sigma = $\pm$ 3 n.mi.) is assumed to occur along a line perpendicular to the pure collision course (relative bearing line). Courses are then generated through the resulting probability zone with the interceptor flying straight lines parallel to the correct pure collision course at the center of the distribution. At lock-on the interceptor is placed on a constant L/W =3g turn. This is the point in the analysis where actual settling time values are needed. Without these the results are optimistic since no reaction or evaluation time is charged to the pilot. The criteria for success are that the launching error can be reduced

to 10° before R_{min} is reached and that the gimbal angle required does not exceed that available during the lock-on to Rmin interval. The analysis was accomplished through programming on an IBM computer.

Figure 56 illustrates some of the results obtained to date. On this figure three approach aspects ($\tau_o = 0^{\circ}, 30^{\circ}$, and 60°) have been investigated. For these approach aspects three speed conditions have been investigated (V_T/V_F = 1.0, 0.8, 0.45) where V_F = Mach 2 at 30,000 feet. For each of the approach aspects the heading angle (Ψ) associated is given. The gimbal limits are the same as used previously; $\pm 41^{\circ}$ in azimuth, $+47^{\circ}$, -38° in elevation. The coordinates of the resulting group of curves are probability of successful arrival to missile launch in percent versus interceptor relative angle off the target's nose in degrees. The geometry is illustrated by the sketch at the bottom of this figure.

For $V_F = V_T$ = Mach 2.0 in the head-on case, the probability of successful arrival to missile launch is 46%. Under the same conditions except that initial position of interceptor relative to the target's nose is 30°, this probability is 52% but drops to zero when initial position relative to the target is 60°. At 60° the gimbal angle required exceeds the capability of the radar, therefore the target cannot be seen by the radar. Also the interceptor will be in a position, determined by the vectoring inaccuracy, from which he cannot convert to a successful attack since he has no speed advantage. Referring to the curve for V_T/V_F = 0.8 it is seen that the probability of success for the head-on case is 48%. When the interceptor approaches from 30° the probability is increased to 82%. Beyond 30° the probability of success drops off rapidly and is back down to 50% at 60° off the target's nose. The primary reason for the marked drop-off in probability is gimbal angle limitation. When the target's speed is reduced as illustrated on the curve representative of V_T/V_F = 0.45, the probability of success is 69% for $\tau_o = 0$, 86% for $\tau_o = 30^{\circ}$, and 85% for $\tau_o = 60^{\circ}$. This later curve represents what is perhaps an acceptable performance from the system when only the degrading effects of vectoring inaccuracy and gimbal angle limits are considered. Unfortunately, this corresponds to todays tactical situation. It is expected that the target of interest to this system will yield results lying in the V_T/V_F= 0.8 to 1.0 region. For these speed conditions it is obvious that the system is in difficulty except in very restricted zones (30° aspect for V_T/V_F = 0.8).

Figure 57 gives the results of the investigation to determine the effect of interceptor slow-down to V_{cruise} on probability of success. It

can be seen from the resulting curves that the probability of success is increased for the head-on case only. For other aspect angles the probability is reduced because of the increased penalty paid by lack of speed advantage.

Degradation Caused by Other Tactical Conditions

The preceding section detailed an investigation (preliminary) of the effects of two degrading factors on probability of successful attack; namely vectoring inaccuracy, and gimbal limits. The effects of several other degrading factors will be included in the final study results. These are as follows:

1. Effects of target maneuver - this is currently under investigation and will be reported in the near future.

2. Effects of weather and clutter - to date the effects of weather and clutter on the performance of the AI radar and missile seeker have not been included. However, much of these data are in hand and will be included in the final study. For example, Fig. 7 shows calculated low altitude performance of the AI radar. These curves will be verified by findings of tests conducted at NATC, Patuxent, and the results incorporated in the study. Figures 58, 59, and 60 show the effects of rain on the current AI radar detection performance. This information will be supplemented by work performed at NAMTC, Pt. Mugu.

3. Effects of countermeasures - basic work on this phase of the study has been reported in NRL Reports 4720, 4785, and 4949. The results of these basic studies will be applied to this study program.

4. Limits imposed by interceptor tactics including climb capability, endurance, and dead time. These factors are currently under investigation.

Remaining Study

Several of the items which are included under this category have been mentioned above. These, along with additional study effort, are listed below.

1. Extension of system settling time study to include all of the applicable conditions related to the current tactical situation. These include examination of courses starting at lock-on ranges related to

head-on case, larger initial errors at lock-on, additional altitude and speed conditions.

2. Extension of the settling time study to include F8U-3 performance.

3. Extraction of results from the settling study based upon allowable launch errors obtained from Pt. Mugu.

4. Inclusion of these results in the probability of success analysis.

5. Analysis of the effects of other degrading factors such as weather, clutter, countermeasures, and interceptor capabilities (climb, endurance and dead time).

6. Introduction of additional thrust to go from V_{cruise} to V_{max} in the problem areas studied.

7. Inclusion of effects of missile hydraulic limitations.

PHASE IV - SYSTEM PERFORMANCE UNDER EXPECTED TACTICAL CONDITIONS WITH ADDITION OF CURRENTLY PROPOSED IMPROVEMENTS

The study to date has indicated that improvement in subsystem performance is needed if successful missile launches at an acceptable probability level are to be achieved. For example, Fig. 56 shows that when the only degrading factors considered are those of vectoring inaccuracy and gimbal angle limits, the resulting probability of success is, in general, unacceptable. When additional degrading factors are considered, it is predictable that these probabilities will be reduced even further. It is thus very important to investigate regions of possible improvement to the subsystem elements in order that overall system tactical use capability can be improved. The following details some of the areas of improvement to AI radar performance which have been investigated to date.

AN/APQ-72 & 74 Improvements in Fair Weather

Fair weather improvements considered for the AN/APQ-72 & 74 radars in this study to date are automatic alarm, search volume optimization, bandwidth switching, bright display, improved receiver crystals and triangle vectoring. The latter item is not an improvement to the radar per se, but rather an improvement to the vectoring phase of the problem

which will result in better detection range performance of the AI radar, and improved capability in converting from a detection to successful missile launch. The aforementioned fair weather improvements are discussed in Westinghouse Air Arm Analytical Section Technical Memo No. 176 which is included as Appendix VII to this report. Detailed information is given in this Appendix. The pertinent factors are briefly reviewed in the following sections.

"Automatic Alarm" was considered as a possible improvement because the AN/APQ-50 radar has demonstrated capability of tracking signals that human operator could not see on the scope and thus could not detect. A method discussed in Appendix VII was investigated to determine whether or not this capability could be utilized to provide increased detection range performance by the sound of an alarm when the radar received signals too weak for an operator to see. It was concluded that such a scheme could lead to improved range performance in a clutter-free environment. No improvement can be expected in the presence of clutter due to the sounding of too many false alarms. Therefore "Automatic Alarm" has been ruled out as an improvement because various sources of clutter are ever present in the detection problem.

Search volume optimization has been studied because it is known that the volume of space looked at by the AI radar today is not ideal for target detection. The probability of detecting a target is the product of two probabilities.

(1) the probability that the target is in the area scanned

(2) the probability of detection of a target within the scanned area

To optimize the search area, the area scanned should include only the area of target uncertainty. The area scanned should not be too large because increased frame time and reduced hits per scan will cause a reduction in detection range. Appendix VII gives a more detailed discussion of this item. The area searched is a direct function of vectoring accuracy and therefore any scheme that results in smaller vectoring errors will permit a smaller search area. A smaller search area will result in longer detection ranges. The resulting improvement in AI radar detection performance from increased efficiency of volume search along with other improvements are shown on Fig. 61, which is a summation of results of the study detailed in Appendix VII. The contours of Fig. 61 are smoothed contours with data actually calculated at every 30°. This

smoothing is unimportant since the degree of improvement is the factor which will be used in later study effort. The coordinates of the graph of Fig. 61 are range in nautical miles versus aspect angle in degrees relative to the nose. The detection range contour labeled (2) in Fig. 61 shows the improvement gained by a reduction of the search area alone to 33.6° x 11.8°.

This search area is not optimum in terms of detection range performance alone. However, when a balance between range performance and mechanization difficulty is achieved this search area is approximately correct. Referring to curve (2) of Fig. 61 and using curve (1) as the reference point (head-on case) it is seen that approximately 10% improvement in AI detection range performance is achieved at the 85% probability level with this reduction in search area.

Bandwidth switching for the search mode was considered because a narrower IF bandwidth results in a decrease of noise power. Bandwidth reduction from the present 4 mcps to 1.12 mcps in search was studied and it is concluded that this will yield a net improvement of approximately 16% in detection range at the 85% probability level as shown in Fig. 61 (curve (4)).

A bright display is still under study, and while no definite conclusions can be drawn at this time concerning the actual amount of detection improvement to be realized, it is estimated that 12% increase in range capability will result if current trends in other areas such as maintenance, reliability, and complexity are continued. However, latent (but lost) in the basic equipment are many db of theoretical range performance. This loss is caused by a "high resistance" connection between the equipment and the operator. If some of the lost db can be recovered, the effects of bright display may well be much more pronounced than the estimated 12%.

Resulting Effects of Improvements on Attack Zones

Means of achieving improved system performance has been discussed in the preceding section. It is believed that all of the improvements analyzed in this section can go in during the time schedule of this equipment. In addition, it is believed that the vectoring inaccuracy in azimuth and range can be reduced from $\pm$ 3 n.mi. to $\pm$ 2 n.mi. Figures 62 and 63 show the effects, as a function of aspect angle, on system performance of including the improvements discussed.

Figure 62 shows the results of improving AI detection capability. In this figure it is assumed that the current AI detection performance is that given for V_F = 1940 ft/sec at 50,000 feet altitude (12-13 n.mi.). The current gimbal angle coverage is used ($\pm$ 41° az; +47°, -38° el.). The vectoring inaccuracy is that currently available (1 Sigma = 3 n.mi. in azimuth and range). The interceptor is at the same altitude as the target (co-altitude attack). The coordinates of the graph are probability of successful arrival to missile launch in percent versus range increment improvements in nautical miles with 0 representing the current range performance. Three speed conditions are examined (V_T/V_F = 1, 0.8, and 0.45 where V_F = 1940 ft/sec). Three approach aspect angles (τ_o) have been examined. Referring to the left hand side of Fig. 62, it is seen that for τ_o = 60° and for V_T/V_F = 1, no increase in system probability results as the range is increased upward to that previously predicted for the realizable improvements. This is due to the fact that detection range is not the limiting parameter for this approach aspect. The limiting parameters are jointly interceptor-pilot capability, and gimbal angle limits. For τ_o = 30° there is a marked improvement as range is increased. The probability of success increases from 52% for the current situation to approximately 72% for range increases predicted in the preceding section (6.8 n.mi.). If 8 n.mi. range improvement can be realized the probability of success would be increased to 73%. For the case of τ_o = 0° the improvement is more obvious. Here the primary limiting factor is AI detection range performance. As shown the range improvement predicted (6.8 n.mi.) would result in improved system probability from that currently available (46%) to 82%.

Referring next to the center of Fig. 62, the improvements resulting from detection increase for V_T/V_F = 0.8 are shown. Again, for τ_o = 60° there is no improvement in probability of success since the limiting parameters are other than detection range. For τ_o = 30° the probability of success increases from 82% for the current situation to 96% when the range is increased 8 n.mi. For τ_o = 0° the probability of success is increased from that currently available (48%) to 96% as the range is increased to 8 n.mi.

The right hand plot of Fig. 62 gives the results of range improvement on the case of V_T/V_F = 0.45. Here the most startling improvement occurs at τ_o =0°.

Figure 63 illustrates the effect of vectoring inaccuracy improvement on the probability of successful arrival to missile launch. As stated previously, it is hoped that the vectoring inaccuracy will be reduced

to ± 2 n.mi. for the 1 Sigma value in range and azimuth. With this in mind, it is important to investigate the resulting effects on system usefulness. The conditions now are the same as originally with the antenna gimbal limits again ± 41° in azimuth and +47°, -38° in elevation and the 85% probability of detection in the 12-13 n.mi. region. Referring to the left hand side of Fig. 63 it is seen that for V_T/V_F = 1 and V_F = 1940 ft/sec that for $\gamma_o = 60°$ there is no improvement in probability of success. As stated previously the limitations for this case are primarily interceptor-pilot capability and gimbal angle limits. For the cases $\gamma_o = 0°$ and 30° there is a large improvement. For $\gamma_o = 0°$, a 3 n.mi. vectoring inaccuracy results in a probability of success of 46%. This is improved to 60% when the inaccuracy is reduced to 2 n.mi. A corresponding improvement results for $\gamma_o = 30°$.

Referring to the center of Fig. 63, the case of V_T/V_F = 0.8 where V_F = 1940 ft/sec is shown. As for the previous situation, there is no improvement for the condition where $\gamma_o = 60°$. For $\gamma_o = 30°$, the probability of success is improved from that currently available (82%) to 91% when the vectoring inaccuracy is reduced to 2 n.mi. For the case of $\gamma_o = 0°$ the improvement is from that currently available (48%) to 71%. The right hand side of Fig. 63 illustrates the case of V_T/V_F = 0.45.

Figure 64 gives the results of analysis to date of increased gimbal angle limits. The basic situation is identical to those of the previous two figures. Assuming that currently a ± 40°(approximately) box is covered by antenna gimbals, the effect of improving these limits are shown. For example, when V_T/V_F = 1 and V_F = 1940 ft/sec (as shown on the left plot) and $\gamma_o = 60°$ going from ± 40° to ± 57° (believed to be approximately maximum which can be realized), a probability of success improvement of 19.5% results. If a full ± 60° could be realized the improvement would be 41%. For the case of $\gamma_o = 30°$ going from ± 40° to ± 57° results in 10% improvement. If a full ± 60° would be realized the improvement would be 16%. For the case of $\gamma_o = 0°$ there is no improvement when gimbal angle limits are varied for ± 40° to ± 60° because detection range and vectoring inaccuracy are the sensitive parameters in this region.

For the case of V_F = 1940 ft/sec and V_T/V_F = 0.8 there is no improvement for runs originating from $\gamma_o = 0$. The reason is the same as given above. The case of $\gamma_o = 60°$ has not been completed but the trend is evident. $\gamma_o = 30°$ has not been examined yet.

When the speed ratio is reduced to V_T/V_F = 0.45 there is no improvement for the cases of $\gamma_o = 0$ and $\gamma_o = 30°$. The case of $\gamma_o = 60°$ has not been included, but it is predictable that it will not be influenced by gimbal angle changes.

It is believed that all of the improvement investigated regarding AI radar range performance can be incorporated in the system in the time interval available for system development. Referring back to Fig. 61, it is seen that each of these improvements separately buys very little. All of the improvements listed on this figure are needed. It is hoped that the improvement in vectoring inaccuracy discussed above will materialize during this same time interval but actual system performance estimates should not be predicated upon this hope. The gimbal angle coverage increase investigated is certainly desirable. However, the extent of this increase must be balanced with state of the art capability and other system requirements such as increase dish size to get additional range needed especially in the forward hemisphere.

Figure 65 gives the resulting probability of success curves for the case where the 85% probability of detection has been increased to 19 n.mi. and the gimbal angle coverage increased to $\pm$ 57° (estimated maximum possible). The method of presentation is the same as that of Fig. 56. The lower curve, shown with a dashed line, was taken from Fig. 56 and is for the case of 85% probability of detection occurring at 12-13 n.mi. and gimbal angle coverage of $\pm$ 41° azimuth and +47°, -38° in elevation. Comparing this to the solid curve resulting from the new detection ranges and gimbal limits for $V_T/V_F = 1$, a major improvement is apparent. For example, when $\gamma_o = 0$ the improvement is from that currently available (46%) to 75% probability of success. When $\gamma_o = 30°$ the improvement is from that currently available (52%) to 89% probability of success. When $\gamma_o = 60°$ the improvement is from that currently available (0%) to 8% probability of success. The other two curves on Fig. 65 are approximations. Since the 19 n.mi. was achieved for $V_T/V_F = 1$ head-on, it is obvious that this range will be larger for $V_T/V_F = 0.8$ and 0.45. The error in range is approximately 10% for the case of $V_T/V_F = 0.45$. However, its effect is minor in nature, with the most pronounced error occurring for $\gamma_o = 0$. The trends are obvious from examination of Fig. 65.

It is obvious from examination of the preceding figure that it is desirable to increase system performance above that available with all of the improvement investigated to this point. It is important to remember that to this point only a few of the degrading factors present in the tactical situation have been examined. When more of these are considered, the overall system performance will be reduced even further. This is especially true for head-on, high-speed attacks. Figures 66 through 68 detail the effects on the improved system probability of success of varying some of the sensitive parameters. It can be shown, very simply, that for the high-speed intercept and forward hemisphere cases, (particularly in a cone of $\pm$ 45° off target's nose), range is the most

sensitive parameter. Figure 66 shows the results of increasing range on probability of successful arrival to missile launch when the basic system is one which contains all of the preceding improvements ($R_{85\%}$ = 19 n.mi. antenna gimbals ± 57°). Referring to the left side of Fig. 66 (V_T/V_F = 1, V_F = 1940 ft/sec) it is seen that for γ_0 = 0 and 30° the effect of increasing the 19 n.mi. range resulting from the discussed improvements to 27 n.mi. is approximately 20%. It is important to recognize that this is a region where increased performance is very important. For the case of V_T/V_F = 0.8 the improvement of adding 8 additional miles detection range varies from 15% (from a probability of 84% to a probability of 99%) for γ_0 = 0 to 8% (from a probability of 92% to a probability of 100%) for γ_0 = 30°. When V_T/V_F = 0.45 there is essentially no improvement resulting from increased AI detection range.

Figure 67 shows the results of improving vectoring accuracy when the detection angle is 19 n.mi. and the gimbal limits are ± 57° (maximum believed available). For the high-speed case V_T/V_F = 1 and γ_0 = 0 the improvement resulting from reducing the vectoring inaccuracy to 2 n.mi. is 12% (from a probability of 76% to a probability of 88%). When γ_0 = 30° the improvement is 5% (from a probability of 89% to a probability of 94%). When γ_0 = 60° the improvement is 3% (from a probability of 8% to a probability of 11%). When the target speed is reduced to V_T/V_F = 0.8 the improvement varies from 9% (from a probability of 84% to a probability of 93%) for γ_0 = 0 to 3% (from a probability of 91% to a probability of 94%) when γ_0 = 30°. When V_T/V_F = 0.45 there is essentially no improvement resulting from improving vectoring inaccuracy.

Figure 68 gives the results of increasing the gimbal angle coverage. The region of interest is that of increasing the gimbal angle coverage from ± 57° up. The curves on this figure show the effects of going from 57° to 67°. However, these results are academic in nature since gimbal angles much in excess of 57° will be extremely difficult to achieve.

Remaining Study Elements

The preceding sections have shown, in preliminary form, the results of incorporating certain improvements upon system probability of success. In addition, the sensitivity of the resulting system performance to variation of several parameters has been demonstrated. All of the improvement study findings thus far presented have assumed a clear weather, countermeasures-free environment. Additional "improvement" items intended to increase system performance under clutter, weather, and countermeasure

conditions will be investigated. Some of the "improvements" to be evaluated are as follows:

(1) Effects of polarization switching in a foul weather environment: some of the study effort on this parameter has been completed. Figures 69 through 71 give the theoretical range performance resulting from the use of circular polarization. Comparing these results with the performance curves given previously for vertical polarization, it is concluded that circular polarization would be superior only under high altitude conditions with rain at the target. Practical realization of circular polarization is technically difficult. It is relatively easy to produce circular polarization under laboratory conditions. However, to propagate circularly polarized waves through the waveguide, antenna, and radome complex is quite difficult. It is believed that no advantage can currently be realized by going to circular polarization.

(2) Investigation of system performance improvement through the use of a larger AI radar antenna: the calculation of range performance improvement resulting from the use of a large dish is straightforward and can be incorporated in this study program in the near future. However, in the two systems of interest, a balance between dish size and gimbal angle coverage based upon optimum overall system performance and mechanical feasibility should be reached before design effort toward the end antenna system is finalized. The achievement of this balance is based upon relatively complex analysis and cannot be predicted at this point in the study program.

(3) Situation display to enhance overall system performance: it is believed that a situation display, similar to the Triangle System, is essential if the desired ultimate use capability of the system is to be approached. While the availability of the Triangle System for use in the time era of interest is questionable at this date, every effort should be exerted toward the development of this or a more optimum situation display.

(4) Antijam features for the AI radar: the use of backbias techniques, automatic homing on jamming, broadbanding, jittered PRF, high-altitude feed, improved AFC and nonsaturating AGC are under investigation. The results of NRL analyses of these features have been reported to the Bureau of Aeronautics (NRL Report 4949).

(5) Antijam features for the Sparrow III seeker: NRL has investigated AJ features for this seeker. The results of this investigation

have been reported to BUAER (NRL Report 4720) and will be included in this study.

(6) Relocation of CW injection plumbing: several schemes have been proposed for relocating the CW injection components. These schemes are, in effect, an effort to allow the use of a larger dish concurrently with larger gimbal angle coverage. These schemes will be studied and the resulting effects upon system performance included.

PHASE V - STUDY TO DETERMINE AND ASSESS REALIZABLE IMPROVEMENTS

As this study continues, NRL and Westinghouse Analytical Section will investigate the feasibility (both technical and time-wise) of incorporating those items which result in important improvement of system performance. Action recommendations will then be made to the Bureau. This is a continuing process and will not necessarily wait for the presentation of a final report. To date, the following proposed actions can be recommended as a result of the preliminary analysis which has been presented.

(1) The incorporation of optimized search area, bright display (enhanced operator environment), and bandwidth switching can be achieved during the time available for the development of this system. Collectively they represent a major improvement in system performance.

(2) While the exact availability date for a situation display such as the Triangle System is not predictable at the present time, concerted effort should be directed towards its development. The incorporation of such a display will represent a major improvement in overall system performance capability.

(3) While the analysis to date has indicated that additional range above that realized from Items (1) and (2) above is very desirable, the incorporation of such items as a larger dish should be delayed until sufficient analysis is completed either under this study program or by the fire control contractor (preferably by the contractor) to allow arrival at an optimum balance between dish size and gimbal angle coverage.

PHASE VI - STUDY OF IR TIE-IN FOR AI FIRE CONTROL SYSTEMS

Up to this point in the study program, the analysis method has been first to investigate the performance resulting from the use of

available equipments and then to indicate possible improvements. To date the undefined state of the IR capability in the AI fire control system is such that this procedure cannot be followed. In lieu of this method the Navy study will first establish deficient areas of the primary fire control system. An investigation will then be made to determine if such secondary items as IR can help in these deficient areas.

PHASE VII - REPEAT STUDY PHASE I-VI FOR SPARROW III WITH IR SEEKER

To date, NRL has insufficient information on the Sparrow III IR seeker. This phase is a contractual item of the study program. Analysis will commence as soon as information is supplied by the contractor.

PHASE VIII - REPEAT STUDY PHASE I-VI FOR SIDEWINDER

This phase is a contractual item of the study program. A memorandum (Sidewinder I and IA Description, Westinghouse Technical Memo 220) has been prepared. This memorandum is currently being reviewed for accuracy by NOTS. In addition, NOTS is supplying estimates on the performance of Sidewinder IC. As soon as these data are in hand, analysis will commence.

IMPORTANT SYSTEM REQUIREMENTS NOT CONTRACTUALLY COVERED

As any study program progresses, many new areas of importance are brought to light. This is true of the current study. The contract as it now exists will not cover many of these items. Among these are:

a. Breakaway and illumination requirements.

b. Interceptor recovery (doctrine) after launch.

c. Sparrow II head for Sparrow III missile.

In addition, certain phases of the study should be extended.

a. Additional approach angles about the target should be studied in the snap-up phase. This study will only consider the head-on case with and without vectoring inaccuracy.

b. More detailed study of items where data is not currently available should be considered.

The Naval Research Laboratory strongly recommends that the current study program be extended to cover the above items or that a new study program be initiated to cover them.

CONCLUSIONS AND RECOMMENDATIONS

Introduction

The data presented in this study summary is only partially complete. There are many areas where much work remains to be done before all phases of the study can be tied together in an exact fashion. Even though the study is only partially complete, inferences can be drawn which will be useful in

(1) formulation of the basic system configuration

(2) development of a situation display

(3) formulation of tactical doctrine guide lines

(4) revision of operational concept for usage of secondary missile seekers

(5) establishing applicability of secondary AI fire control systems, such as IR, to the deficient areas of the primary AI fire control system

(6) establishing lowest acceptable limits defining a useful Navy system

(7) starting immediate action on Items 1-6 above in order that useful attainment of operational requirement objectives can be achieved

As is evident from the material presented in this report, and from conferences with BUAER and participating contractors, findings of the current Navy Study Program are vital to the management of a tactically useful F4H-1 and F6U-3 Weapon System. Factors contributing importantly to the validity of this study include its technical direction by the Navy and its use of Navy approved inputs.

Detailed Recommendations and Conclusions

1. The preliminary results of the study indicate that for co-altitude high-speed attacks under "ideal" conditions with $V_T/V_P = 1$ the interceptor

must start its approach from forward of 70° off the target's nose if it is to get into a position to launch a missile.

2. It can be easily shown from the study results that when additional time is added for systems preparation (currently estimated as 27 seconds total) most of this forward 70° zone will be eliminated. In the case of $V_T/V_F = 1$ for attacks occurring at 30,000 and 50,000 feet, approximately a 10° zone (from 60° to 70° off the target's nose) would remain.

3. When V_T/V_F is reduced to 0.8, attacks can originate from around the clock for ideal conditions. However, when the total system settling time is considered, it can be shown that approximately the forward 60° is eliminated from the usable attack zone.

4. When the interceptor is slowed down to V_{cruise} additional time is available for forward hemisphere attack. However, when the target is a high speed one, the approach aspect is even more restricted. For example, when the target is flying at Mach 2.0 at 30,000 feet the interceptor must approach from forward of 40° off its nose.

5. When the target speed is Mach 2.0 and the interceptor speed is Mach 2.0 or V_{max} and pull-up attacks are employed under ideal conditions, successful engagements are restricted to 7,000 feet altitude differential for targets flying at 30,000 feet altitude and higher. No capability exists for targets flying at 65,000 feet altitude.

6. When the target speed is reduced to Mach 0.9 and the interceptor is flying at Mach 2.0 or V_{max}, successful engagements are restricted to altitude differentials of 17,000 feet or less for targets flying at 50,000 feet altitude or higher. When the target altitude is 30,000 feet or less, successful pull-up engagements can occur from sea level to co-altitude.

7. For the cases where the interceptor is slowed down to Mach 0.9 at the start of pull-up, no capability exists for pull-up attacks against either a Mach 2.0 or Mach 0.9 target at altitudes of 65,000 feet or higher.

8. For the pull-up attacks at 50,000 feet or less, a greater altitude differential capability exists when the interceptor is slowed down to Mach 0.9 than for the cases where V_F = Mach 2.0. With the target flying at 50,000 feet (V_T = Mach 2.0), this altitude differential is 10,000 feet.

9. The probability of successful attack when limited by some of the degrading factors such as gimbal angle and vectoring inaccuracies have been in part investigated. When the interceptor is flying at Mach 2.0 in a co-altitude attack and $V_T/V_F = 1$, the probability of successful arrival to missile launch for the nose-on case is 46% and for 30° off the target's nose is 52%. At 60° off the target's nose, the probability goes to zero because of the interceptor's inability to get into position and because of gimbal angle limits.

10. When V_T/V_F is reduced to 0.8 and the engagement occurs at co-altitude, the probability of successful arrival to missile launch is increased to 48% for nose-on, to 82% at 30° off the target's nose, and to 50% at 60° off the target's nose.

11. When the interceptor is slowed down to Mach 0.9 the head-on probability of success goes up but falls off rapidly as the aspect angle from which the engagement starts moves toward the beam. For the case of $V_T/V_F = 1.7$, the probability of successful arrival to missile launch is 71% for nose-on and zero at 30° off the target's nose.

12. Although many of the degrading factors which will be encountered under realistic tactical conditions have not been included in the study to date the results can be inferred. It is predictable that the indicated probability of success values given in Items 9 thru 11 will be reduced markedly.

13. Thus far in the study program the resulting improvement from the use of a bright display, bandwidth switching, and optimized search area have been investigated. The result is an increase in AI detection range from 12.7 n.mi. to 19 n.mi. for a Mach 2.0 interceptor attacking a Mach 2.0 target head-on.

14. The improvement factor given in this report for a bright display is an engineering estimate of that which could result by brightening the current presentation. There are many other "lost" db's which could be recovered through a program of system analysis having as its objective an optimization of the pilot's environment. This program would include the possibility of such items as an NRL type bright display, situation display and general cockpit optimization.

15. When the improvement factors of Item 13 are included and when the antenna gimbal limits are increased to $\pm$ 57° in azimuth and elevation

there is a marked improvement in probability of successful arrival to missile launch. For example, when V_F = Mach 2.0 and V_T/V_F = 1.0 there is an improvement in probability of success of approximately 30% for head-on attacks resulting in a value of 75%.

16. It is believed that the improvements of Item 13 could be incorporated in the system during the time era of interest. The Laboratory would strongly recommend that the Bureau direct the contractors to proceed toward this end.

17. The results of the study program infer that a situation display is a necessity if a tactically useful system is to result. This situation display is important because it can provide data from which the pilot can start an intercept prior to AI radar detection, (Enclosure 1).

18. A preliminary study of the sensitivity of probability of success to AI radar range and gimbal angle limits has been made. The result is that in some areas, especially nose-on, the probability of success is very sensitive to range. In other areas, especially 60° off the nose of the target aft, the probability of success is very sensitive to gimbal angle limits. It is obvious that these features are interdependent. Thus a compromise in mechanization (for example large dish versus gimbal angle coverage) which can result in an approach to maximum overall use capability must be reached before design effort can be specified, (Enclosure 3).

19. The findings of this study could and should be applied in the system design effort being conducted by the various contractors. To this end, the study results and details should be made available to the principal contractors. The impact of this is directly related to the importance of defining the long lead time system elements.

20. The undefined developmental state of IR for the fire control system is such that no current system can be realistically analyzed in terms of its potential contribution to overall system performance. Test information taken under controlled conditions would provide information needed by this study program in order to investigate system deficiencies to determine the applicability of secondary systems, (Enclosure 2).

21. Analysis of system performance resulting from use of the Sparrow III IR Seeker will begin as soon as sufficient data is supplied by the contractor. To date the information available to NRL is not adequate to warrant an analysis.

22. Results of incorporation of the Sidewinder missile in the system will be investigated. Forthcoming study effort will be initially based upon estimates of missile performance, since design of the Sidewinder Ic will not be frozen during the remaining study interval.

23. In order to continue on an uninterrupted basis, it is important at this time for the Bureau of Aeronautics to program an extension to contract NOas 57-663d under the administrative cognizance of the Bureau of Aeronautics AV-3122 and under the technical direction of the Equipment Research Branch, Code 5360, NRL. As detailed in the report, there are important areas where timely coverage will not occur in the current study program. In addition there are problem areas which should be investigated but because of the limited scope of the current program will not be investigated.

24. The Laboratory will forward to the Bureau, under separate cover, a recommended extended study program.

REFERENCES

1. "Flight Test of AN/APQ-50 Radar Set - Phase I, Report 1," NATC, Electronic Test Division, Project TED No. PTREL 43045, 9 Feb 56

2. "Quarterly Engineering Report No.1, The Navy Air-to-Air Missile Study," Westinghouse Electric Corporation, 14 Aug 57, Confidential

3. "Analytical Section Technical Memorandum 25, Revised Radar Range Report," Westinghouse Electric Corporation, 6 Feb 56, Confidential

4. "Report of Conference at Naval Research Laboratory, Develop Input Data and Requirements for Weapon Systems Technical Analysis," NRL 5360-462/57, 11 Jun 57, Secret

ACKNOWLEDGEMENTS

The data presented in this report represents the results, to date, of the Navy's Air-to-Air Missile Study Program. The analytical results including those from which the figures were derived are the results of the computational work underway at Westinghouse Air Arm Division. The authors would like to thank the Analytical Section of this division for their major contribution to this report, and in particular would like to thank Messers R. Clanton, J. Buchan, C. Baida, and B. Van Hook. In addition the authors would like to thank P. Waterman, L. Gilchrist, and W. Hodgson for their assistance in the preparation of this report.

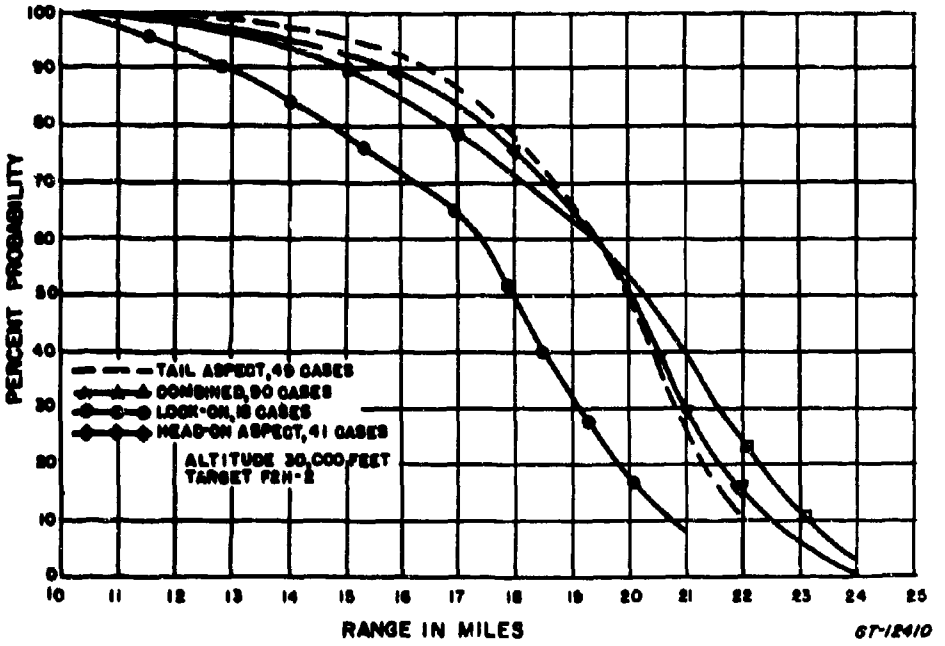

Figure 1 Cumulative Probability of Detection and Lock-On, AN/APQ-50 Radar Set No. 20

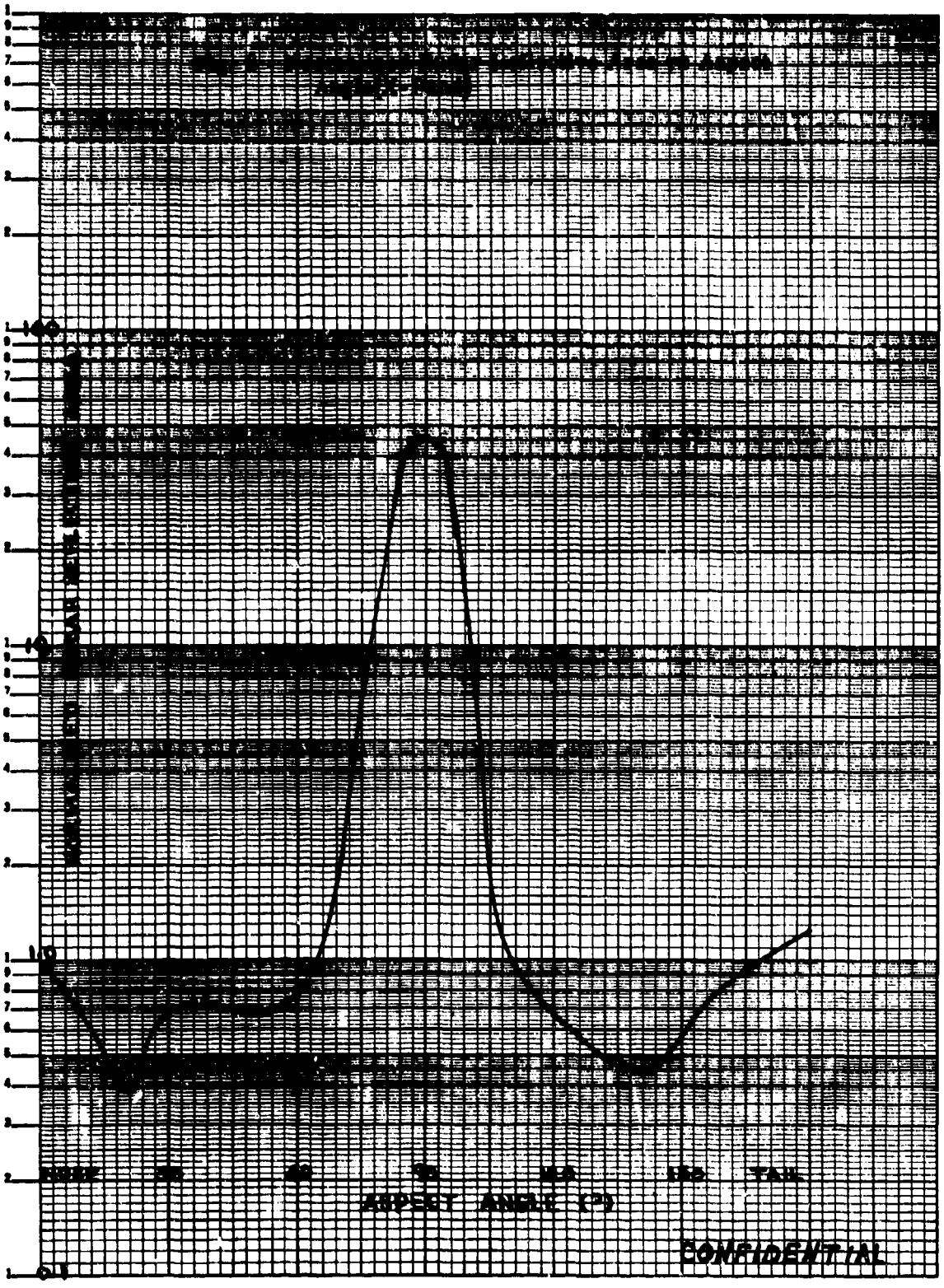
ASPECT ANGLE (P)
CONFIDENTIAL

TABLE 2

LIST OF HORIZONTAL ATTACK STUDY CASES

CASE	ALTITUDE (feet)	VELOCITY OF INTERCEPTOR (feet/sec)	TARGET SPEED (feet/sec)	TARGET TO INTERCEPTOR SPEED RATIO
50HH	50,000	1940	1940	1.0
50HM	50,000	1940	1552	0.8
50HL	50,000	1940	873	0.45
30HH	30,000	1897	1897	1.0
30HM	30,000	1897	1518	0.8
30HL	30,000	1897	854	0.45
1HH	1,000	1189	1189	1.0
1HM	1,000	1189	951	0.8
1HL	1,000	1189	533	0.45
50LH	50,000	873	1940	
50LM	50,000	873	1552	
50LL	50,000	873	873	
30LH	30,000	894	1897	
30LM	30,000	894	1518	
30LL	30,000	894	854	
1LH	1,000	556	1189	
1LM	1,000	556	951	
1LL	1,000	556	533	

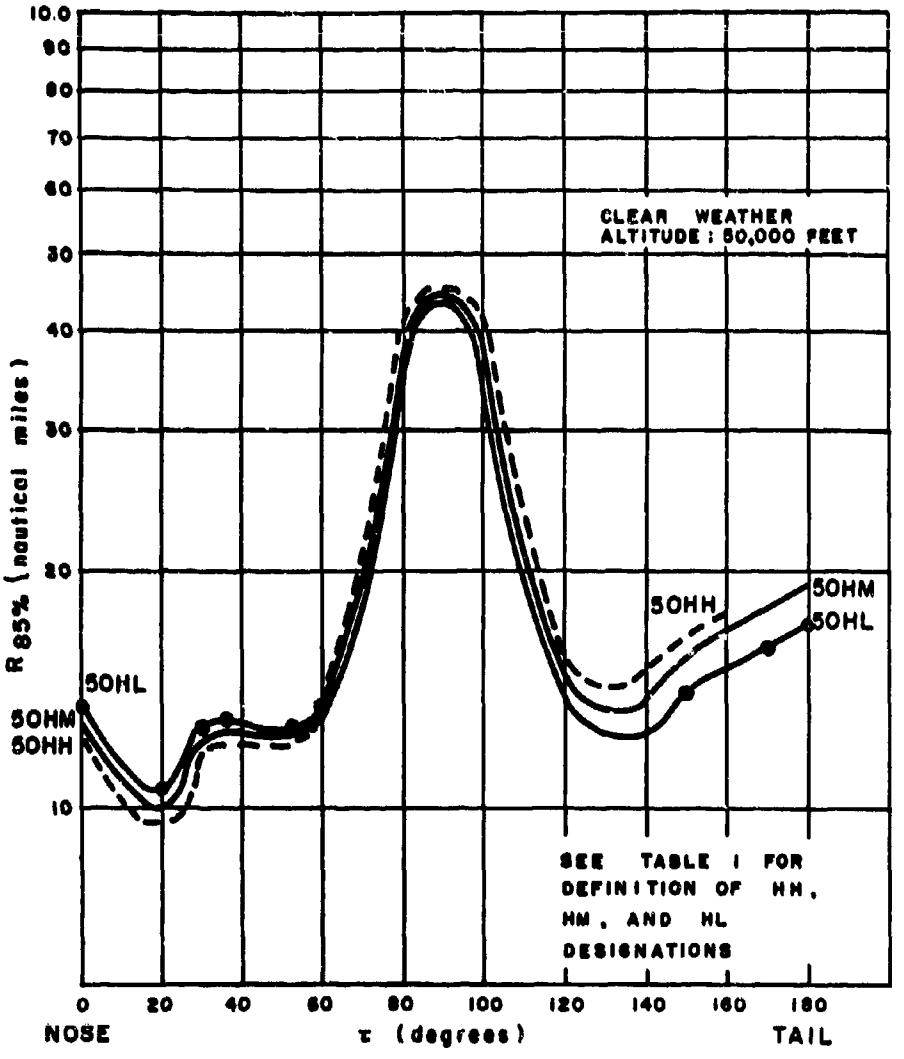

Figure 3. 85% Cumulative Probability Detection Range AN/APQ-72 and AN/APQ-74 versus Angle-off Target (Part 1)

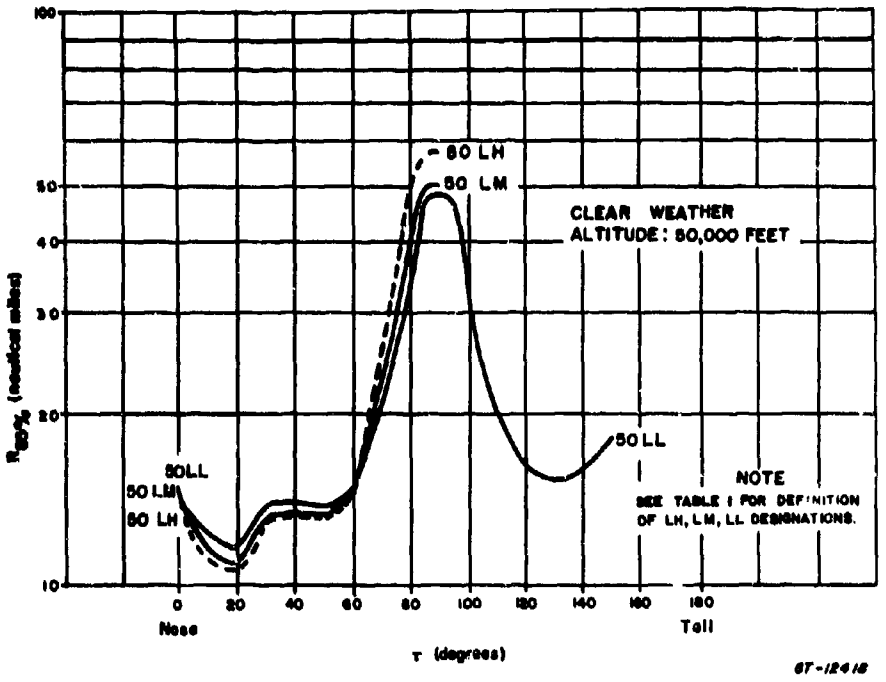

Figure 4. 85% Cumulative Probability Detection Range, AN/APQ-72 and AN/APQ-74 versus Angle-off Target (Part II)

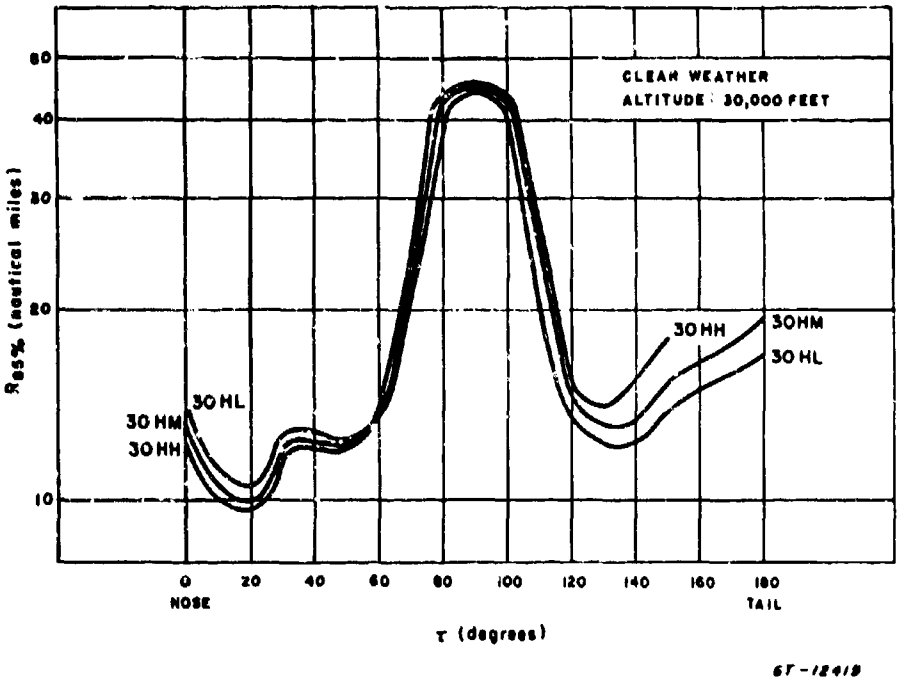

Figure 5. 85% Cumulative Probability Detection Range AN/APQ-72 and AN/APQ-74 versus Angle-off Target (Part III)

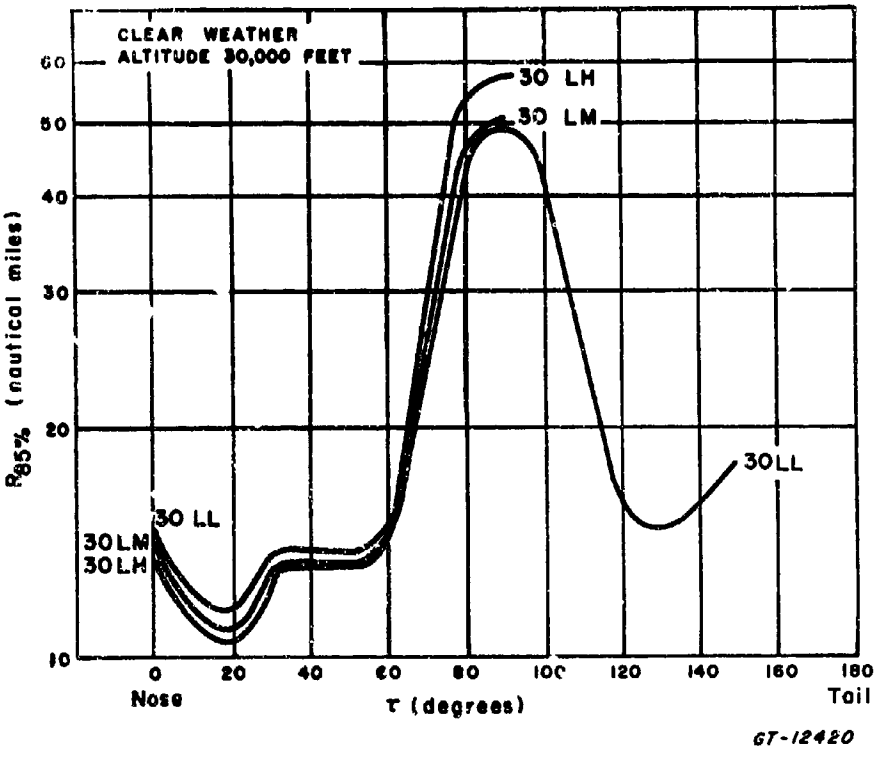

Figure 6. 85% Cumulative Probability Detection Range AN/APQ-72 and AN/APQ-74 versus Angle-off Target (Part IV)

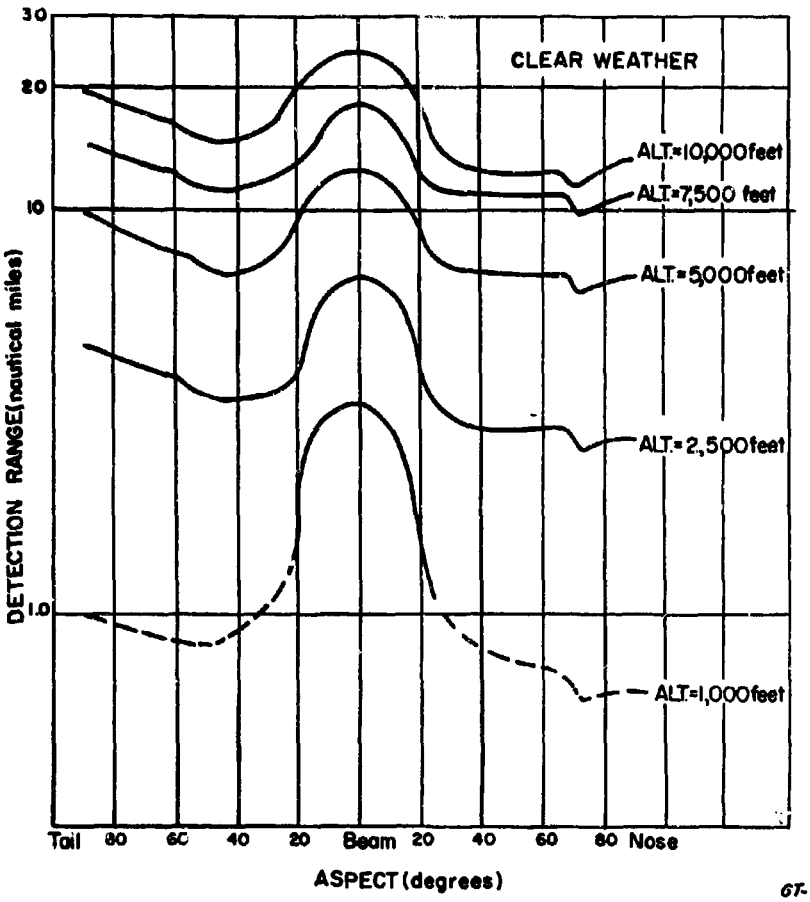

Figure 7. Low Altitude Detection Range - Vertical Polarization (Theoretical)

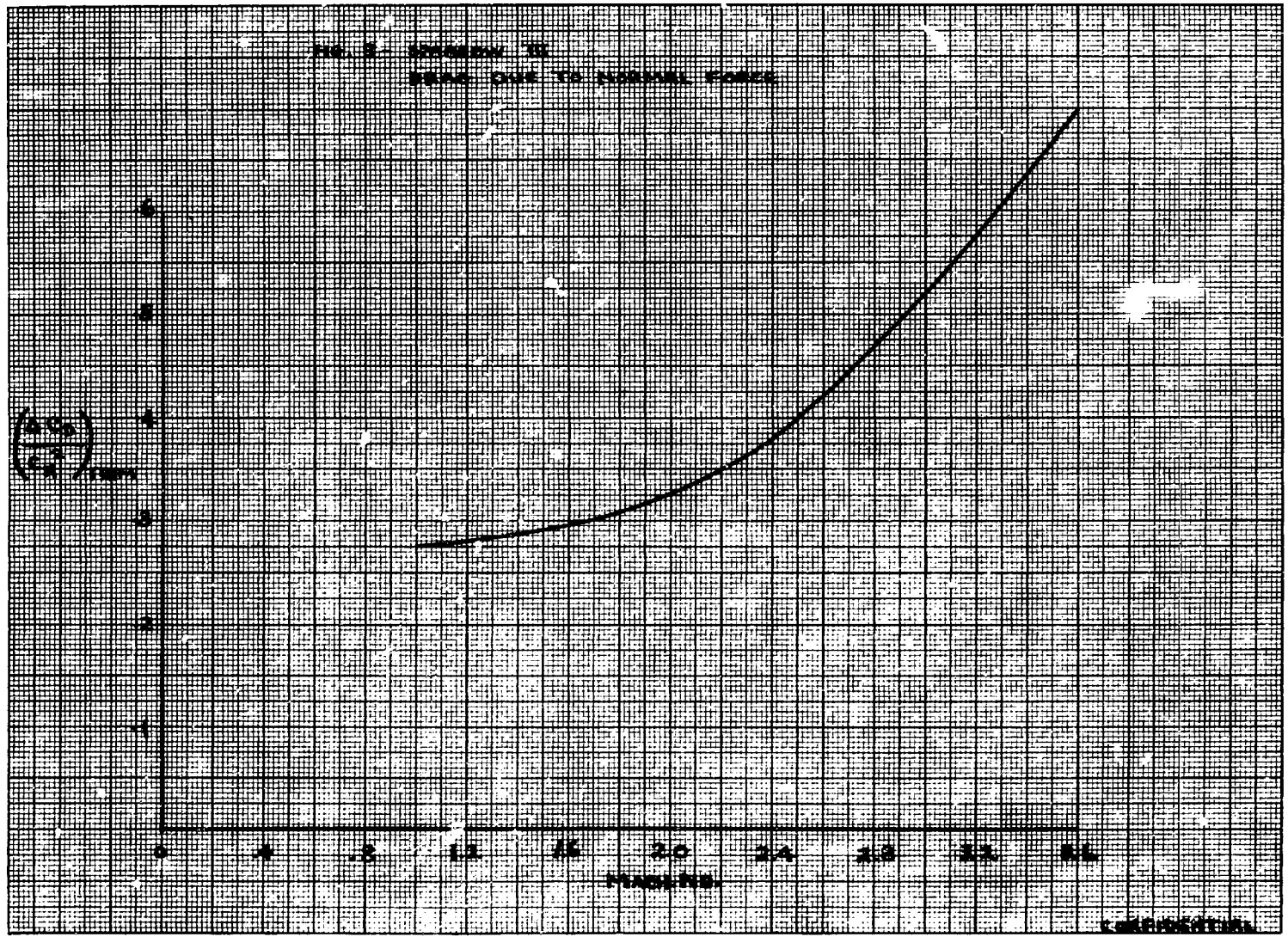
FIG. 2 - INCREASE IN
DRAG DUE TO NORMAL FORCE
$\left(\frac{\Delta C_D}{C_N^2}\right)_{max}$
6
8
4
2
-4
0
.4
.8
1.2
1.6
2.0
2.4
2.8
3.2
3.6
MACH NO.

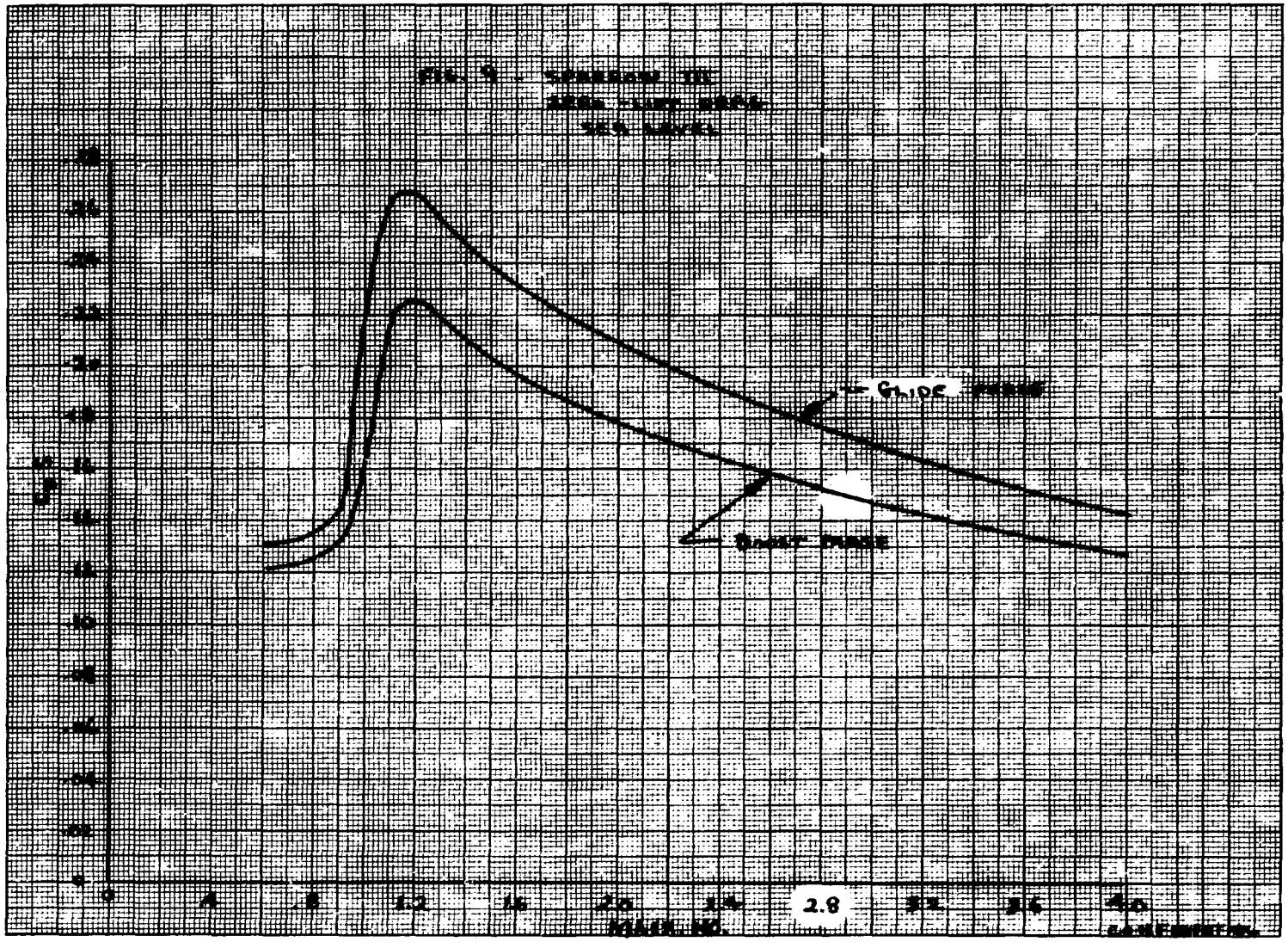
2.8

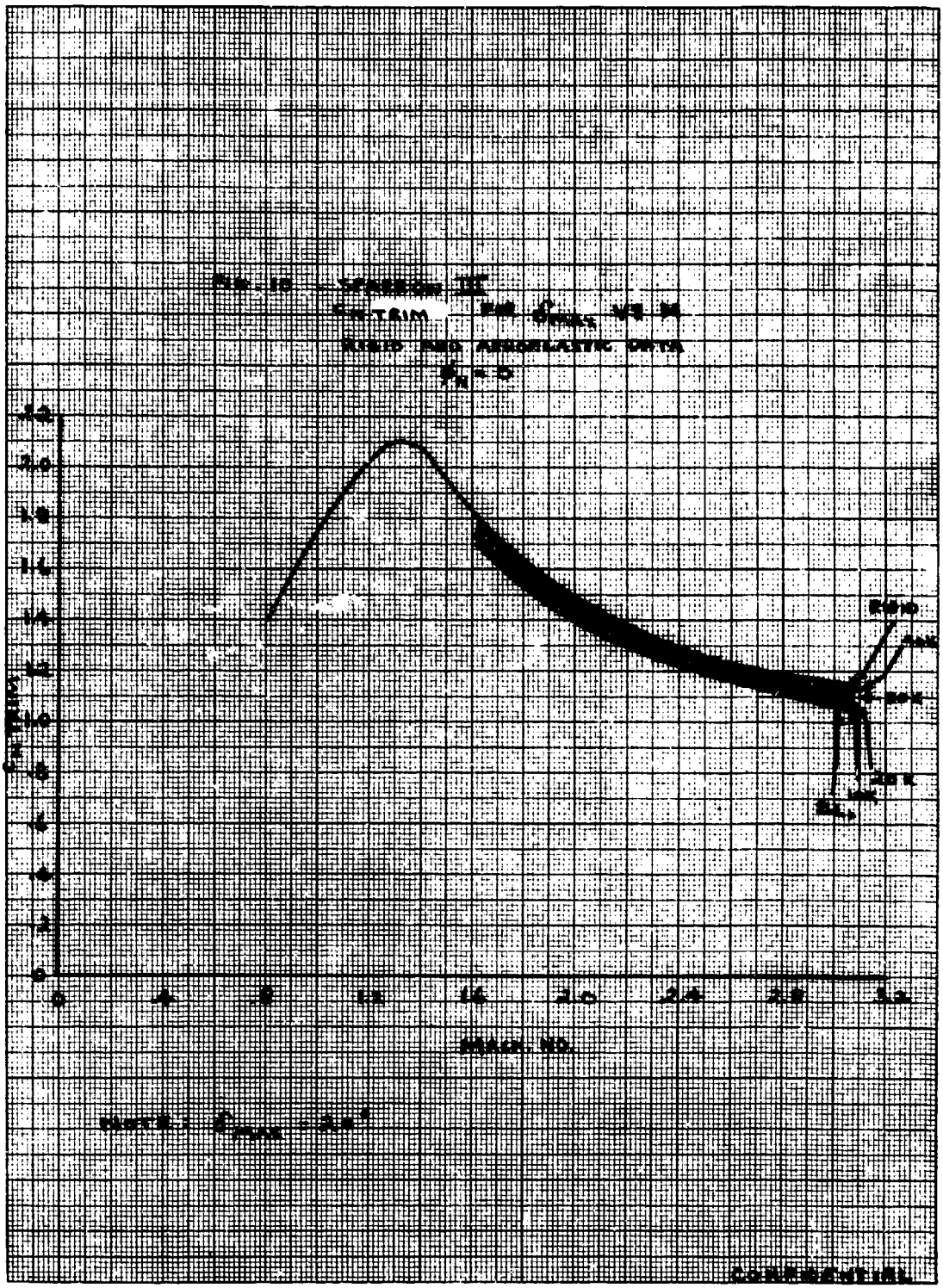
RIGID
AERO
ELASTIC
MACH NO.

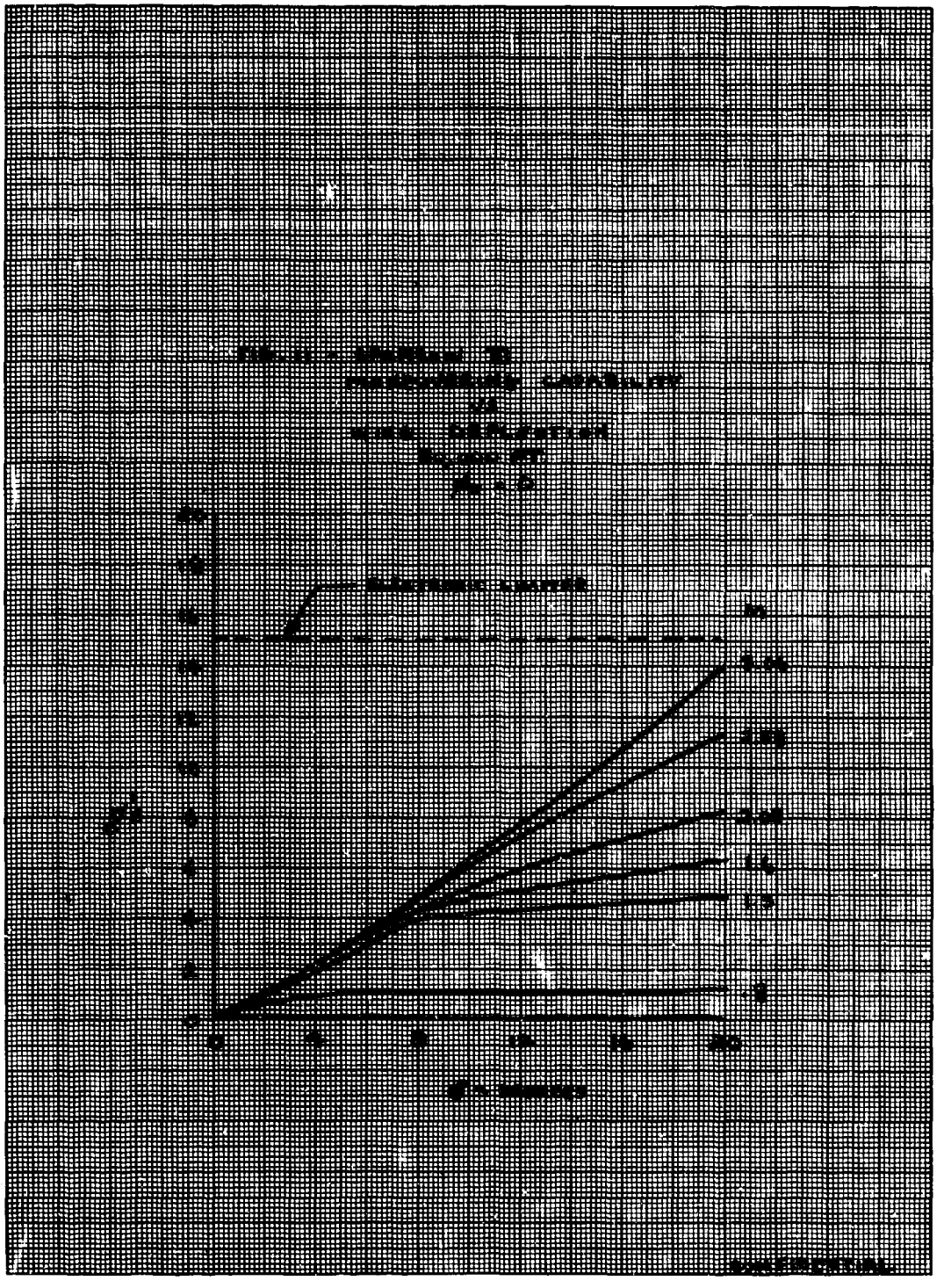

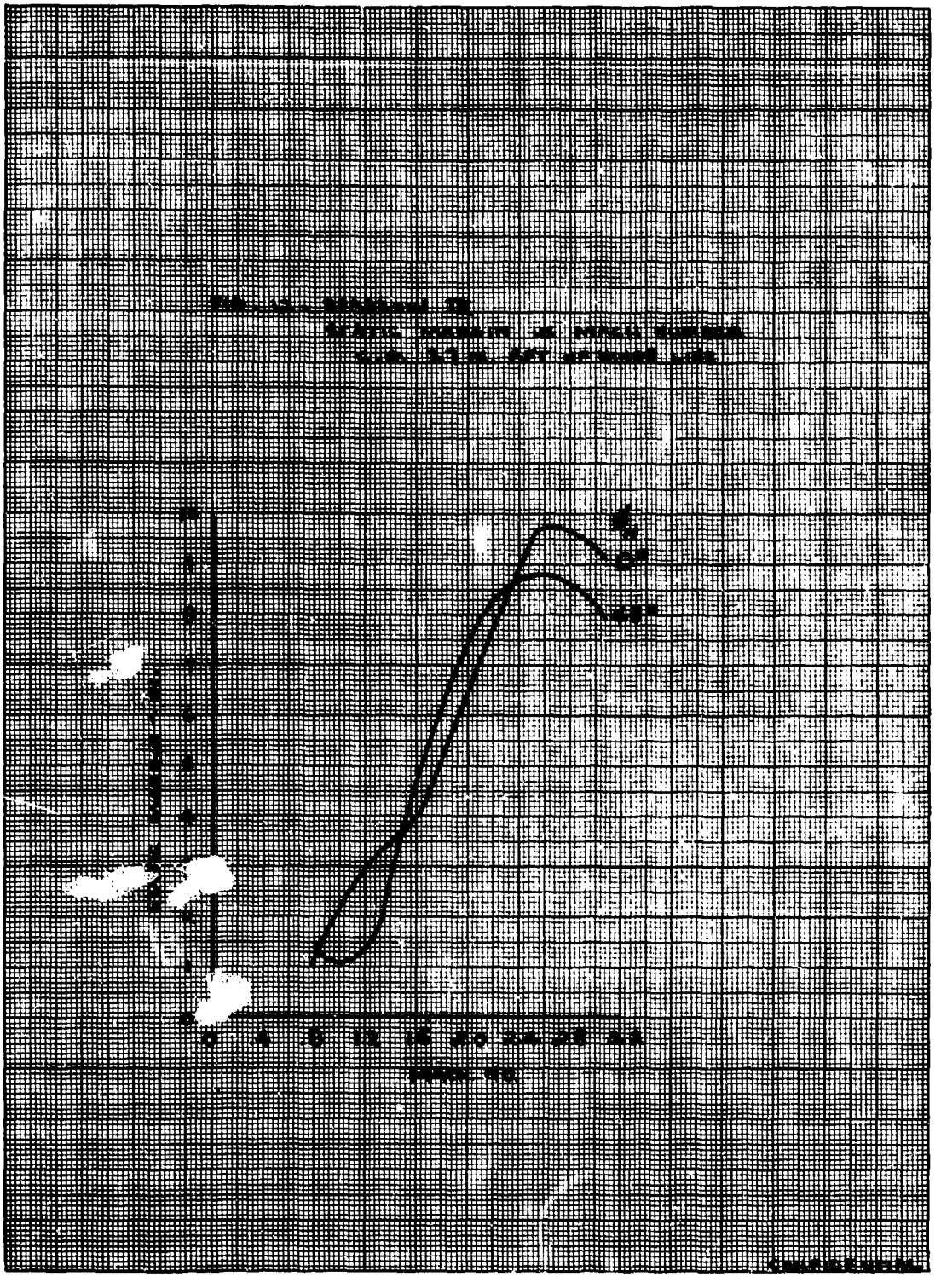

FIG. 15 - SPARROW III AERODELASTIC DATA
NORMAL FORCE COEFFICIENT SLOPES VS MACH NUMBER

$C_{N_\alpha} = (\partial C_N / \partial \alpha)_{\alpha = \delta = 0^\circ}$

$\phi_N = 0$

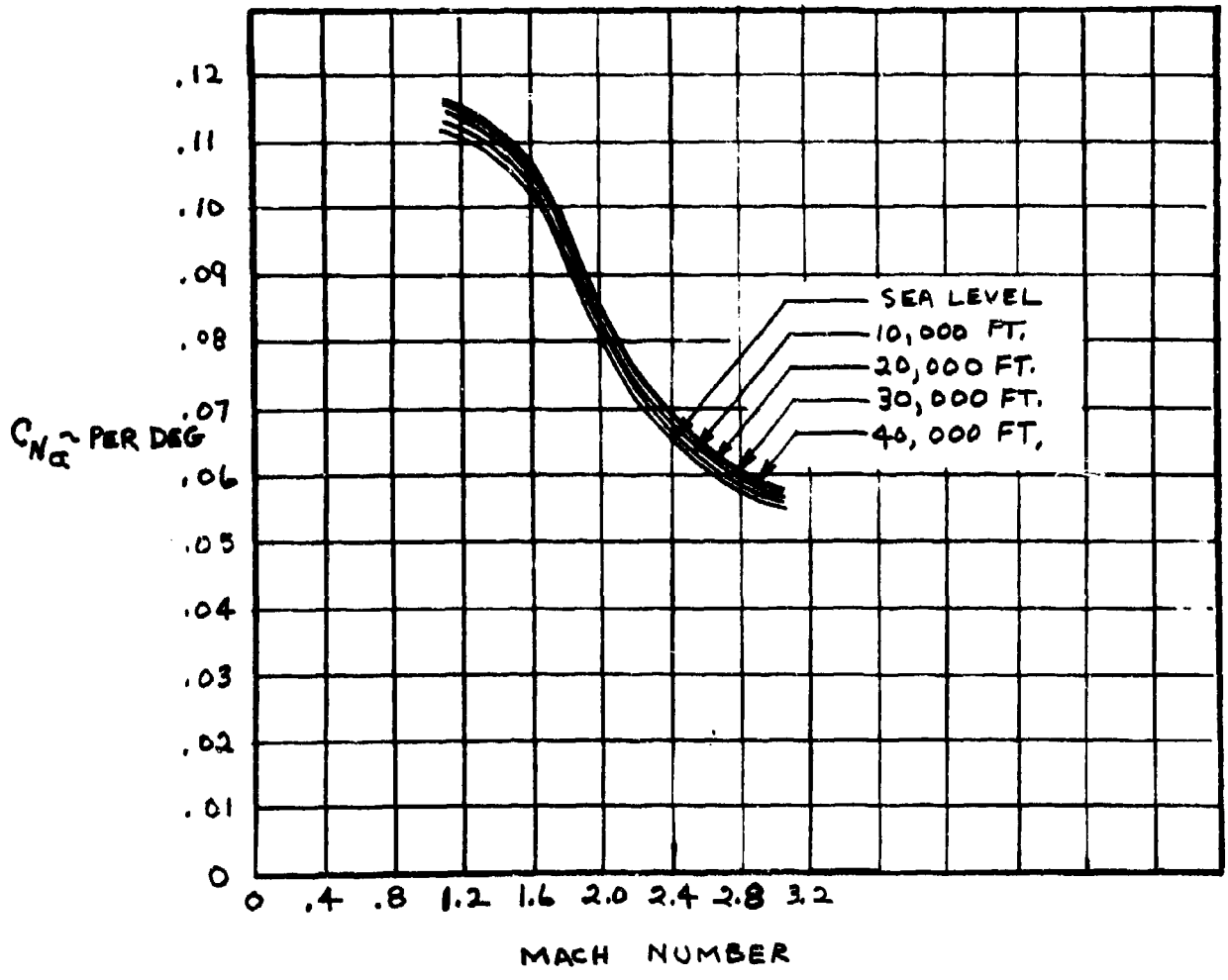

CONFIDENTIAL

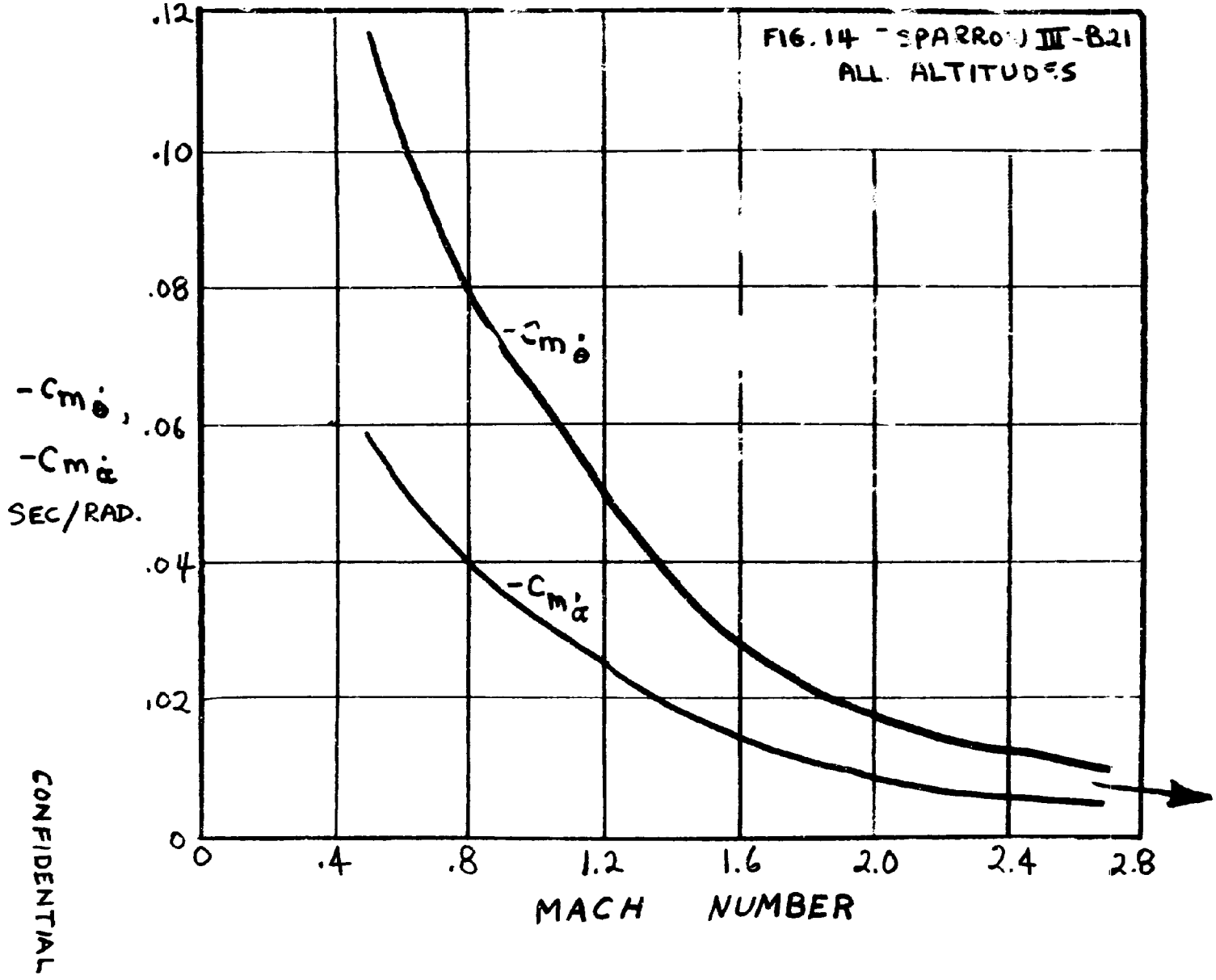

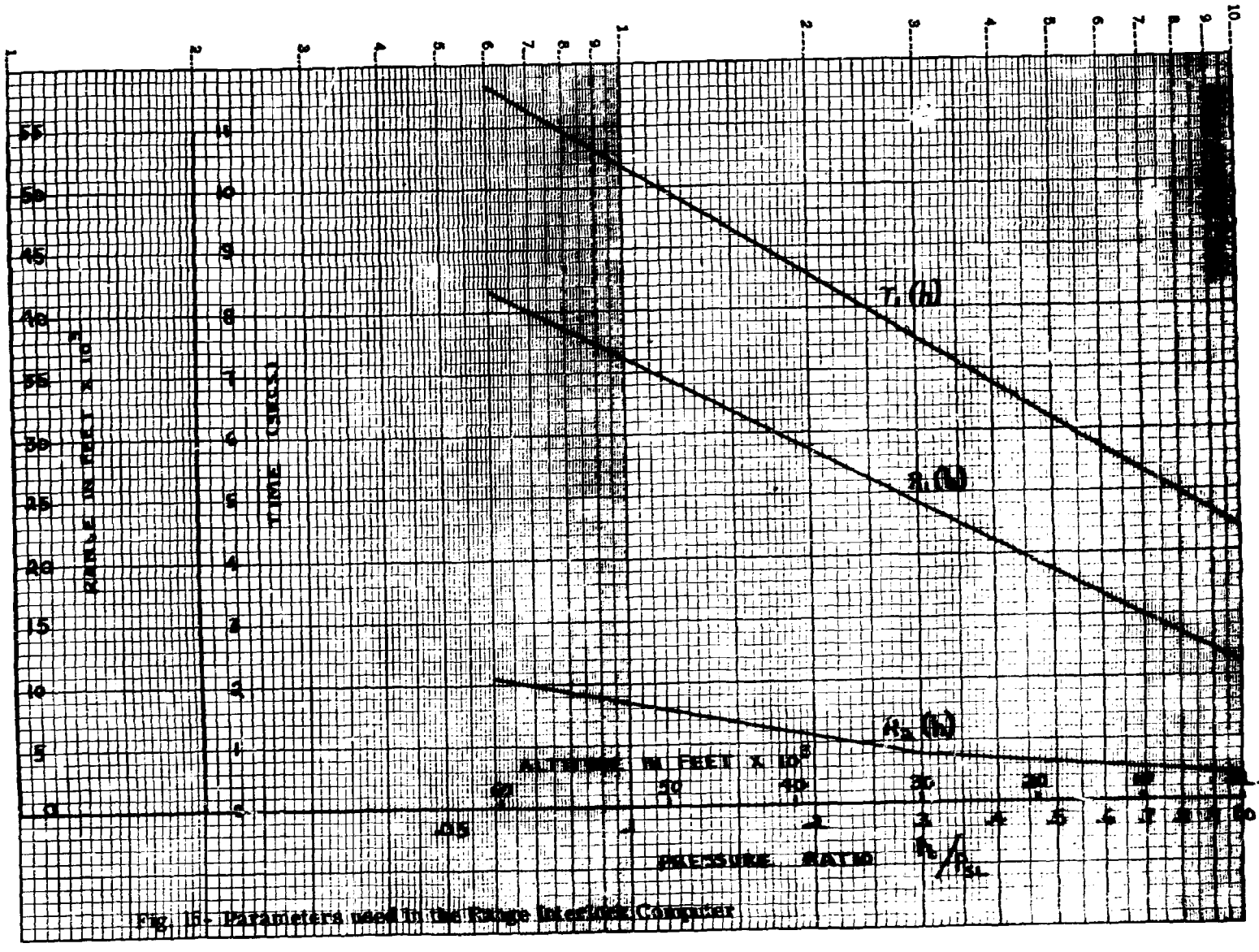

Fig. 15- Parameters used in the Range Interface Computer

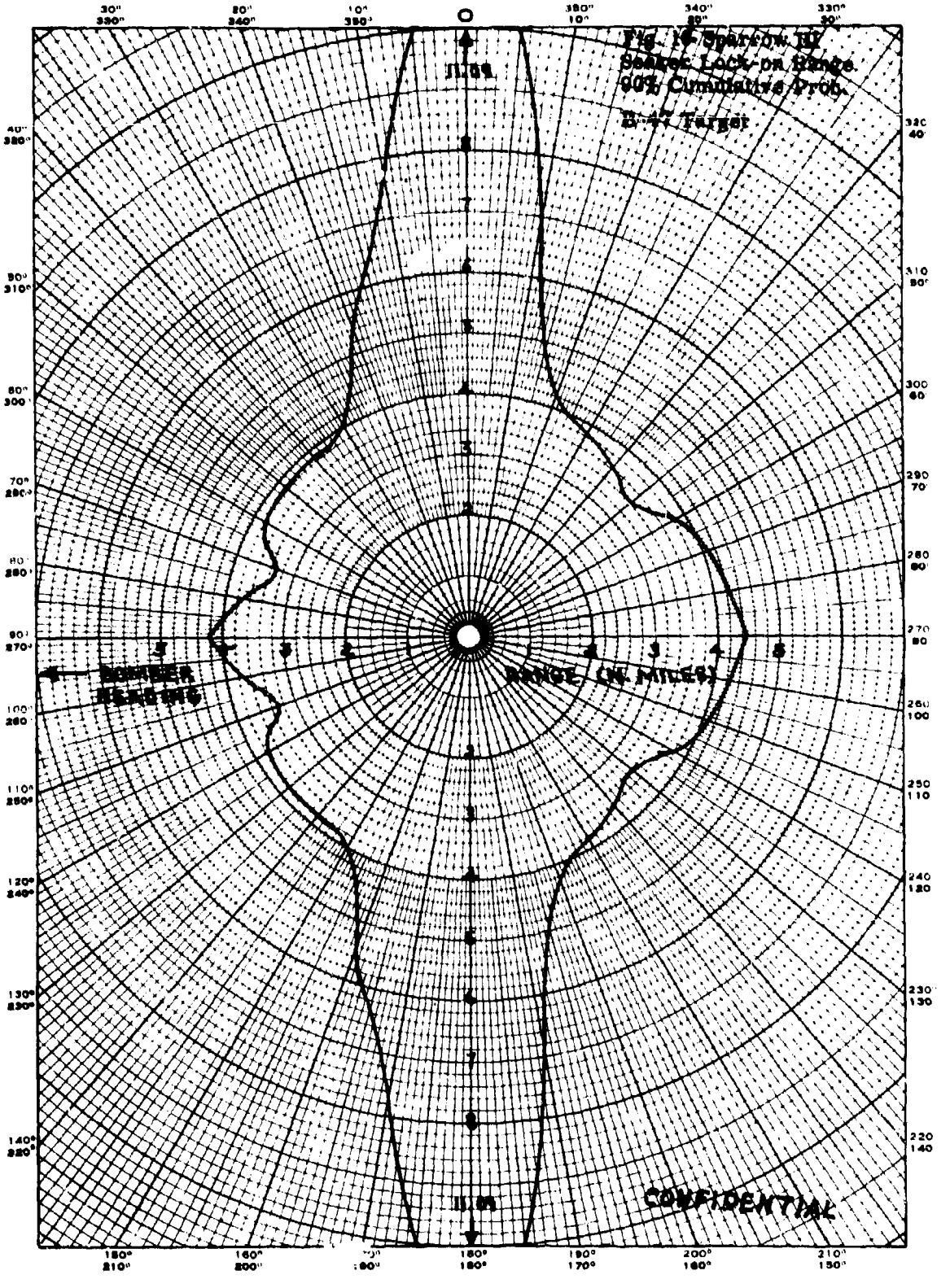
Fig. 16 Sparrow III
Search Lock-on Range
90% Cumulative Prob.
B-47 Target
O
11.5 n
11.0 n
BOMBER HEADING
RANGE (IN MILES)
CONFIDENTIAL

LATERAL Distance FROM TARGET PATH IN FEET x 10³
DISTANCE FROM DETECTION IN FEET x 10³

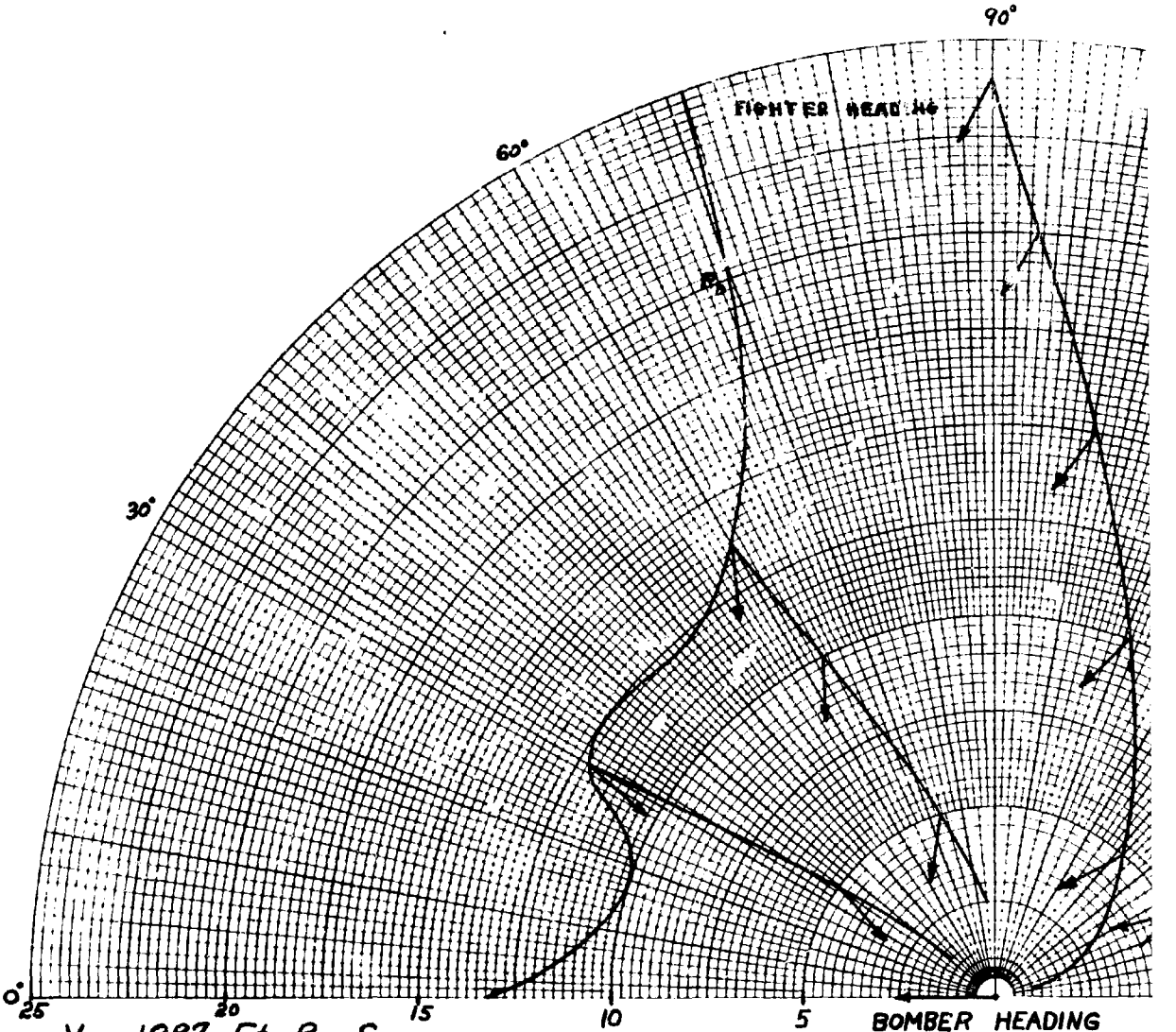

V_F = 1897 Ft. Per Sec.
V_T = 1518 Ft. Per Sec.
ALTITUDE = 30,000 Ft.
⟶ = FIGHTER HEADING

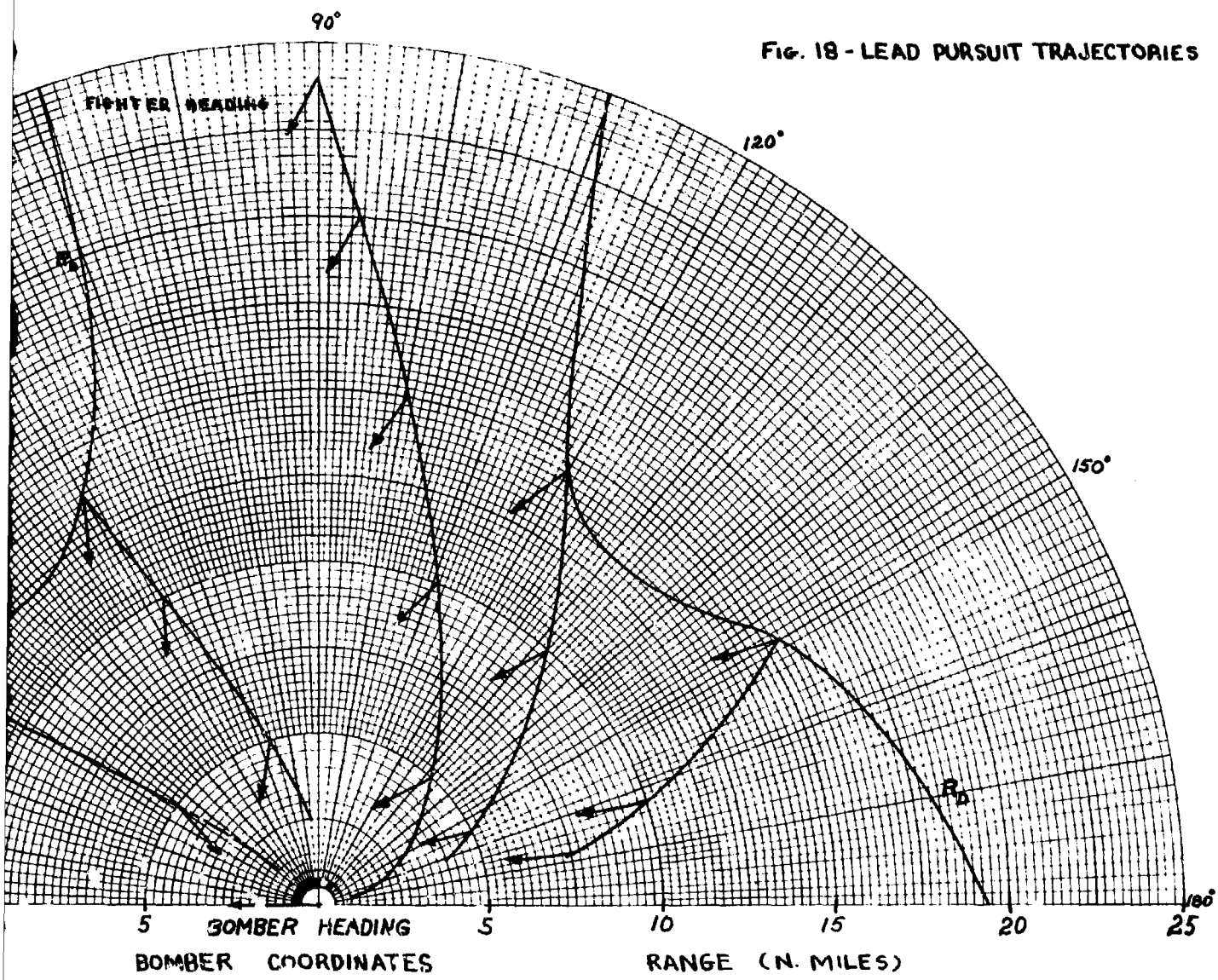

FIG. 18 - LEAD PURSUIT TRAJECTORIES

CONFIDENTIAL

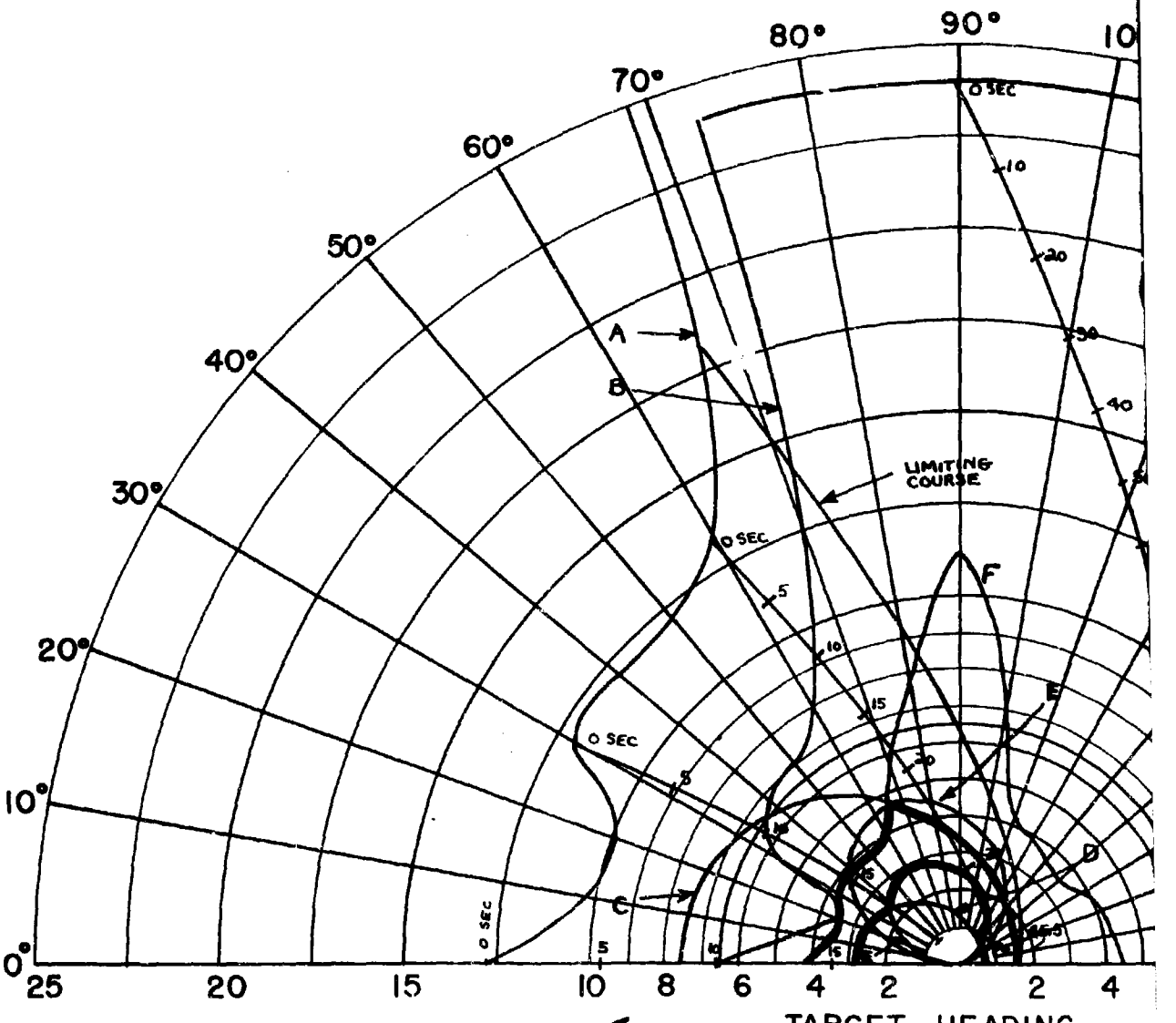

TARGET HEADING

V_F = 1897 FT/SEC (F-4H-1)
V_T = 1897 FT/SEC
ALTITUDE = 30,000 FT.

A - 85% DETECTION RANGE
B - LOCK-ON RANGE (10 SEC. LOCK
C - SPARROW III MAX. AERODYNAM
D - SPARROW III MIN. AERODYNAM
E - CONSTANT LOAD FACTOR LOC
F - 90% SPARROW III SEEKER LC
G - 6.5 N.M. INTERLOCK

FIG. 19 - CO-ALTITUDE LEAD PURSUIT ATTACK ZONE OVERLAYS.

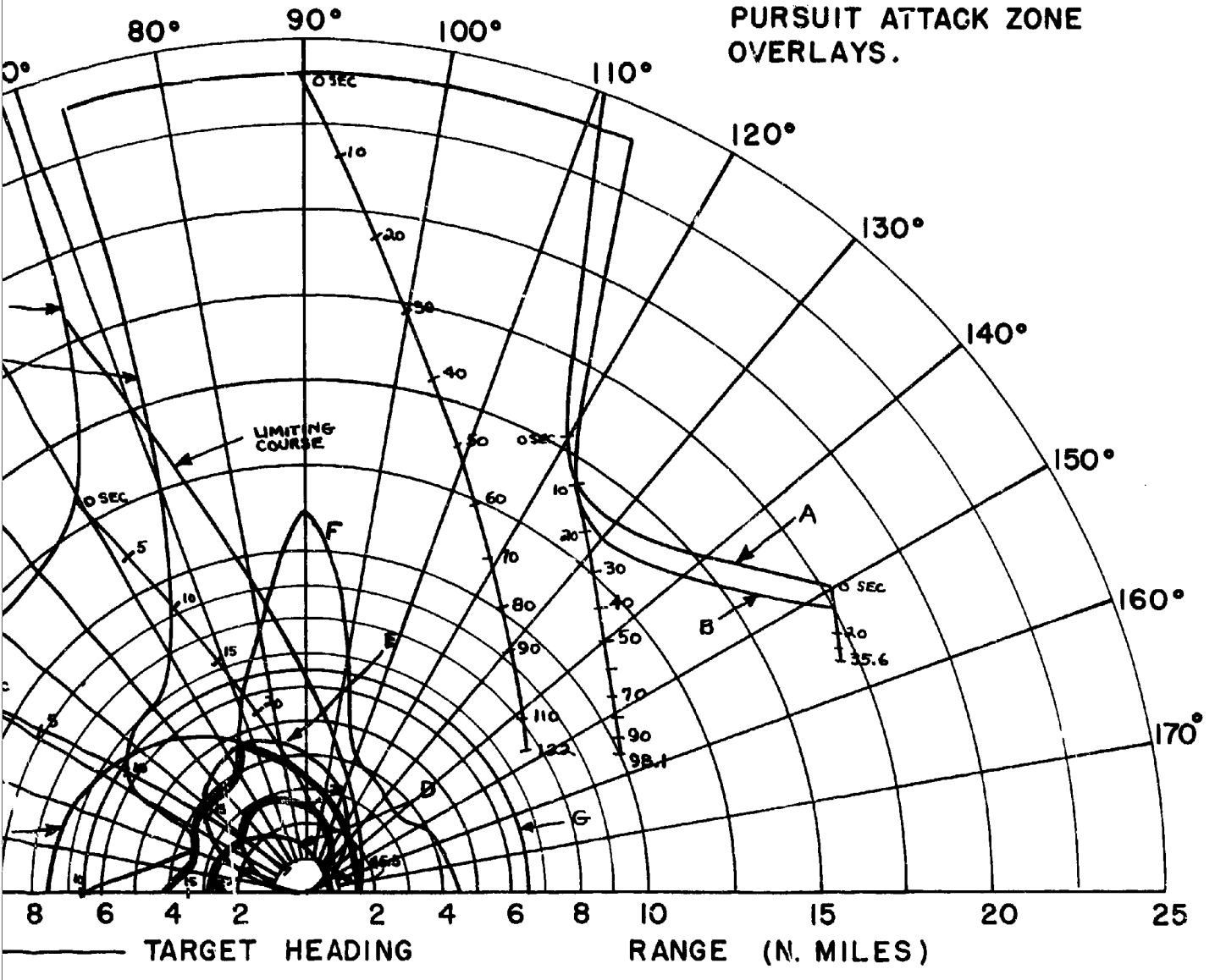

85% DETECTION RANGE
LOCK-ON RANGE (10 SEC. LOCK-ON TIME)
SPARROW III MAX. AERODYNAMIC RANGE
SPARROW III MIN. AERODYNAMIC RANGE
CONSTANT LOAD FACTOR LOCUS ($N_Z = 2,3$)
90% SPARROW III SEEKER LOCK-ON RANGE
6.5 N.M. INTERLOCK

CONFIDENTIAL

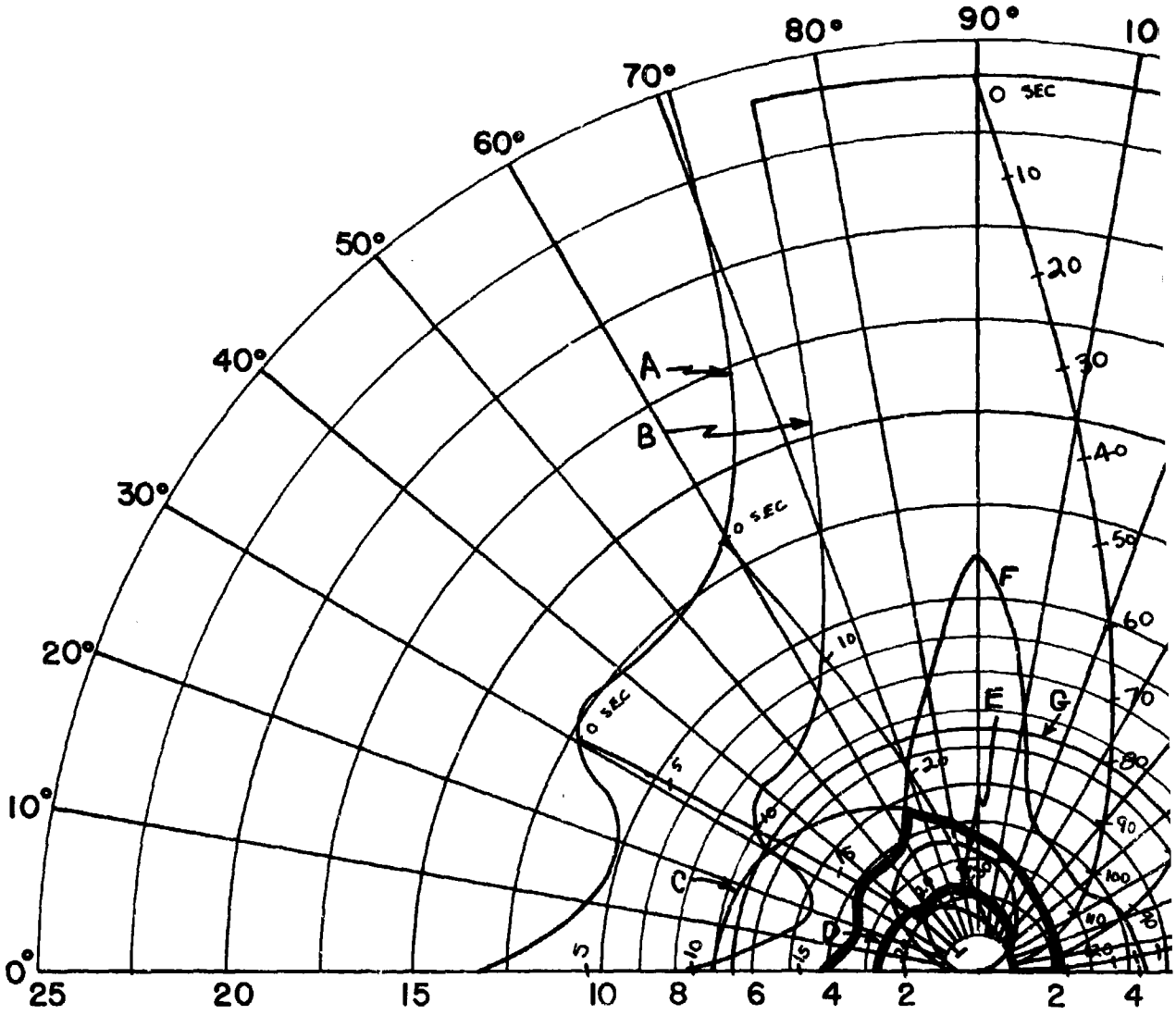

V_F = 1897 FT/SEC (F4H-1)
V_T = 1518 FT/SEC
ALTITUDE = 30,000 FT.

A - 85% DETECTION RANGE
B - LOCK-ON RANGE (10 SEC. LOCK
C - SPARROW III MAX. AERODYNAM
D - SPARROW III MIN. AERODYNAM
E - CONSTANT LOAD FACTOR LO(
F - 90% SPARROW III SEEKER L(
G - 6.5 N.M. INTERLOCK

FIG. 20 - CO-ALTITUDE LEAD PURSUIT ATTACK ZONE OVERLAYS.

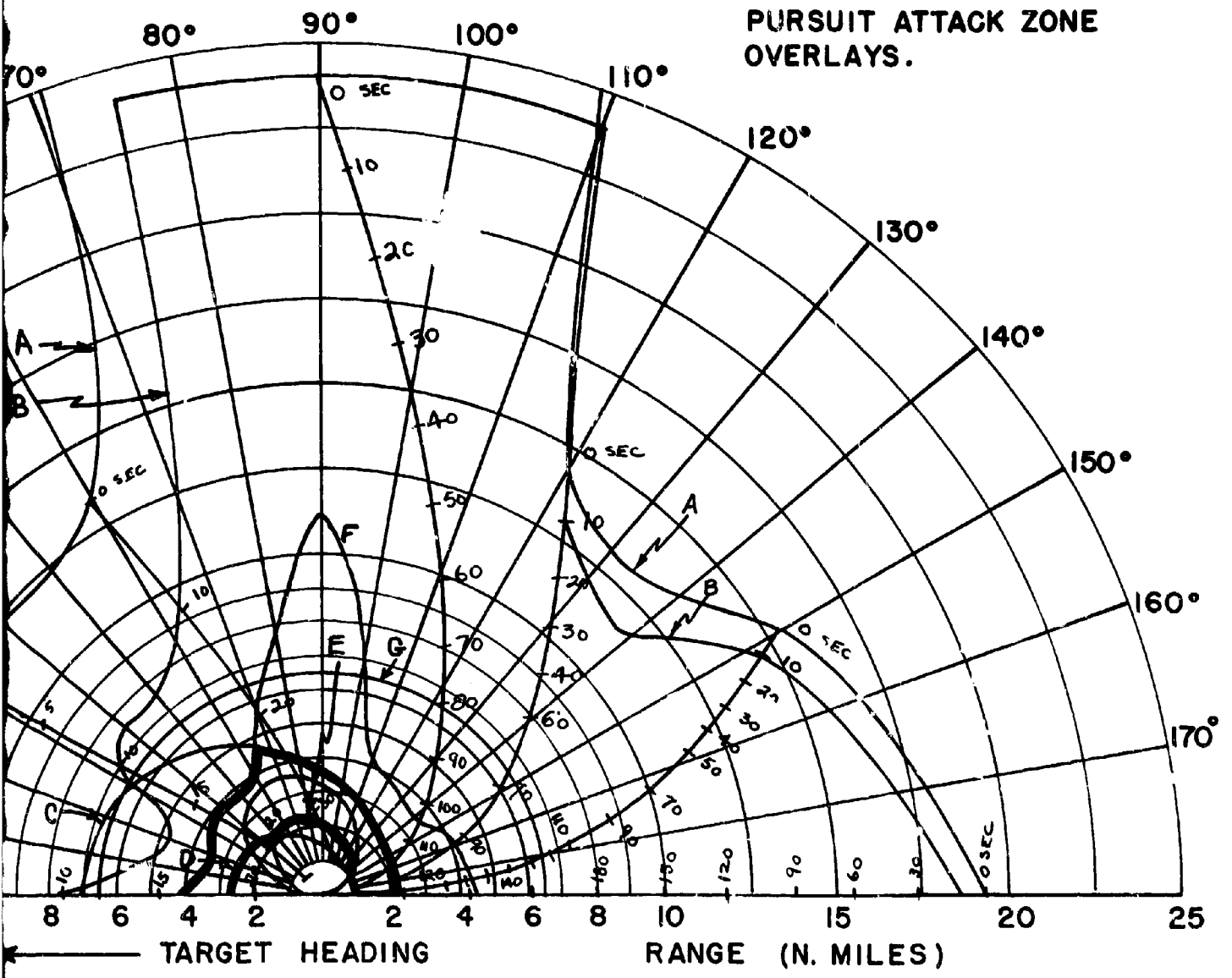

- 85% DETECTION RANGE
- LOCK-ON RANGE (10 SEC. LOCK-ON TIME)
- SPARROW III MAX. AERODYNAMIC RANGE
- SPARROW III MIN. AERODYNAMIC RANGE
- CONSTANT LOAD FACTOR LOCUS (N_Z = 2,3)
- 90% SPARROW III SEEKER LOCK-ON RANGE
- 6.5 N.M. INTERLOCK

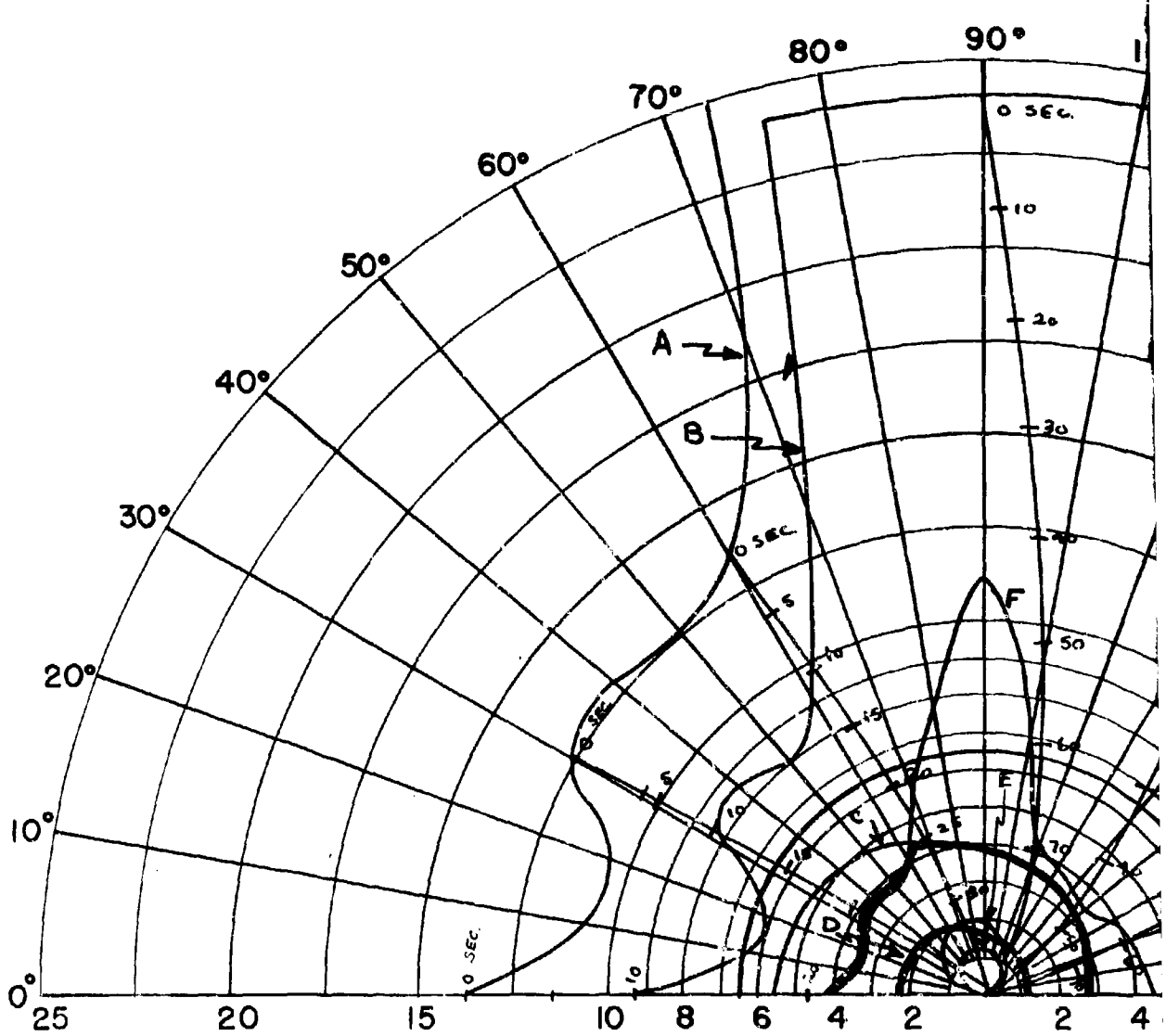

V_F = 1891 FT/SEC (F4H-1)
V_T = 854 FT/SEC
ALTITUDE = 30,000 FT.

A - 85% DETECTION RANGE
B - LOCK-ON RANGE (10 SEC. LOC
C - SPARROW III MAX. AERODYNA
D - SPARROW III MIN. AERODYNA
E - CONSTANT LOAD FACTOR LC
F - 90% SPARROW III SEEKER
G - 6.5 N.M. INTERLOCK

FIG. 21 - CO-ALTITUDE LEAD PURSUIT ATTACK ZONE OVERLAYS.

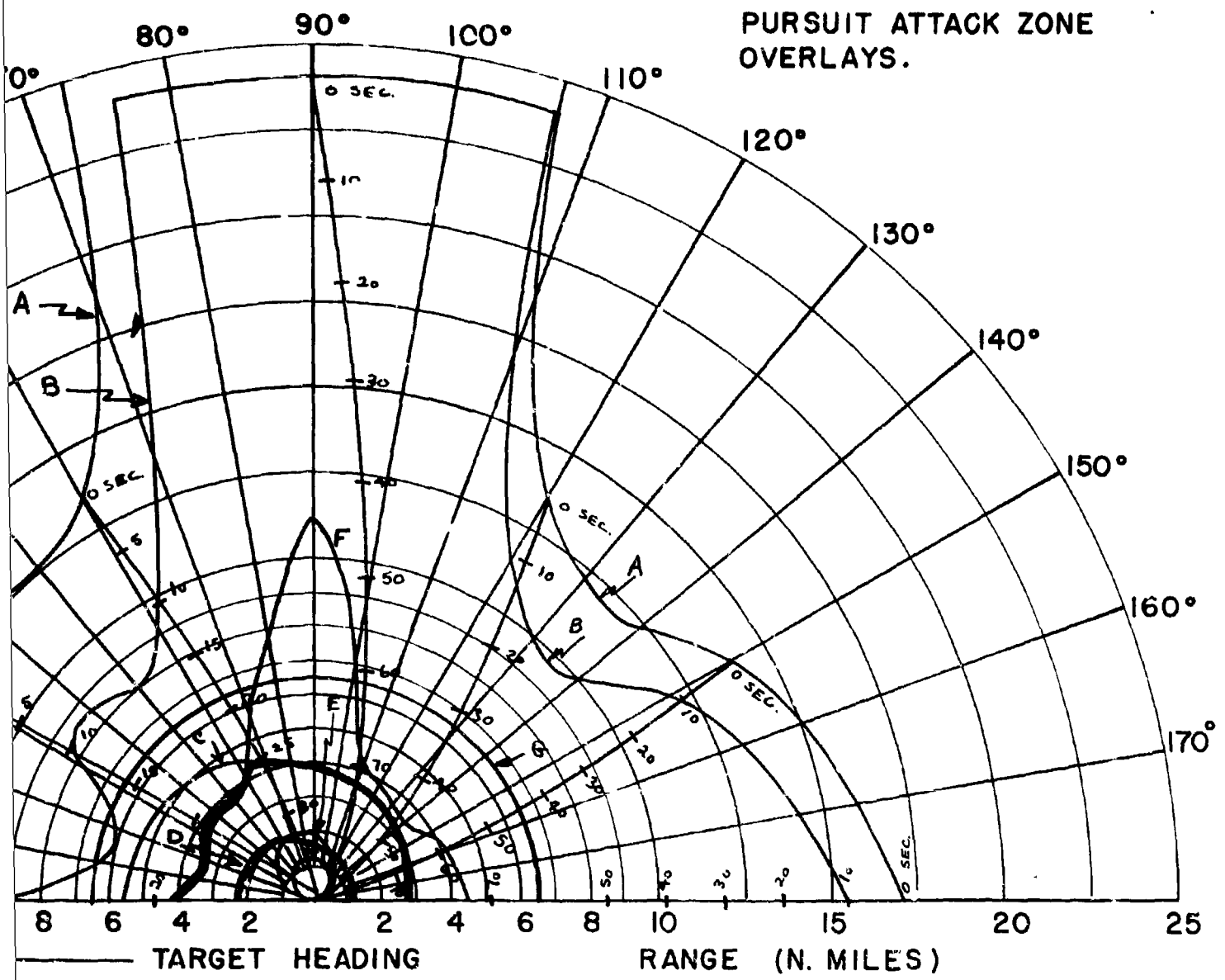

85% DETECTION RANGE
LOCK-ON RANGE (10 SEC. LOCK-ON TIME)
SPARROW III MAX. AERODYNAMIC RANGE
SPARROW III MIN. AERODYNAMIC RANGE
CONSTANT LOAD FACTOR LOCUS (N_Z = 2,3)
90% SPARROW III SEEKER LOCK-ON RANGE
6.5 N.M. INTERLOCK

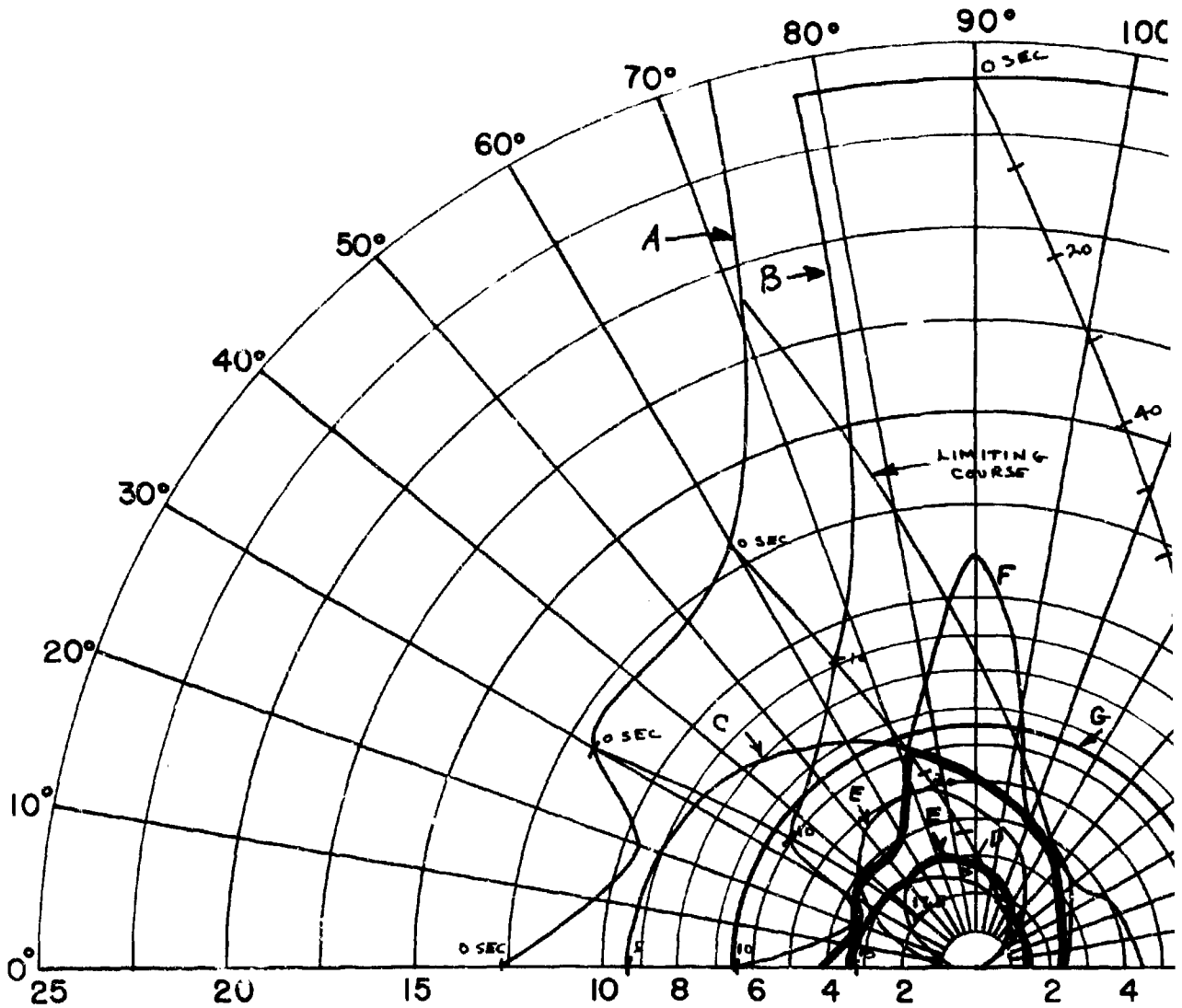

V_F = 1940 FT/SEC (F4H-1)
V_T = 1940 FT/SEC
ALTITUDE = 50,000 FT.

A - 85% DETECTION RANGE
B - LOCK-ON RANGE (10 SEC. LOCK
C - SPARROW III MAX. AERODYNAM
D - SPARROW III MIN. AERODYNAM
E - CONSTANT LOAD FACTOR LOC
F - 90% SPARROW III SEEKER LC
G - 6.5 N.M. INTERLOCK

FIG. 22 - CO-ALTITUDE LEAD PURSUIT ATTACK ZONE OVERLAYS.

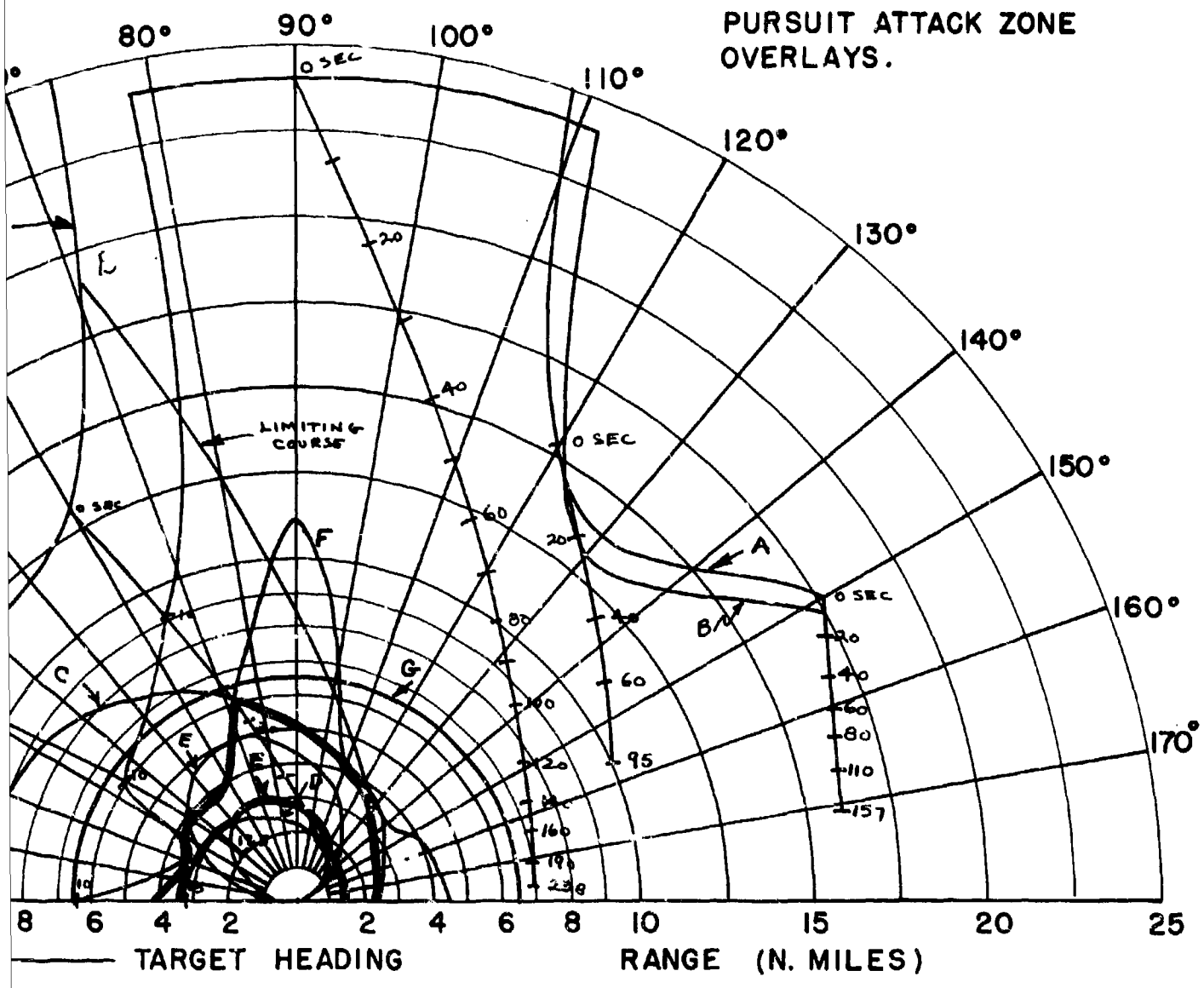

85% DETECTION RANGE
LOCK-ON RANGE (10 SEC. LOCK-ON TIME)
SPARROW III MAX. AERODYNAMIC RANGE
SPARROW III MIN. AERODYNAMIC RANGE
CONSTANT LOAD FACTOR LOCUS (N_z = 2,3)
90% SPARROW III SEEKER LOCK-ON RANGE
6.5 N.M. INTERLOCK

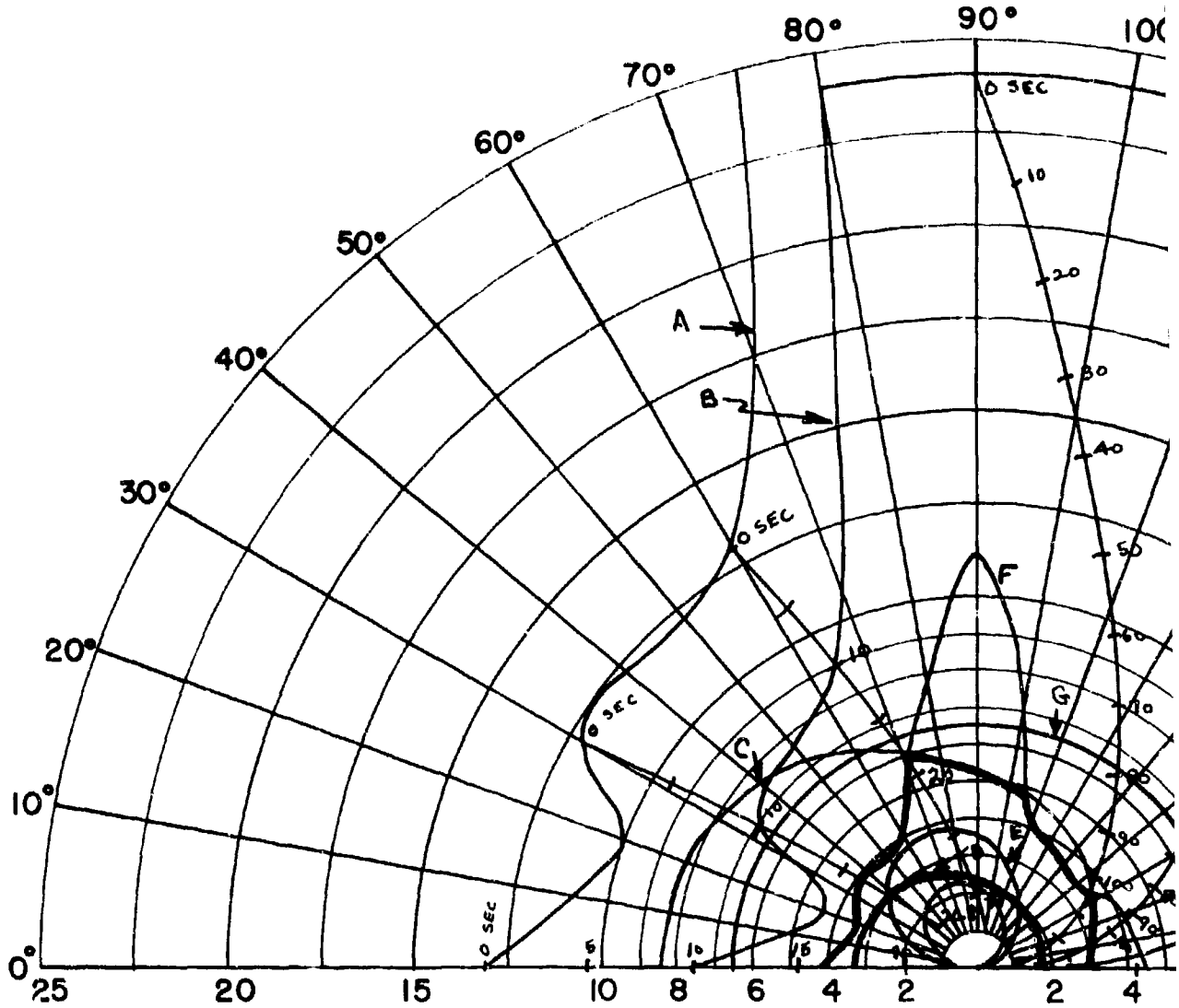

V_F = 1940 FT/SEC (F4H-1)
V_T = 1552 FT/SEC
ALTITUDE = 50,000 FT.

A - 85% DETECTION RANGE
B - LOCK-ON RANGE (10 SEC. LOCK
C - SPARROW III MAX. AERODYNAM
D - SPARROW III MIN. AERODYNAM
E - CONSTANT LOAD FACTOR LOC
F - 90% SPARROW III SEEKER L(
G - 6.5 N.M. INTERLOCK

FIG. 23 - CO-ALTITUDE LEAD PURSUIT ATTACK ZONE OVERLAYS.

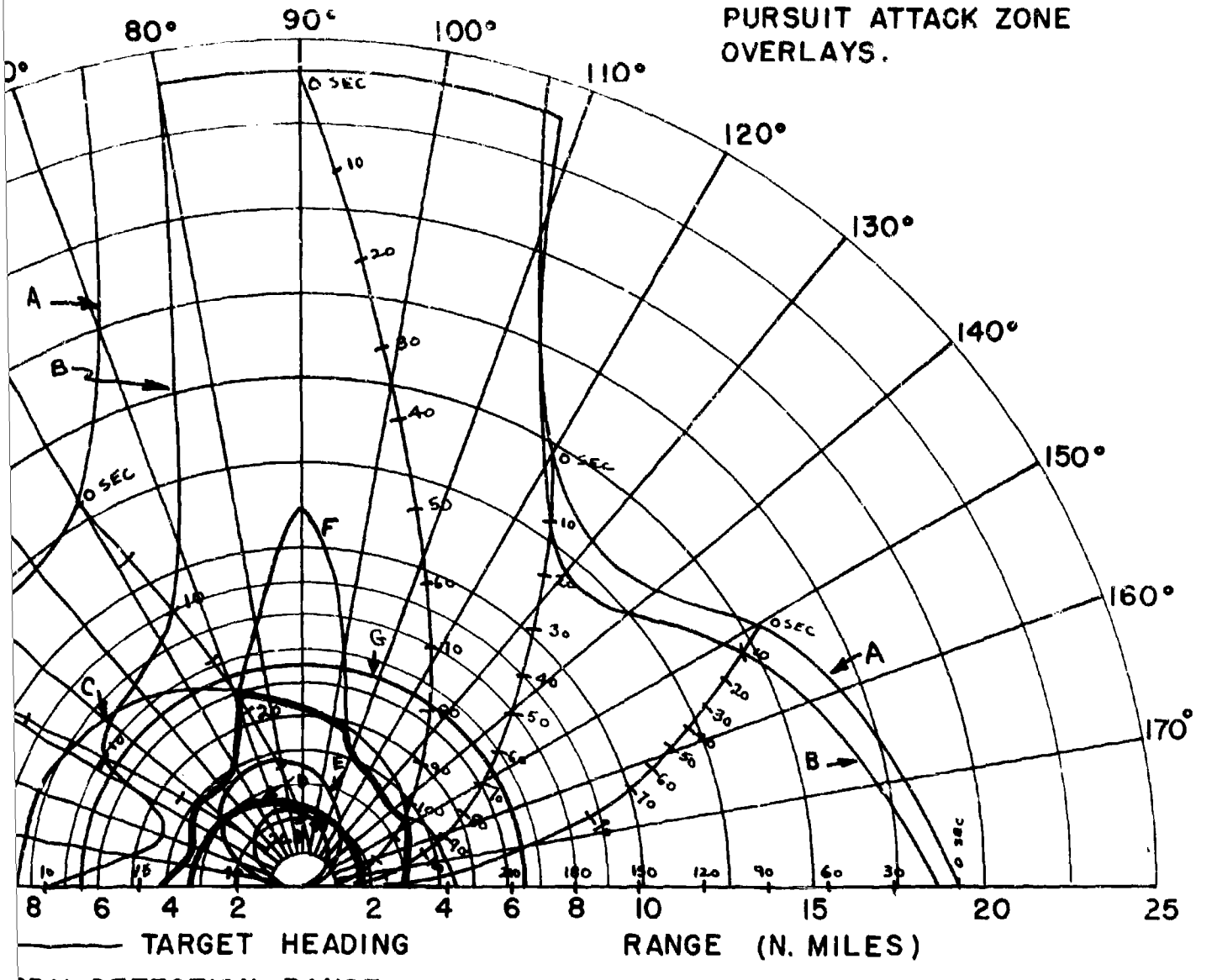

85% DETECTION RANGE
LOCK-ON RANGE (10 SEC. LOCK-ON TIME)
SPARROW III MAX. AERODYNAMIC RANGE
SPARROW III MIN. AERODYNAMIC RANGE
CONSTANT LOAD FACTOR LOCUS (N_Z = 2,3)
90% SPARROW III SEEKER LOCK-ON RANGE
6.5 N.M. INTERLOCK

CONFIDENTIAL 2

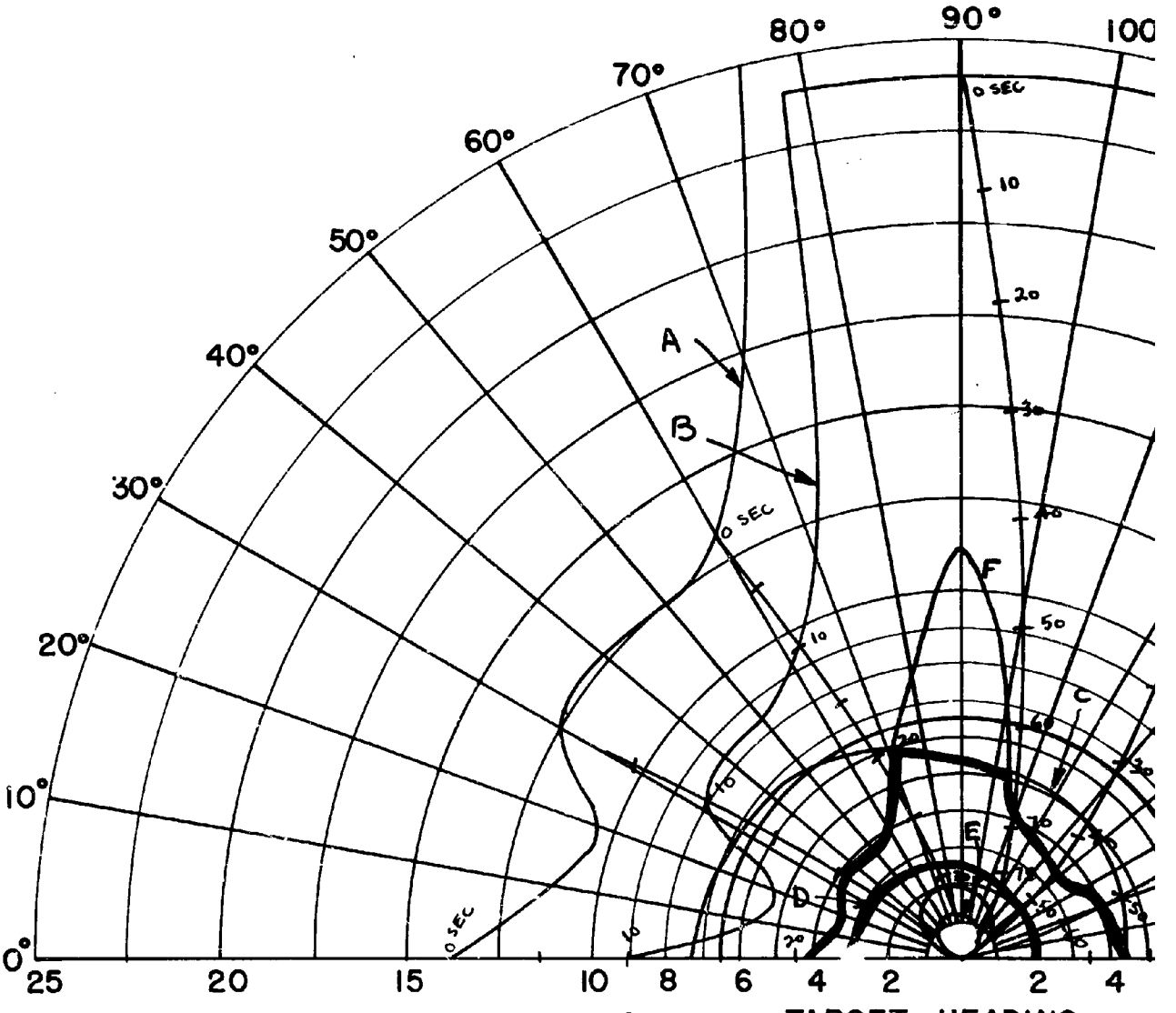

V_F = 194.0 FT/SEC (F4H-1)
V_T = 873 FT/SEC
ALTITUDE = FT.

← TARGET HEADING

A - 85% DETECTION RANGE
B - LOCK-ON RANGE (10 SEC. LOCK
C - SPARROW III MAX. AERODYNAM
D - SPARROW III MIN. AERODYNAM
E - CONSTANT LOAD FACTOR LO
F - 90% SPARROW III SEEKER L
G - 6.5 N.M. INTERLOCK

FIG. 24 - CO-ALTITUDE LEAD PURSUIT ATTACK ZONE OVERLAYS.

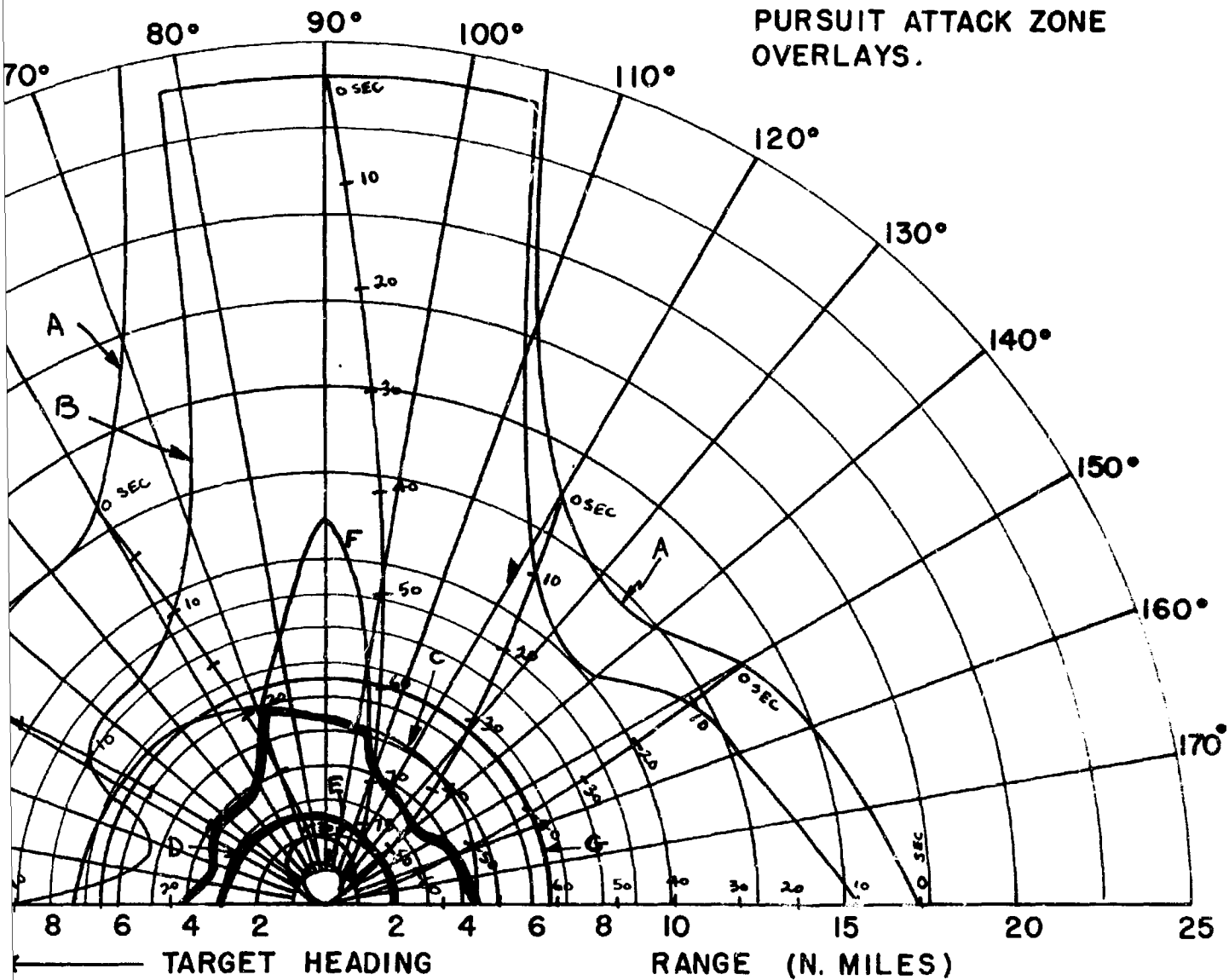

- 85% DETECTION RANGE
- LOCK-ON RANGE (10 SEC. LOCK-ON TIME)
- SPARROW III MAX. AERODYNAMIC RANGE
- SPARROW III MIN. AERODYNAMIC RANGE
- CONSTANT LOAD FACTOR LOCUS (N_Z = 2,3)
- 90% SPARROW III SEEKER LOCK-ON RANGE
- 6.5 N.M. INTERLOCK

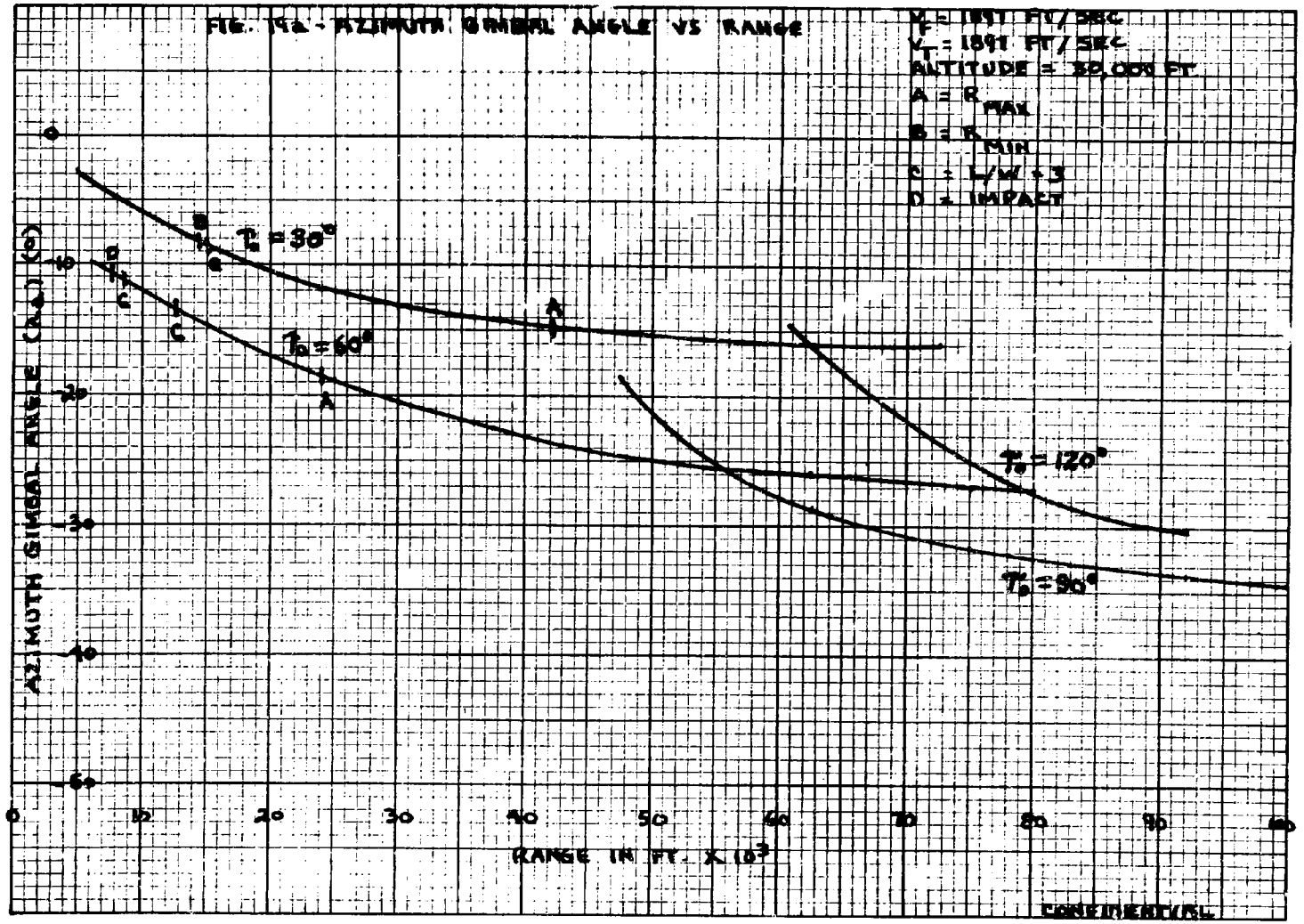
FIG. 14a - AZIMUTH GIMBAL ANGLE VS RANGE
V_F = 1891 FT/SEC
V_T = 1891 FT/SEC
ALTITUDE = 30,000 FT.
A = R_{MAX}
B = R_{MIN}
C = L/W = 3
D = IMPACT
T_o = 30°
T_o = 60°
T_o = 120°
T_o = 90°
AZIMUTH GIMBAL ANGLE (A.G.) (°)
RANGE IN FT. X 10^3
CONFIDENTIAL

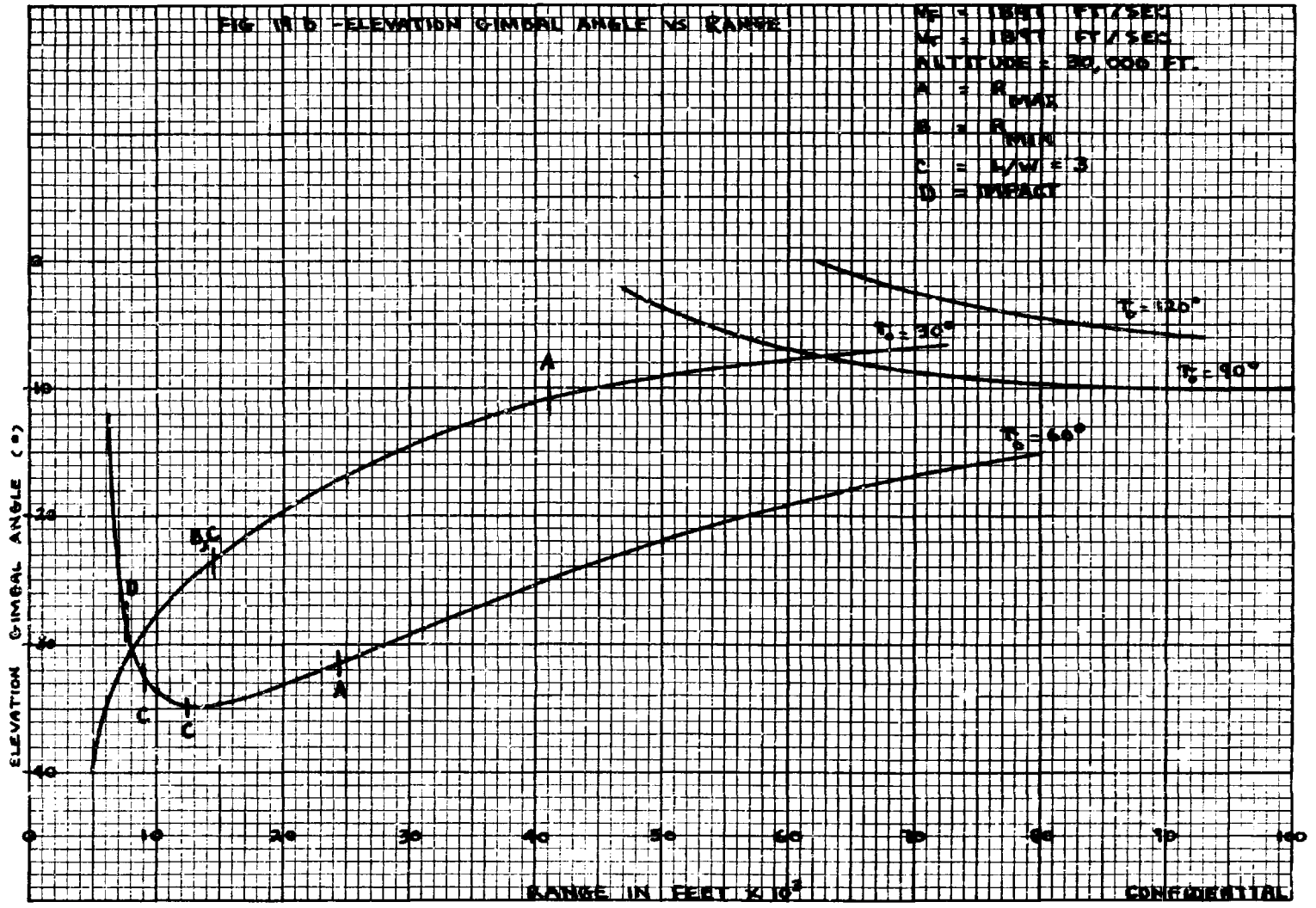
FIG 11 b -ELEVATION GIMBAL ANGLE VS RANGE
V_T = 1845 FT/SEC
V_M = 1977 FT/SEC
ALTITUDE = 30,000 FT.
A = R_{MAX}
B = R_{MIN}
C = L/W = 3
D = IMPACT
γ_c = 120°
γ_c = 30°
γ_c = 90°
γ_c = 60°
A
B
C
D
ELEVATION GIMBAL ANGLE (°)
RANGE IN FEET X 10^3
CONFIDENTIAL

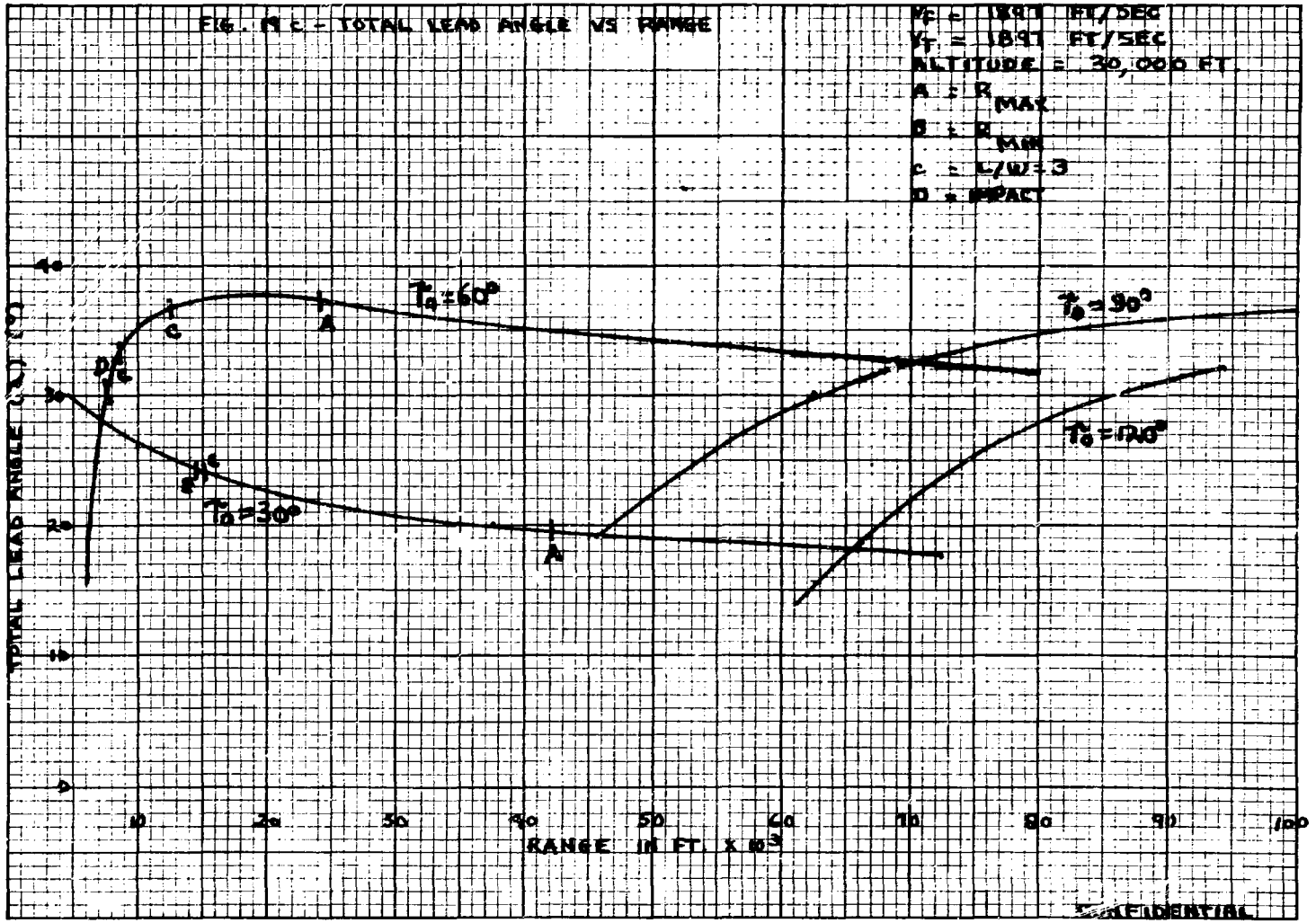
FIG. 19 c - TOTAL LEAD ANGLE VS RANGE
V_F = 1891 FT/SEC
V_T = 1891 FT/SEC
ALTITUDE = 30,000 FT.
A = R_{MAX}
B = R_{MIN}
C = L/W = 3
D = IMPACT
T_0 = 60°
T_0 = 90°
T_0 = 120°
T_0 = 30°
TOTAL LEAD ANGLE (°)
RANGE IN FT. X 10^3
CONFIDENTIAL

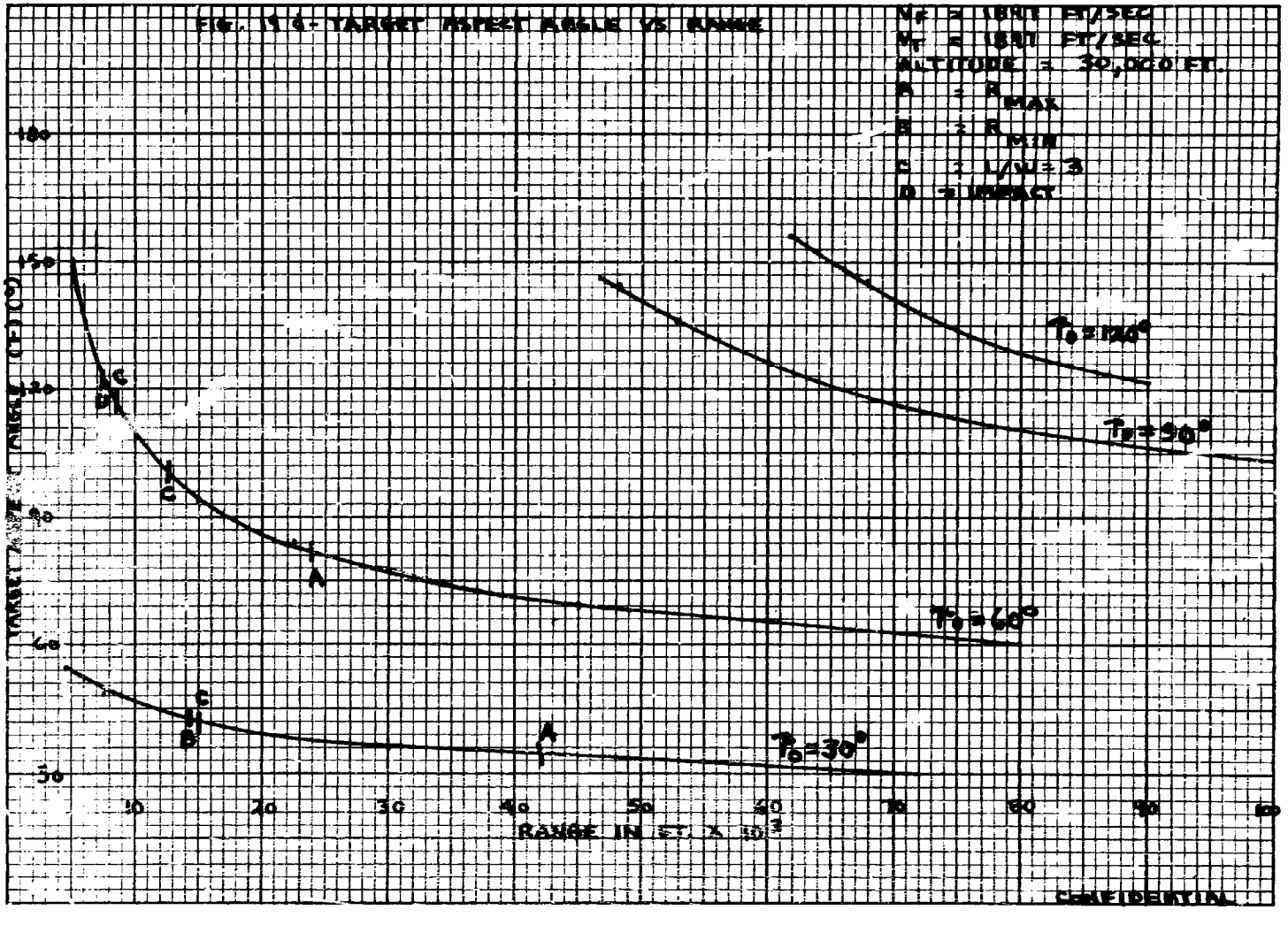
FIG. 19 6 - TARGET ASPECT ANGLE VS RANGE
V_F = 1800 FT/SEC
V_T = 1800 FT/SEC
ALTITUDE = 30,000 FT.
A = R_{MAX}
B = R_{MIN}
C = L/W = 3
D = IMPACT
T_0 = 120°
T_0 = 90°
T_0 = 60°
T_0 = 30°
TARGET ASPECT ANGLE (T) (°)
RANGE IN FT. X 10³
CONFIDENTIAL

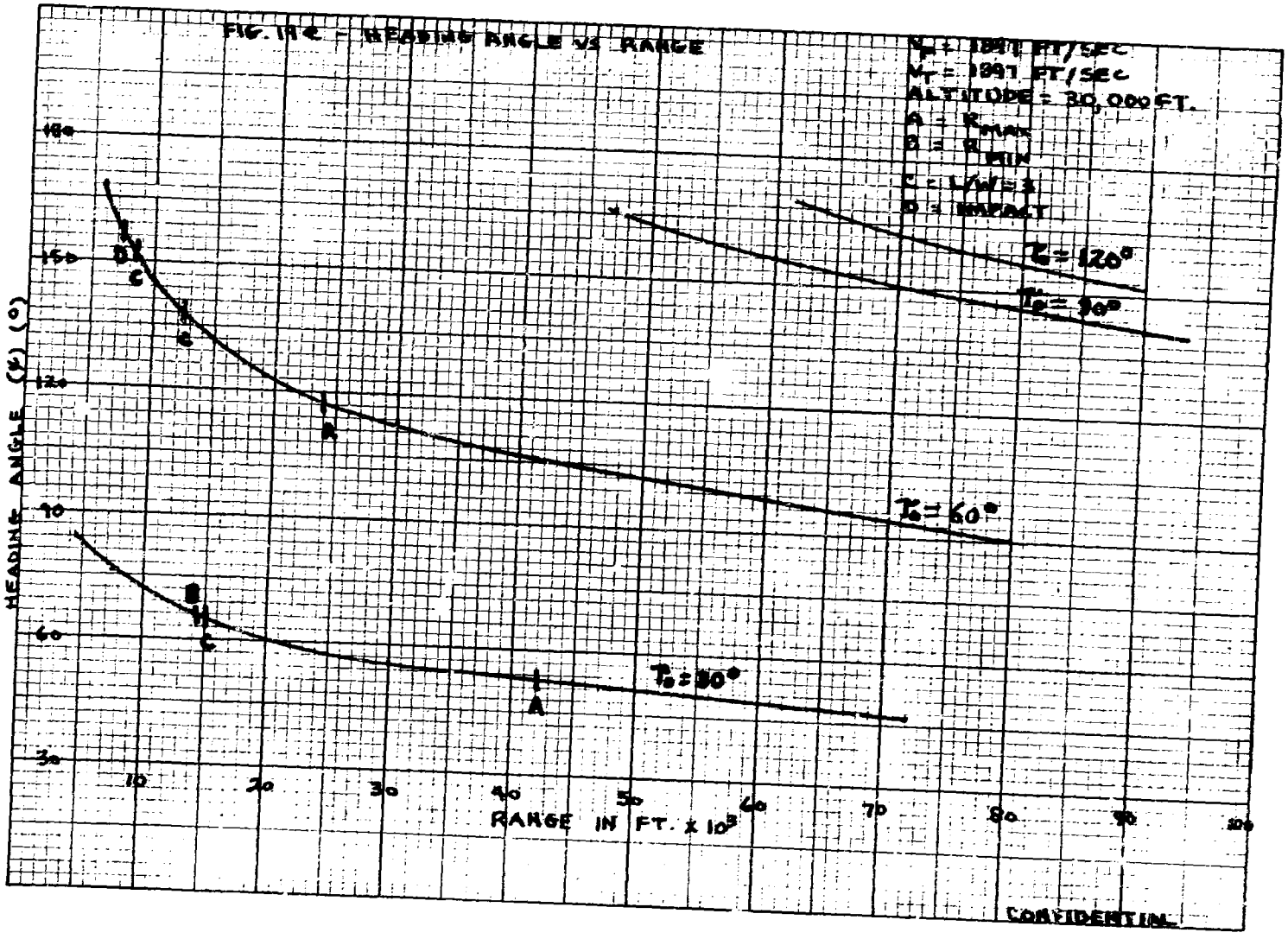
FIG. 11 c - HEADING ANGLE VS RANGE
V_M = 1991 FT/SEC
V_T = 1991 FT/SEC
ALTITUDE = 30,000 FT.
A = R_{MAX}
B = R_{MIN}
C = $L/M^2 = 3$
D = IMPACT
T_o = 120°
T_o = 90°
T_o = 60°
T_o = 30°
HEADING ANGLE (ψ) (°)
RANGE IN FT. x 10^3
CONFIDENTIAL

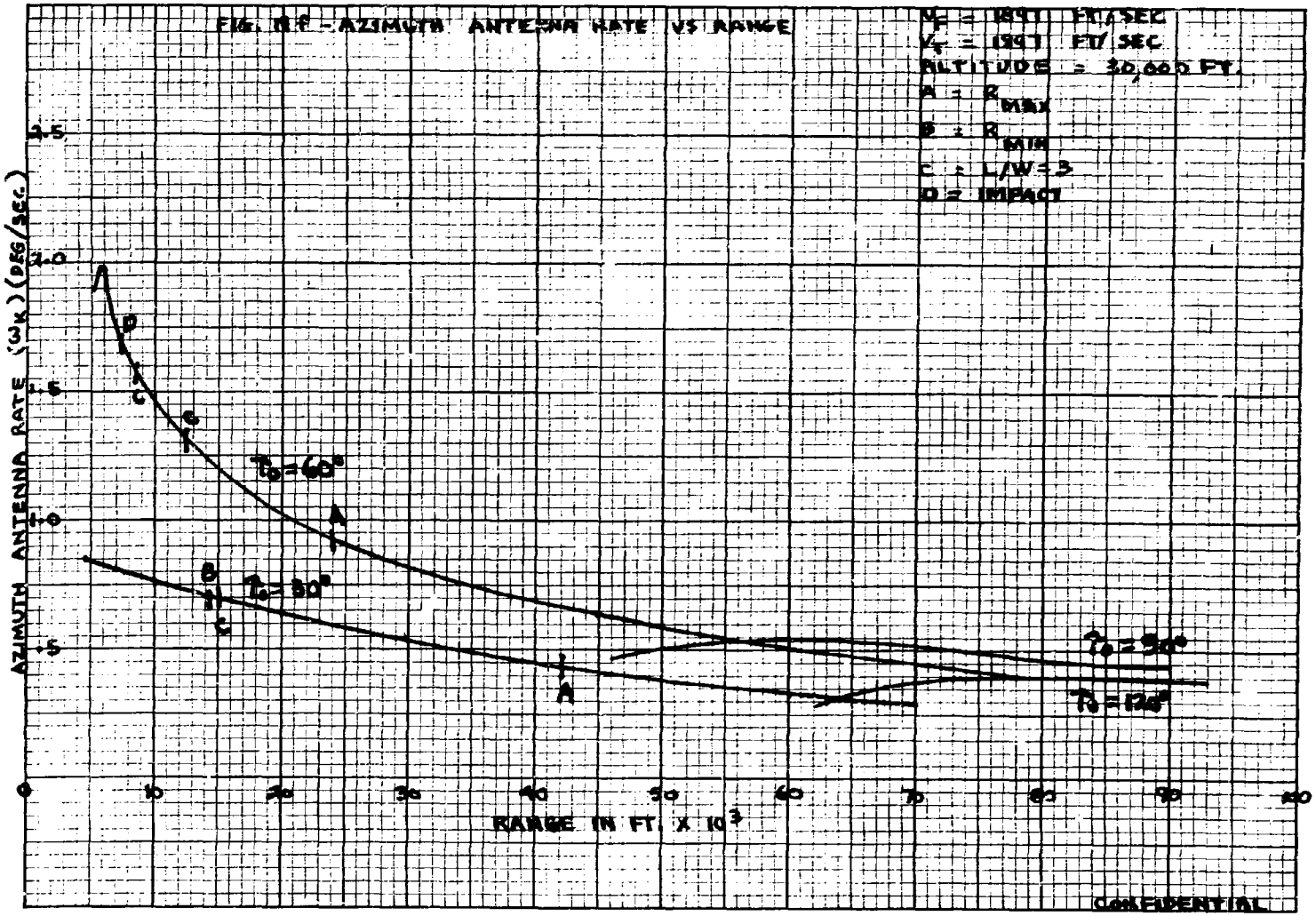
FIG. 11F - AZIMUTH ANTENNA RATE VS RANGE
V_F = 1891 FT/SEC
V_T = 1991 FT/SEC
ALTITUDE = 30,000 FT.
A = R_{MAX}
B = R_{MIN}
C = L/W = 3
D = IMPACT
AZIMUTH ANTENNA RATE (ω_K) (DEG/SEC.)
RANGE IN FT. X 10^3
T_0 = 60°
T_0 = 90°
T_0 = 120°
A
B
C
D
CONFIDENTIAL

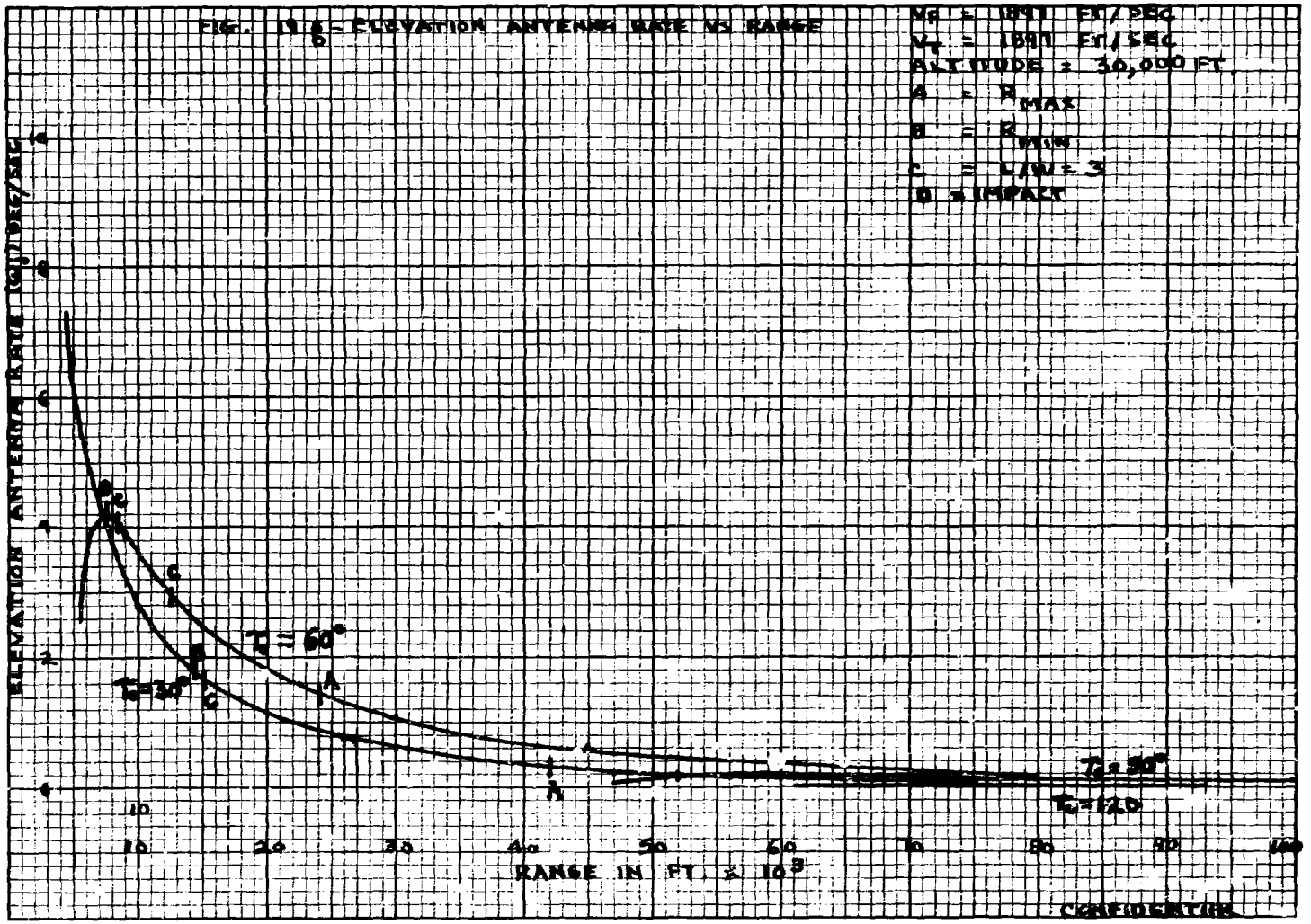
FIG. 19 b - ELEVATION ANTENNA RATE VS RANGE
V_F = 1891 FT/SEC
V_T = 1891 FT/SEC
ALTITUDE = 30,000 FT.
A = R_{MAX}
B = R_{MIN}
C = L/W = 3
D = IMPACT
ELEVATION ANTENNA RATE (MILS/SEC)
RANGE IN FT. x 10^3
T_c=30°
T_c=60°
T_c=90°
T_c=120
CONFIGURATION

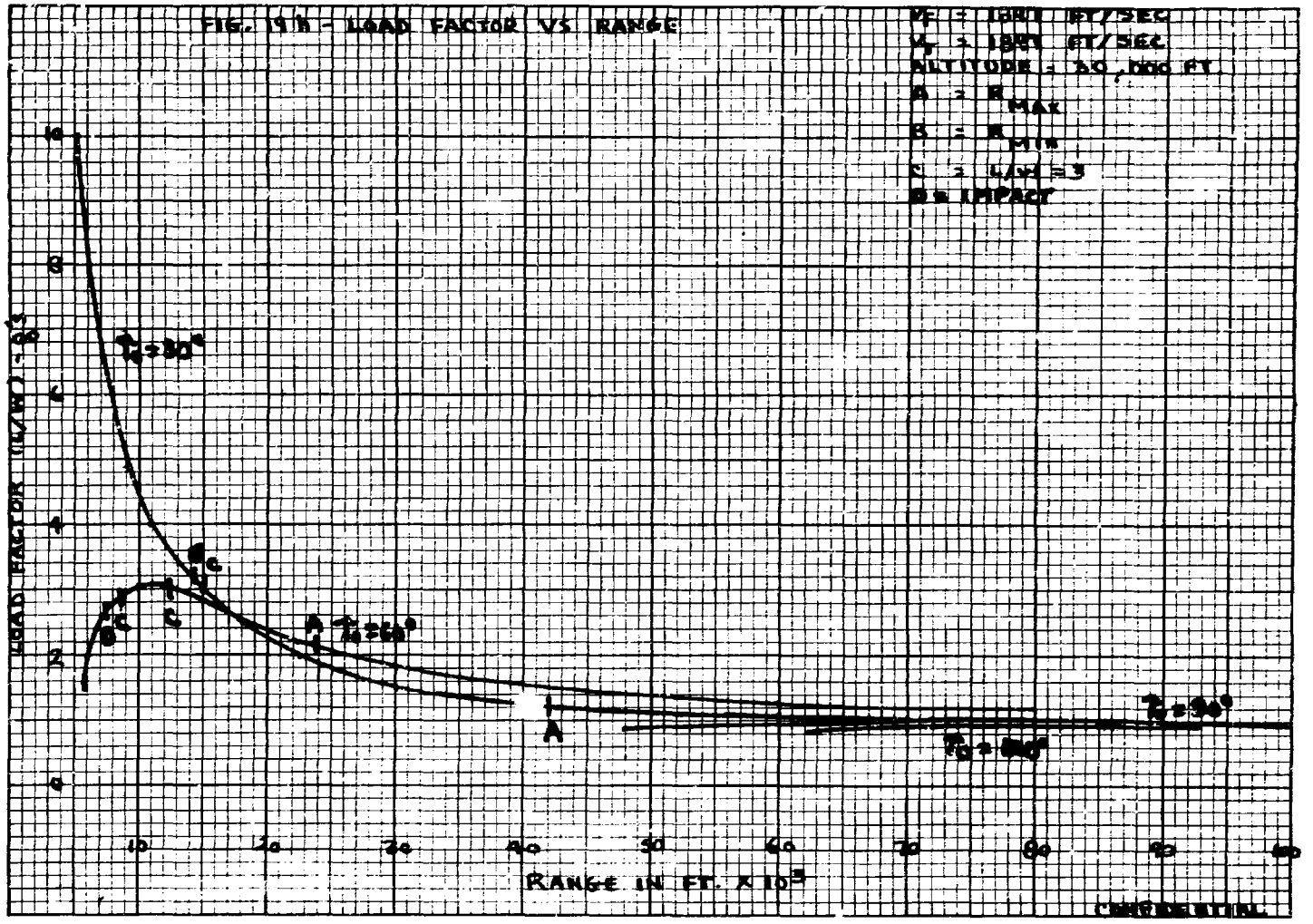
FIG. 19 h - LOAD FACTOR VS RANGE
V_F = 1881 FT/SEC
V_T = 1881 FT/SEC
ALTITUDE = 30,000 FT
A = E MAX
B = E MIN
C = L/W = 3
D = IMPACT
LOAD FACTOR (L/W) - Gs
RANGE IN FT. X 10^3
A
B
C
D
γ_T=30°
γ_T=60°
γ_T=90°
CONFIDENTIAL

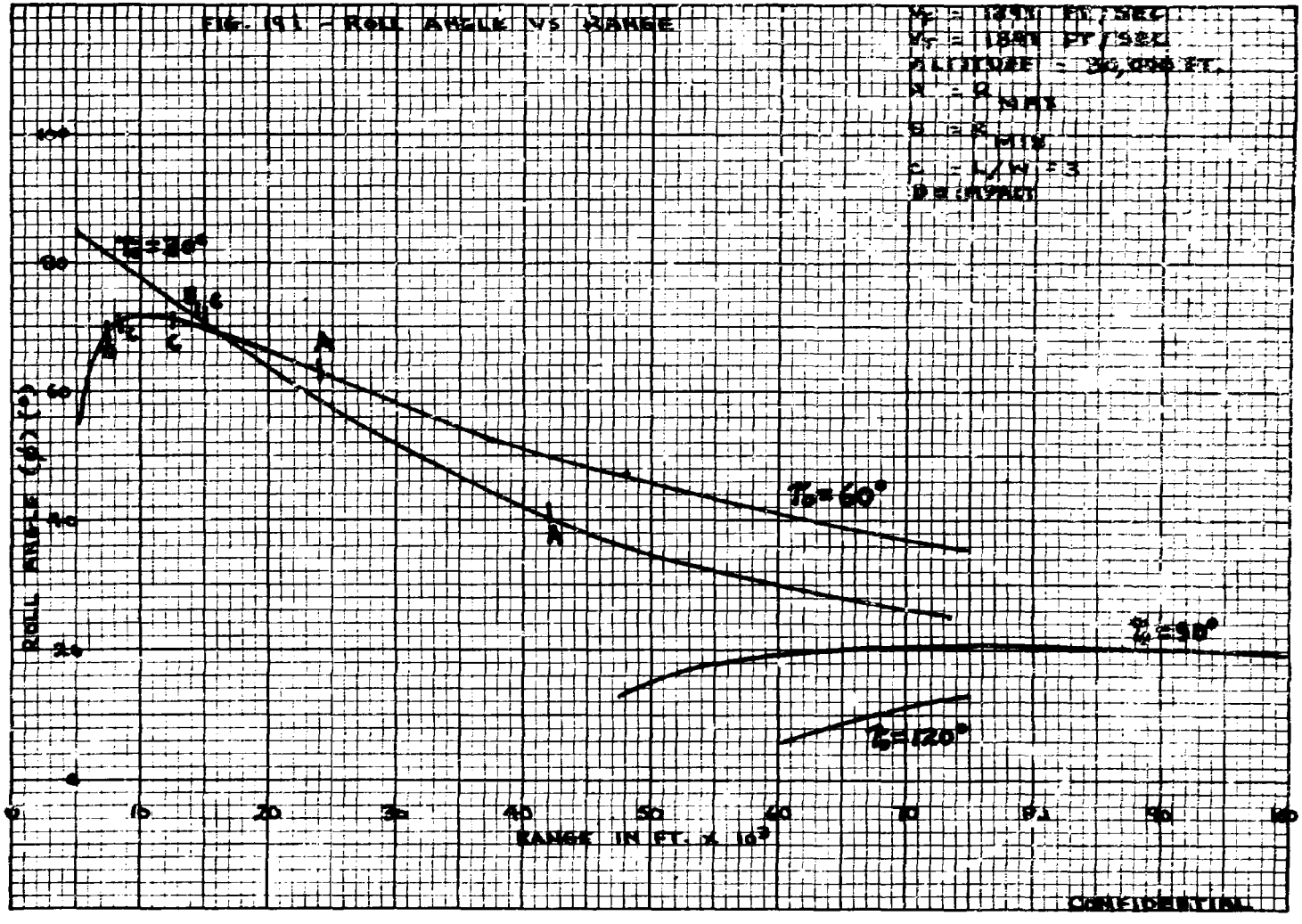
FIG. 191 - ROLL ANGLE VS RANGE
ROLL ANGLE (φ) (DEG)
RANGE IN FT. X 10³
$T_0 = 60°$
$T_0 = 120°$
CONFIDENTIAL

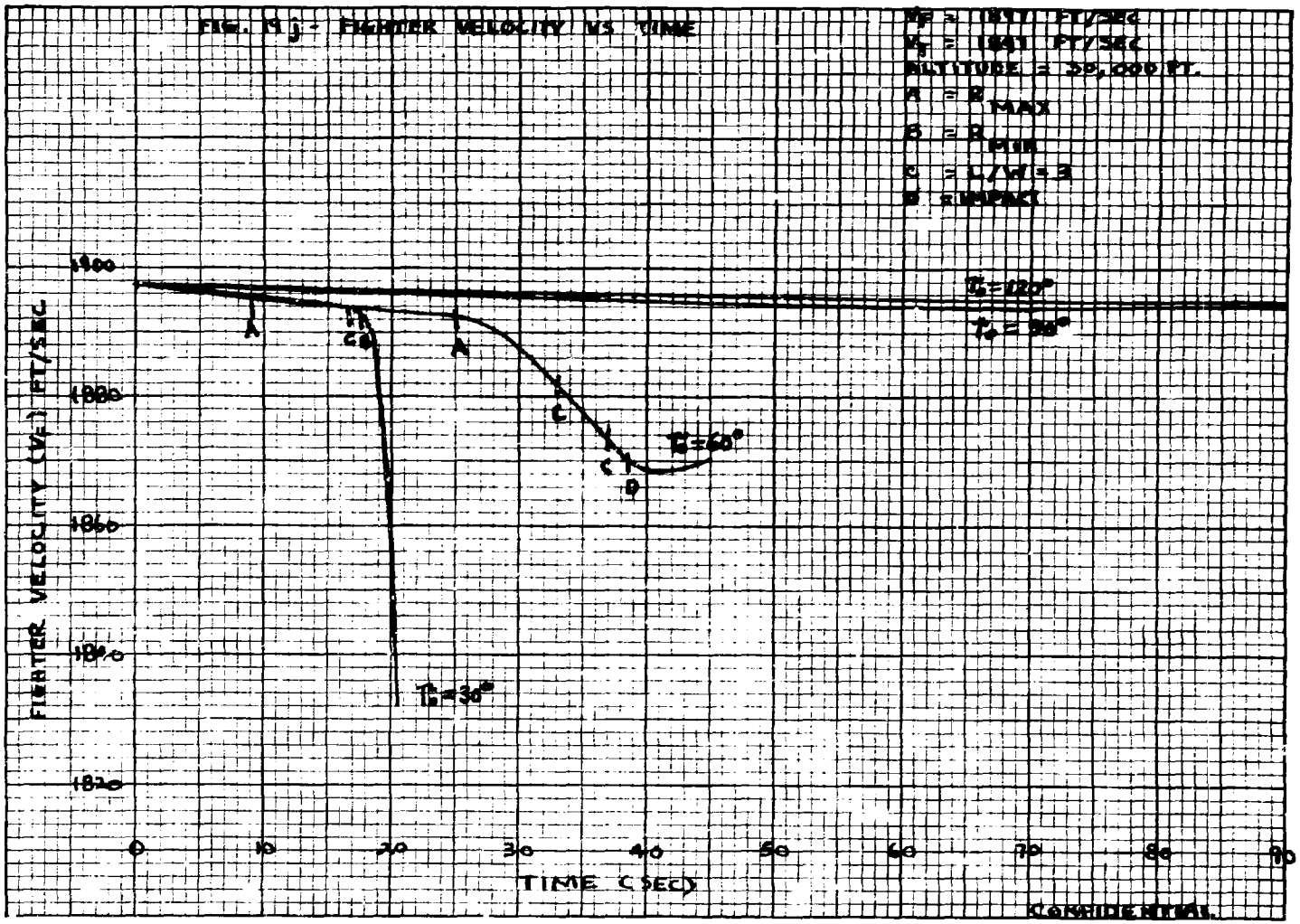
FIG. 19 j - FIGHTER VELOCITY VS TIME
V_F = 1877 FT/SEC
V_T = 1841 FT/SEC
ALTITUDE = 30,000 FT.
A = R MAX
B = R MIN
C = L/W = 3
D = IMPACT
ψ_T = 120°
ψ_T = 90°
ψ_T = 60°
ψ_T = 30°
FIGHTER VELOCITY (V_F) FT/SEC
1900
1880
1860
1840
1820
0
10
20
30
40
50
60
70
80
90
TIME (SEC)
CONFIDENTIAL

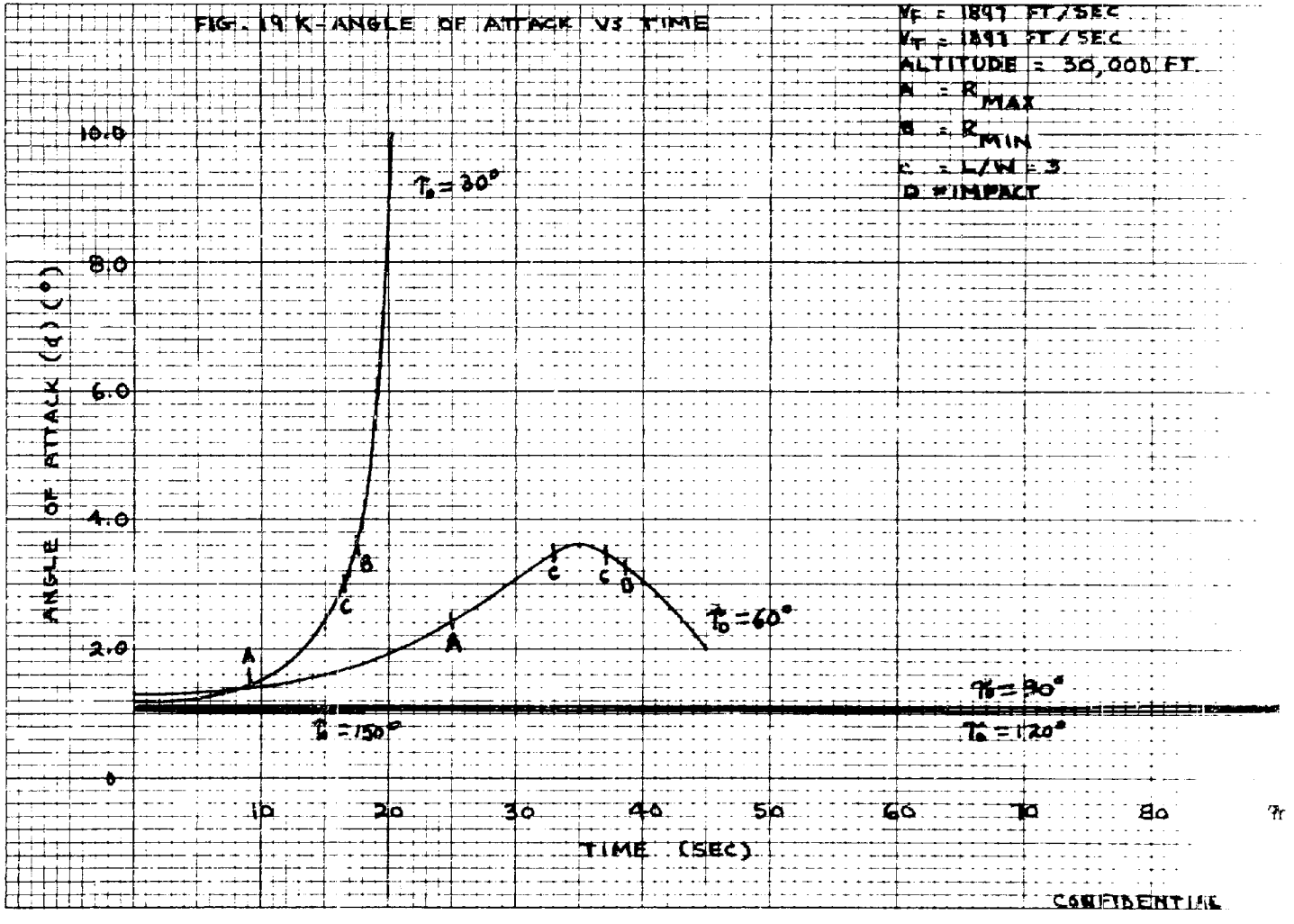
FIG. 19 K - ANGLE OF ATTACK VS TIME
V_F = 1897 FT/SEC
V_T = 1897 FT/SEC
ALTITUDE = 30,000 FT.
A = R_{MAX}
B = R_{MIN}
C = L/W = 3
D = IMPACT
$\gamma_0 = 30°$
$\gamma_0 = 60°$
$\gamma_0 = 90°$
$\gamma_0 = 120°$
$\gamma_0 = 150°$
ANGLE OF ATTACK (α) (°)
TIME (SEC)
10.0
8.0
6.0
4.0
2.0
0
10
20
30
40
50
60
70
80
A
B
C
D
CONFIDENTIAL

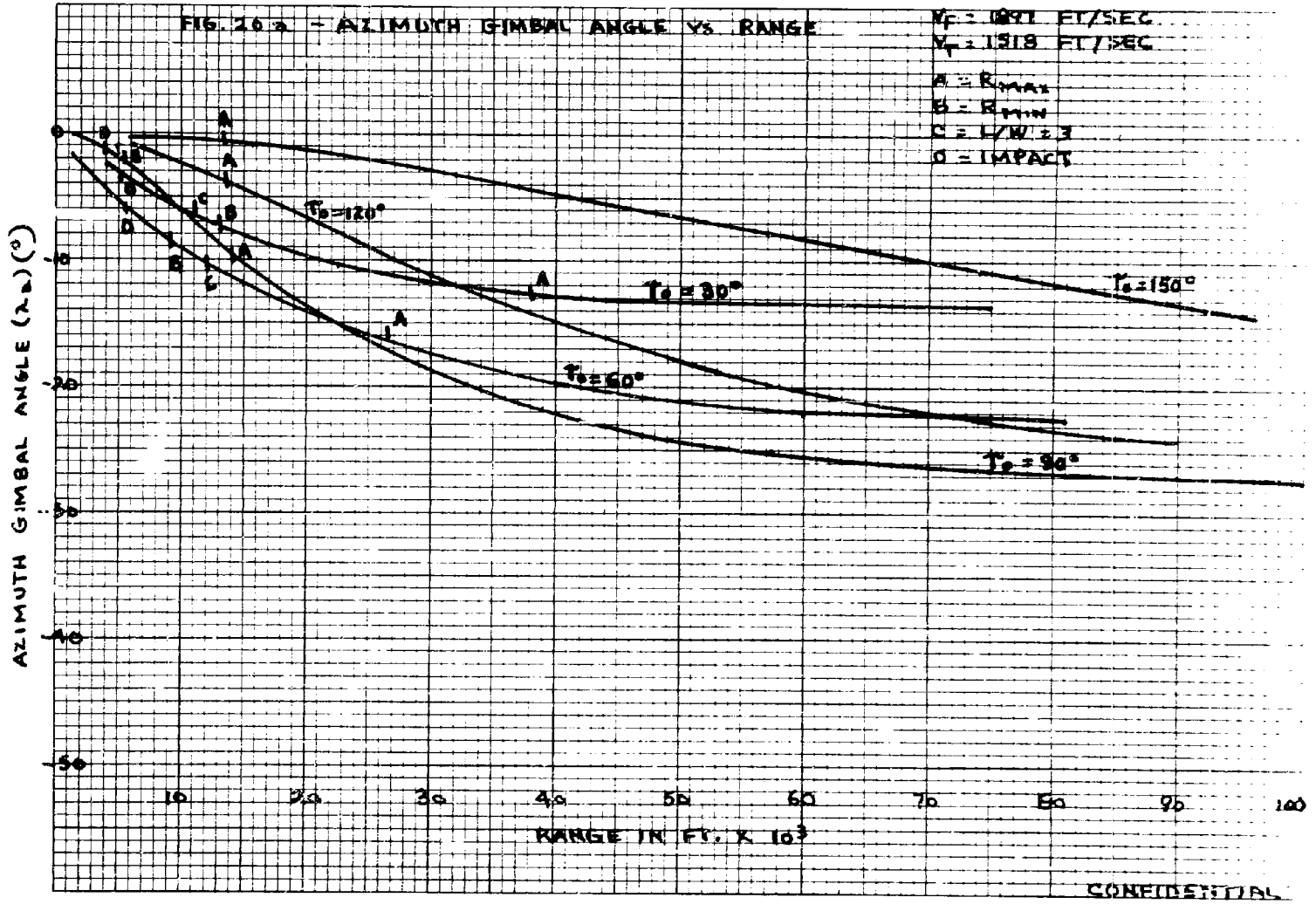
FIG. 20 a - AZIMUTH GIMBAL ANGLE VS RANGE
V_T = 1891 FT/SEC
V_T = 1518 FT/SEC
A = R_{max}
B = R_{min}
C = L/W = 3
D = IMPACT
γ_D=120°
γ_D = 30°
γ_D=150°
γ_D=60°
γ_D = 90°
AZIMUTH GIMBAL ANGLE (λ_a) (°)
0
-10
-20
-30
-40
-50
10
20
30
40
50
60
70
80
90
100
RANGE IN FT. X 10^3
CONFIDENTIAL

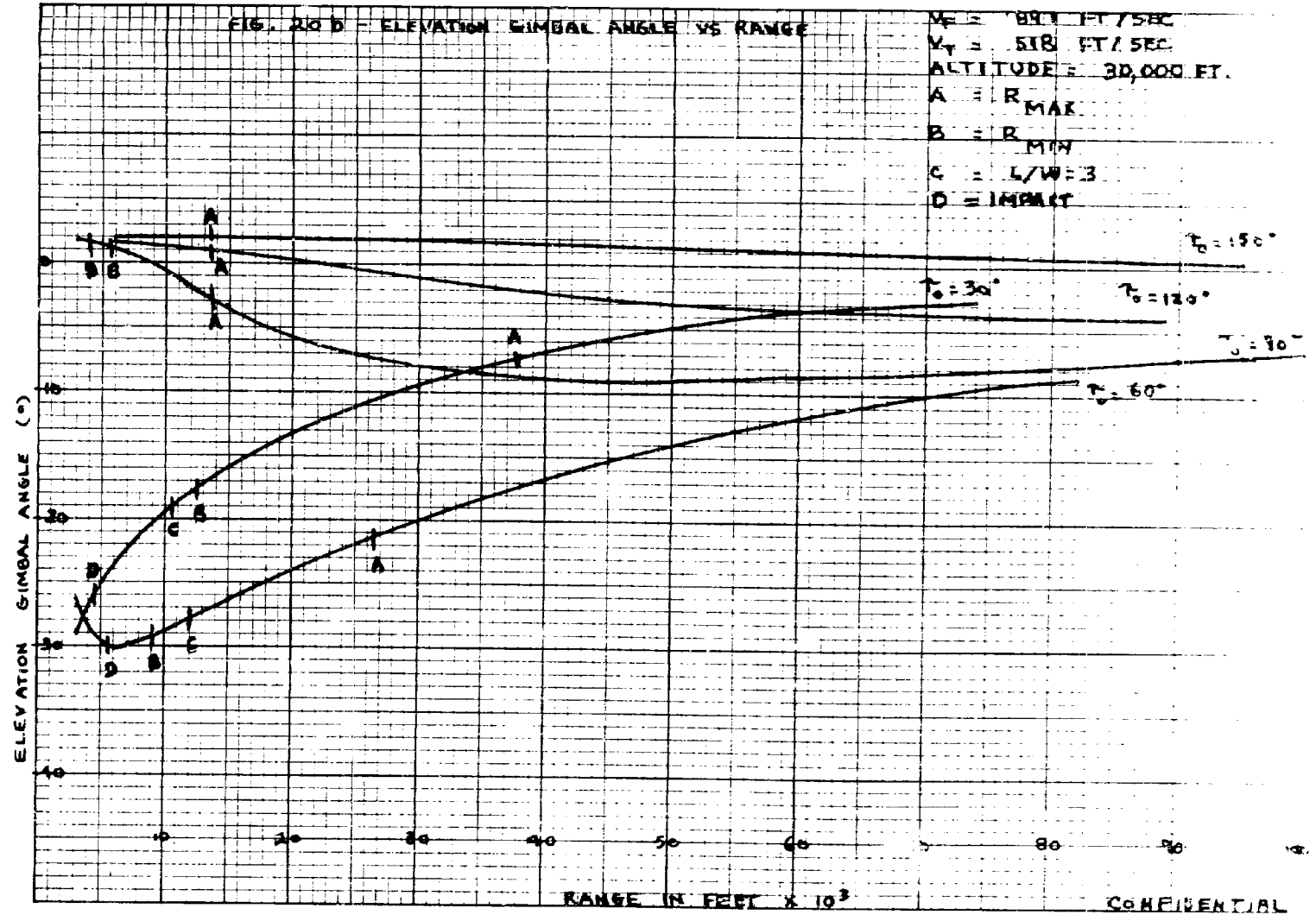
FIG. 20 b - ELEVATION GIMBAL ANGLE VS RANGE
V_F = 891 FT/SEC
V_T = 518 FT/SEC
ALTITUDE = 30,000 FT.
A = R_{MAX}
B = R_{MIN}
C = L/W = 3
D = IMPACT
τ_0 = 150°
τ_0 = 90°
τ_0 = 120°
τ_0 = 60°
ELEVATION GIMBAL ANGLE (°)
RANGE IN FEET X 10^3
CONFIDENTIAL

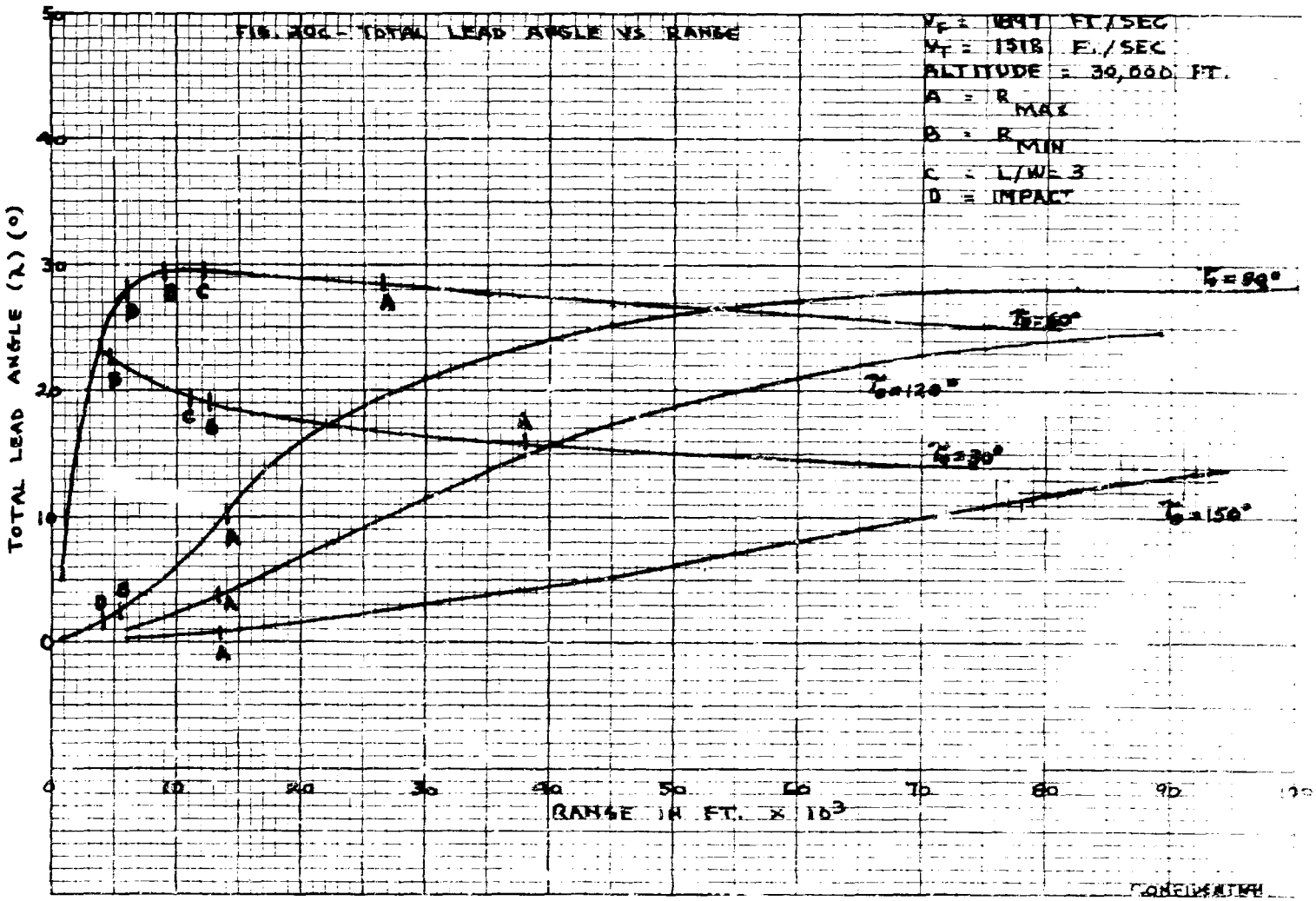
FIG. 20C - TOTAL LEAD ANGLE VS RANGE
V_F = 1891 FT/SEC
V_T = 1518 F./SEC
ALTITUDE = 30,000 FT.
A = R_{MAX}
B = R_{MIN}
C = L/W = 3
D = IMPACT
τ_T = 89°
τ_T = 60°
τ_T = 120°
τ_T = 30°
τ_T = 150°
TOTAL LEAD ANGLE (λ) (°)
RANGE IN FT. × 10^3
CONFIDENTIAL

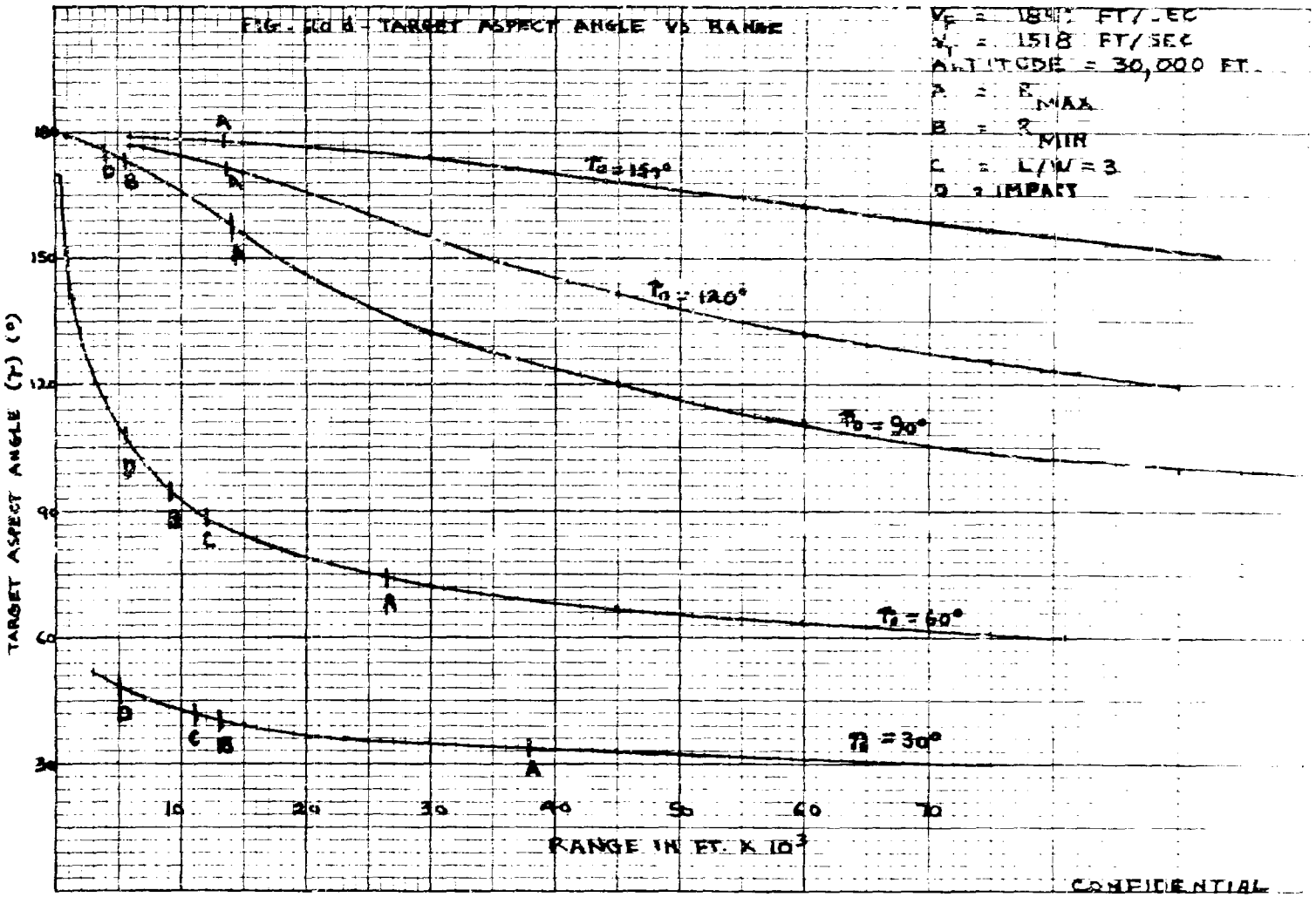
FIG. 6d 8 - TARGET ASPECT ANGLE VS RANGE
V_F = 1847 FT/SEC
V_T = 1518 FT/SEC
ALTITUDE = 30,000 FT.
A = R_{MAX}
B = R_{MIN}
C = L/W = 3
D = IMPACT
T_a = 150°
T_a = 120°
T_a = 90°
T_a = 60°
T_a = 30°
TARGET ASPECT ANGLE (T) (°)
RANGE IN FT. X 10^3
CONFIDENTIAL

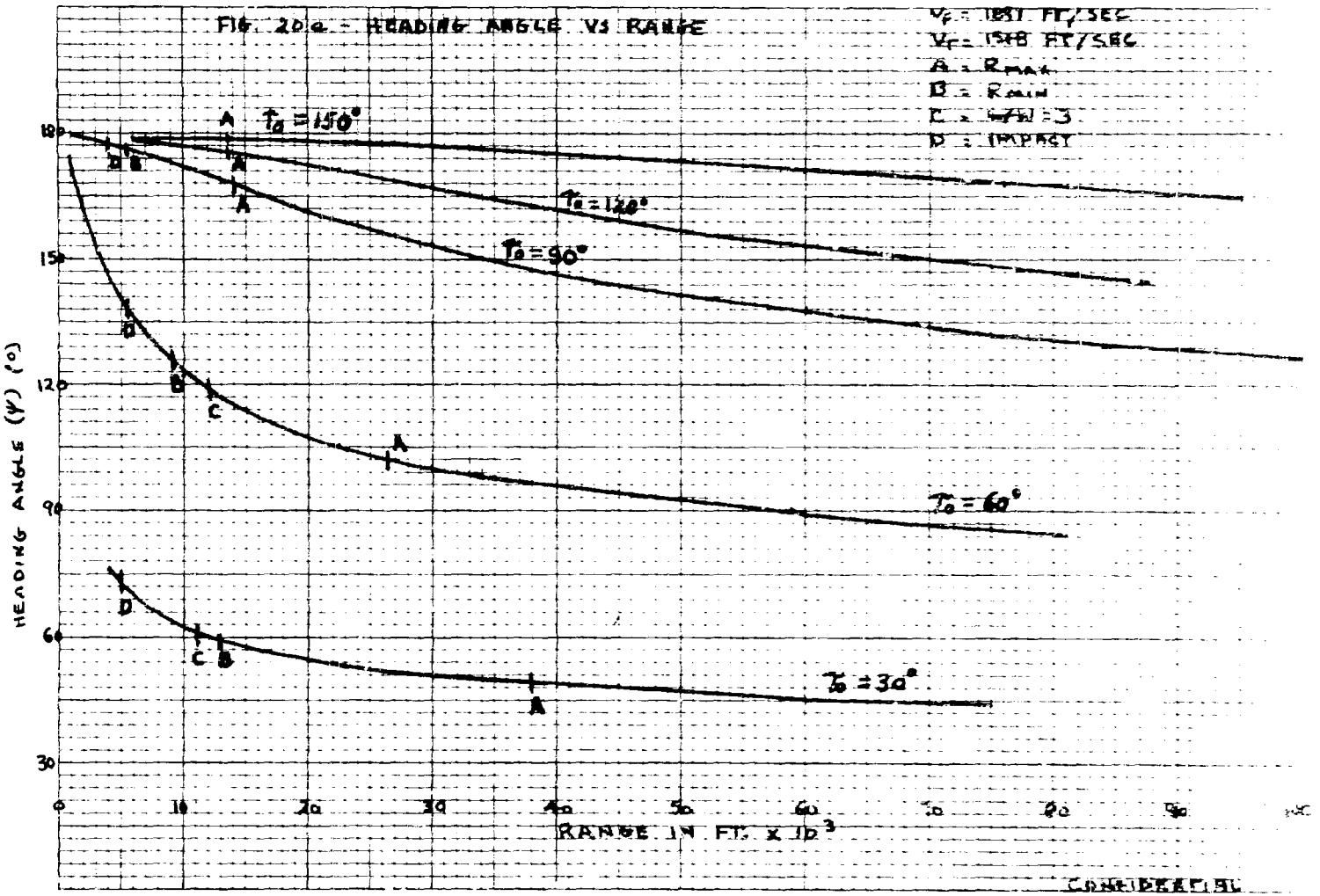
FIG. 20a - HEADING ANGLE VS RANGE
V_f = 1851 FT/SEC
V_f = 1518 FT/SEC
A = R_{max}
B = R_{min}
C = R/R_{min} = 3
D = IMPACT
γ_0 = 150°
γ_0 = 120°
γ_0 = 90°
γ_0 = 60°
γ_0 = 30°
HEADING ANGLE (ψ) (°)
RANGE IN FT. x 10^3
CONFIDENTIAL

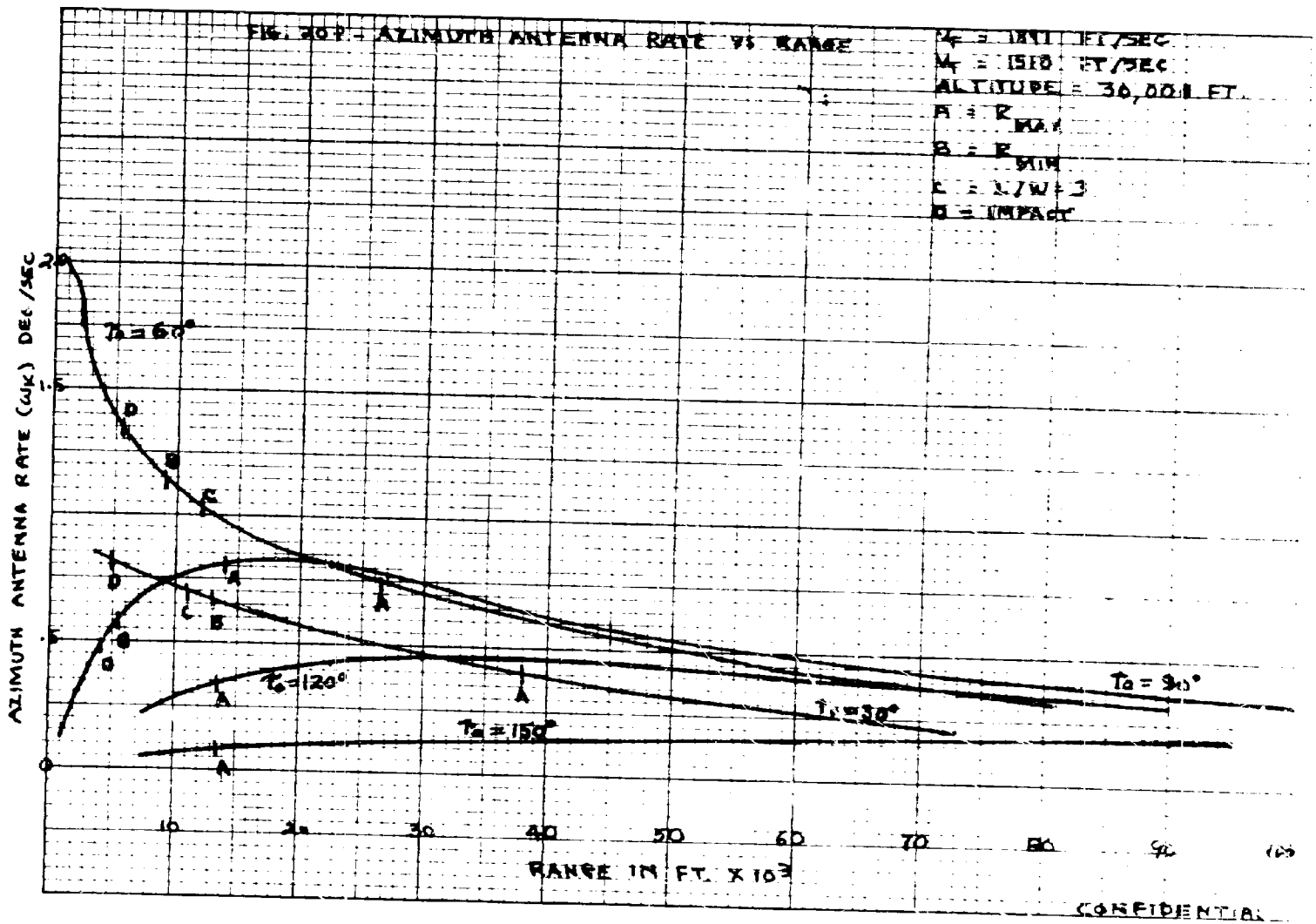
FIG. 207 - AZIMUTH ANTENNA RATE VS RANGE
V_T = 1411 FT/SEC
V_T = 1518 FT/SEC
ALTITUDE = 30,000 FT.
A = R_{MAX}
B = R_{MIN}
L = L/W = 3
D = IMPACT
AZIMUTH ANTENNA RATE (ωK) DEG/SEC
20
0
T_a = 60°
T_a = 120°
T_a = 150°
T_a = 90°
T_a = 30°
A
B
C
D
10
20
30
40
50
60
70
80
90
100
RANGE IN FT. X 10^3
CONFIDENTIAL

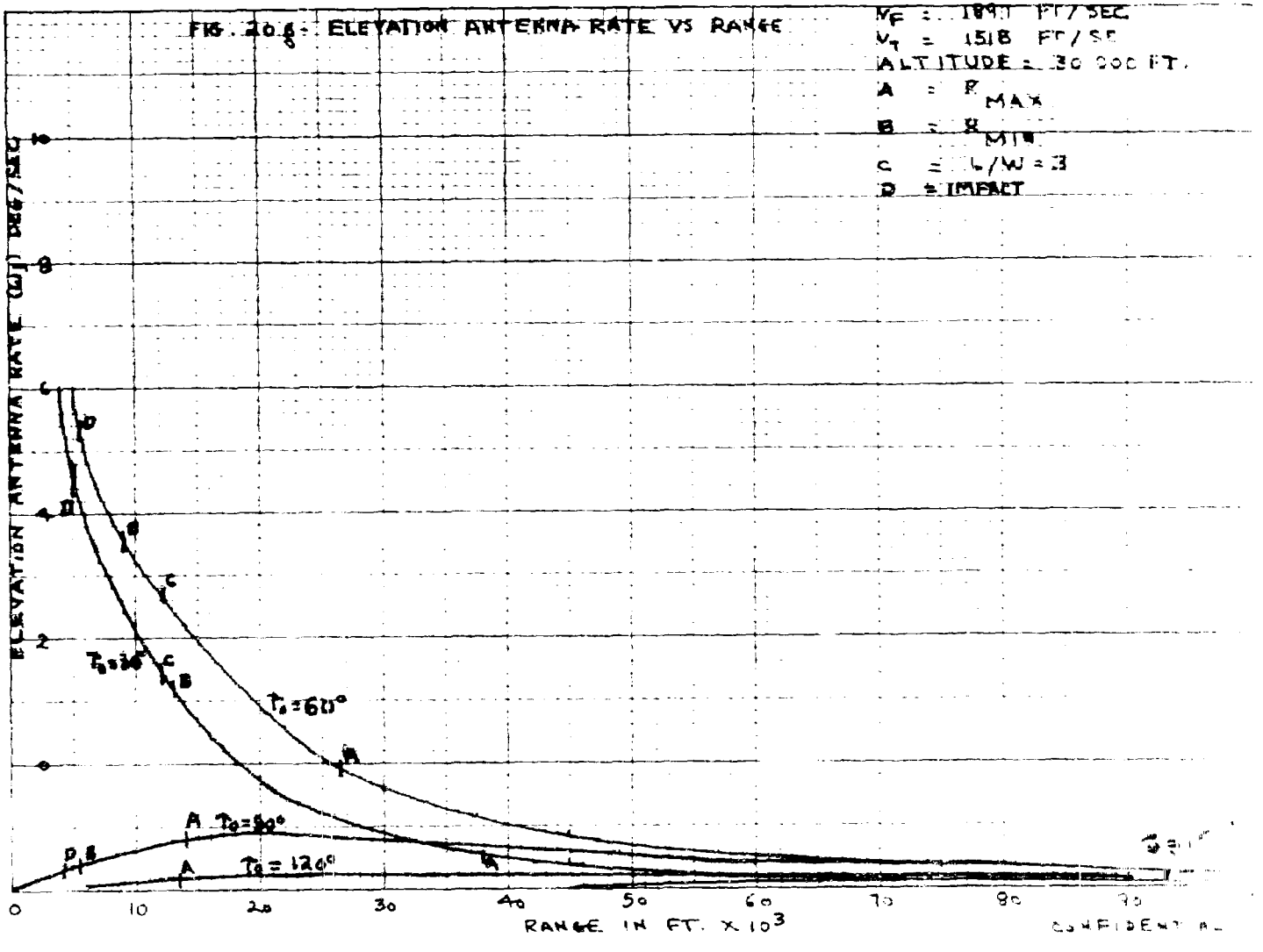
FIG. 20.6 - ELEVATION ANTENNA RATE VS RANGE
V_F = 1891 FT/SEC
V_T = 1518 FT/SEC
ALTITUDE = 30 000 FT.
A = R_{MAX}
B = R_{MIN}
C = L/W = 3
D = IMPACT
ELEVATION ANTENNA RATE (ω) DEG/SEC
RANGE IN FT. X 10^3
T_0=60°
T_0=90°
T_0=120°
0
10
20
30
40
50
60
70
80
90

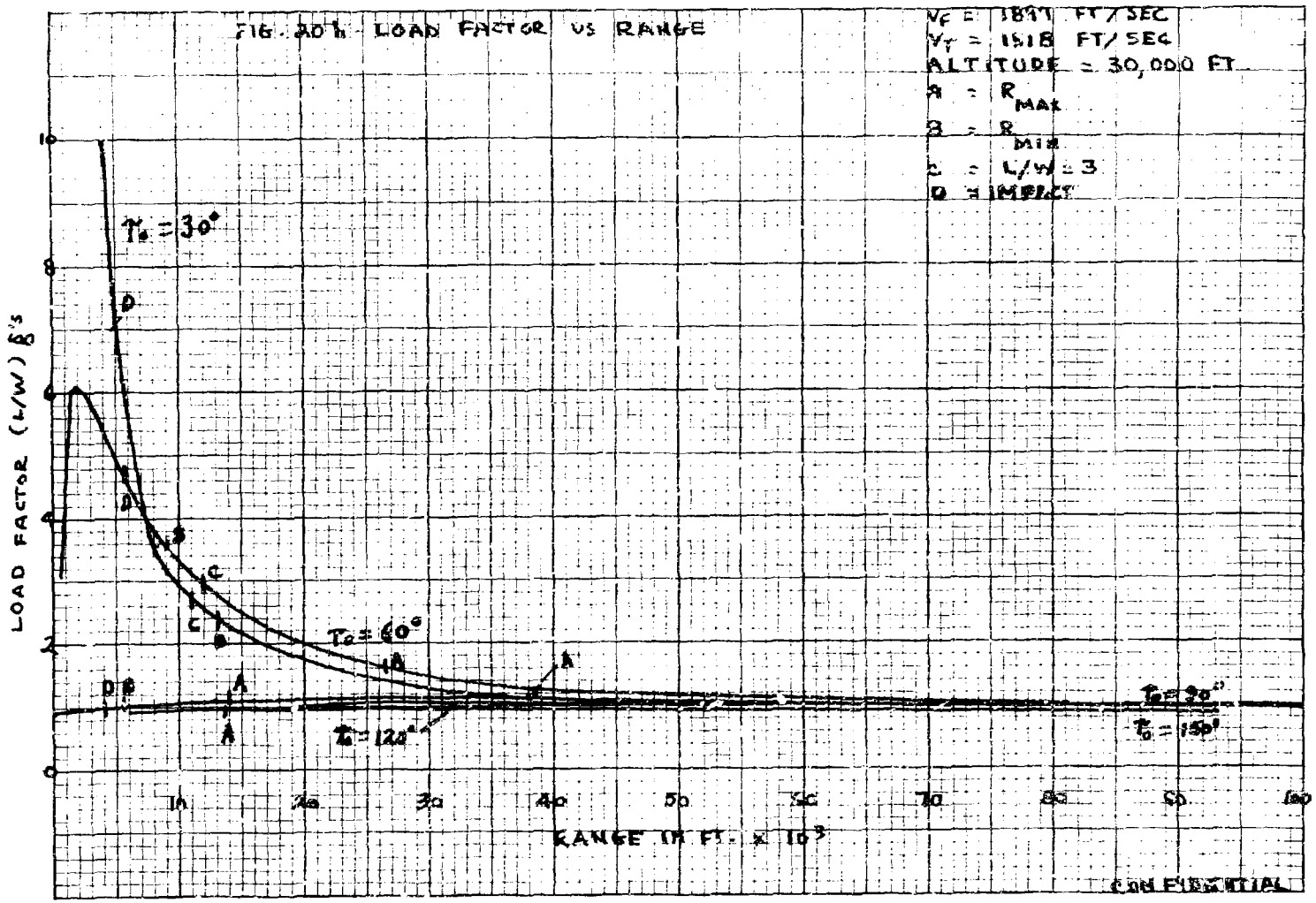
FIG. 20 h - LOAD FACTOR VS RANGE
V_F = 1897 FT/SEC
V_T = 1518 FT/SEC
ALTITUDE = 30,000 FT
A = R_{MAX}
B = R_{MIN}
C = L/W = 3
D = IMPACT
$\gamma_0 = 30°$
$\gamma_0 = 60°$
$\gamma_0 = 120°$
$\gamma_0 = 90°$
$\gamma_0 = 150°$
LOAD FACTOR (L/W) G's
RANGE IN FT. x 10^3
CONFIDENTIAL

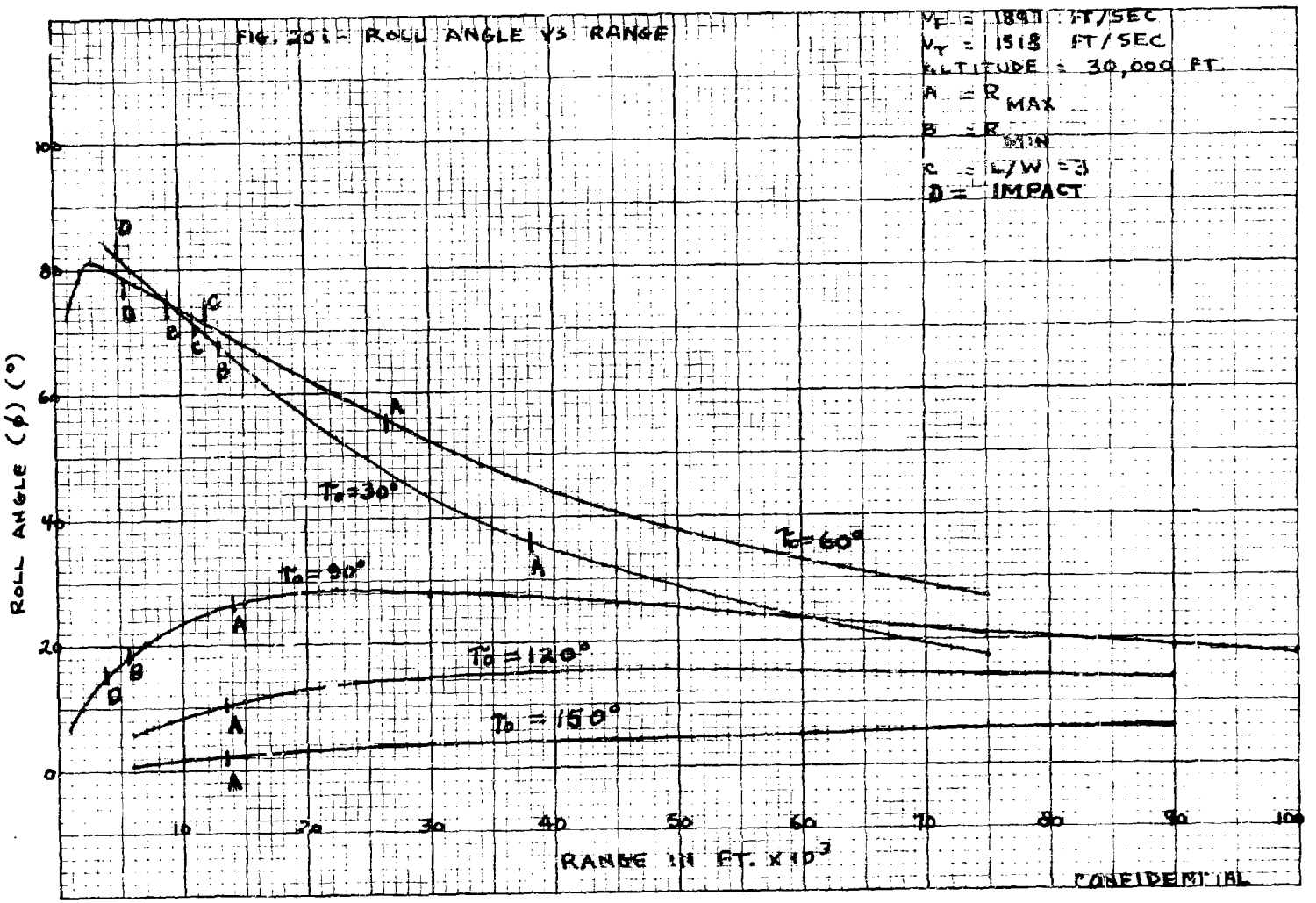
FIG. 201 - ROLL ANGLE VS RANGE
V_F = 1891 FT/SEC
V_T = 1518 FT/SEC
ALTITUDE = 30,000 FT.
A = R_{MAX}
B = R_{MIN}
C = L/W = 3
D = IMPACT
ROLL ANGLE (φ) (°)
RANGE IN FT. X 10^3
T_D=30°
T_D=60°
T_D=90°
T_D=120°
T_D=150°
CONFIDENTIAL

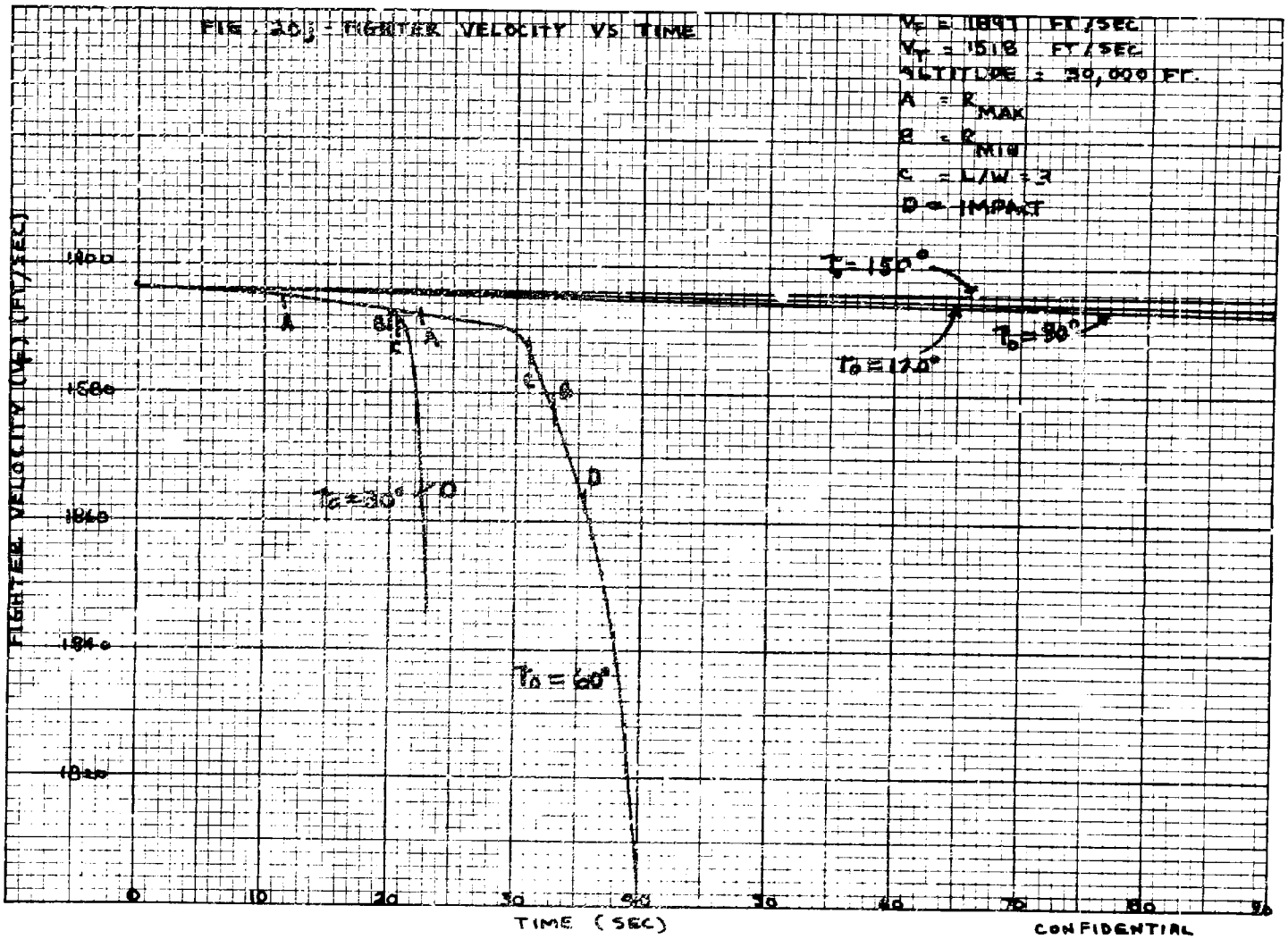
FIG. 20 - FIGHTER VELOCITY VS TIME
V_F = 1189 FT/SEC
V_T = 1518 FT/SEC
ALTITUDE = 30,000 FT.
A = R_{MAX}
B = R_{MIN}
C = L/W = 3
D = IMPACT
τ_c = 150°
τ_D = 90°
τ_D = 120°
τ_D = 30°
τ_D = 60°
FIGHTER VELOCITY (V_F) (FT/SEC)
1400
1560
1840
1840
1800
0
10
20
30
40
50
60
70
80
90
TIME (SEC)
CONFIDENTIAL

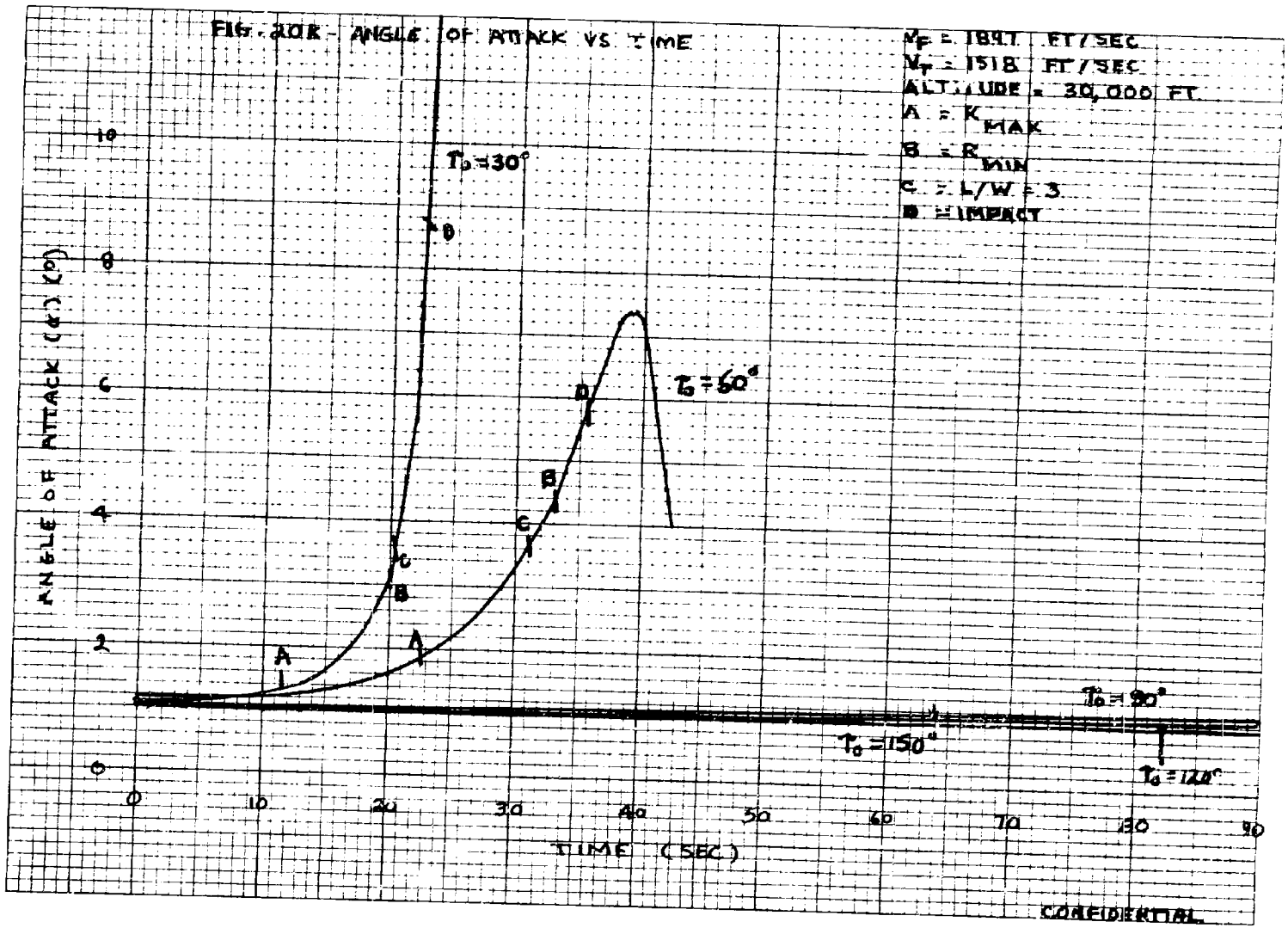
FIG. 20K - ANGLE OF ATTACK VS TIME
V_F = 1847 FT/SEC
V_T = 1518 FT/SEC
ALTITUDE = 30,000 FT
A = K_{MAX}
B = R_{MIN}
C = L/W = 3
D = IMPACT
T_0 = 30°
T_0 = 60°
T_0 = 90°
T_0 = 120°
T_0 = 150°
ANGLE OF ATTACK (α) (°)
TIME (SEC)
0
2
4
6
8
10
20
30
40
50
60
70
80
90
A
B
C
D
CONFIDENTIAL

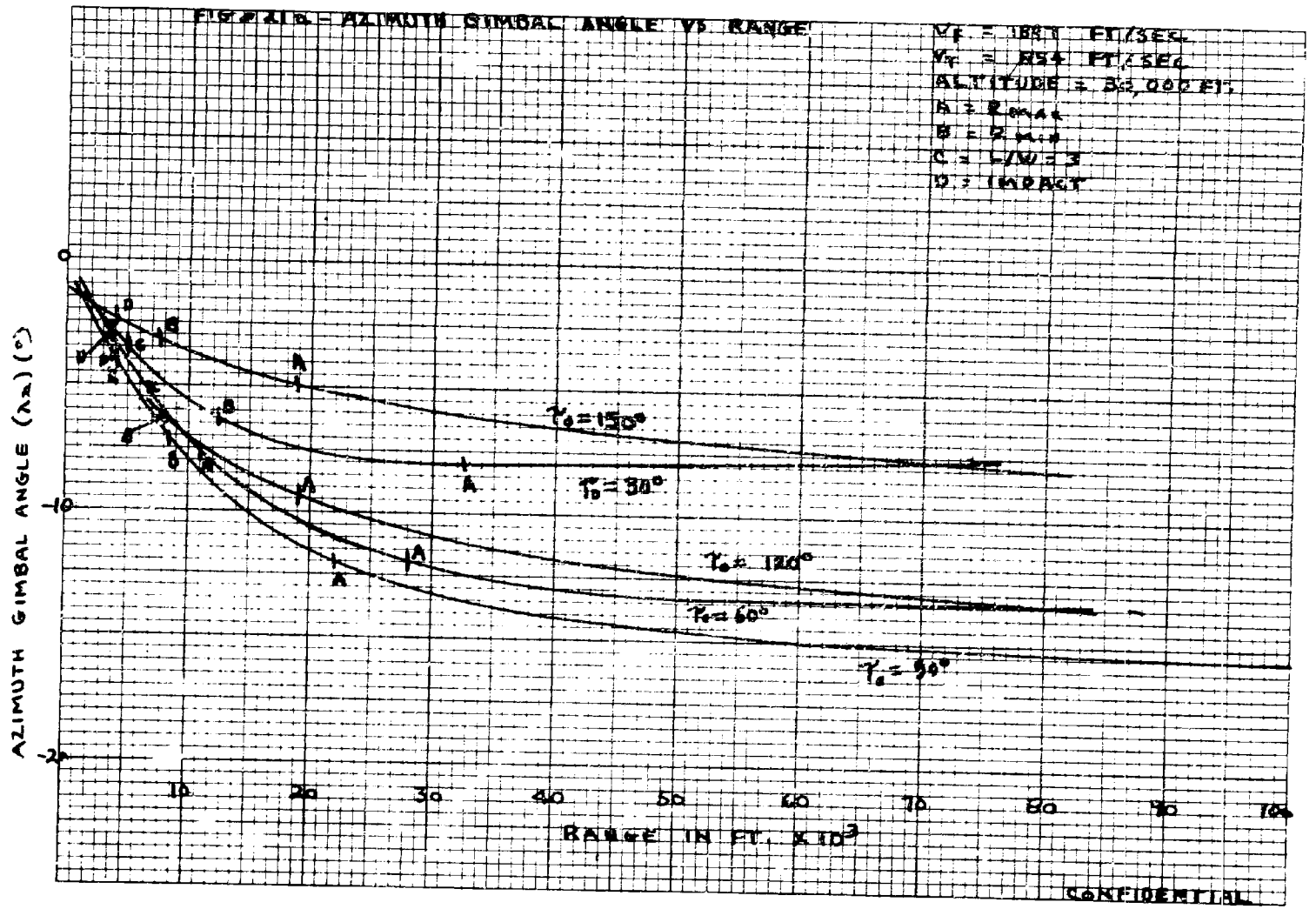
FIGURE 21b - AZIMUTH GIMBAL ANGLE VS RANGE
V_F = 1881 FT/SEC
V_T = 854 FT/SEC
ALTITUDE = 32,000 FT.
A = Rmax
B = Rmin
C = L/W = 3
D = IMPACT
γ_o = 150°
γ_o = 90°
γ_o = 120°
γ_o = 60°
γ_o = 30°
AZIMUTH GIMBAL ANGLE (λ_a) (°)
0
-10
-20
10
20
30
40
50
60
70
80
90
100
RANGE IN FT. X 10^3
CONFIDENTIAL

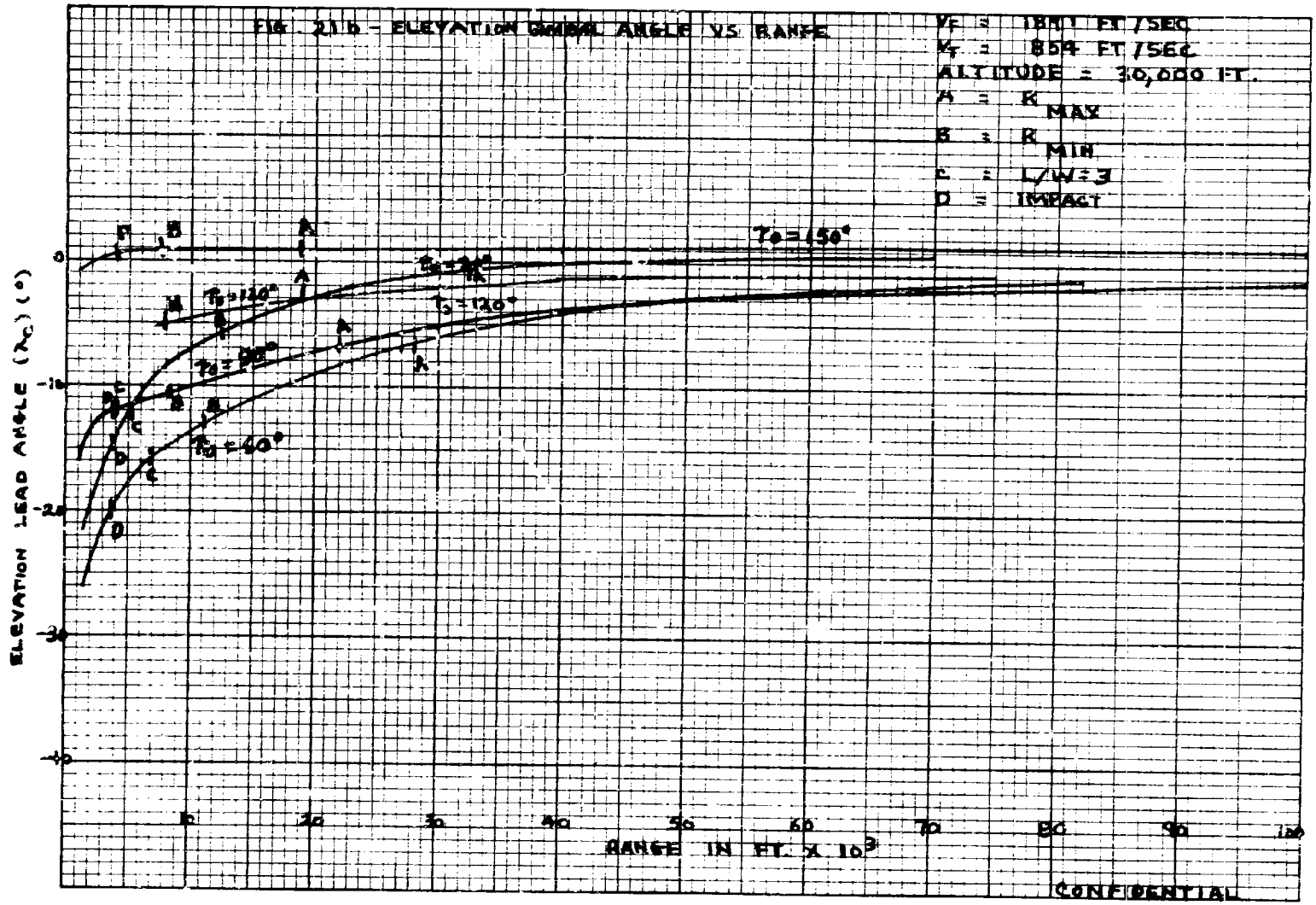
FIG. 21b - ELEVATION GIMBAL ANGLE VS RANGE
V_F = 1811 FT/SEC
V_T = 859 FT/SEC
ALTITUDE = 30,000 FT.
A = R MAX
B = R MIN
C = L/W=3
D = IMPACT
T_θ=150°
T_θ=120°
T_θ=90°
T_θ=60°
T_θ=40°
ELEVATION LEAD ANGLE (λ_G) (°)
0
-10
-20
-30
-40
10
20
30
40
50
60
70
80
90
100
RANGE IN FT. X 10^3
CONFIDENTIAL

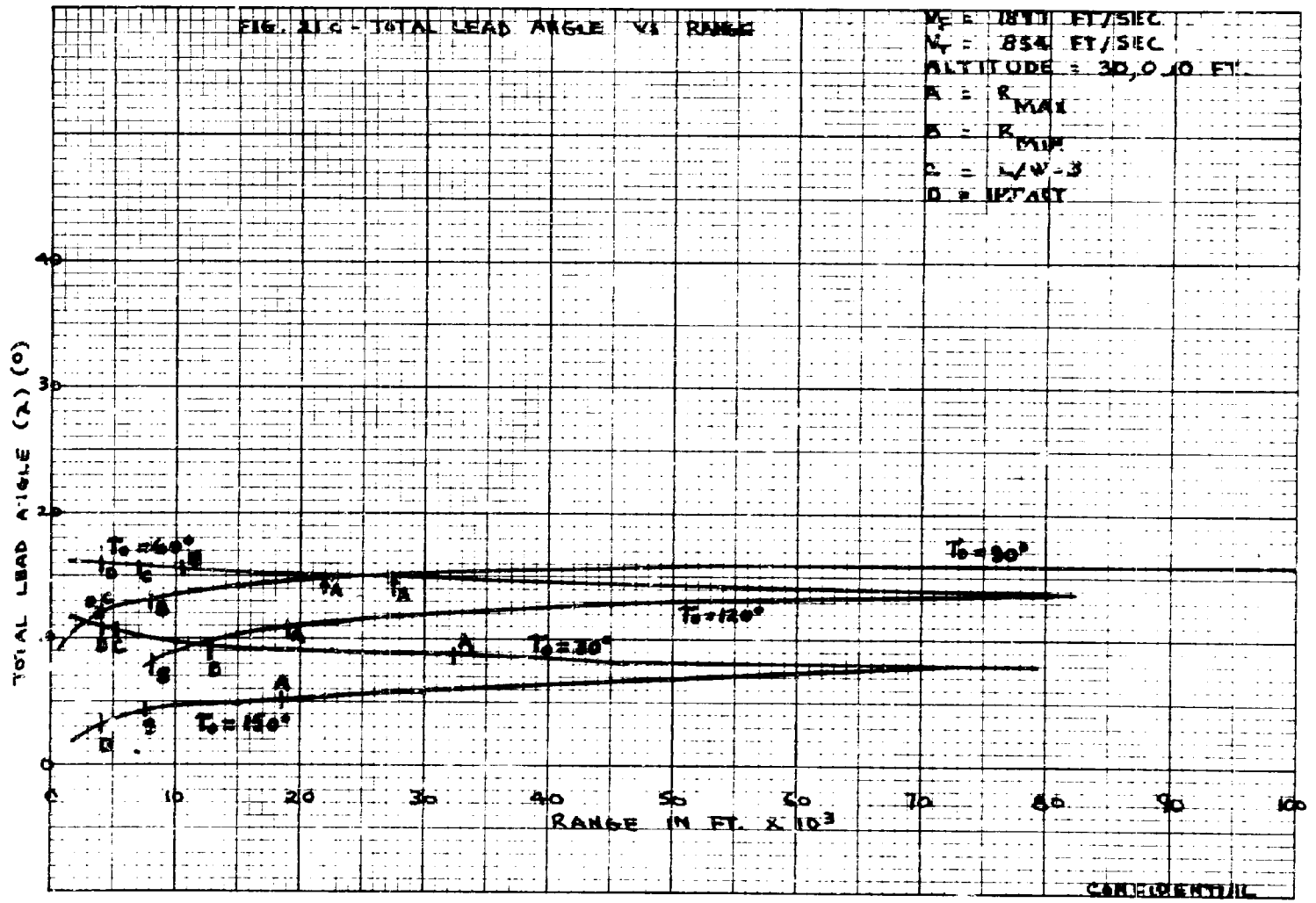
FIG. 21 C - TOTAL LEAD ANGLE VS RANGE
V_F = 1811 FT/SEC
V_T = 854 FT/SEC
ALTITUDE = 30,000 FT
A = R_{MAX}
B = R_{MIN}
C = L/W-3
D = IMPACT
TOTAL LEAD ANGLE (λ) (°)
RANGE IN FT. X 10^3
T_0 = 60°
T_0 = 90°
T_0 = 120°
T_0 = 30°
T_0 = 150°
CONFIDENTIAL

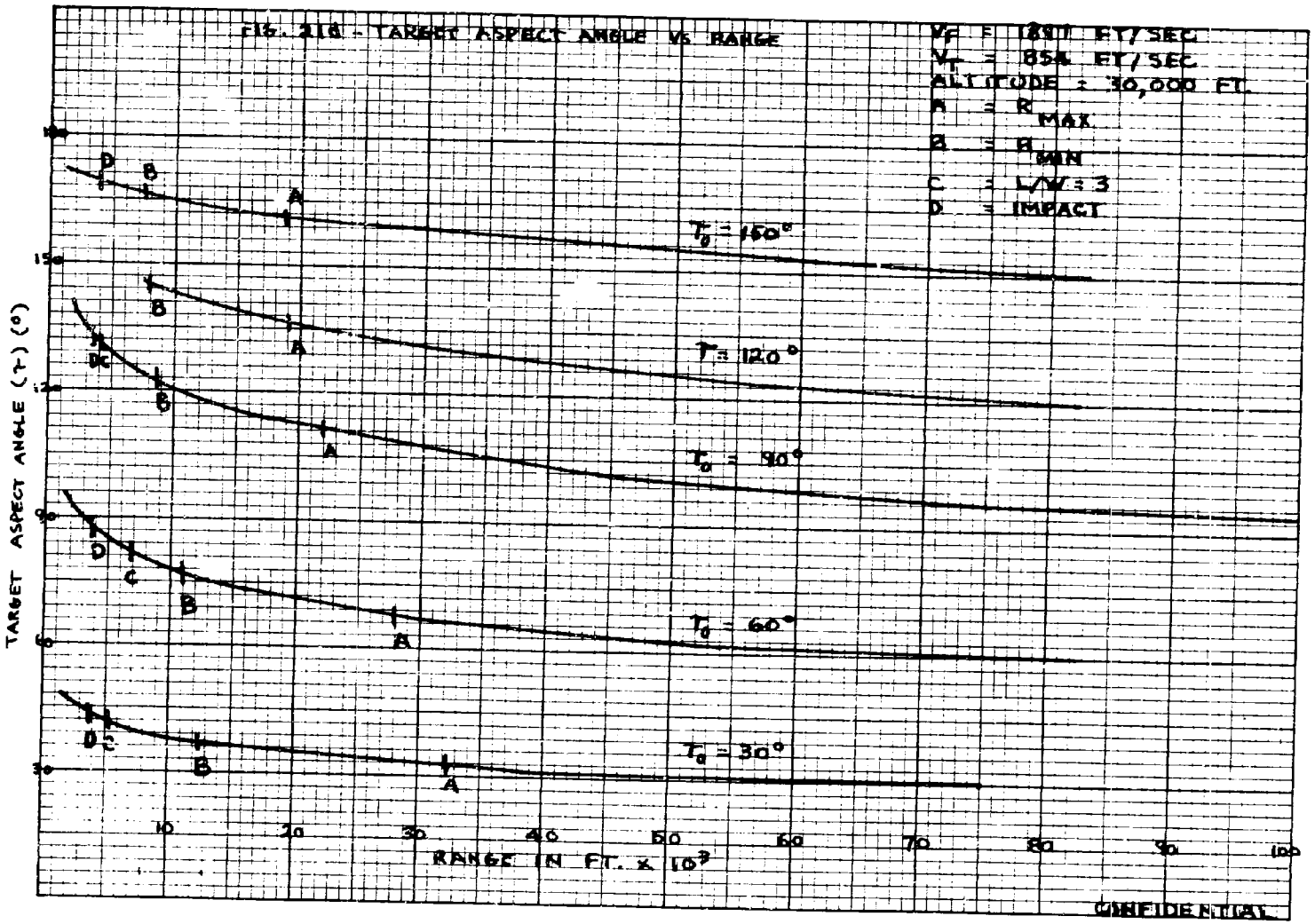
FIG. 21B - TARGET ASPECT ANGLE VS RANGE
V_F = [illegible] FT/SEC.
V_T = 854 FT/SEC.
ALTITUDE = 30,000 FT.
A = R_{MAX}
B = R_{MIN}
C = L/V = 3
D = IMPACT
T_0 = 150°
T_0 = 120°
T_0 = 90°
T_0 = 60°
T_0 = 30°
TARGET ASPECT ANGLE (T) (°)
RANGE IN FT. x 10^3
CONFIDENTIAL

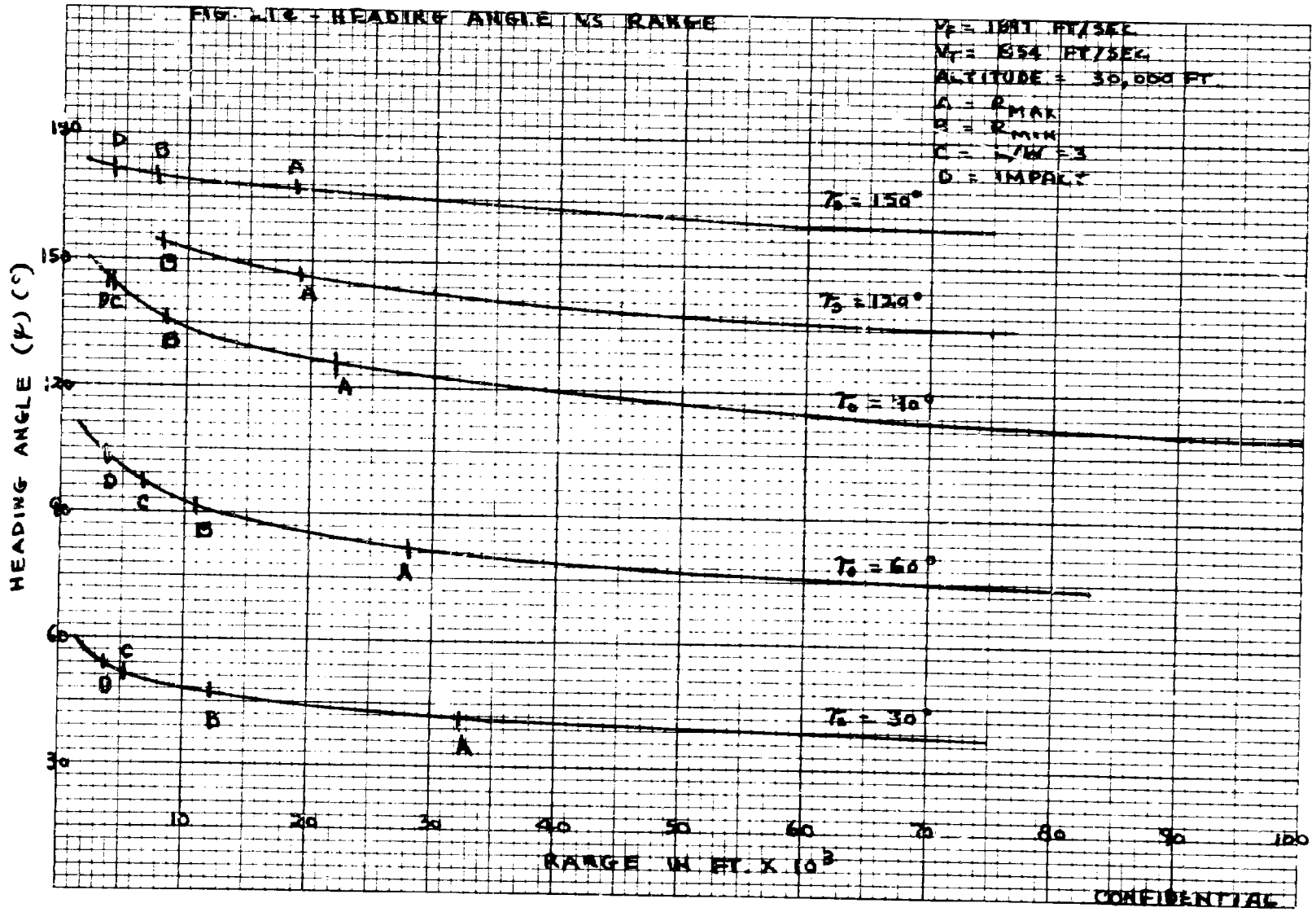
FIG. 11c - HEADING ANGLE VS RANGE
V_P = 1081 FT/SEC
V_T = 854 FT/SEC
ALTITUDE = 30,000 FT
A = R_{MAX}
B = R_{MIN}
C = λ/W = 3
D = IMPACT
T_0 = 150°
T_0 = 120°
T_0 = 90°
T_0 = 60°
T_0 = 30°
HEADING ANGLE (Ψ) (°)
RANGE IN FT. X 10^3
CONFIDENTIAL

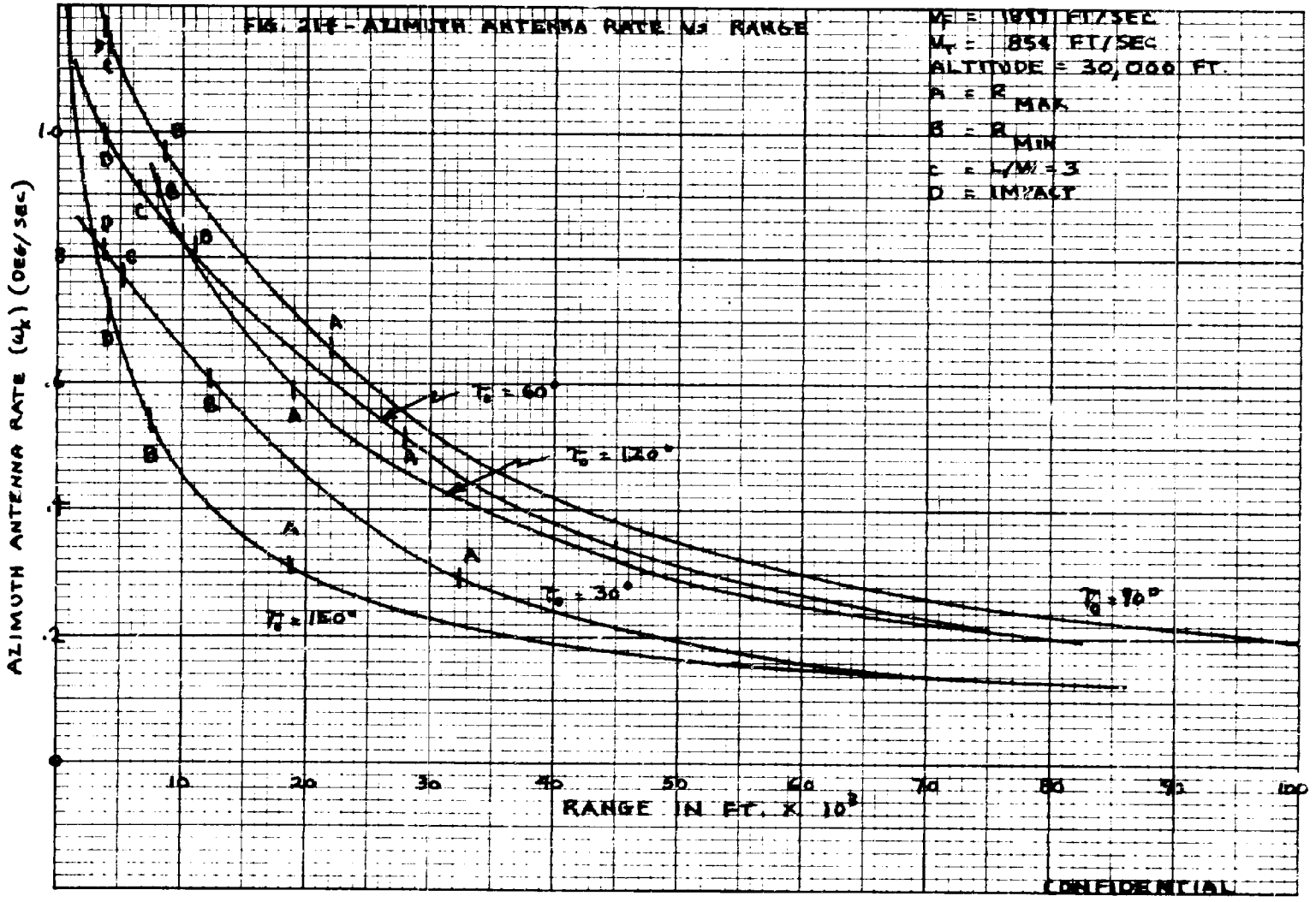
FIG. 21F - AZIMUTH ANTENNA RATE VS RANGE
V_F = 1851 FT/SEC
V_T = 854 FT/SEC
ALTITUDE = 30,000 FT.
A = R MAX.
B = R MIN
C = L/M = 3
D = IMPACT
T_0 = 60°
T_0 = 120°
T_0 = 30°
T_0 = 150°
T_0 = 90°
AZIMUTH ANTENNA RATE (ω_k) (DEG/SEC)
RANGE IN FT. X 10^3
CONFIDENTIAL

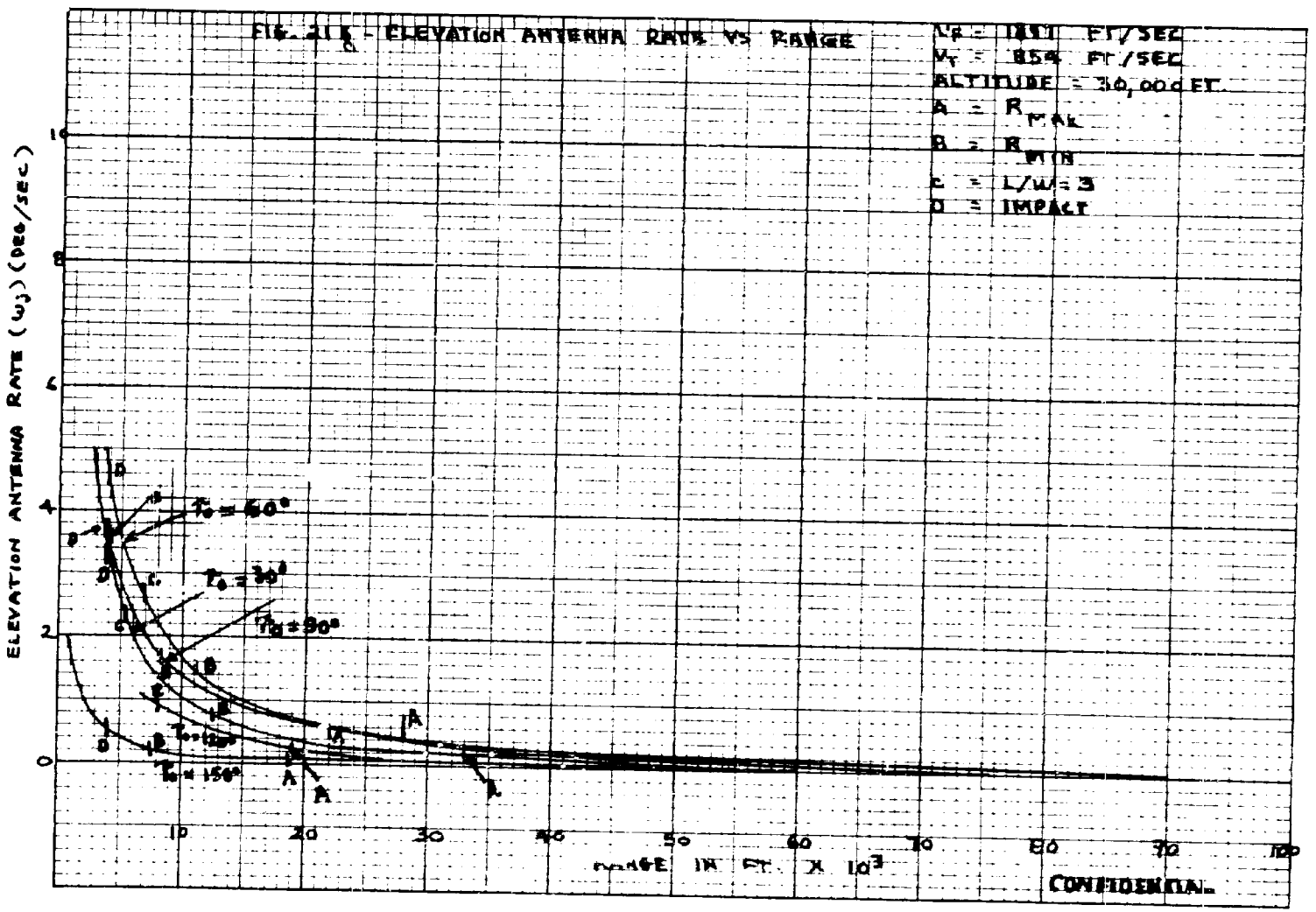
FIG. 21 b - ELEVATION ANTENNA RATE VS RANGE
V_F = 1851 FT/SEC
V_T = 854 FT/SEC
ALTITUDE = 30,000 FT.
A = R_{MAX}
B = R_{MIN}
C = L/W = 3
D = IMPACT
ELEVATION ANTENNA RATE (ω_3) (DEG/SEC)
γ_0 = 60°
γ_0 = 30°
γ_0 = 90°
γ_0 = 120°
γ_0 = 150°
RANGE IN FT. X 10^3
CONFIDENTIAL

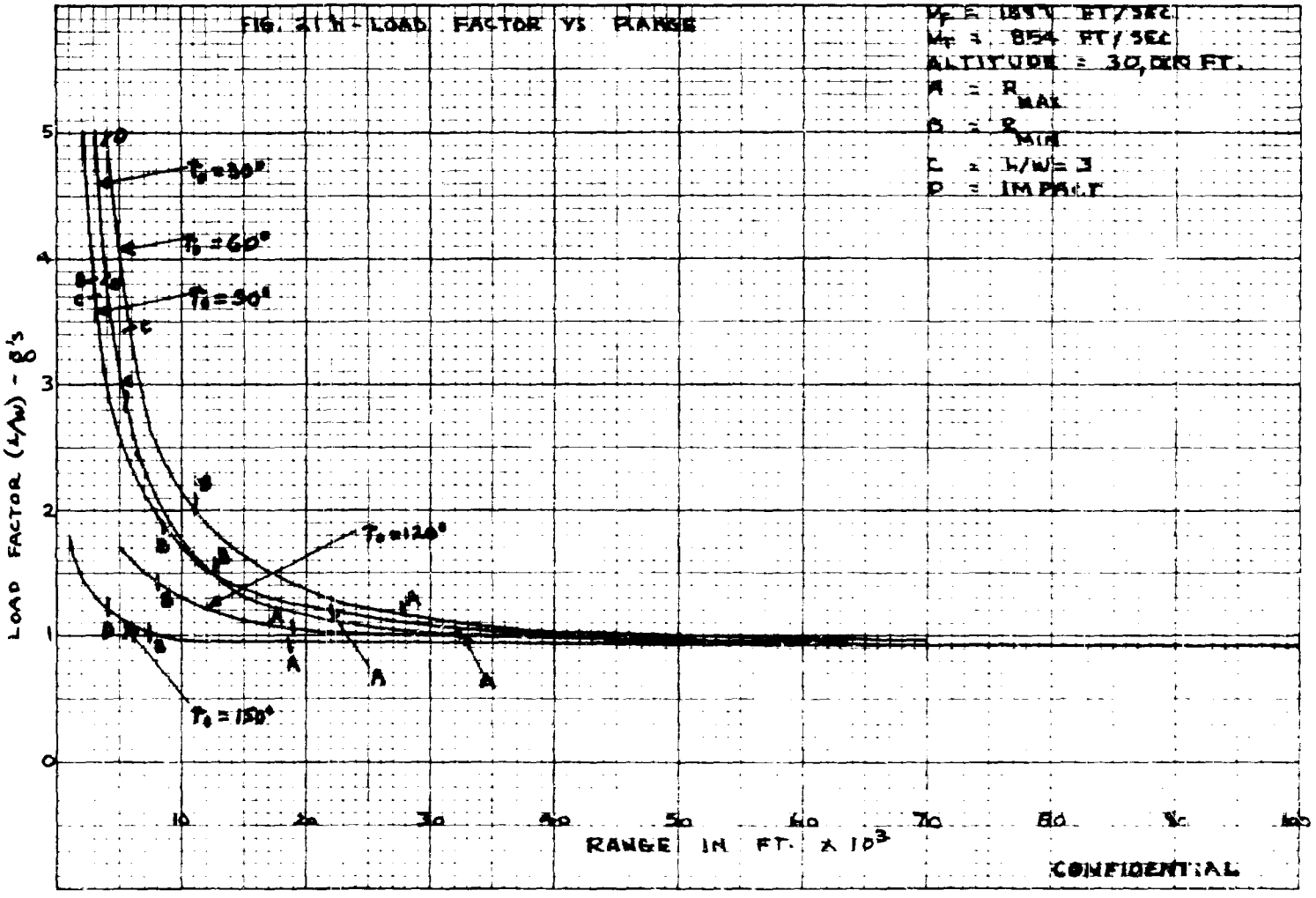
FIG. 21 h - LOAD FACTOR VS RANGE
V_F = 1897 FT/SEC
V_M = 854 FT/SEC
ALTITUDE = 30,000 FT.
A = R_{MAX}
B = R_{MIN}
C = h/w = 3
D = IMPACT
T_0 = 30°
T_0 = 60°
T_0 = 90°
T_0 = 120°
T_0 = 150°
LOAD FACTOR (L/W) - G'S
RANGE IN FT. X 10^3
CONFIDENTIAL

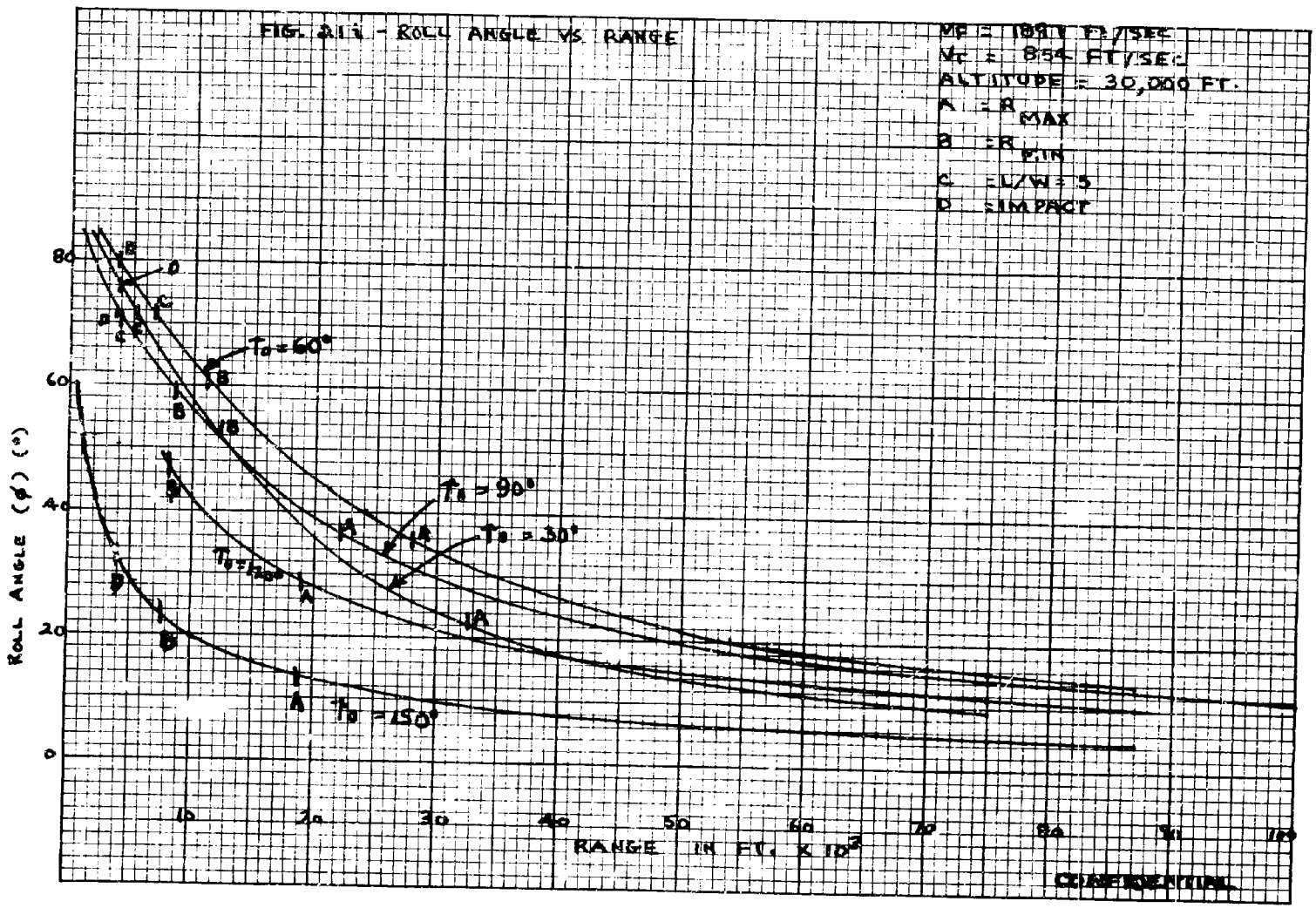
FIG. 21 - ROLL ANGLE VS RANGE
V_F = 1891 FT/SEC
V_T = 854 FT/SEC
ALTITUDE = 30,000 FT.
A = R_{MAX}
B = R_{MIN}
C = L/W = 5
D = IMPACT
$T_\theta = 60°$
$T_\theta = 90°$
$T_\theta = 30°$
$T_\theta = 150°$
ROLL ANGLE (ϕ) (°)
RANGE IN FT. X 10^3
CONFIDENTIAL

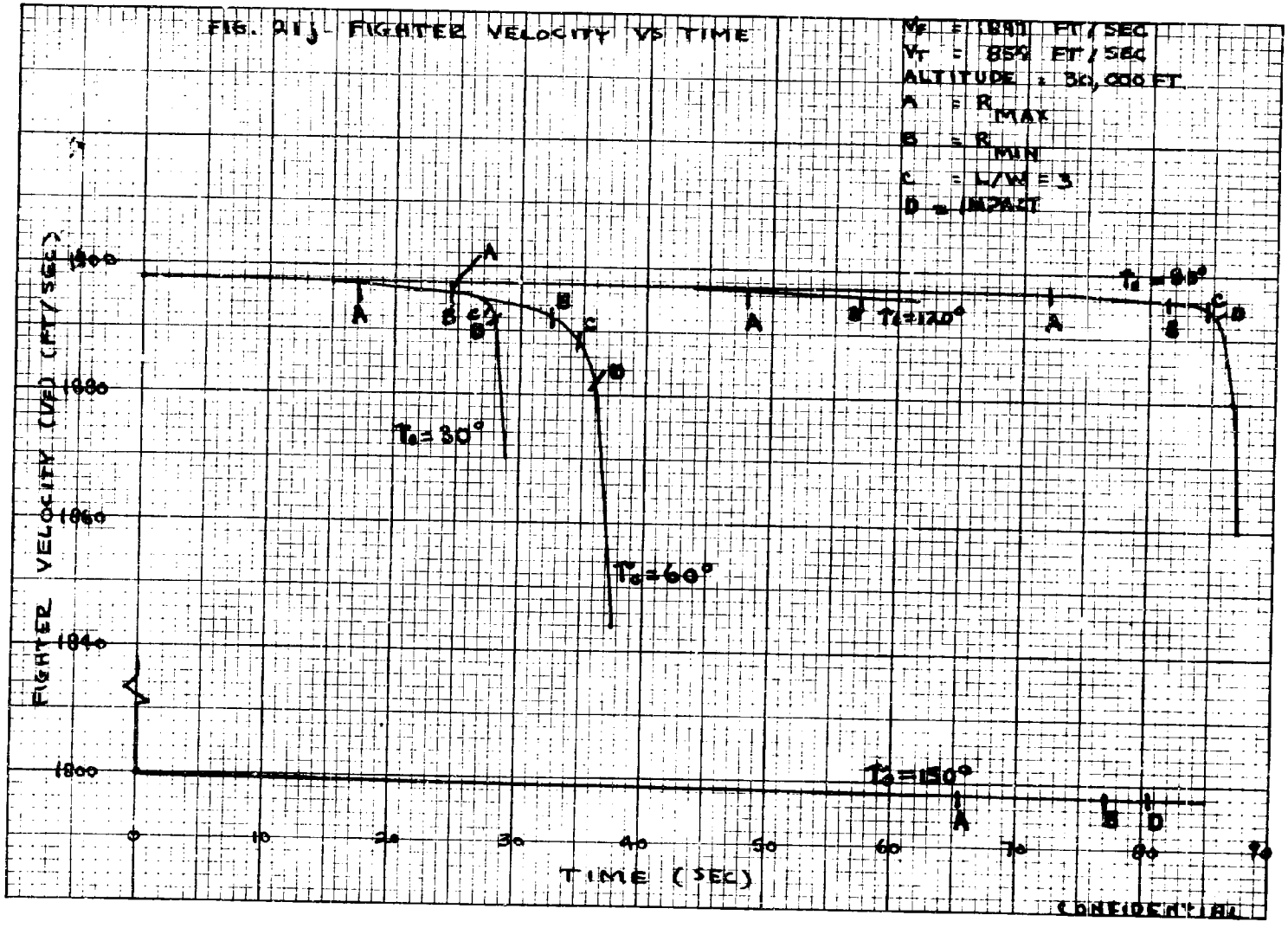
FIG. 21j - FIGHTER VELOCITY VS TIME
V_M = 1881 FT/SEC
V_T = 856 FT/SEC
ALTITUDE = 36,000 FT
A = R_{MAX}
B = R_{MIN}
C = L/W = 3
D = IMPACT
FIGHTER VELOCITY (V_F) (FT/SEC)
1900
1880
1860
1840
1800
TIME (SEC)
0
10
20
30
40
50
60
70
80
90
T_d = 30°
T_d = 60°
T_d = 120°
T_d = 150°
T_d = 90°
A
B
C
D
CONFIDENTIAL

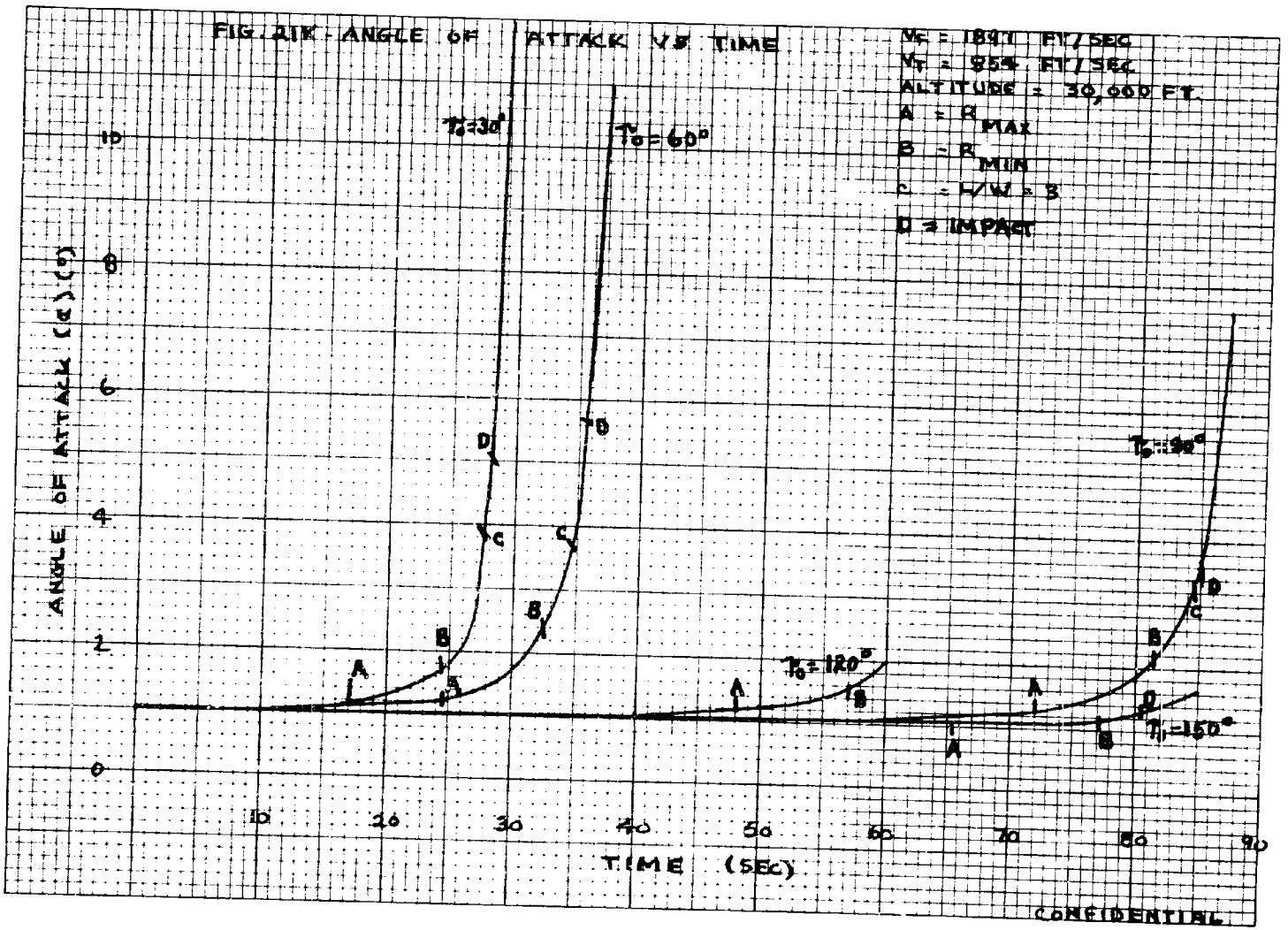
FIG. 21K - ANGLE OF ATTACK VS TIME
V_E = 18971 FT/SEC
V_T = 9554 FT/SEC
ALTITUDE = 30,000 FT.
A = R_{MAX}
B = R_{MIN}
C = H/W = 3
D = IMPACT
γ_0=30°
γ_0=60°
γ_0=90°
γ_0=120°
γ_0=150°
ANGLE OF ATTACK (α) (°)
TIME (SEC)
0
2
4
6
8
10
10
20
30
40
50
60
70
80
90
CONFIDENTIAL

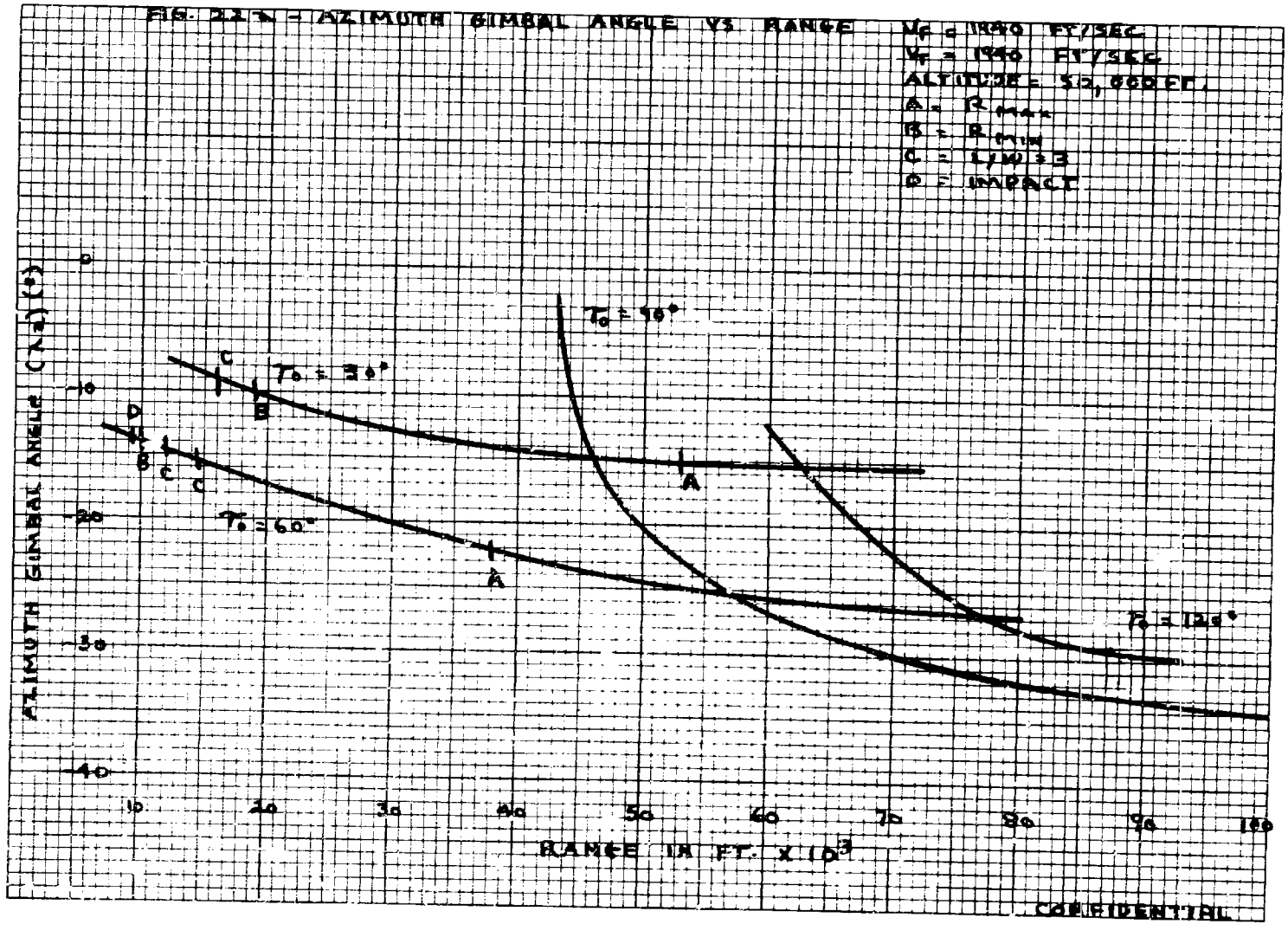
FIG. 22 N - AZIMUTH GIMBAL ANGLE VS RANGE
V_C = 1440 FT/SEC.
V_T = 1440 FT/SEC.
ALTITUDE = 52,000 FT.
A = R max.
B = R min
C = t/m = 3
D = IMPACT
AZIMUTH GIMBAL ANGLE (Na)(°)
RANGE IN FT. X 10^3
T_o = 90°
T_o = 30°
T_o = 60°
T_o = 120°
A
B
C
D
0
-10
-20
-30
-40
10
20
30
40
50
60
70
80
90
100
CONFIDENTIAL

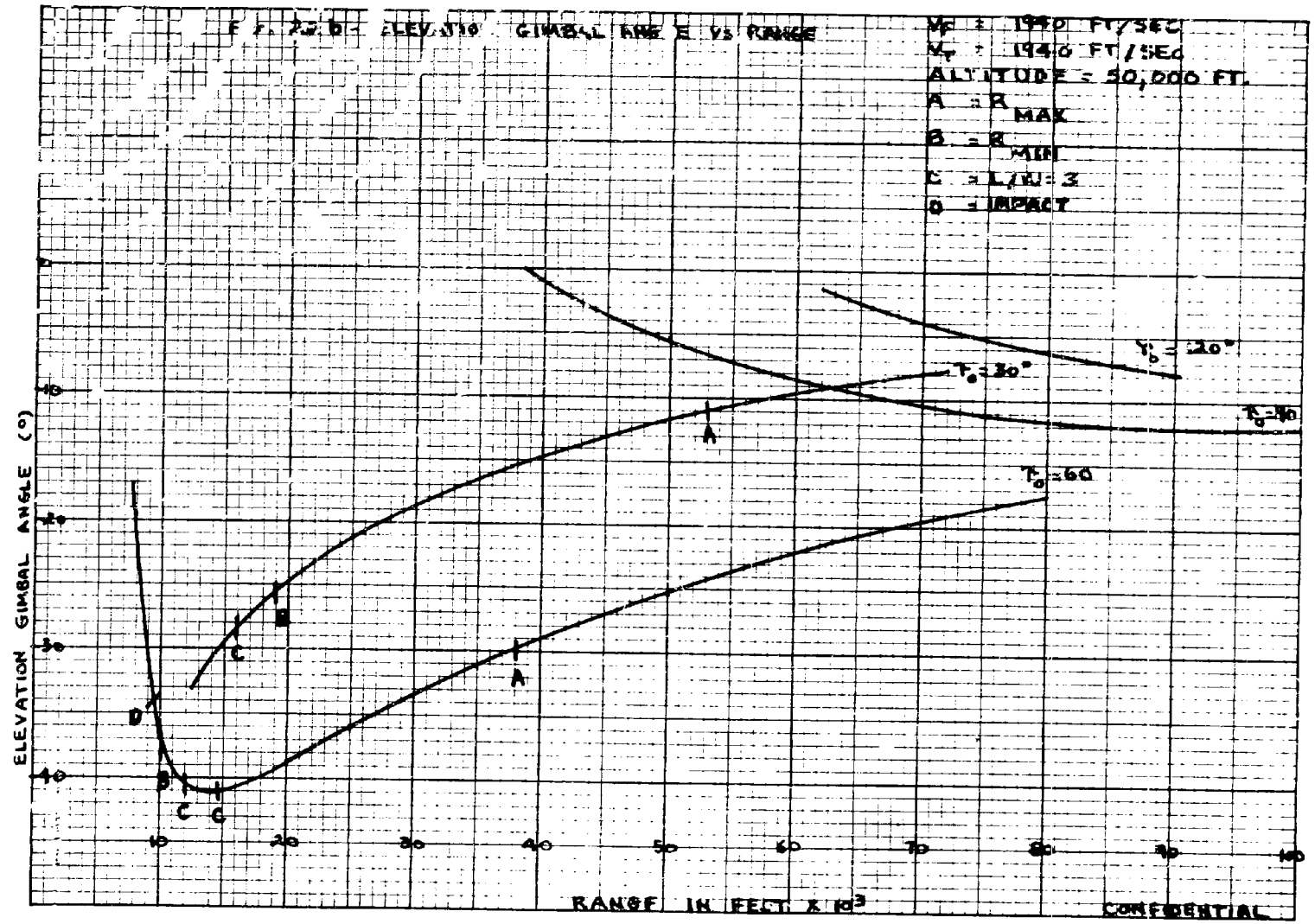
F.F. 2-D ELEVATION GIMBAL ANGLE VS RANGE
V_F = 1990 FT/SEC
V_T = 1946 FT/SEC
ALTITUDE = 50,000 FT.
A = R_{MAX}
B = R_{MIN}
C = L/D = 3
D = IMPACT
γ_b = -20°
γ_b = -30°
γ_b = -60
ELEVATION GIMBAL ANGLE (°)
RANGE IN FEET X 10^3
CONFIDENTIAL

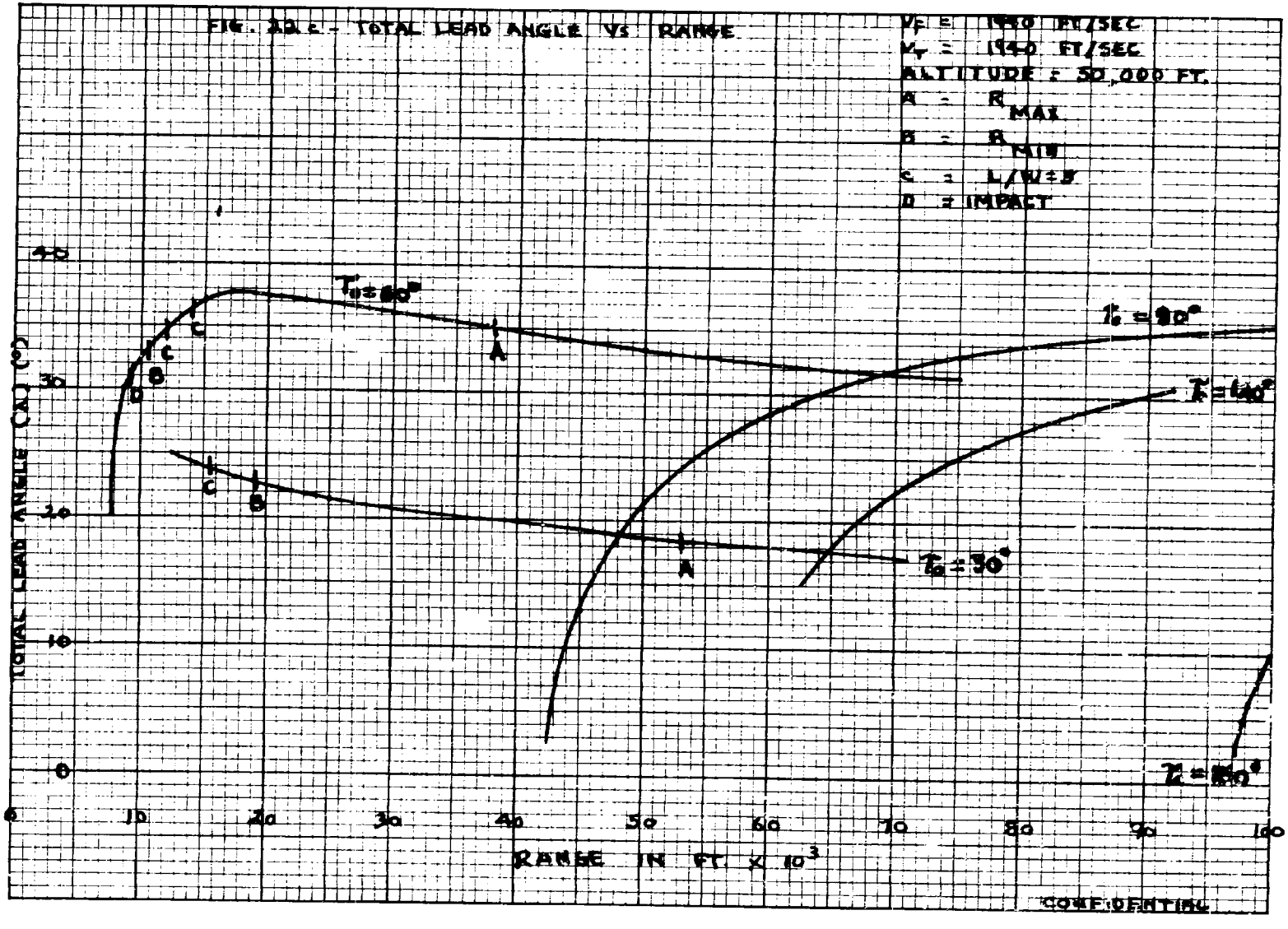
FIG. 22 c - TOTAL LEAD ANGLE VS RANGE
V_F = 1980 FT/SEC
V_T = 1940 FT/SEC
ALTITUDE = 50,000 FT.
A = R_{MAX}
B = R_{MIN}
C = L/W = 5
D = IMPACT
$T_0 = 90°$
$T_0 = 60°$
$T_0 = 30°$
A
B
C
D
TOTAL LEAD ANGLE (A.L.) (°)
40
30
20
10
0
0
10
20
30
40
50
60
70
80
90
100
RANGE IN FT. X 10^3
CONFIDENTIAL

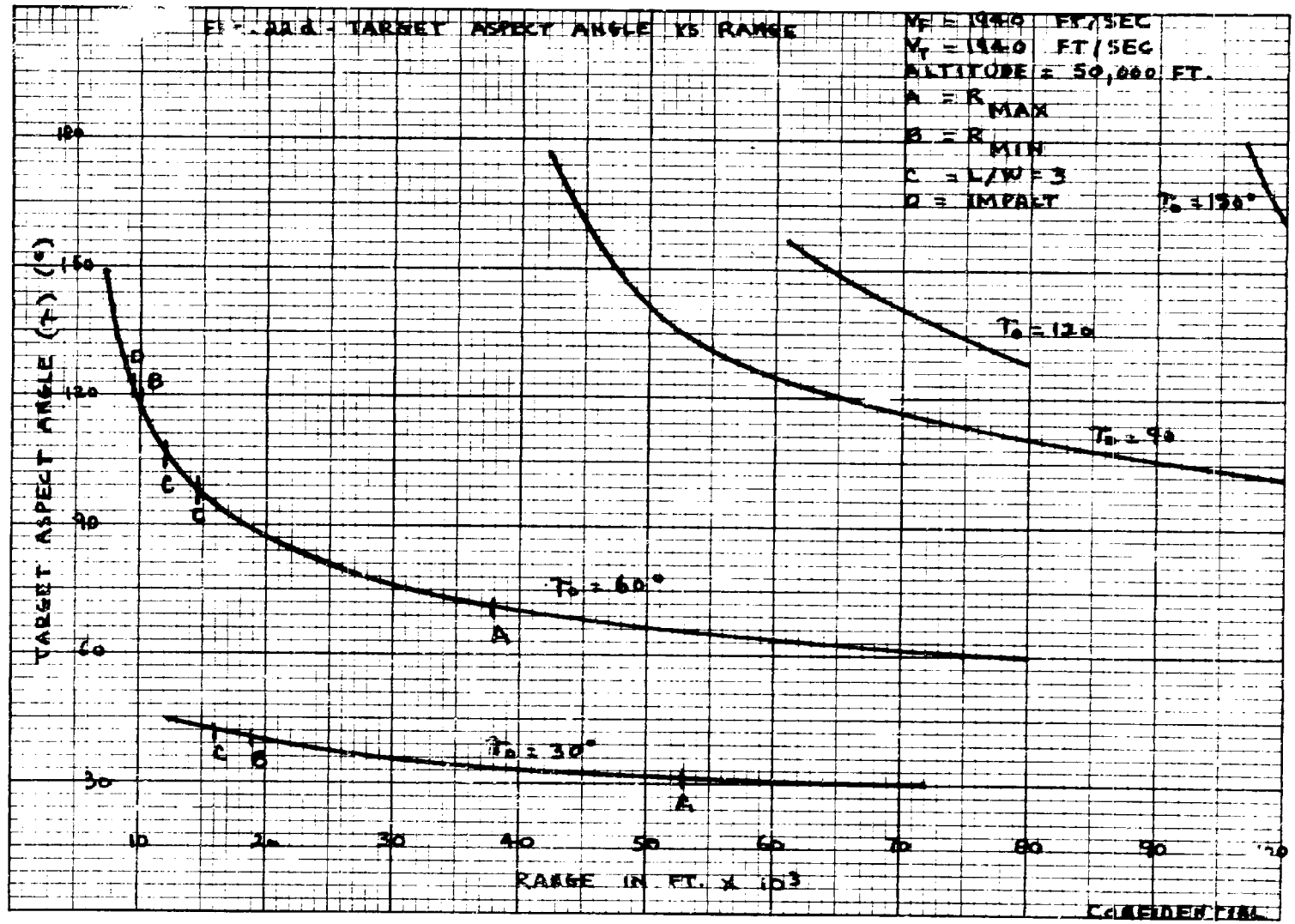
FIG. 22 d - TARGET ASPECT ANGLE VS RANGE
V_F = 1940 FT/SEC
V_T = 1540 FT/SEC
ALTITUDE = 50,000 FT.
A = R_{MAX}
B = R_{MIN}
C = L/W = 3
D = IMPACT
T_0 = 150°
T_0 = 120
T_0 = 90
T_0 = 60°
T_0 = 30°
TARGET ASPECT ANGLE (T) (°)
180
150
120
90
60
30
10
20
30
40
50
60
70
80
90
RANGE IN FT. x 10^3
CONFIDENTIAL

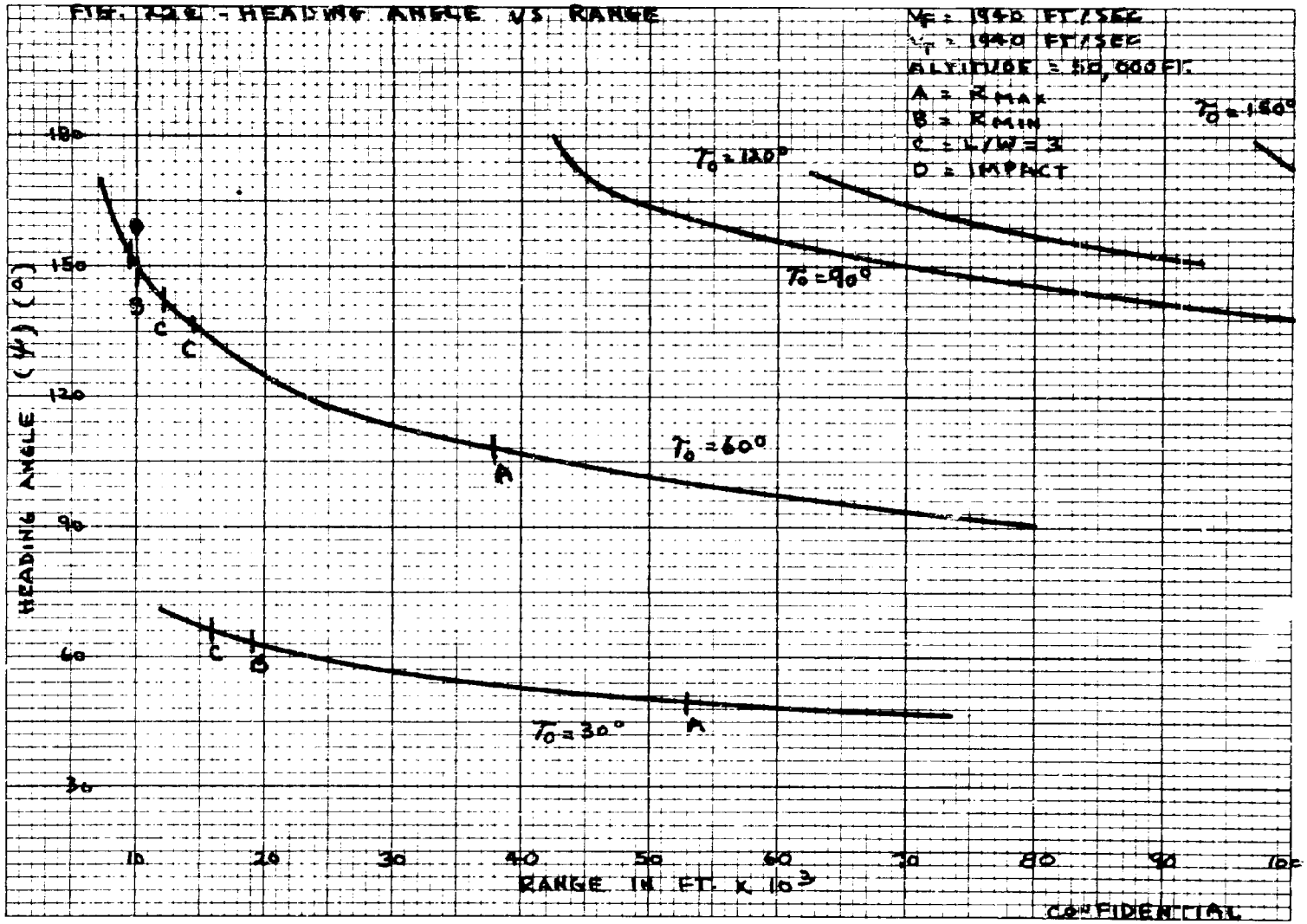
FIG. 202 - HEADING ANGLE VS RANGE
V_F = 1940 FT/SEC
V_T = 1940 FT/SEC
ALTITUDE = 50,000 FT.
A = R_{MAX}
B = R_{MIN}
C = L/W = 3
D = IMPACT
γ_0 = 150°
γ_0 = 120°
γ_0 = 90°
γ_0 = 60°
γ_0 = 30°
HEADING ANGLE (ψ) (°)
180
150
120
90
60
30
10
20
30
40
50
60
70
80
90
100
RANGE IN FT. X 10^3
CONFIDENTIAL

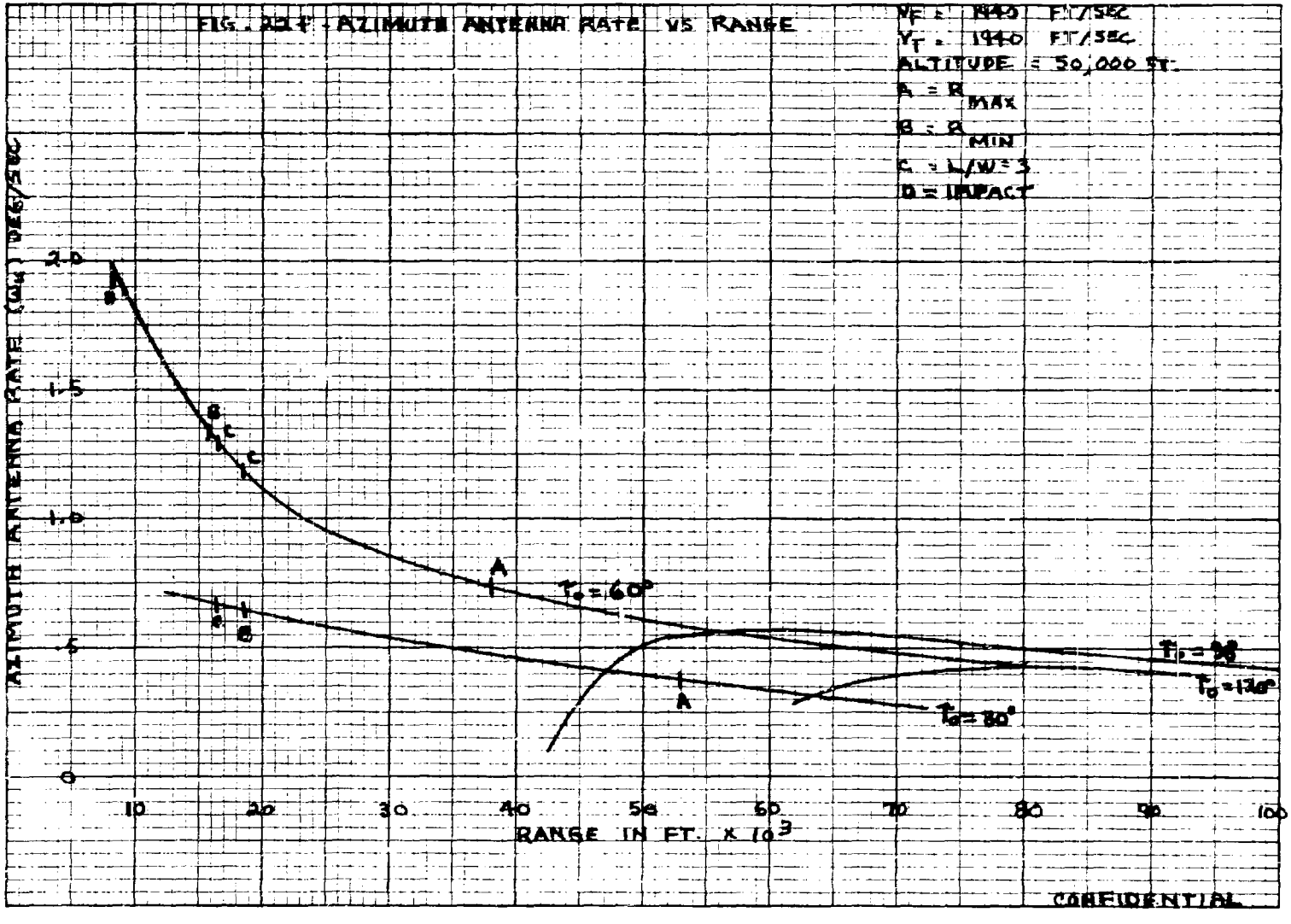
FIG. 22 f - AZIMUTH ANTENNA RATE VS RANGE
V_F = 840 FT/SEC
V_T = 1440 FT/SEC
ALTITUDE = 50,000 FT.
A = R_{MAX}
B = R_{MIN}
C = L/W = 3
D = IMPACT
AZIMUTH ANTENNA RATE (ω_A) DEG/SEC
2.0
1.5
1.0
.5
0
10
20
30
40
50
60
70
80
90
100
RANGE IN FT. X 10^3
A
B
C
D
T_θ = 60°
T_θ = 80°
T_θ = 120°
CONFIDENTIAL

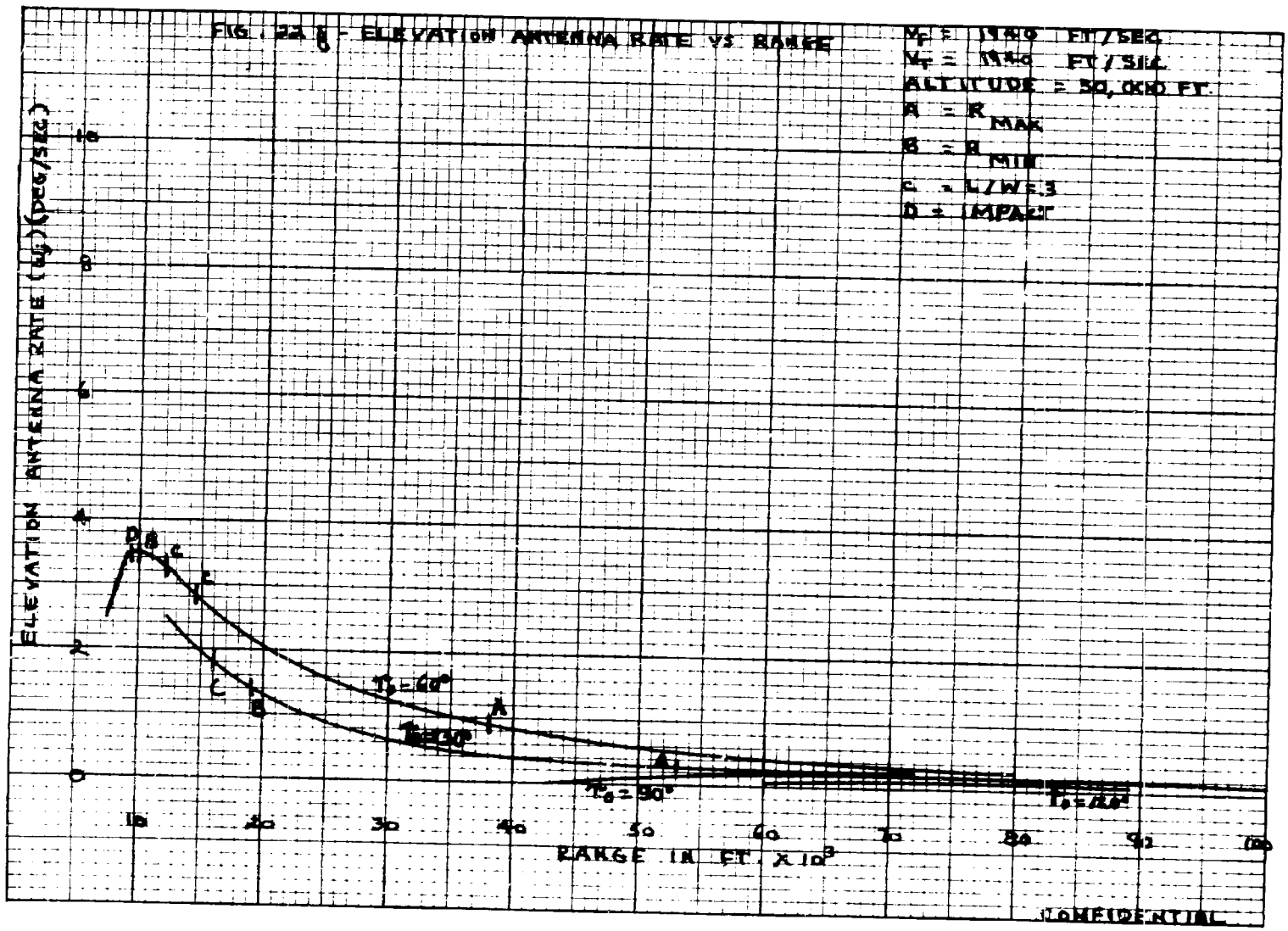
FIG. 22 - ELEVATION ANTENNA RATE VS RANGE
V_F = 1440 FT/SEC
V_T = 1440 FT/SEC
ALTITUDE = 50,000 FT
A = R_{MAX}
B = R_{MIN}
C = L/W=3
D = IMPACT
ELEVATION ANTENNA RATE ($\dot{\theta}$) (DEG/SEC)
RANGE IN FT. X 10^3
γ_0=60°
γ_0=30°
γ_0=90°
γ_0=45°
CONFIDENTIAL

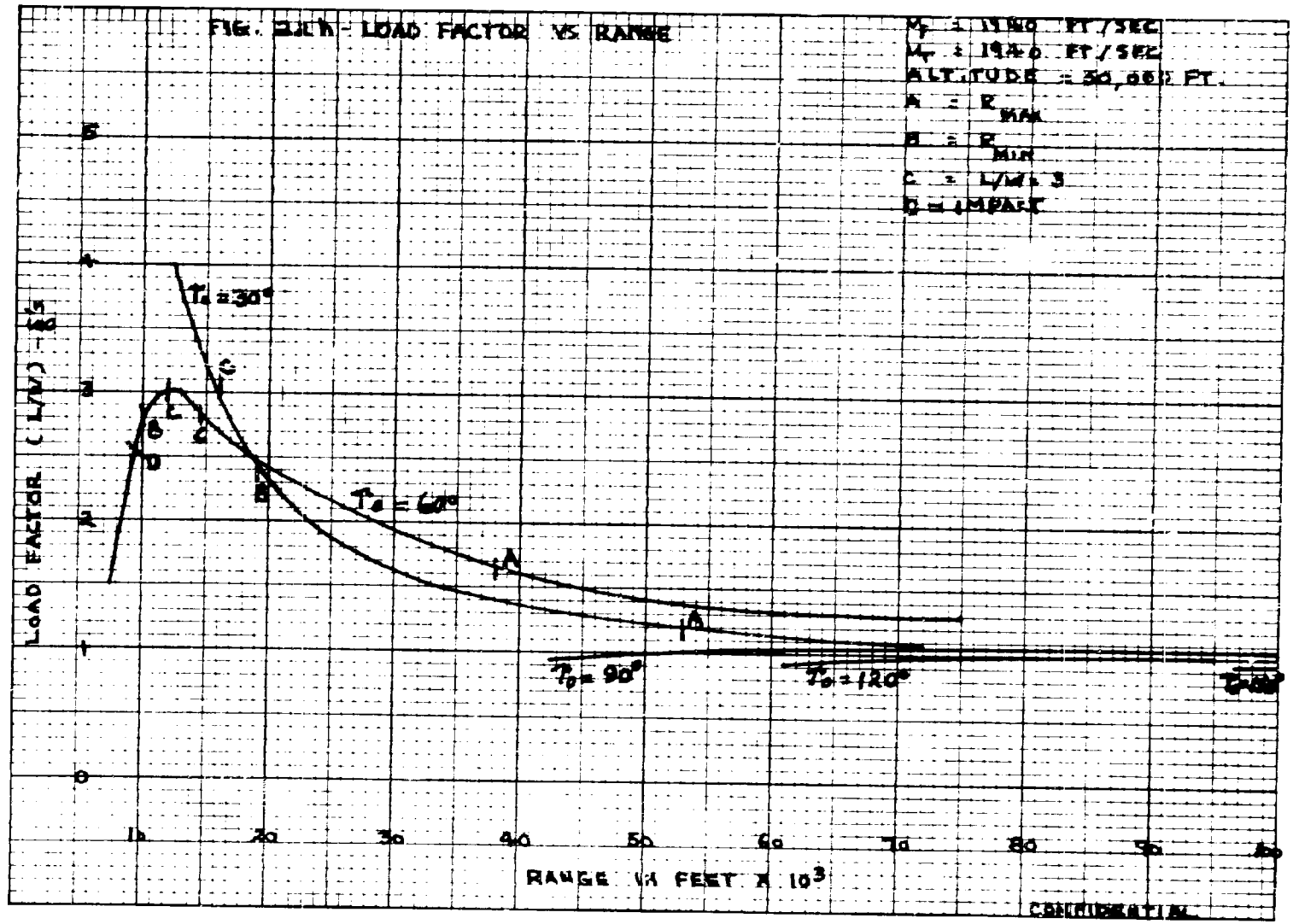
FIG. 22th - LOAD FACTOR VS RANGE
V_p = 1190 FT/SEC
V_T = 1940 FT/SEC
ALTITUDE = 30,000 FT.
A = R_{MAX}
B = R_{MIN}
C = L/W = 3
D = IMPACT
LOAD FACTOR (L/W) - g's
$T_\theta = 30°$
$T_\theta = 60°$
$T_\theta = 90°$
$T_\theta = 120°$
A
B
C
D
RANGE IN FEET X 10^3
CONTINUOUS TURN

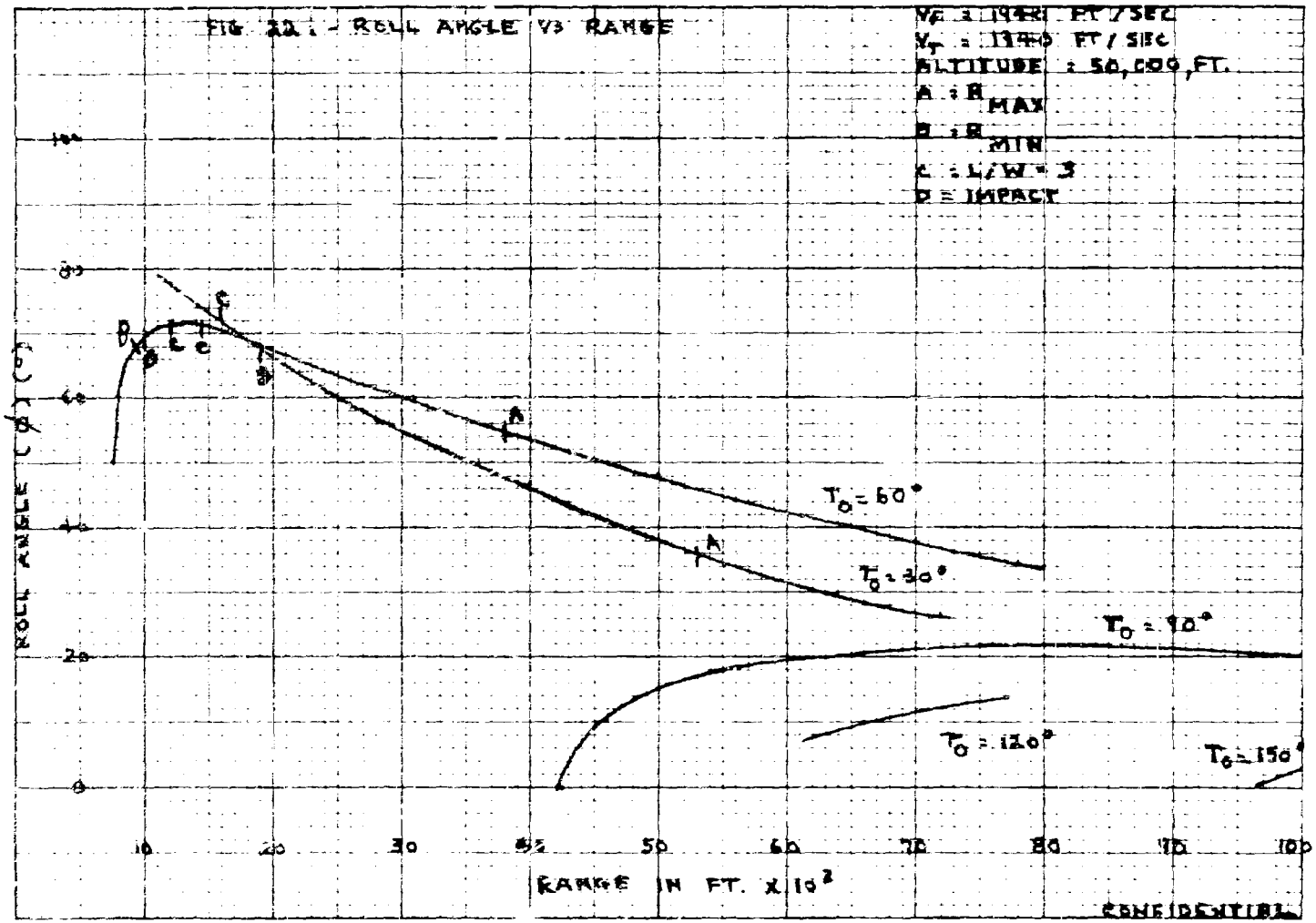
FIG 22 :- ROLL ANGLE VS RANGE
V_E = 1948 FT/SEC
V_T = 1349 FT/SEC
ALTITUDE = 50,000 FT.
A = R_{MAX}
B = R_{MIN}
L = L/W = 3
D = IMPACT
T_0 = 60°
T_0 = 90°
T_0 = 120°
T_0 = 150°
ROLL ANGLE (φ)
RANGE IN FT. X 10^2
CONFIDENTIAL

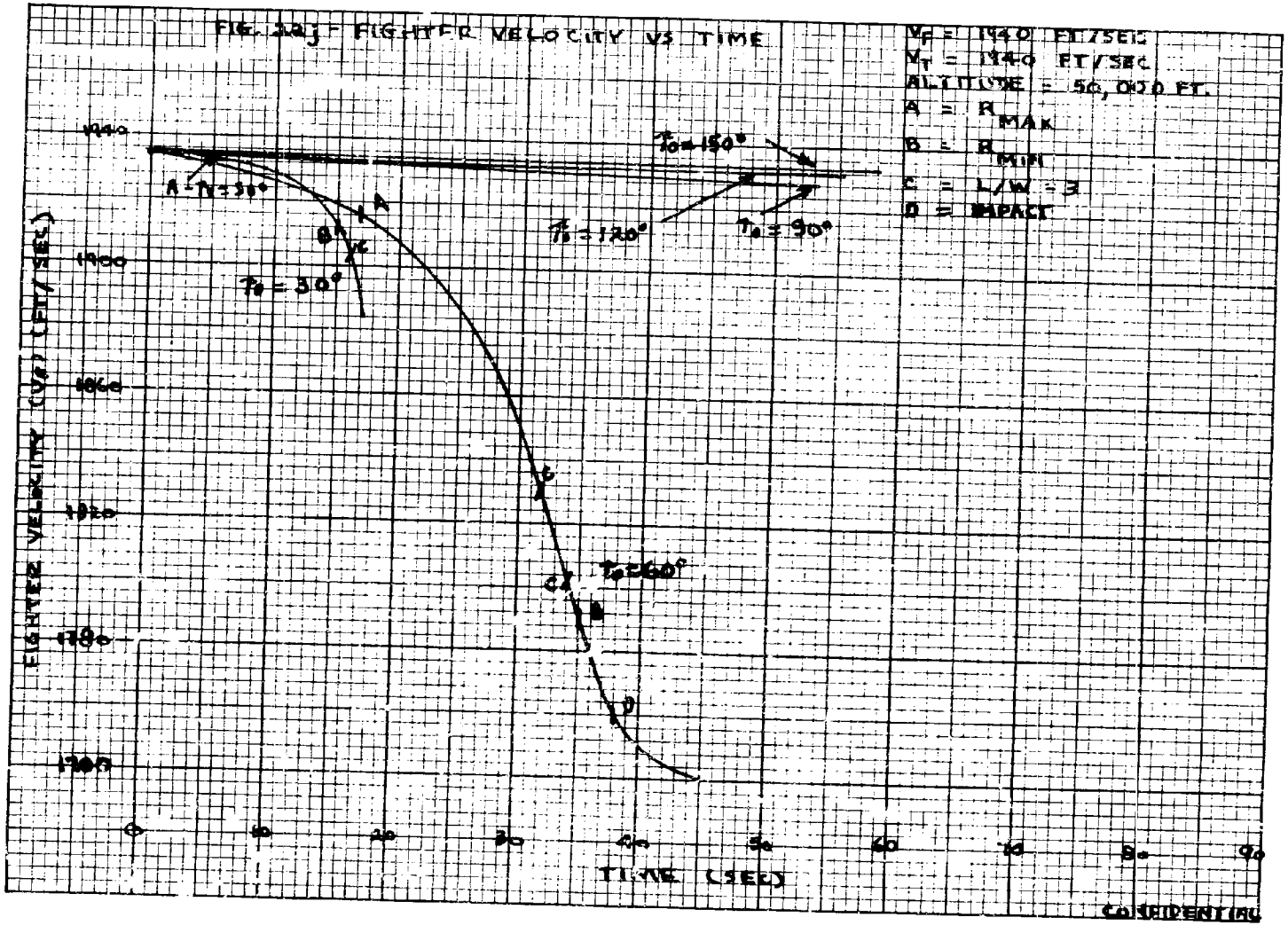
FIG. 22j - FIGHTER VELOCITY VS TIME
V_F = 1940 FT/SEC
V_T = 1940 FT/SEC
ALTITUDE = 50,000 FT.
A = R_{MAX}
B = R_{MIN}
C = L/W = 3
D = IMPACT
T_{10}=150°
T_0=120°
T_0=90°
T_0=60°
T_0=30°
A-T=30°
FIGHTER VELOCITY (VF) (FT/SEC)
TIME (SEC)
CONFIDENTIAL

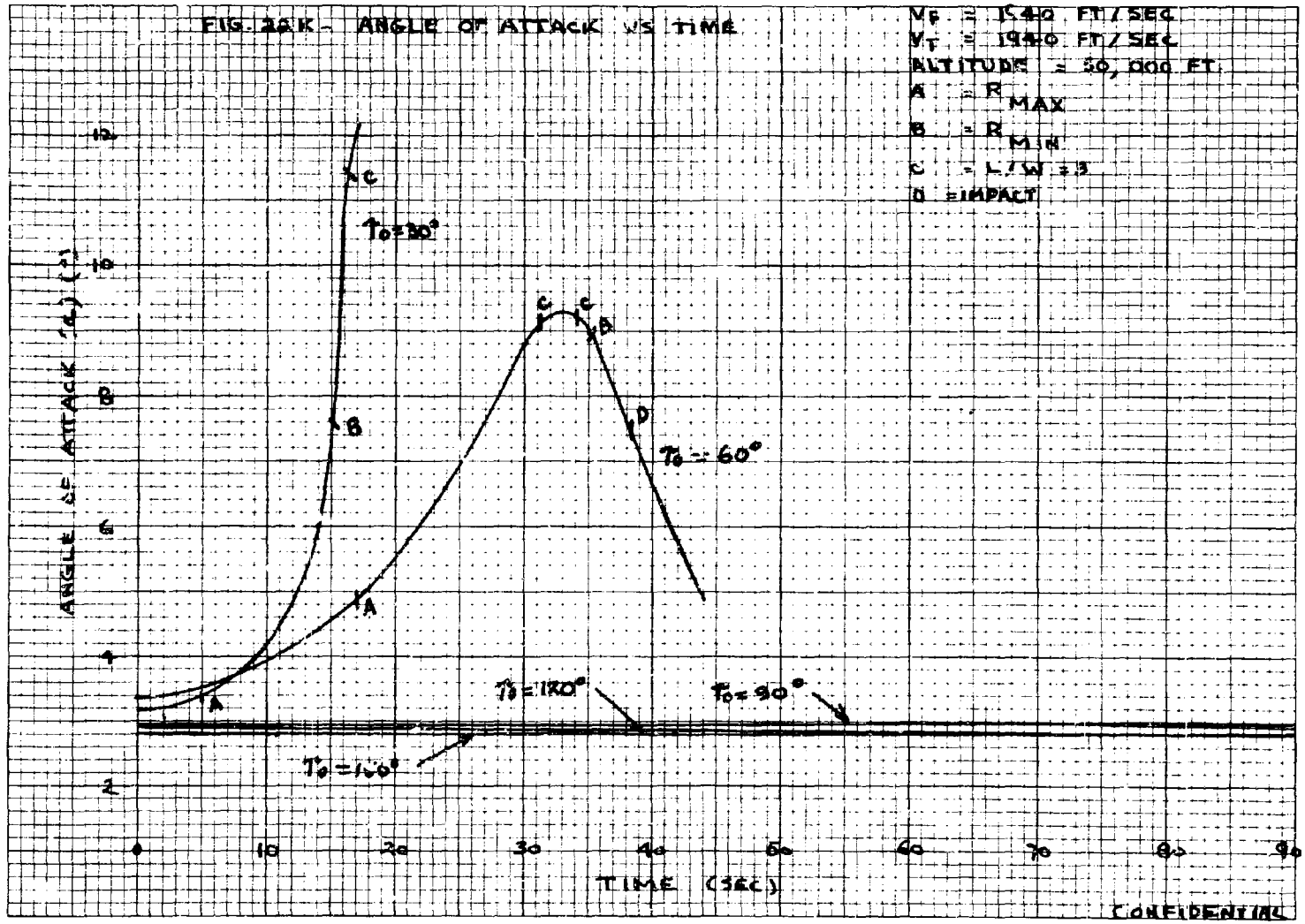
FIG. 20 K - ANGLE OF ATTACK VS TIME
V_E = 15440 FT/SEC
V_T = 19440 FT/SEC
ALTITUDE = 50,000 FT.
A = R_{MAX}
B = R_{MIN}
C = L/W = 3
D = IMPACT
ANGLE OF ATTACK (α) (°)
TIME (SEC)
T_0=30°
T_0=60°
T_0=90°
T_0=120°
T_0=150°
A
B
C
D
CONFIDENTIAL

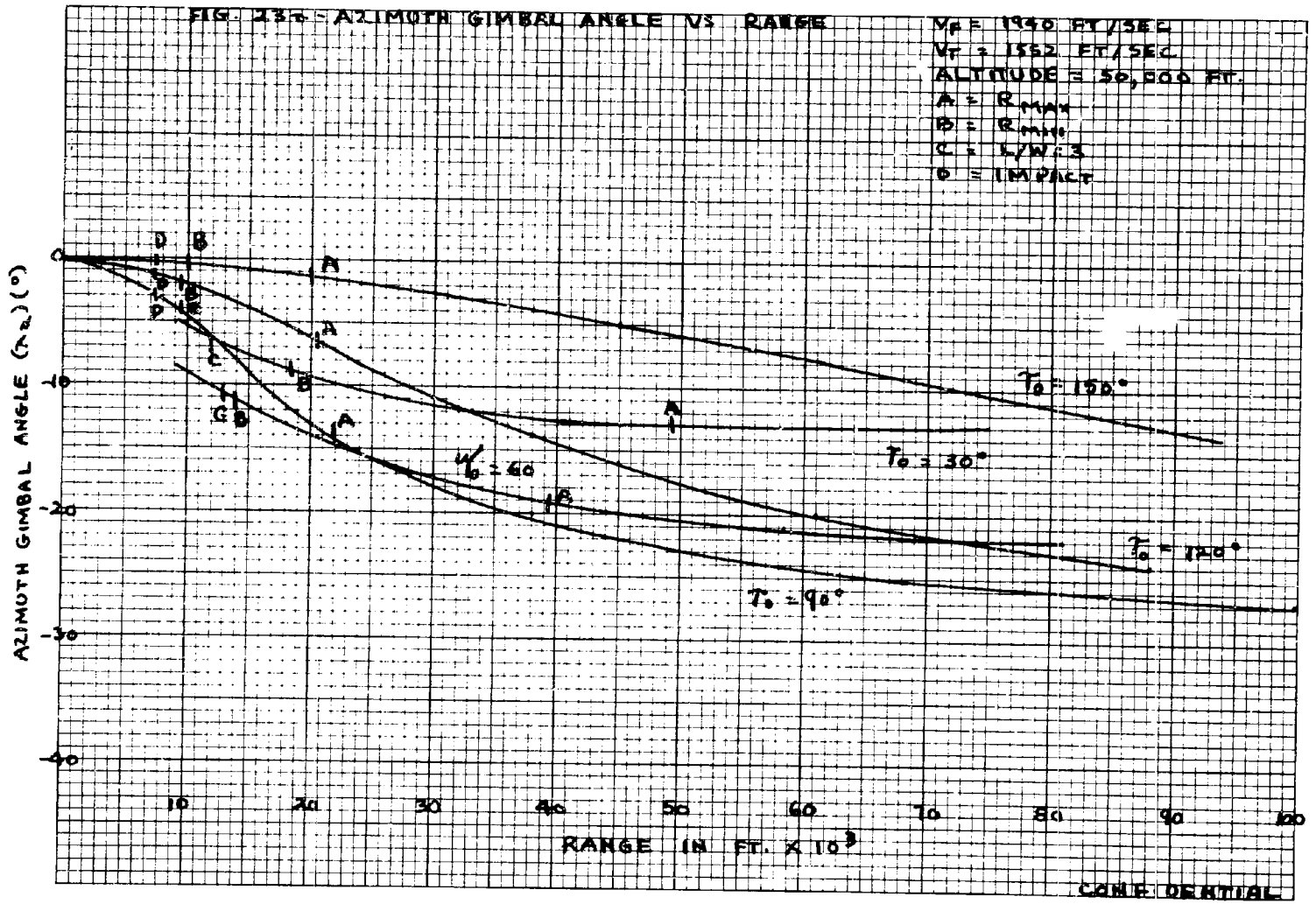
FIG. 23a - AZIMUTH GIMBAL ANGLE VS RANGE
V_F = 1940 FT/SEC
V_T = 1552 FT/SEC
ALTITUDE = 50,000 FT.
A = R_{max}
B = R_{min}
C = L/W = 3
D = IMPACT
AZIMUTH GIMBAL ANGLE (γ_{GL}) (°)
0
-10
-20
-30
-40
10
20
30
40
50
60
70
80
90
100
RANGE IN FT. X 10^3
T_0 = 150°
T_0 = 30°
ψ_0 = 60
T_0 = 120°
T_0 = 90°
CONFIDENTIAL

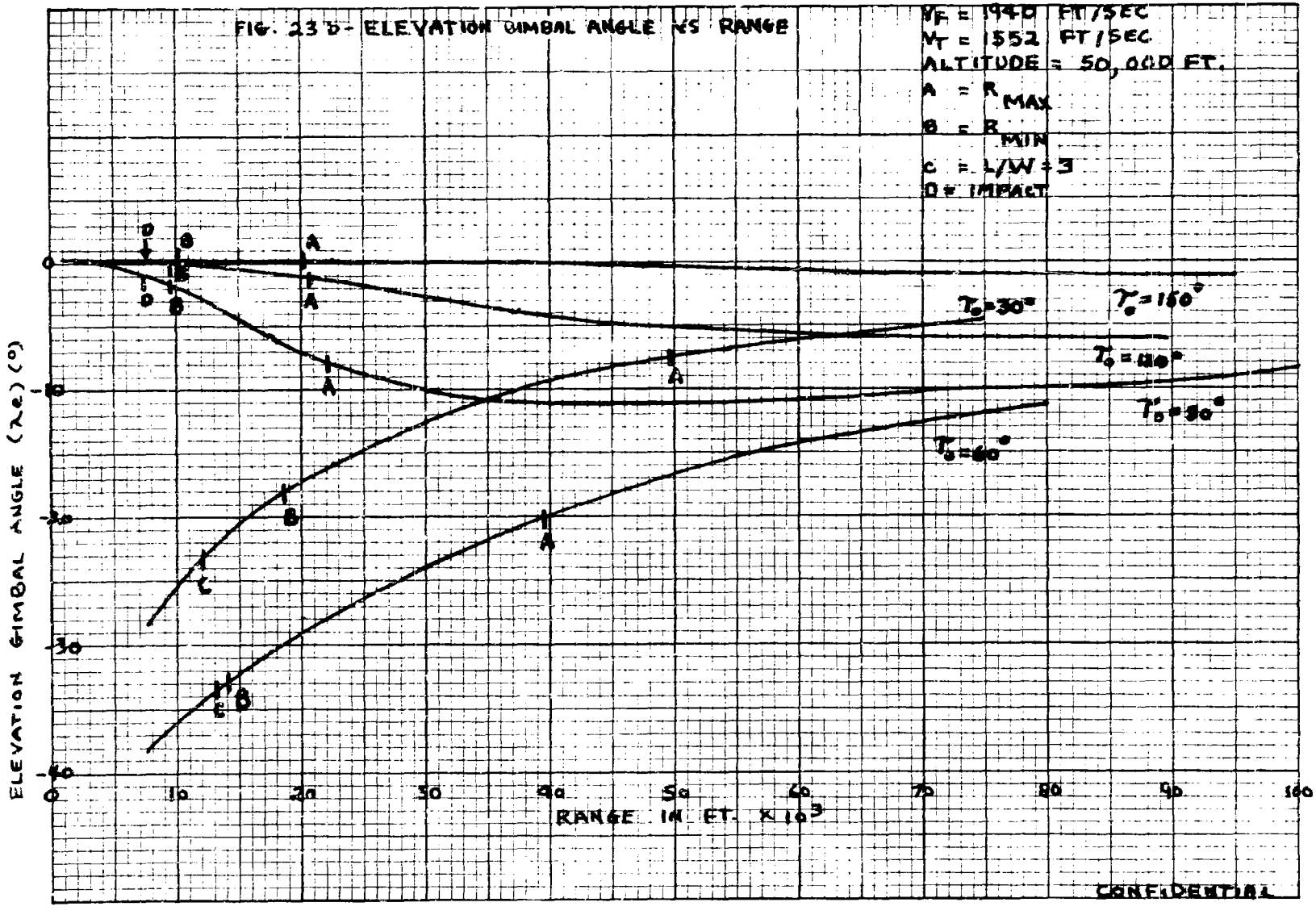
FIG. 23 b - ELEVATION GIMBAL ANGLE VS RANGE
V_F = 1940 FT/SEC
V_T = 1552 FT/SEC
ALTITUDE = 50,000 FT.
A = R_{MAX}
B = R_{MIN}
C = L/W = 3
D = IMPACT
T_o=30°
T_o=150°
T_o=120°
T_o=90°
T_o=60°
ELEVATION GIMBAL ANGLE (λε) (°)
RANGE IN FT. X 10^3
CONFIDENTIAL

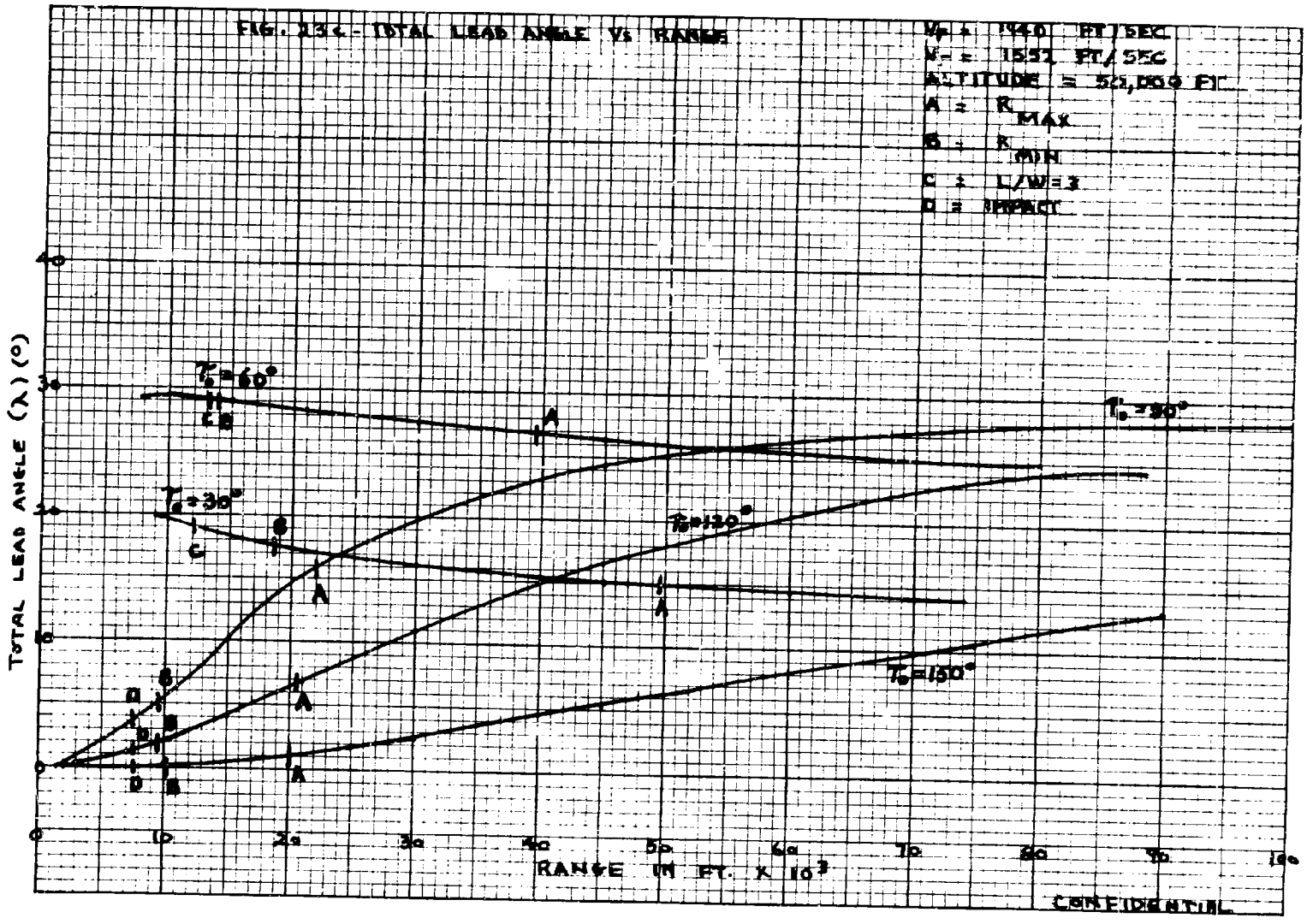
FIG. 23c - TOTAL LEAD ANGLE Vs RANGE
V_p = 1440 FT/SEC
V_T = 1552 FT/SEC
ALTITUDE = 50,000 FT
A = R_{MAX}
B = R_{MIN}
C = L/W = 3
D = IMPACT
TOTAL LEAD ANGLE (λ) (°)
RANGE IN FT. X 10^3
T_o=60°
T_o=30°
T_o=120°
T_o=150°
CONFIDENTIAL

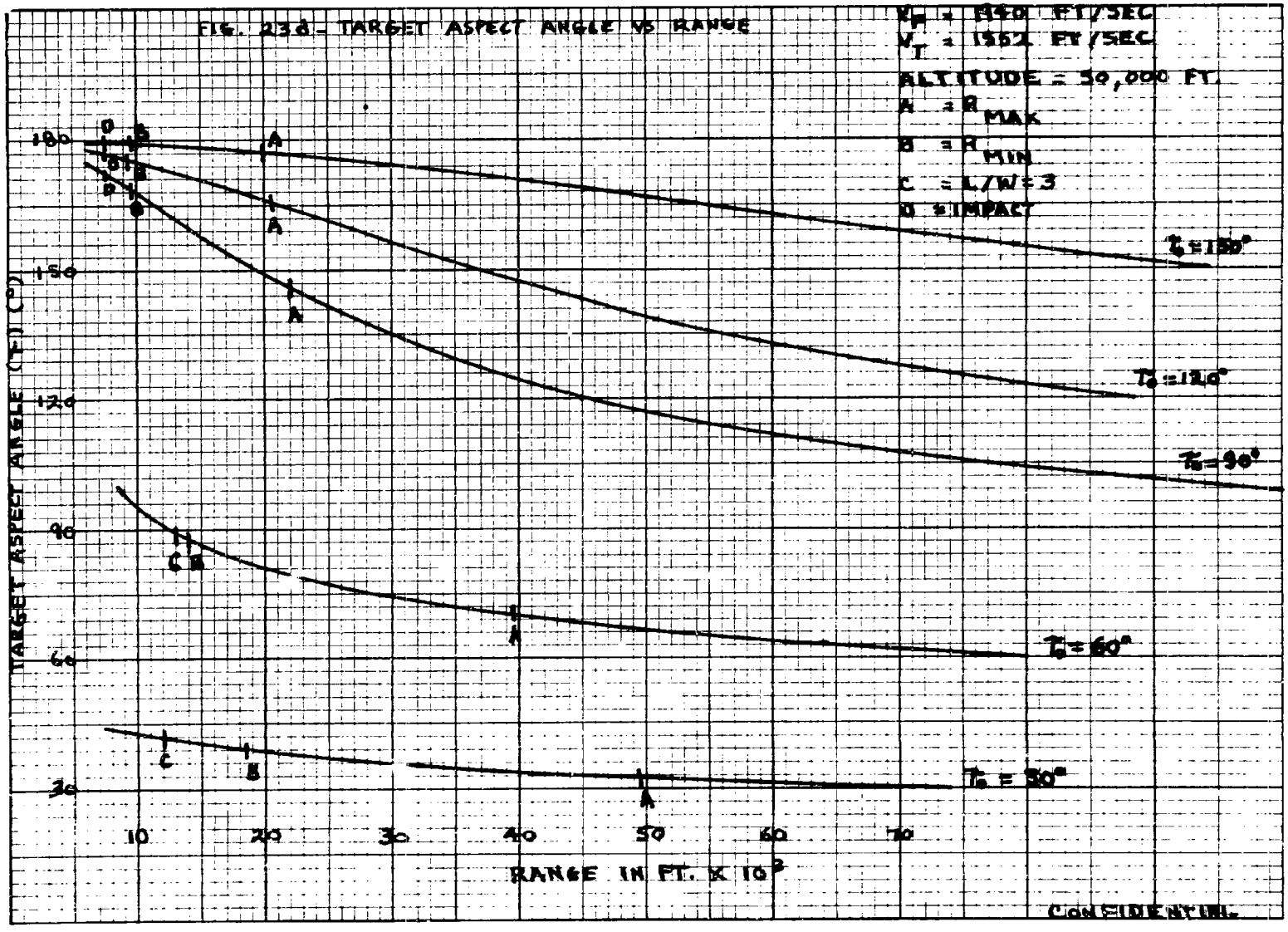
FIG. 23a - TARGET ASPECT ANGLE VS RANGE
V_M = 1450 FT/SEC
V_T = 1552 FT/SEC
ALTITUDE = 50,000 FT.
A = R_{MAX}
B = R_{MIN}
C = L/W = 3
D = IMPACT
T_0 = 150°
T_0 = 120°
T_0 = 90°
T_0 = 60°
T_0 = 30°
TARGET ASPECT ANGLE (T_0) (°)
180
150
120
90
60
30
10
20
30
40
50
60
70
RANGE IN FT. X 10^3
CONFIDENTIAL

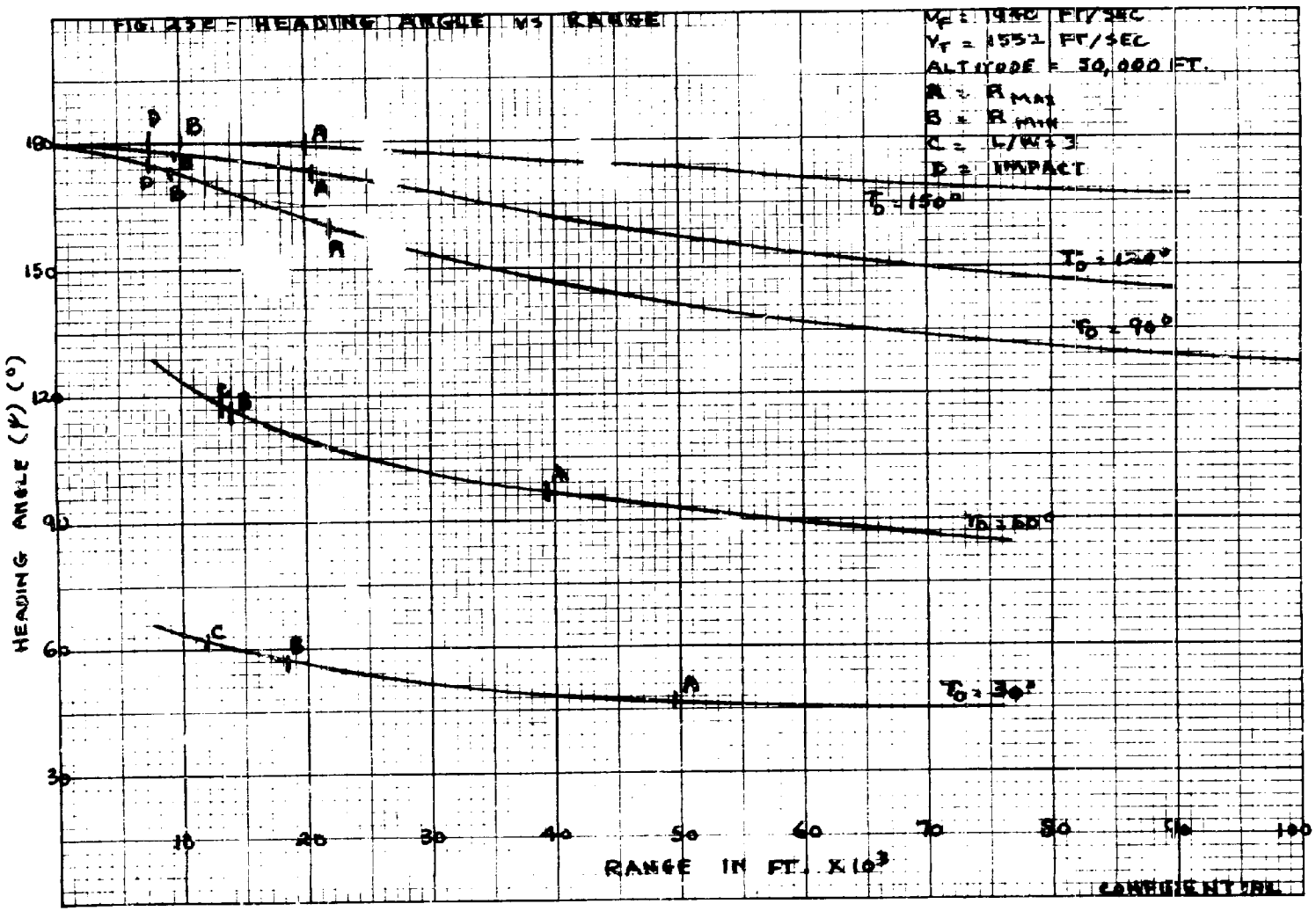
FIG. 232 - HEADING ANGLE VS RANGE
V_F = 1940 FT/SEC
V_T = 1552 FT/SEC
ALTITUDE = 30,000 FT.
A = R_{MAX}
B = R_{MIN}
C = L/W = 3
D = IMPACT
τ_0 = 150°
τ_0 = 120°
τ_0 = 90°
τ_0 = 60°
τ_0 = 30°
HEADING ANGLE (Ψ) (°)
180
150
120
90
60
30
10
20
30
40
50
60
70
80
90
100
RANGE IN FT. X 10^3
CONFIDENTIAL

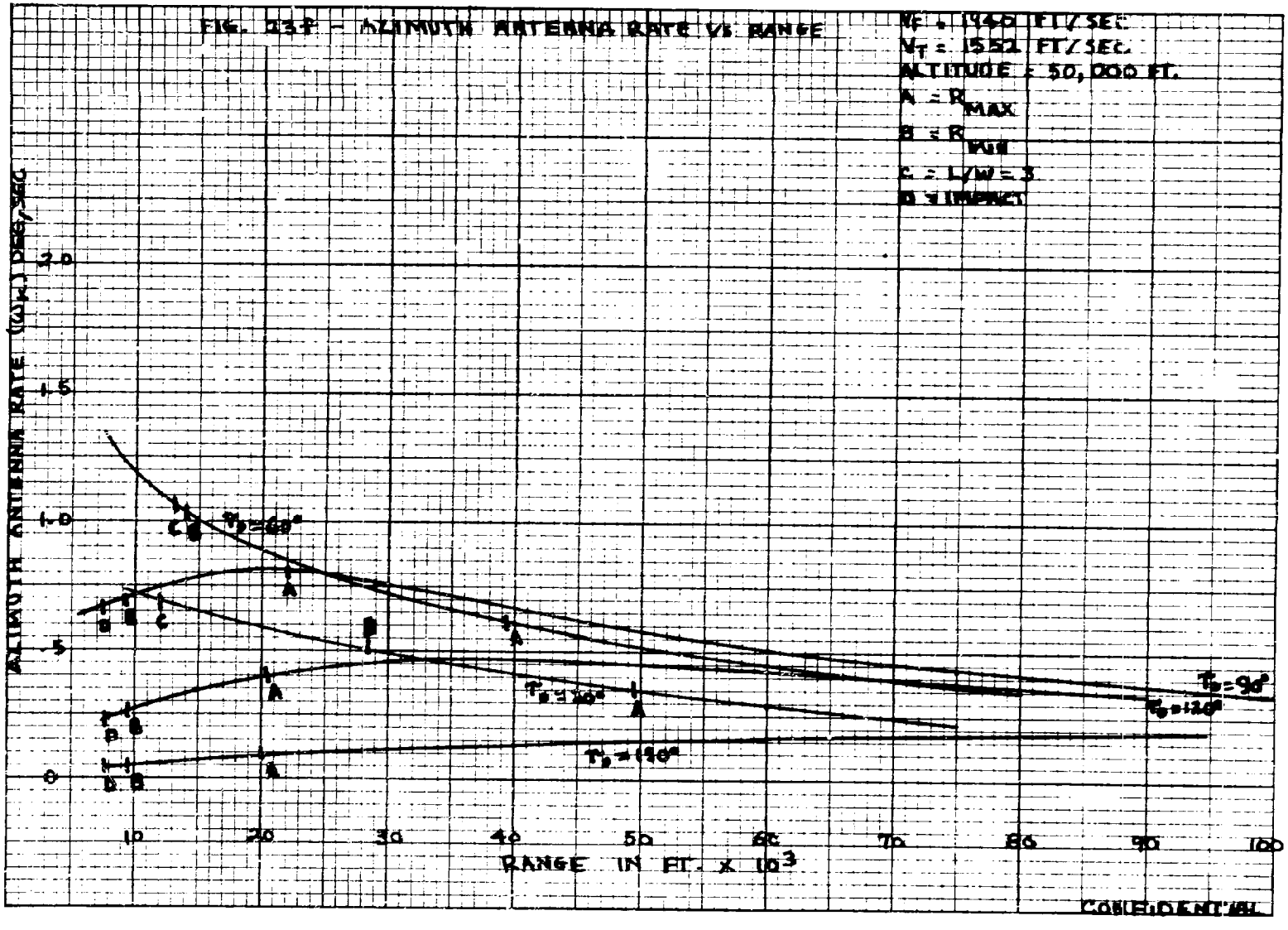
FIG. 23F - AZIMUTH ANTENNA RATE VS RANGE
V_F = 1440 FT/SEC.
V_T = 1552 FT/SEC.
ALTITUDE = 50,000 FT.
A = R_{MAX}
B = R_{MIN}
C = L/W = 3
D = IMPACT
AZIMUTH ANTENNA RATE ($\dot{\Omega}_W$) DEG/SEC
2.0
1.5
1.0
.5
0
T_D=60°
T_D=90°
T_D=120°
T_D=150°
10
20
30
40
50
60
70
80
90
100
RANGE IN FT. X 10^3
CONFIDENTIAL

FIG. 23 - ELEVATION ANTENNA RATE VS RANGE

V_f = 1440 FT/SEC
V_T = 152 FT/SEC
ALTITUDE = 50,000 FT.
A = R_{MAX}
B = R_{MIN}
C = L/W = 3
D = IMPACT

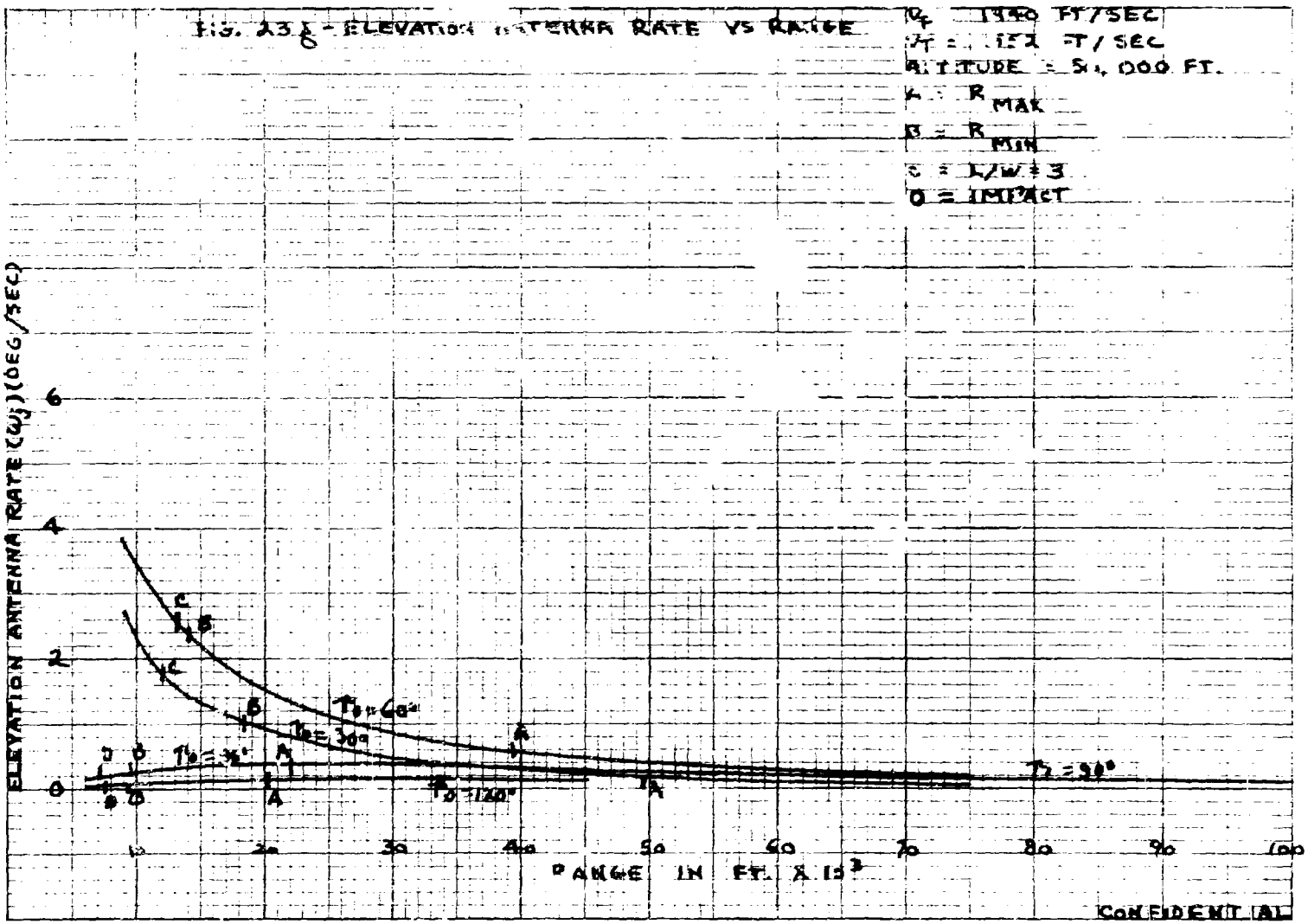

CONFIDENTIAL

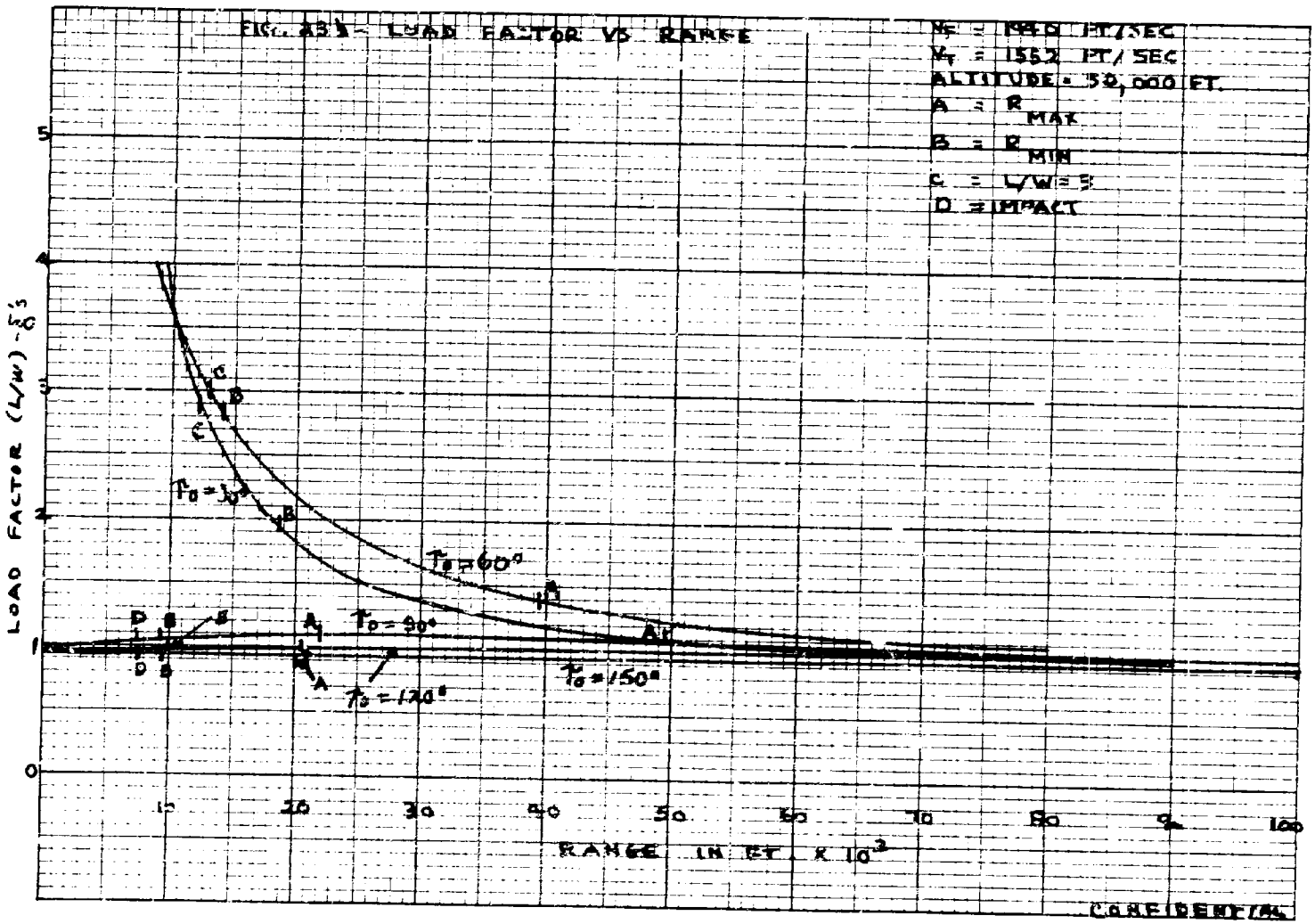
FIG. 33 - LOAD FACTOR VS RANGE
V_F = 1440 FT/SEC
V_T = 1552 FT/SEC
ALTITUDE = 50,000 FT.
A = R_{MAX}
B = R_{MIN}
C = L/W = 5
D = IMPACT
LOAD FACTOR (L/W) - n_c
RANGE IN FT. X 10^3
T_D = 30°
T_D = 60°
T_D = 90°
T_D = 120°
T_D = 150°
0
1
2
3
4
5
10
20
30
40
50
60
70
80
90
100
CONFIDENTIAL

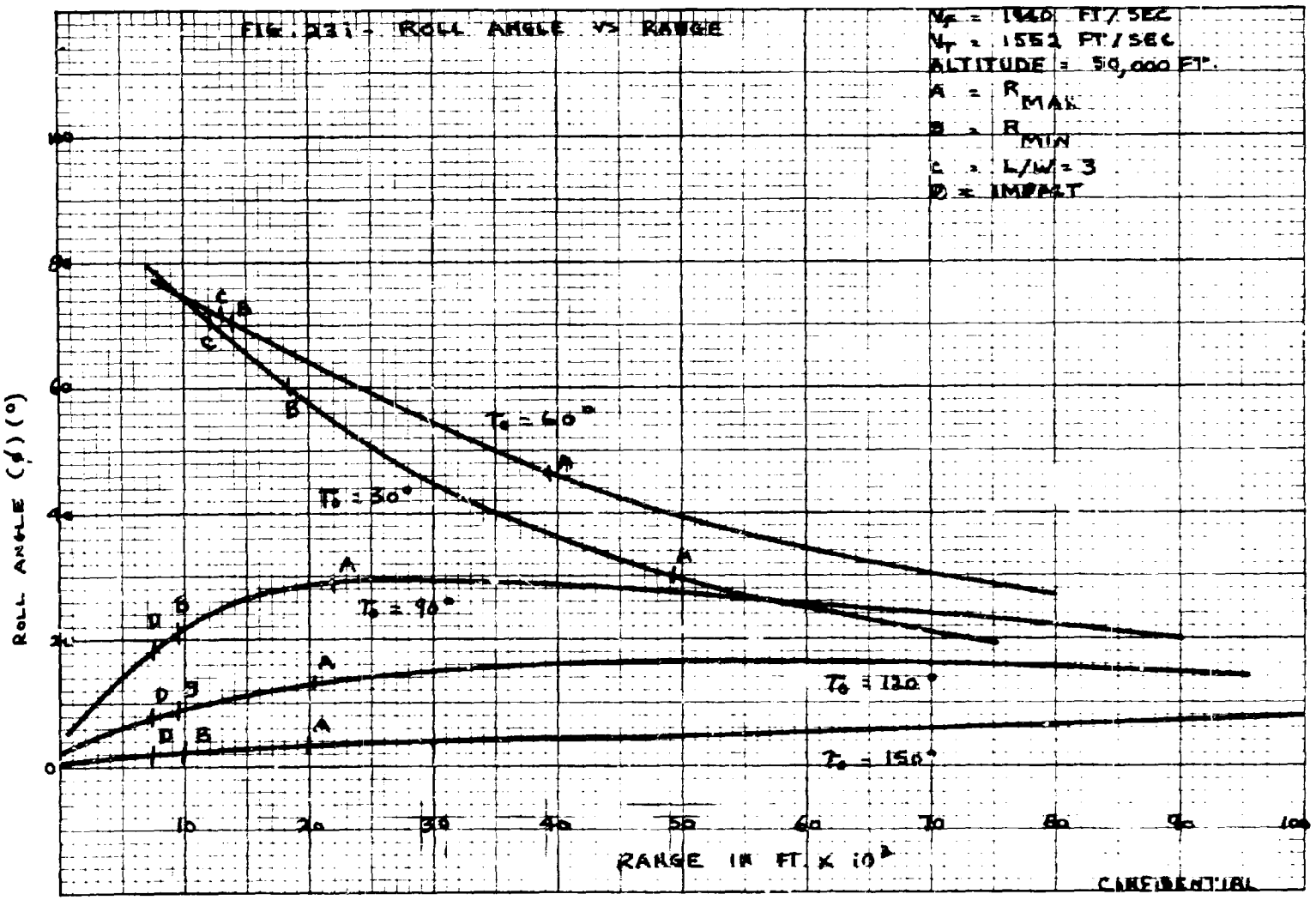
FIG. 231 - ROLL ANGLE VS RANGE
V_F = 1440 FT/SEC
V_T = 1552 FT/SEC
ALTITUDE = 50,000 FT.
A = R_{MAX}
B = R_{MIN}
C = L/W = 3
D = IMPACT
T_0 = 60°
T_0 = 30°
T_0 = 90°
T_0 = 120°
T_0 = 150°
ROLL ANGLE (φ) (°)
RANGE IN FT. X 10^3
CONFIDENTIAL

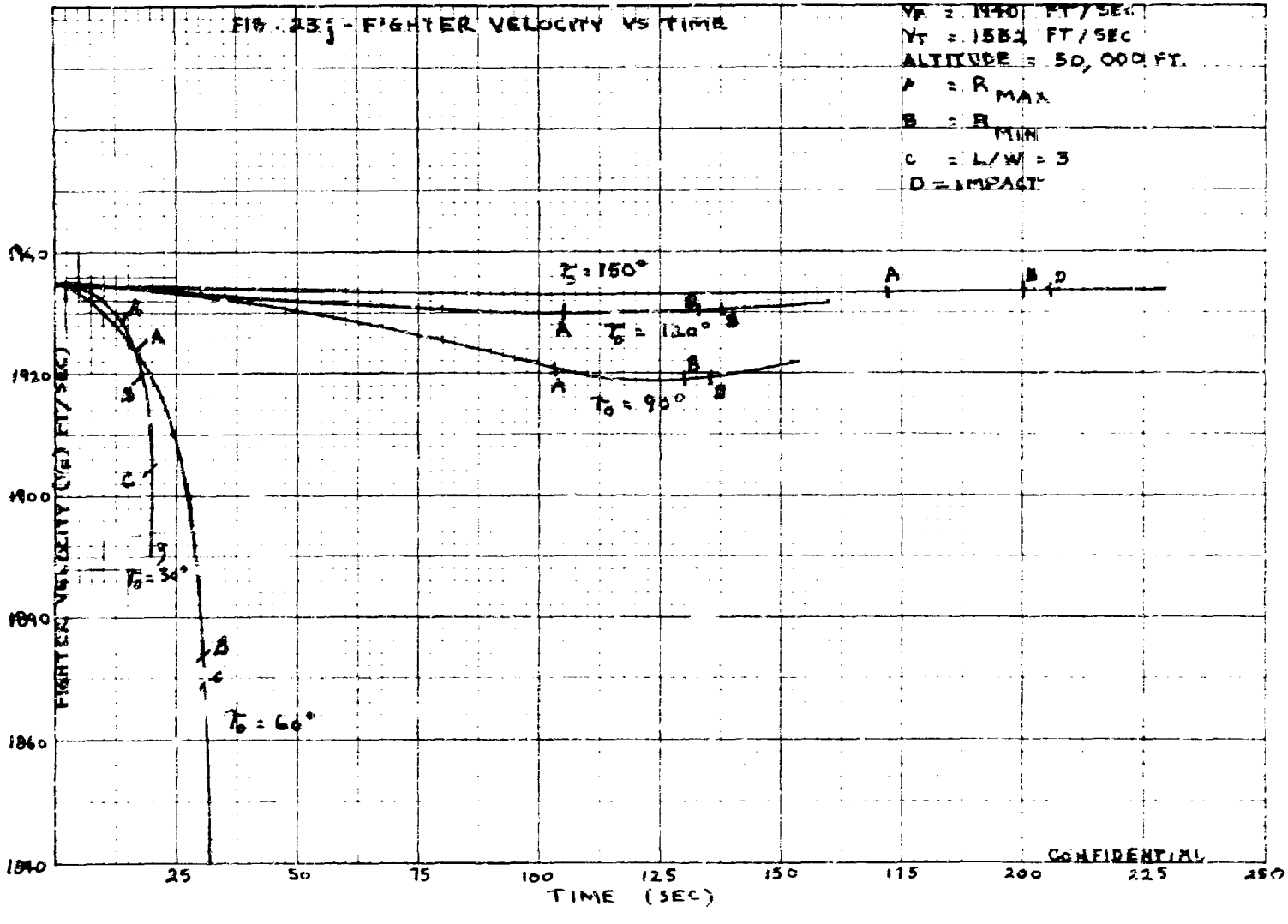
FIG. 23j - FIGHTER VELOCITY VS TIME
V_F = 1940 FT/SEC
V_T = 1552 FT/SEC
ALTITUDE = 50,000 FT.
A = R_{MAX}
B = R_{MIN}
C = L/W = 3
D = IMPACT
τ_0 = 150°
τ_0 = 120°
τ_0 = 90°
τ_0 = 34°
τ_0 = 64°
FIGHTER VELOCITY (V$_F$) FT/SEC
TIME (SEC)
1940
1920
1900
1880
1860
1840
25
50
75
100
125
150
175
200
225
250
CONFIDENTIAL

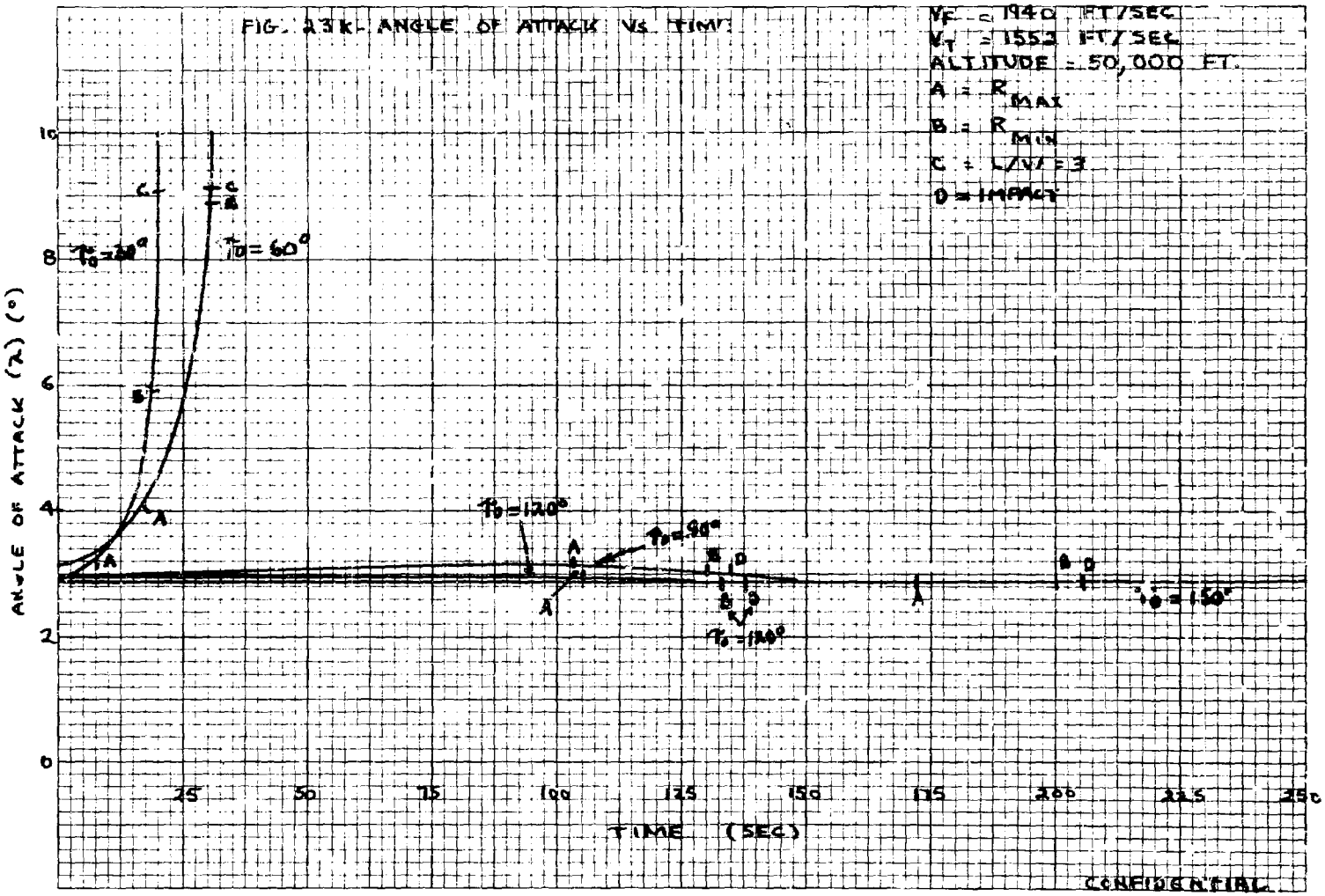
FIG. 23k- ANGLE OF ATTACK Vs TIME
V_F = 1940 FT/SEC
V_T = 1552 FT/SEC
ALTITUDE = 50,000 FT.
A = R_{MAX}
B = R_{MIN}
C = L/W = 3
D = IMPACT
ANGLE OF ATTACK (α) (°)
TIME (SEC)
γ_0 = 150°
γ_0 = 120°
γ_0 = 90°
γ_0 = 60°
γ_0 = 30°
CONFIDENTIAL

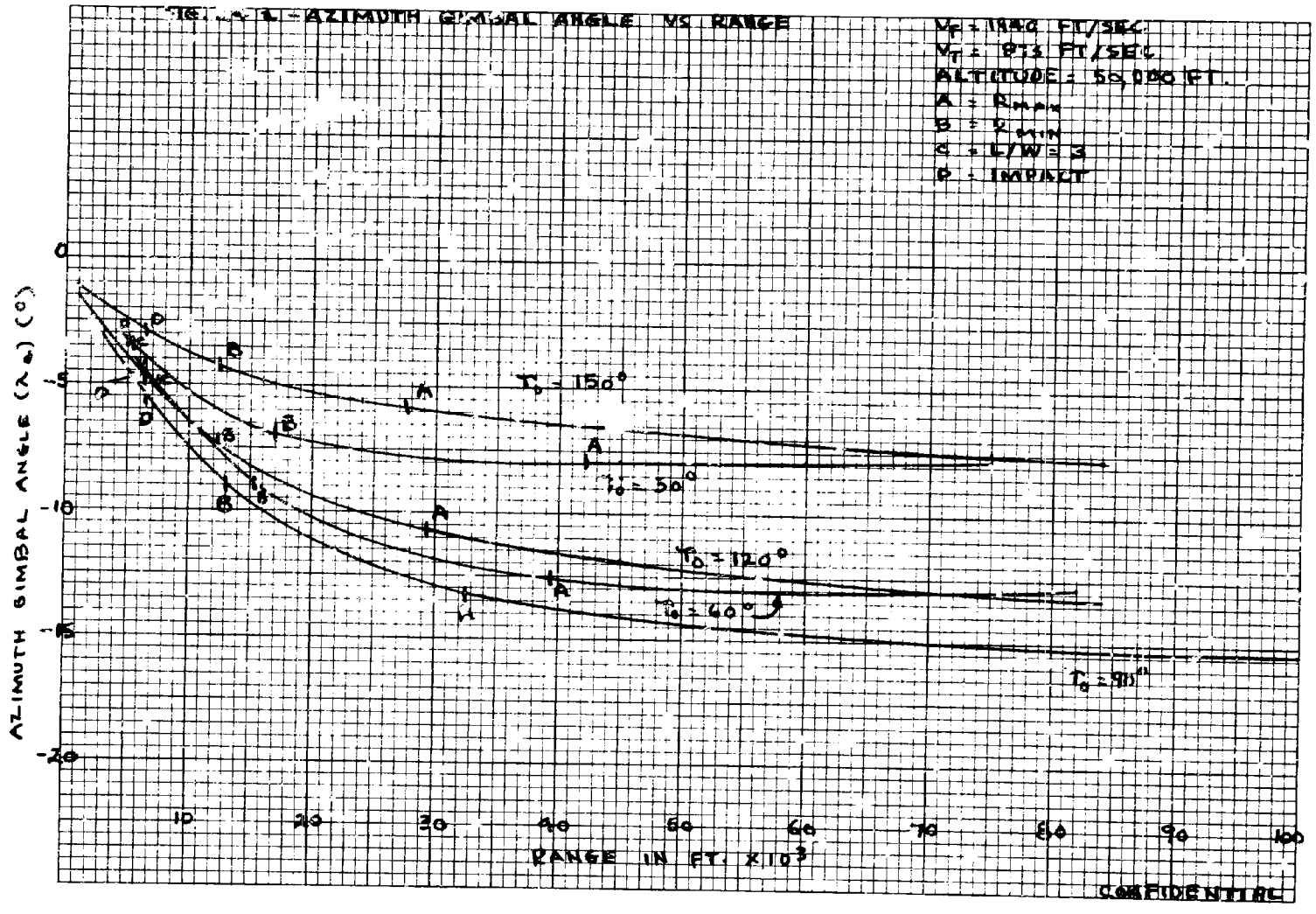
FIG. 4.1 - AZIMUTH GIMBAL ANGLE VS RANGE
V_F = 1440 FT/SEC
V_T = 875 FT/SEC
ALTITUDE = 50,000 FT.
A = R_{max}
B = R_{min}
C = L/W = 3
P = IMPACT
AZIMUTH GIMBAL ANGLE (λ_a) (°)
0
-5
-10
-15
-20
T_0 = 150°
T_0 = 90°
10
20
30
40
50
60
70
80
90
100
RANGE IN FT. X 10^3
CONFIDENTIAL

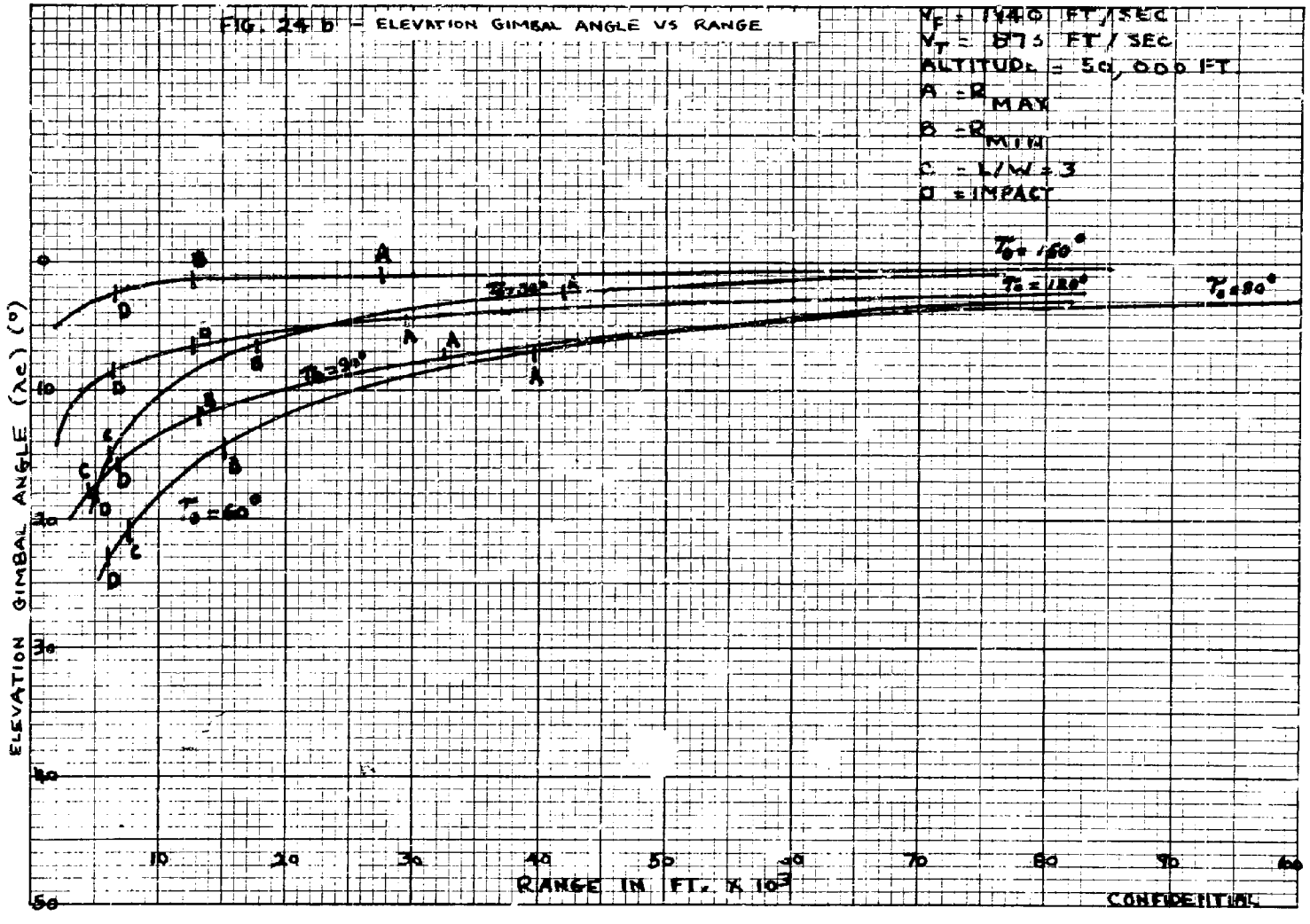
FIG. 24 b - ELEVATION GIMBAL ANGLE VS RANGE
V_F = 1140 FT/SEC
V_T = 875 FT/SEC
ALTITUDE = 50,000 FT
A = R_{MAX}
B = R_{MIN}
C = L/W = 3
D = IMPACT
$\gamma_0 = 150°$
$\gamma_0 = 120°$
$\gamma_0 = 90°$
$\gamma_0 = 30°$
$\gamma_0 = 60°$
ELEVATION GIMBAL ANGLE (λ_E) (°)
RANGE IN FT. X 10^3
CONFIDENTIAL

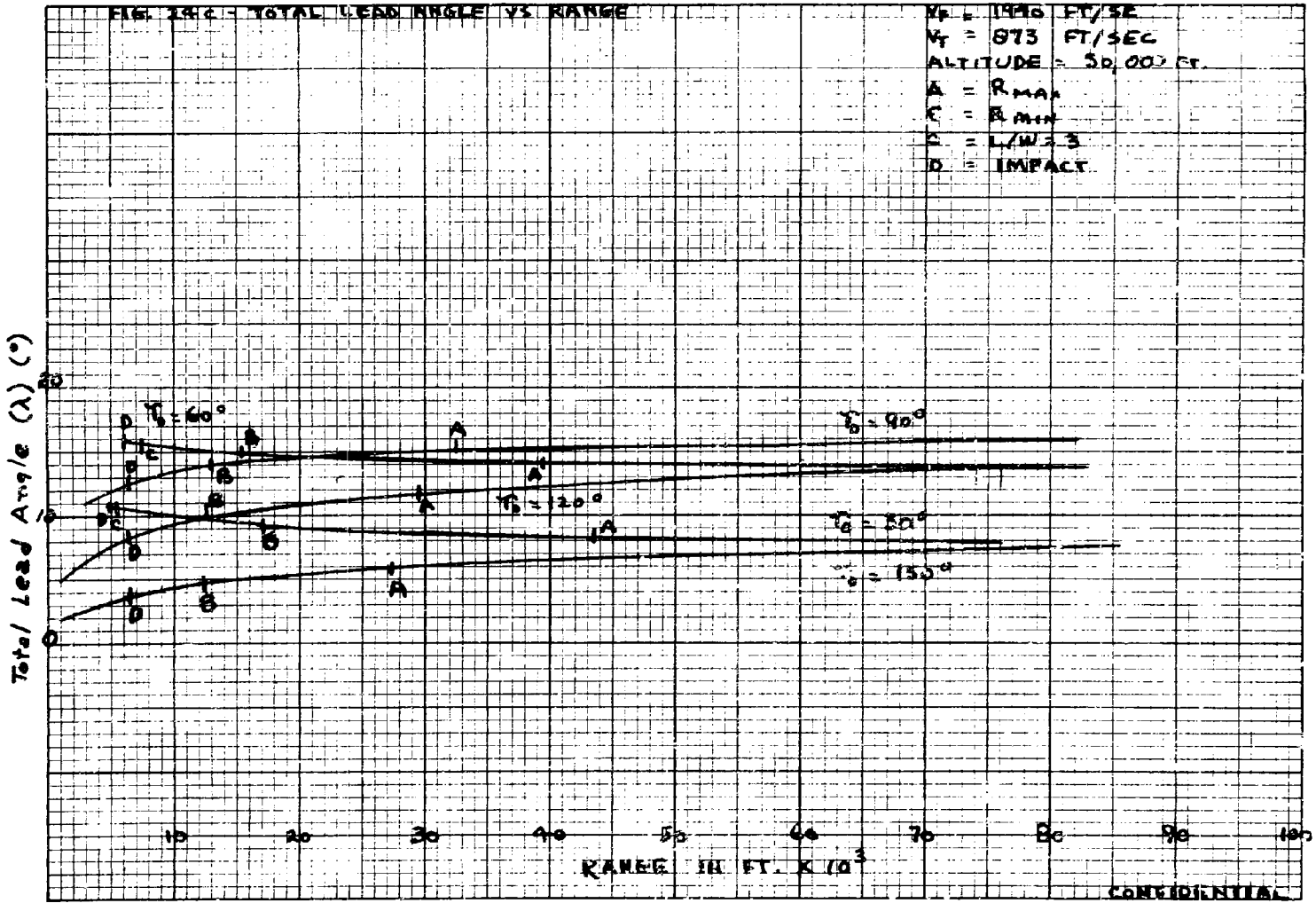
FIG. 14c - TOTAL LEAD ANGLE VS RANGE
V_p = 1990 FT/SEC
V_T = 873 FT/SEC
ALTITUDE = 50,000 FT.
A = R_{MAX}
C = R_{MIN}
D = IMPACT
Total Lead Angle (λ) (°)
20
10
0
γ_0 = 60°
γ_0 = 90°
γ_0 = 120°
γ_0 = 150°
10
20
30
40
50
60
70
80
90
100
RANGE IN FT. X 10^3
CONFIDENTIAL

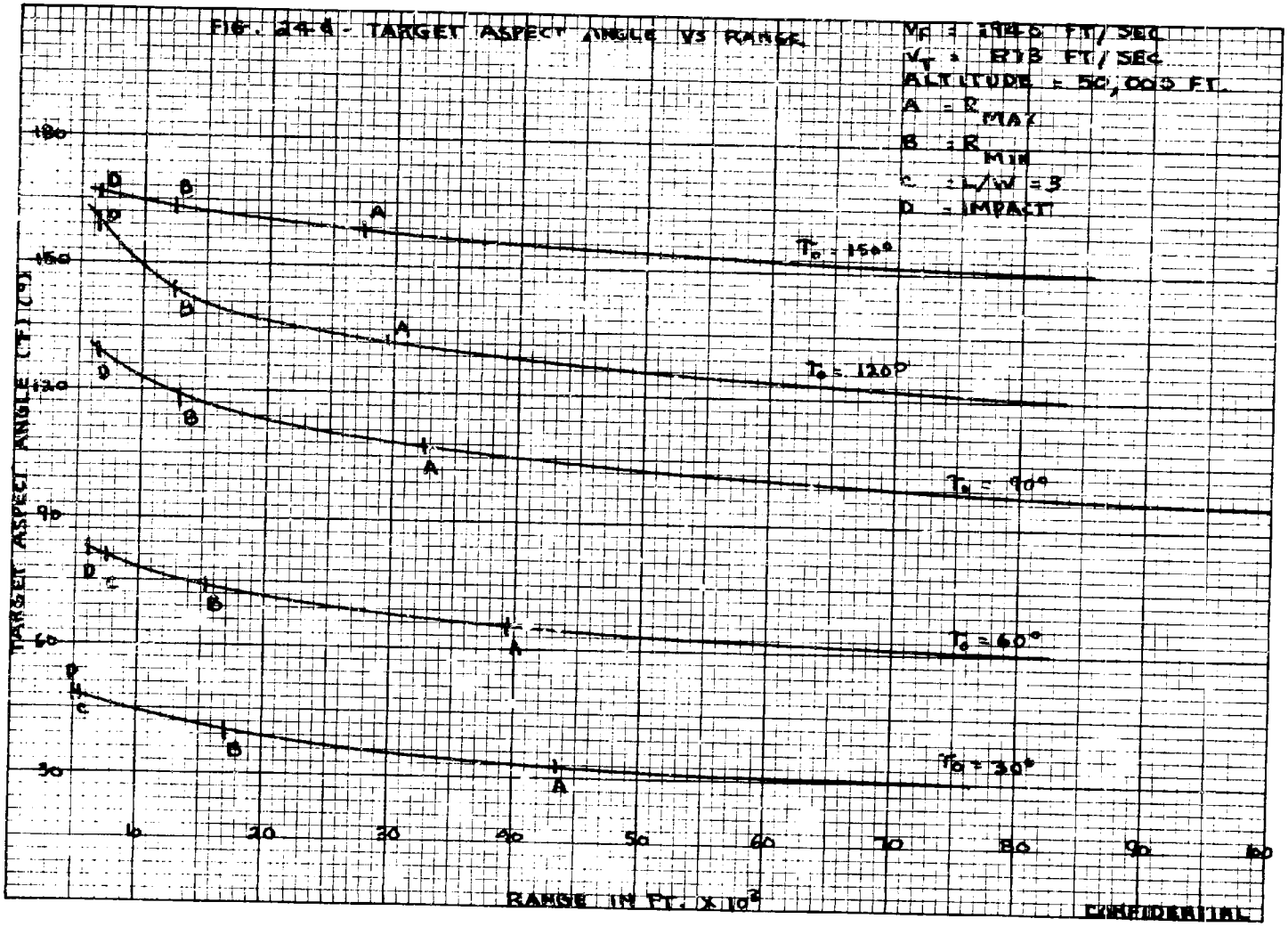
FIG. 24-9 - TARGET ASPECT ANGLE VS RANGE
V_M = 1845 FT/SEC
V_T = 873 FT/SEC
ALTITUDE = 50,000 FT.
A = R_{MAX}
B = R_{MIN}
C = L/W = 3
D = IMPACT
T_θ = 150°
T_θ = 120°
T_θ = 90°
T_θ = 60°
T_θ = 30°
TARGET ASPECT ANGLE (T_θ)
180
150
120
90
60
30
10
20
30
40
50
60
70
80
90
100
RANGE IN FT. X 10^2
CONFIDENTIAL

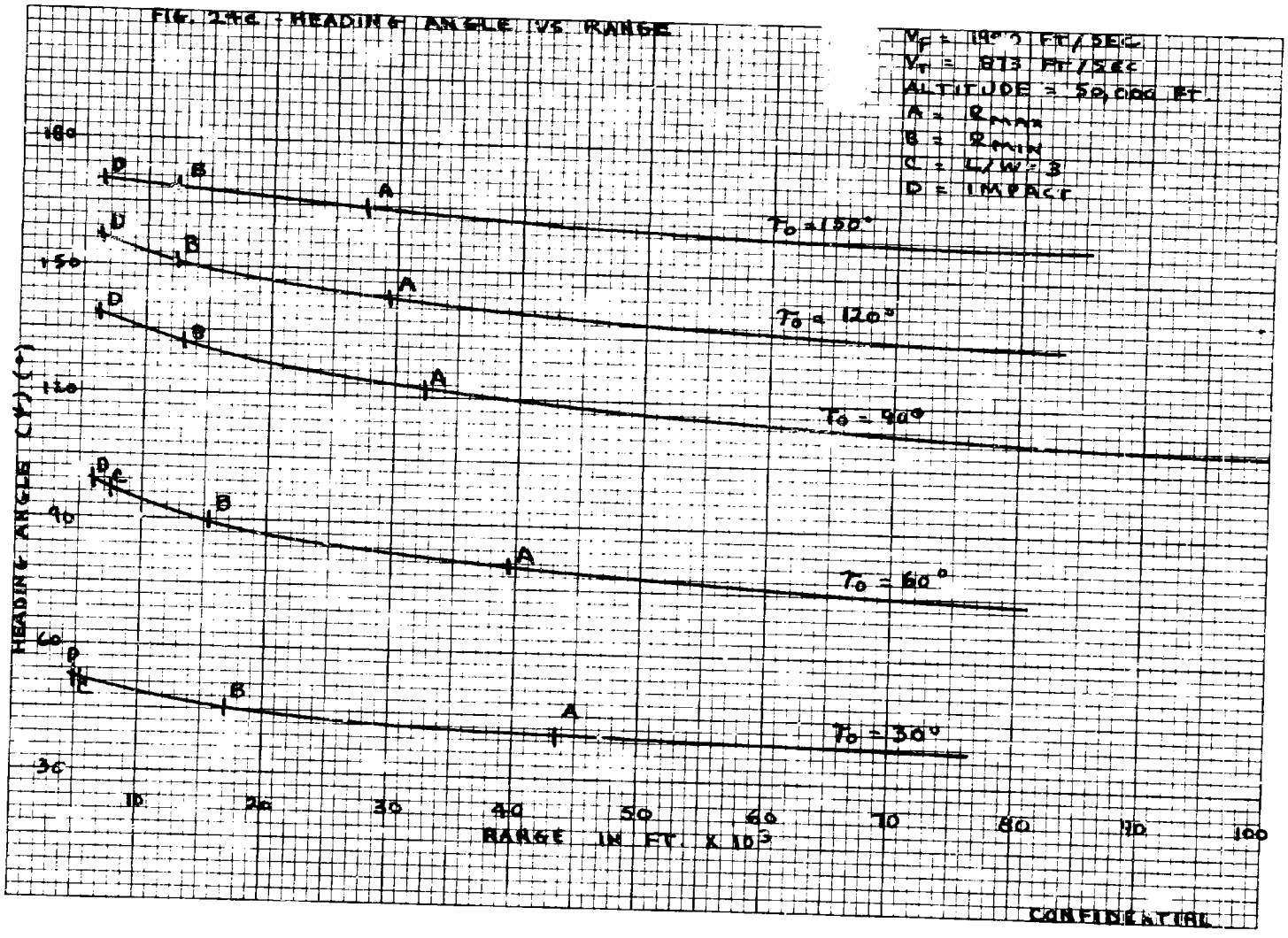
FIG. 24c : HEADING ANGLE VS RANGE
V_F = 1400 FT/SEC
V_T = 873 FT/SEC
ALTITUDE = 50,000 FT.
A = R_{max}
B = R_{min}
C = L/W = 3
D = IMPACT
T_0 = 150°
T_0 = 120°
T_0 = 90°
T_0 = 60°
T_0 = 30°
HEADING ANGLE (ψ) (°)
180
150
120
90
60
30
10
20
30
40
50
60
70
80
90
100
RANGE IN FT. X 10³
CONFIDENTIAL

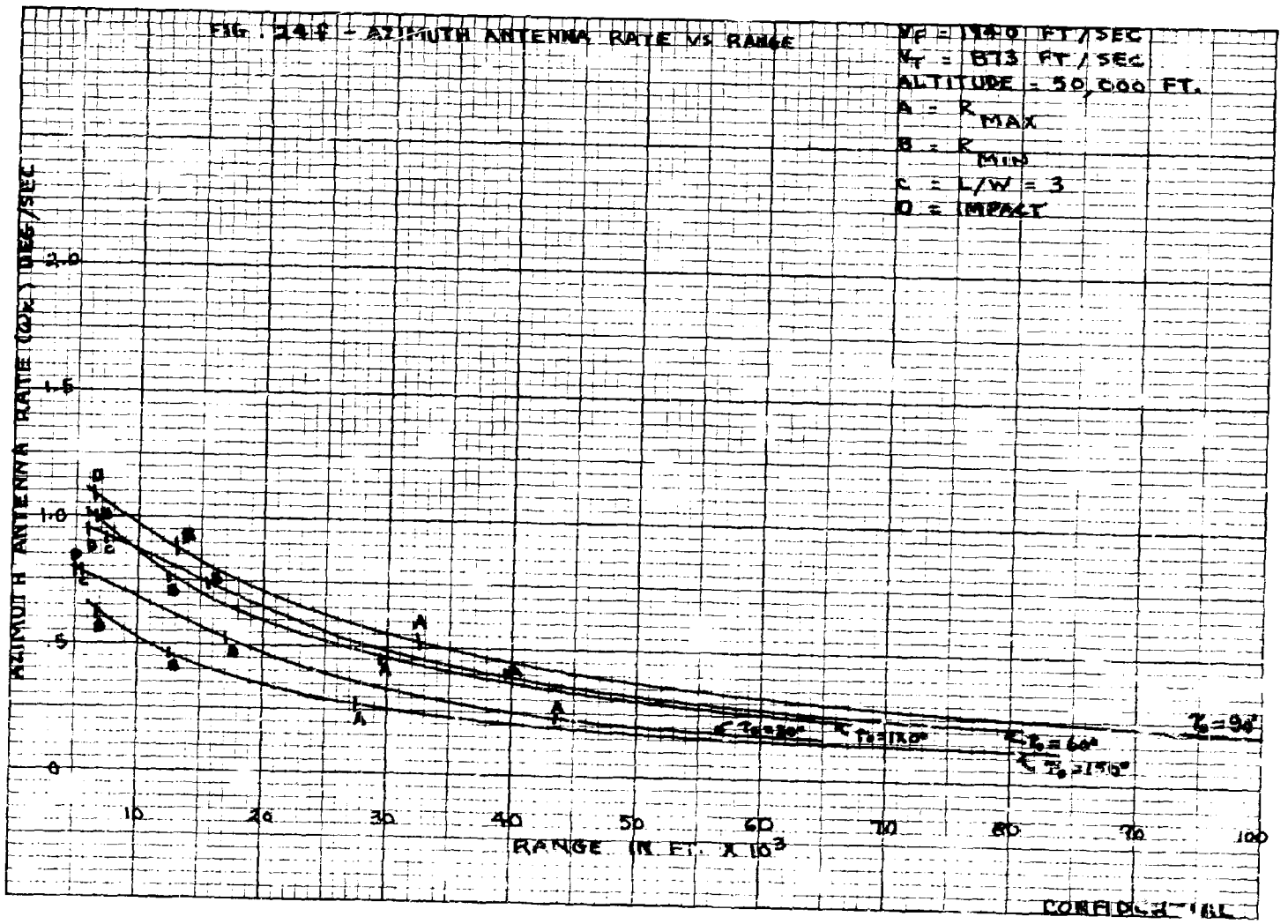
FIG. 24f - AZIMUTH ANTENNA RATE VS RANGE
V_f = 1340 FT/SEC
V_T = 873 FT/SEC
ALTITUDE = 50,000 FT.
A = R_{MAX}
B = R_{MIN}
c = L/W = 3
D = IMPACT
AZIMUTH ANTENNA RATE ($\dot{\psi}_L$) DEG/SEC
2.0
1.5
1.0
.5
0
10
20
30
40
50
60
70
80
90
100
RANGE IN FT. X 10^3
ψ_0 = 90°
ψ_0 = 120°
ψ_0 = 150°
ψ_0 = 60°
ψ_0 = 30°
CORRIDOR

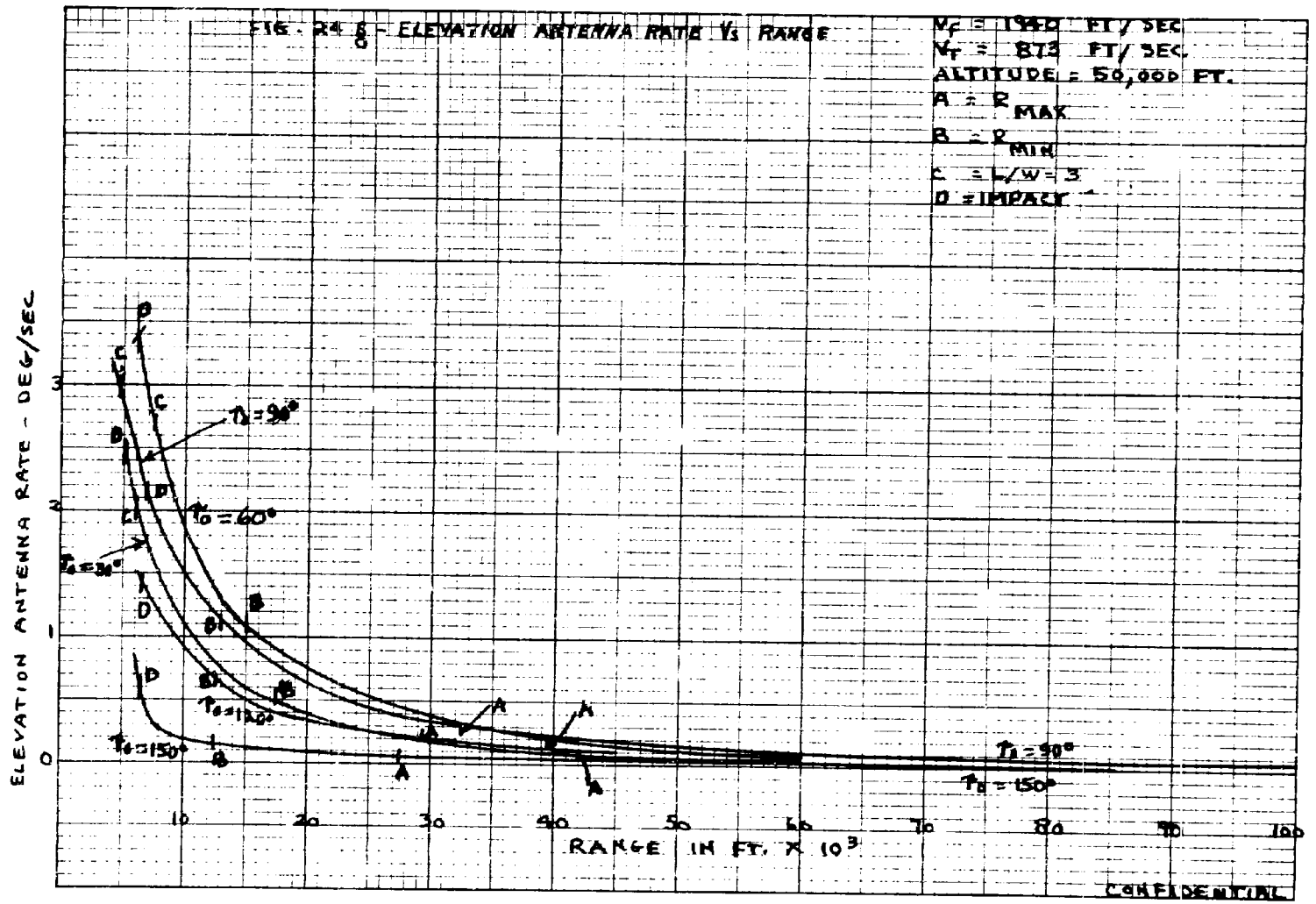
FIG. 24 $\frac{S}{G}$ - ELEVATION ANTENNA RATE $\dot{\gamma}_s$ RANGE
V_C = 1950 FT/SEC
V_T = 873 FT/SEC
ALTITUDE = 50,000 FT.
A = R_{MAX}
B = R_{MIN}
C = L/W = 3
D = IMPACT
ELEVATION ANTENNA RATE - DEG/SEC
RANGE IN FT. X 10^3
γ_T = 90°
γ_T = 60°
γ_T = 30°
γ_T = 120°
γ_T = 150°
γ_T = 90°
γ_T = 150°
CONFIDENTIAL

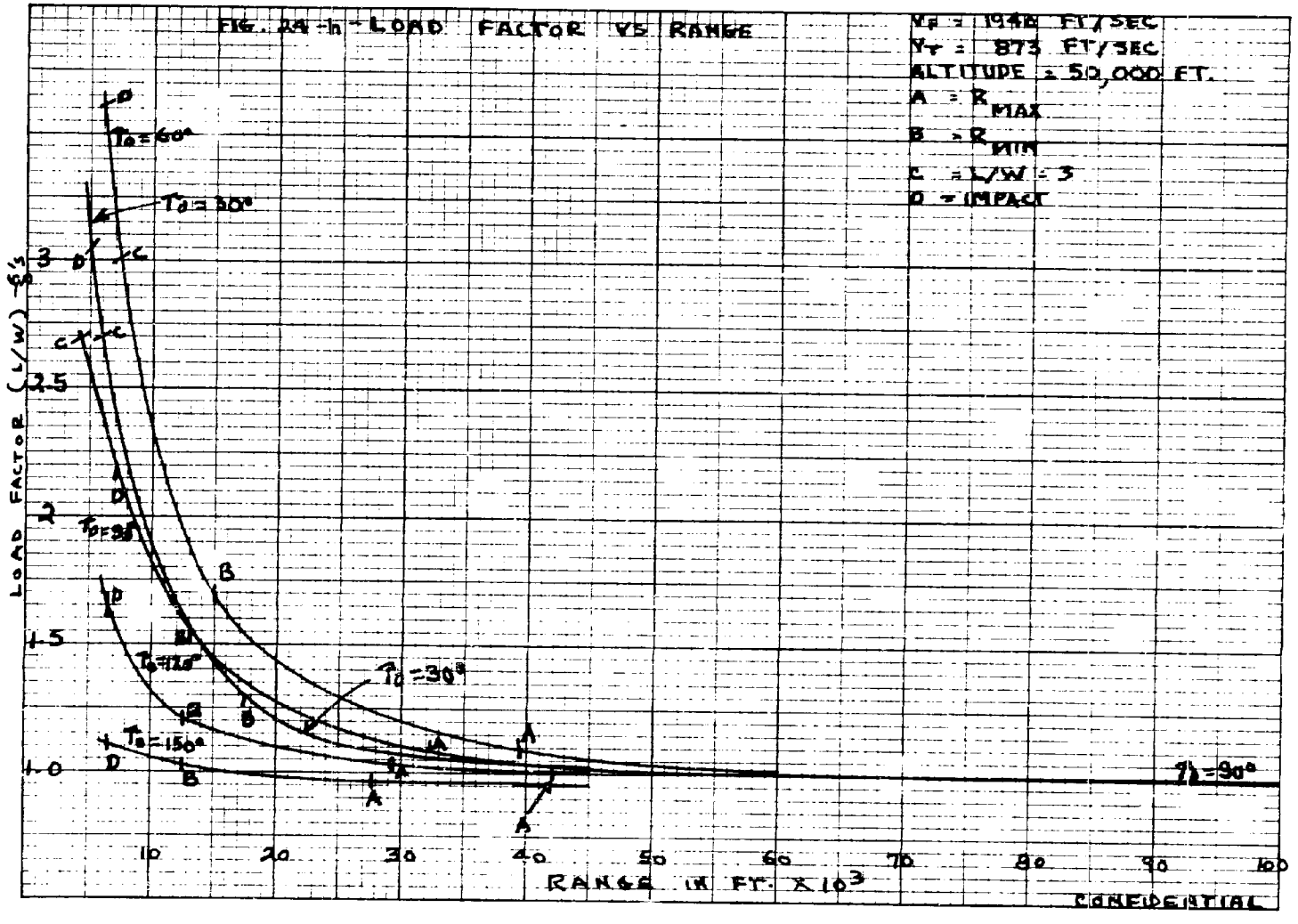
FIG. 24-h - LOAD FACTOR VS RANGE
V_F = 1948 FT/SEC
V_T = 873 FT/SEC
ALTITUDE = 50,000 FT.
A = R_{MAX}
B = R_{MIN}
C = L/W = 3
D = IMPACT
LOAD FACTOR (L/W) - G's
RANGE IN FT. X 10^3
T_D=60°
T_D=30°
T_D=30°
T_D=12°
T_D=30°
T_D=150°
T_D=90°
CONFIDENTIAL

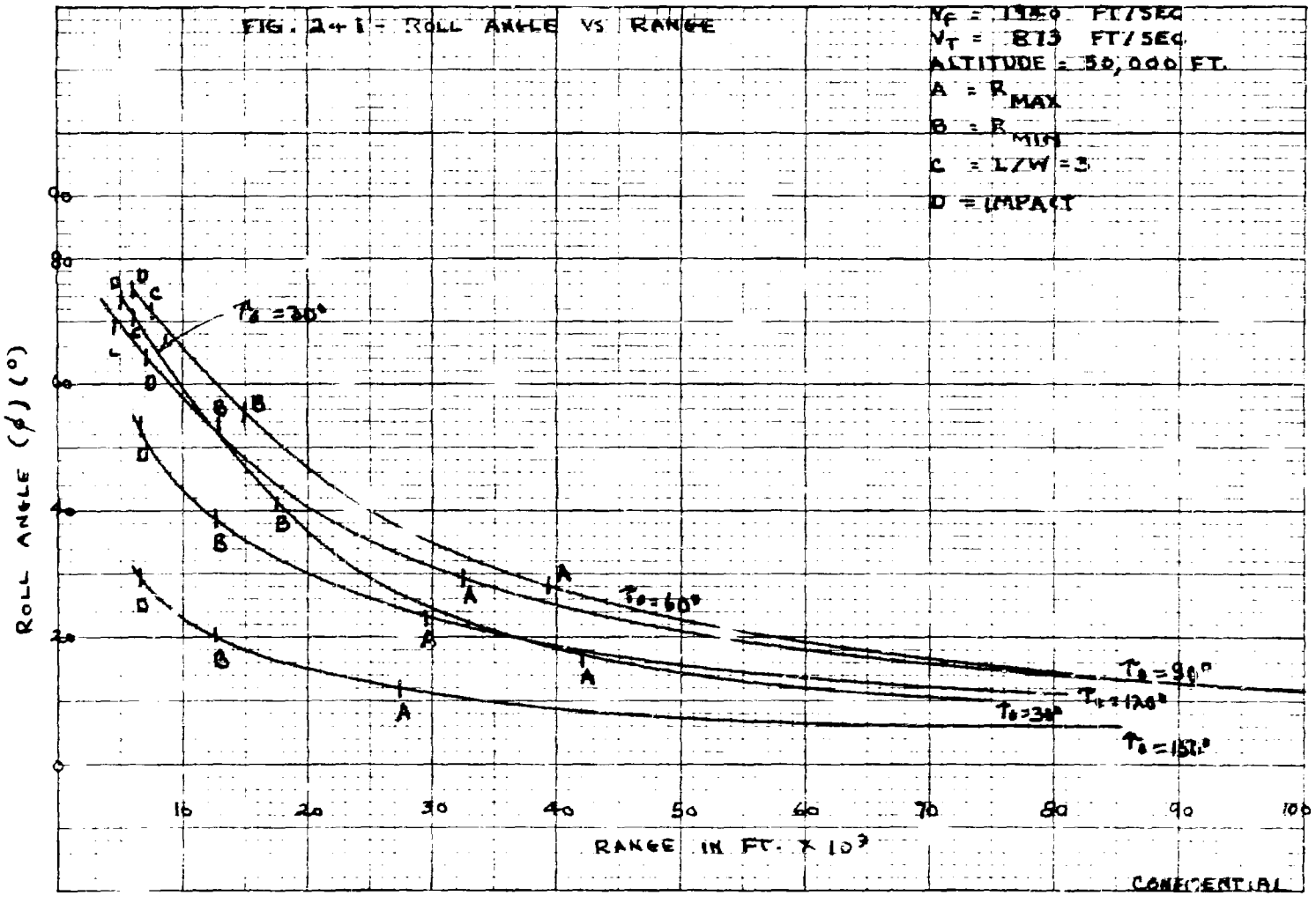
FIG. 24-1 - ROLL ANGLE VS RANGE
V_F = 1150 FT/SEC
V_T = 873 FT/SEC
ALTITUDE = 50,000 FT.
A = R_{MAX}
B = R_{MIN}
C = L/W = 3
D = IMPACT
T_θ = 30°
T_θ = 60°
T_θ = 90°
T_θ = 120°
T_θ = 135°
T_θ = 150°
ROLL ANGLE (φ) (°)
RANGE IN FT. X 10^3
CONFIDENTIAL

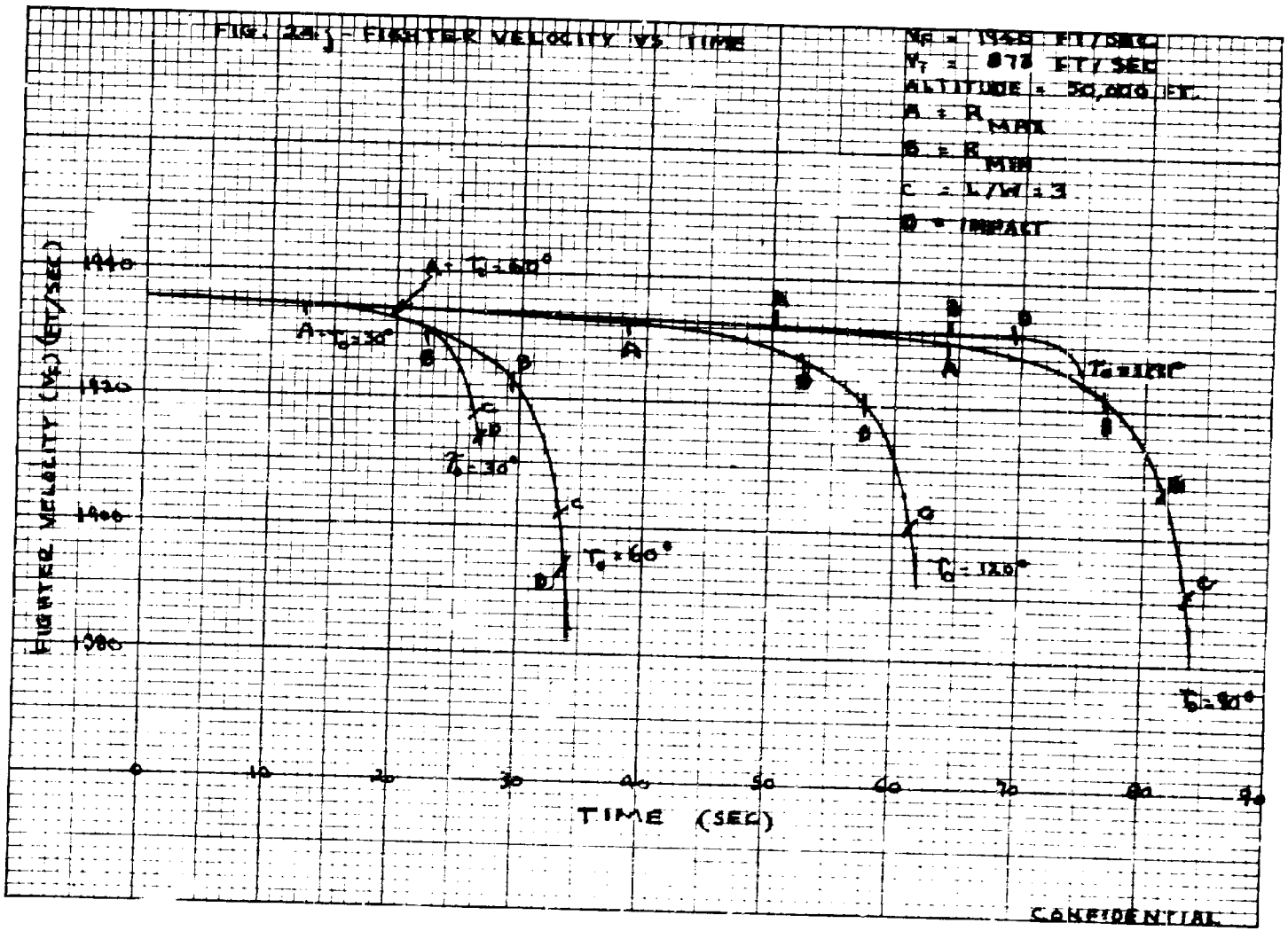
FIG. 23 - FIGHTER VELOCITY VS TIME
V_F = 1945 FT/SEC
V_T = 873 FT/SEC
ALTITUDE = 50,000 FT.
A = R_{MAX}
B = R_{MIN}
C = L/W = 3
D = IMPACT
FIGHTER VELOCITY (V_F) (FT/SEC)
1440
1420
1400
1380
0
10
20
30
40
50
60
70
80
90
TIME (SEC)
T_0 = 60°
T_0 = 30°
T_0 = 120°
T_0 = 90°
CONFIDENTIAL

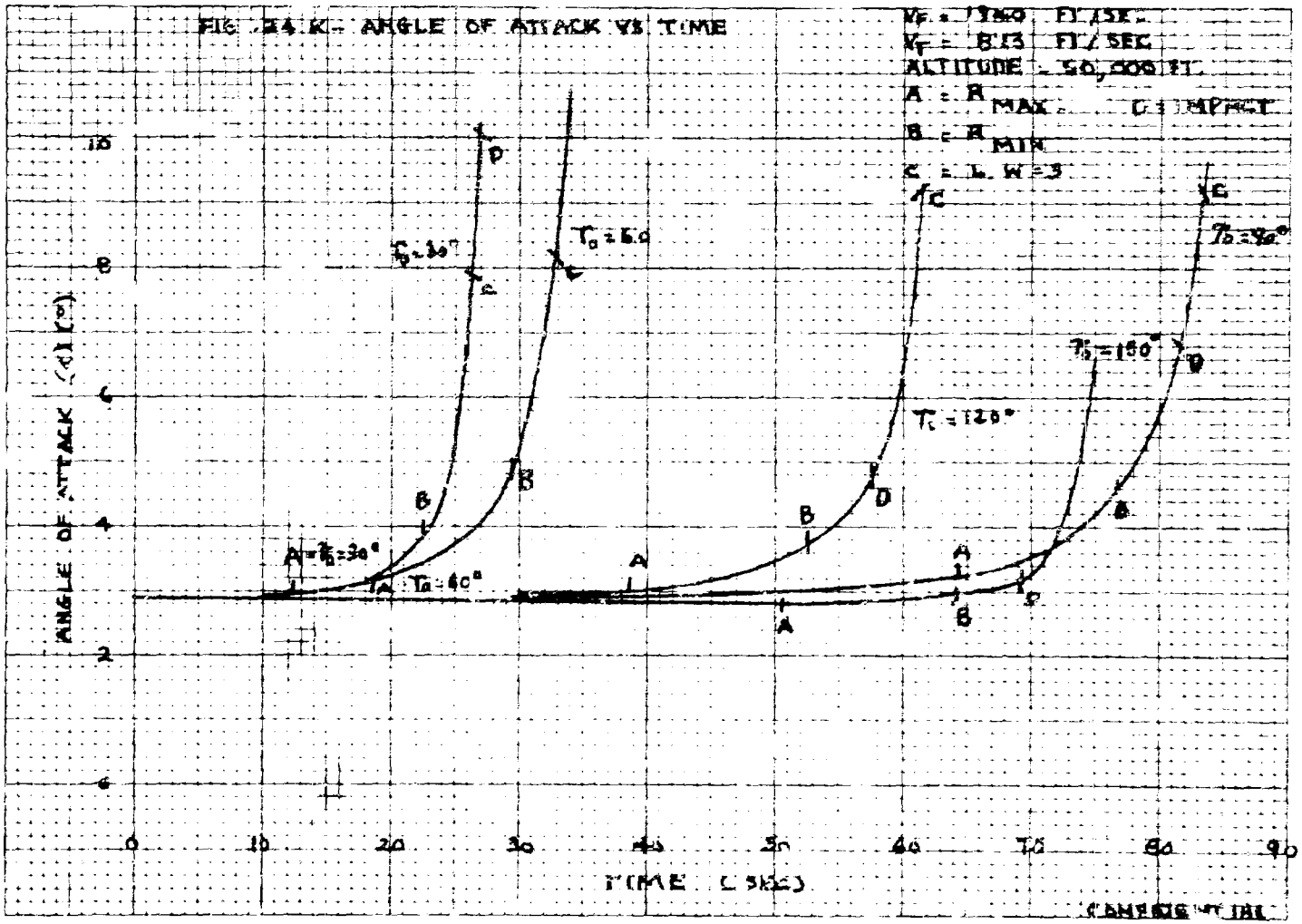
FIG. 24 K - ANGLE OF ATTACK VS TIME
V_F = 13,160 FT/SEC
V_F = 8,173 FT/SEC
ALTITUDE = 50,000 FT.
A = R MAX.
B = R MIN.
C = L. W = 3
C = IMPACT
T_0 = 30°
T_0 = 60°
T_0 = 120°
T_0 = 150°
T_0 = 180°
ANGLE OF ATTACK (α) (°)
TIME (SEC)
CAMBER AT IMP

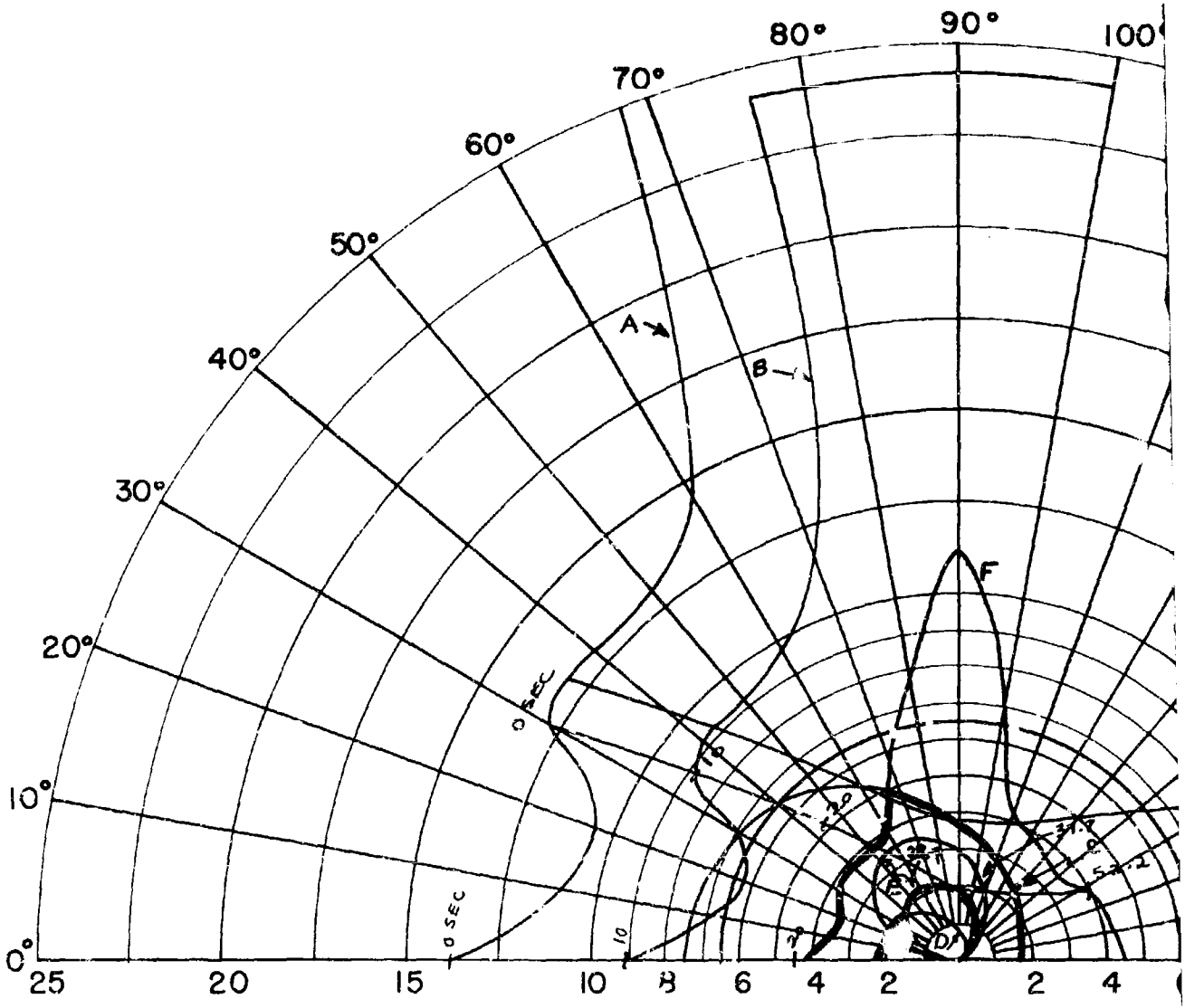

TARGET HEADING

V_F = 894 FT/SEC (F4H-1)
V_T = 1897 FT/SEC
ALTITUDE = 30,000 FT.

A - 85% DETECTION RANGE
B - LOCK-ON RANGE (10 SEC. LOCK-
C - SPARROW III MAX. AERODYNAMI
D - SPARROW III MIN. AERODYNAMI
E - CONSTANT LOAD FACTOR LOCU
F - 30% SPARROW III SEEKER LOC
G - 6.5 N.M. INTERLOCK

FIG. 25- CO-ALTITUDE LEAD PURSUIT ATTACK ZONE OVERLAYS.

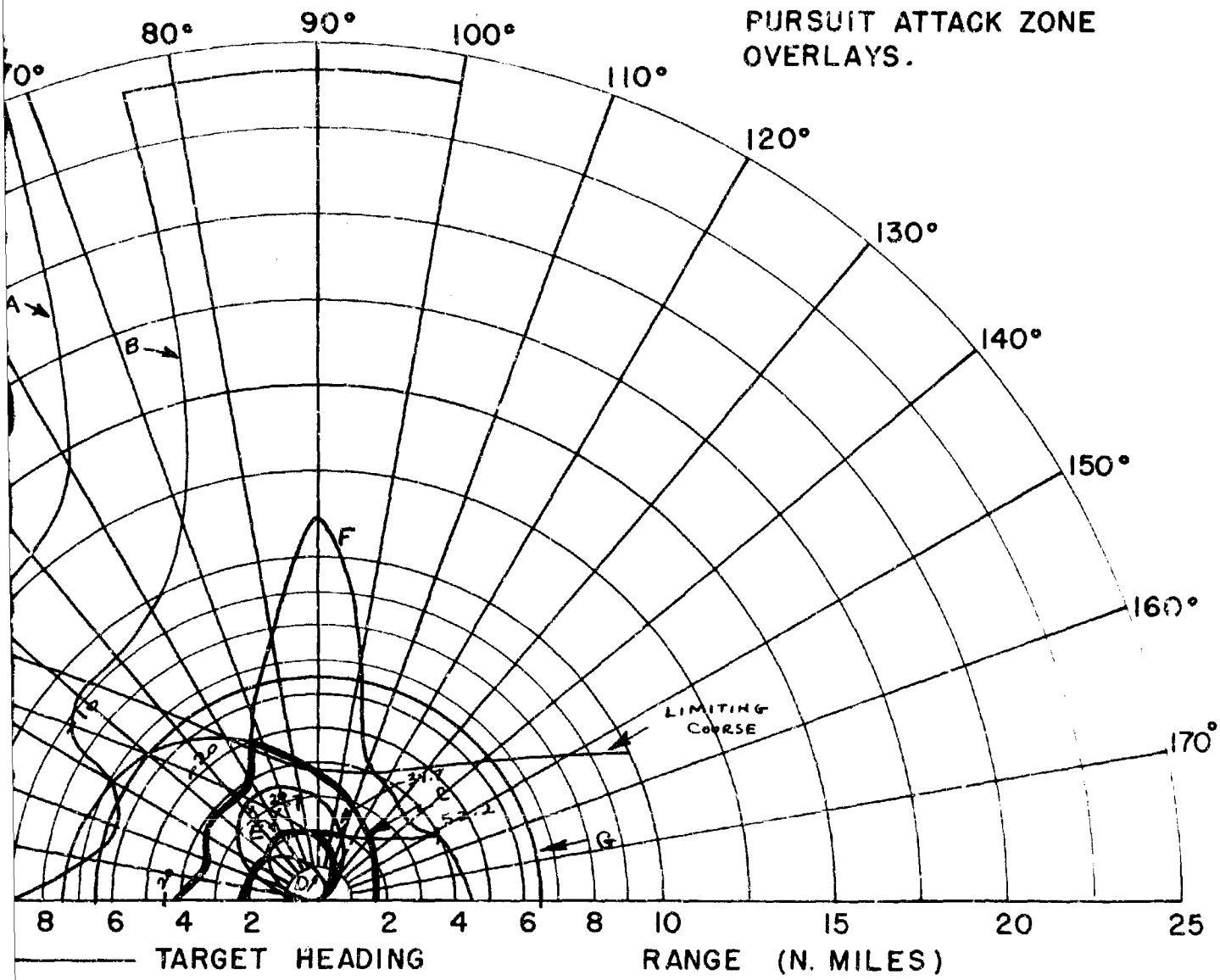

85% DETECTION RANGE
LOCK-ON RANGE (10 SEC. LOCK-ON TIME)
SPARROW III MAX. AERODYNAMIC RANGE
SPARROW III MIN. AERODYNAMIC RANGE
CONSTANT LOAD FACTOR LOCUS (N_Z = 2,3)
90% SPARROW III SEEKER LOCK-ON RANGE
6.5 N.M. INTERLOCK

CONFIDENTIAL

2

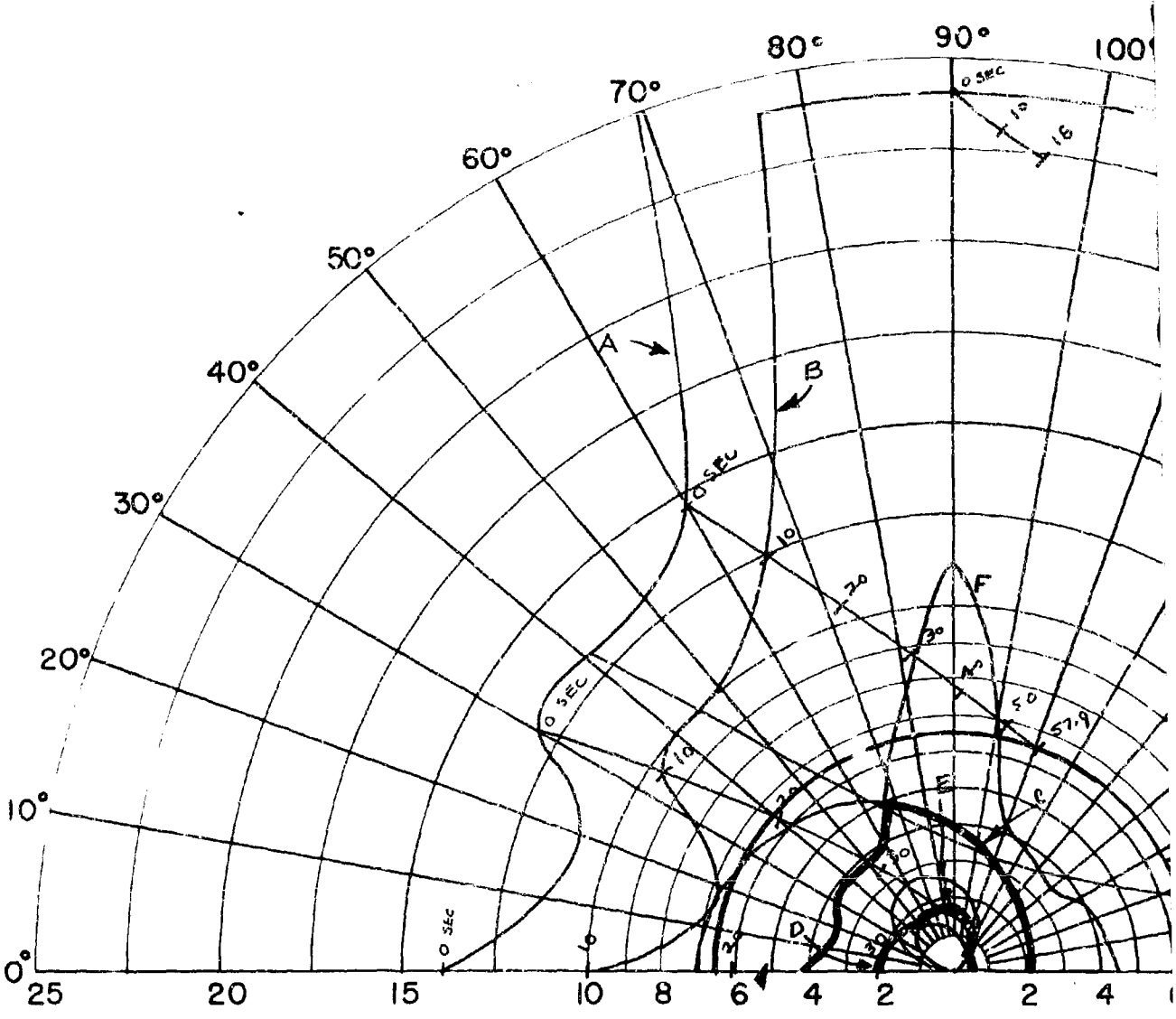

V_F = 894 FT/SEC (F4H-1)
V_T = 1518 FT/SEC
ALTITUDE = 30,000 FT.

A - 85% DETECTION RANGE
B - LOCK-ON RANGE (10 SEC. LOCK-
C - SPARROW III MAX. AERODYNAMI
D - SPARROW III MIN. AERODYNAMI
E - CONSTANT LOAD FACTOR LOCU
F - 90% SPARROW III SEEKER LO
G - 6.5 N.M. INTERLOCK

FIG. 26 - CO-ALTITUDE LEAD PURSUIT ATTACK ZONE OVERLAYS.

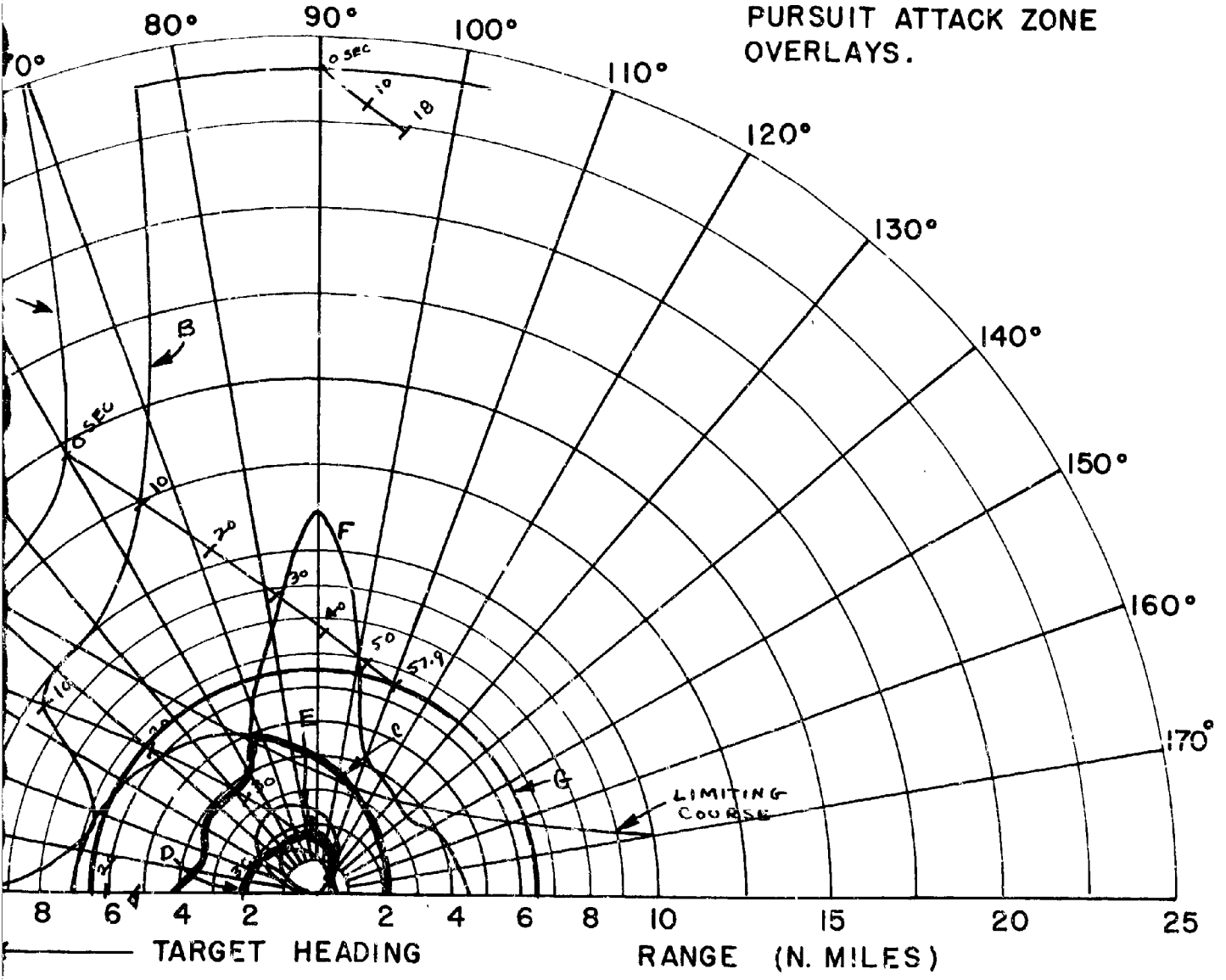

- 85% DETECTION RANGE
- LOCK-ON RANGE (10 SEC. LOCK-ON TIME)
- SPARROW III MAX. AERODYNAMIC RANGE
- SPARROW III MIN. AERODYNAMIC RANGE
- CONSTANT LOAD FACTOR LOCUS (N_Z = 2,3)
- 90% SPARROW III SEEKER LOCK-ON RANGE
- 6.5 N.M. INTERLOCK

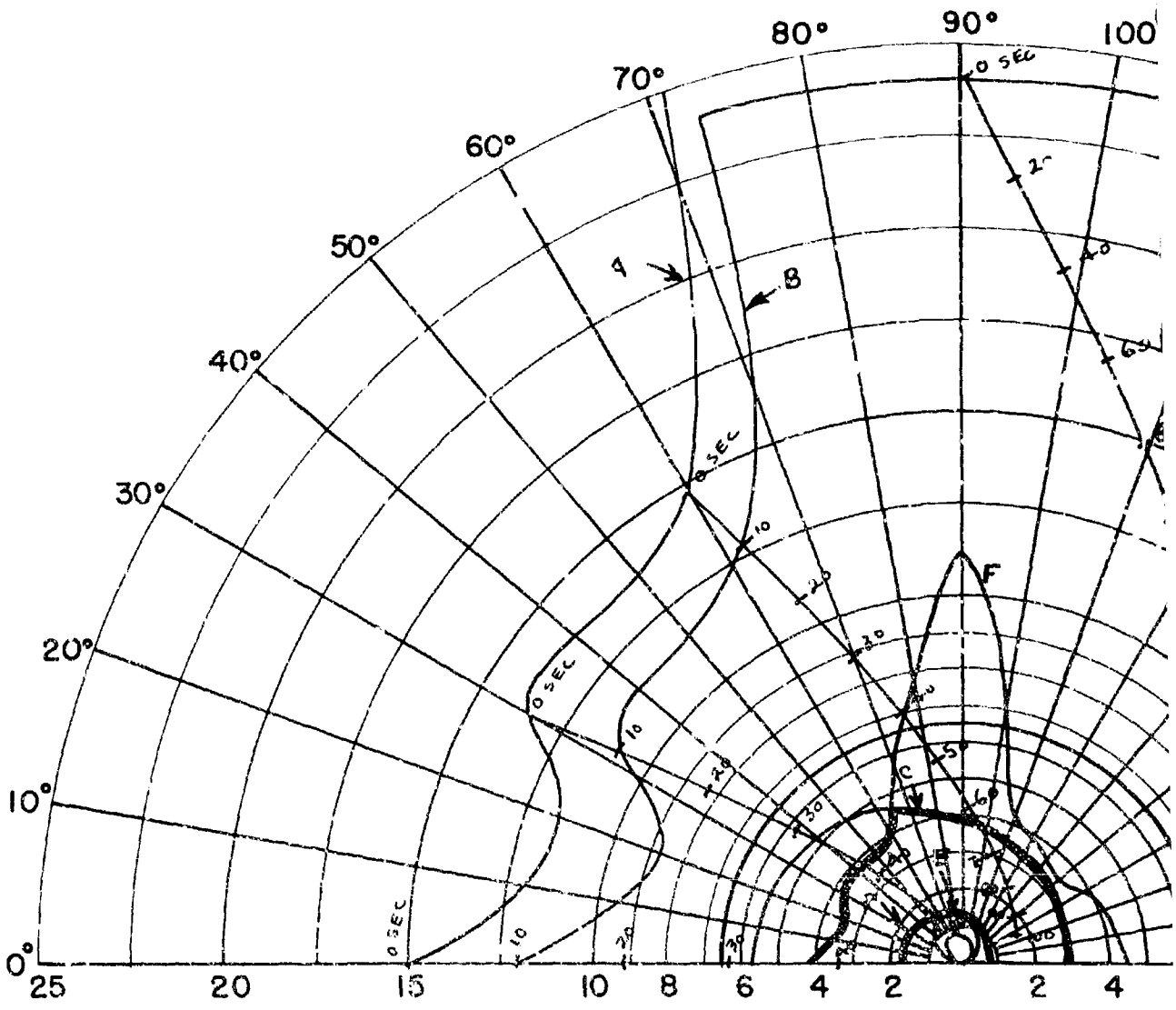

TARGET HEADING

V_F = 894 FT/SEC (F4H-1)
V_T = 854 FT/SEC
ALTITUDE = 30,000 FT.

A - 85% DETECTION RANGE
B - LOCK-ON RANGE (10 SEC. LOCK-
C - SPARROW III MAX. AERODYNAMI
D - SPARROW III MIN. AERODYNAMI
E - CONSTANT LOAD FACTOR LOC
F - 90% SPARROW III SEEKER LO
G - 6.5 N.M. INTERLOCK

FIG. 27 - CO-ALTITUDE LEAD PURSUIT ATTACK ZONE OVERLAYS.

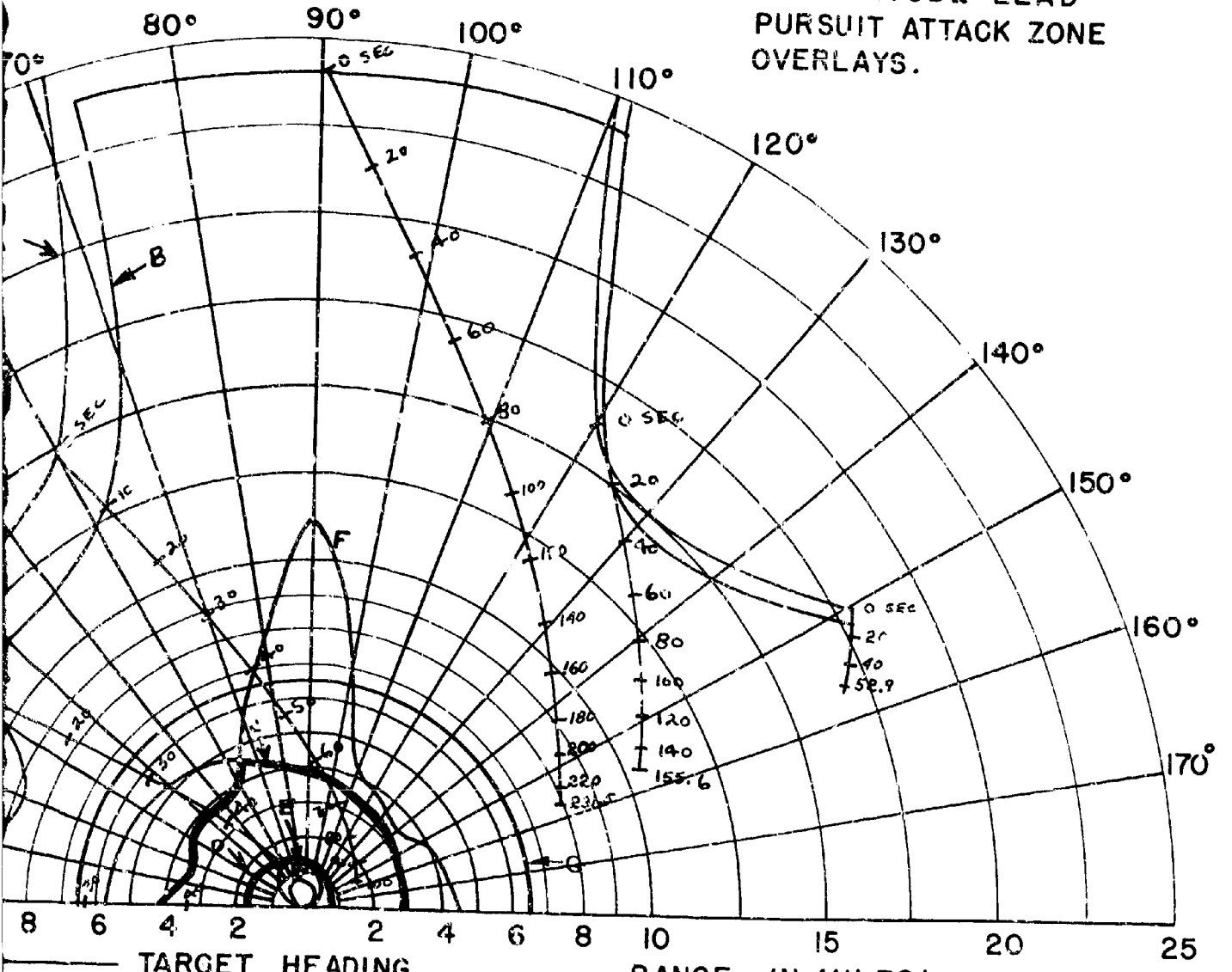

——— TARGET HEADING

85% DETECTION RANGE
LOCK-ON RANGE (10 SEC. LOCK-ON TIME)
SPARROW III MAX. AERODYNAMIC RANGE
SPARROW III MIN. AERODYNAMIC RANGE
CONSTANT LOAD FACTOR LOCUS (N_z = 2,3)
90% SPARROW III SEEKER LOCK-ON RANGE
6.5 N.M. INTERLOCK

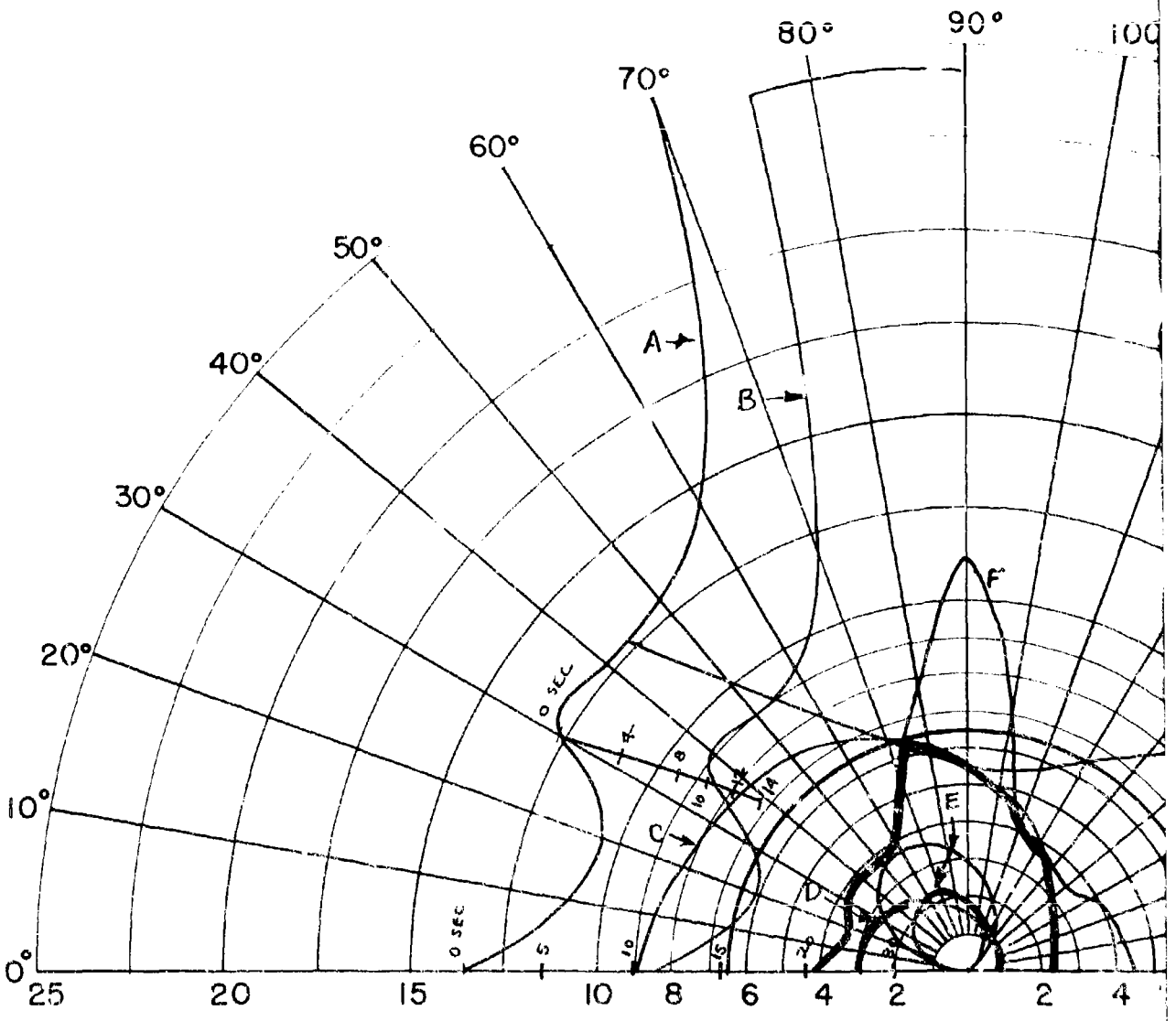

V_F = 873 FT/SEC (F4H-1)
V_T = 1940 FT/SEC
ALTITUDE = 50,000 FT.

A - 85% DETECTION RANGE
B - LOCK-ON RANGE (10 SEC. LOCK
C - SPARROW III MAX. AERODYNAM
D - SPARROW III MIN. AERODYNAM
E - CONSTANT LOAD FACTOR LO
F - 30% SPARROW III SEEKER L
G - 6.5 N.M. INTERLOCK

FIG. 28 - CO-ALTITUDE LEAD PURSUIT ATTACK ZONE OVERLAYS.

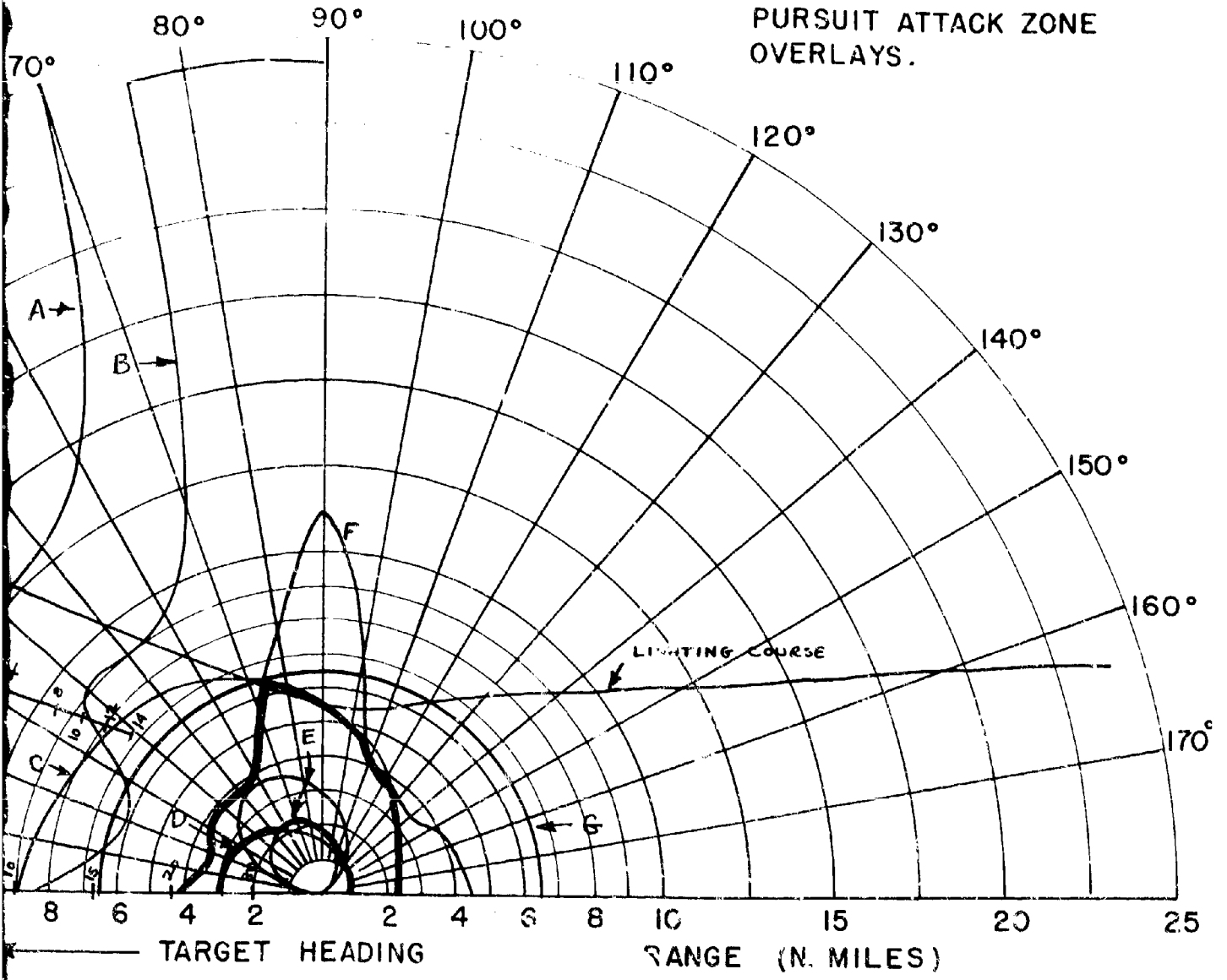

- 85% DETECTION RANGE
- LOCK-ON RANGE (10 SEC. LOCK-ON TIME)
- SPARROW II MAX. AERODYNAMIC RANGE
- SPARROW III MIN. AERODYNAMIC RANGE
- CONSTANT LOAD FACTOR LOCUS ($N_Z = 2,3$)
- 90% SPARROW III SEEKER LOCK-ON RANGE
- 6.5 N.M. INTERLOCK

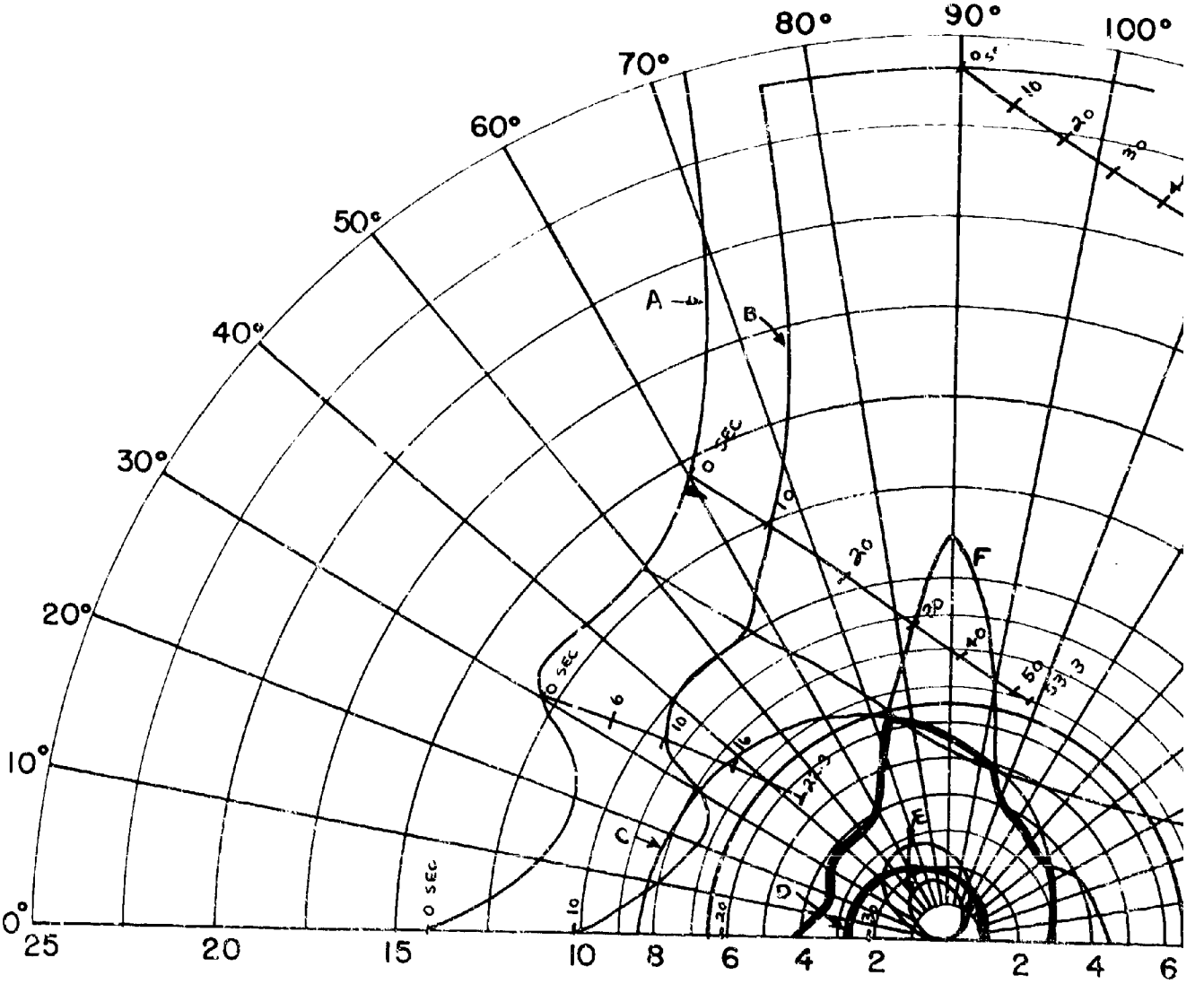

V_F = 873 FT/SEC (F4H-1)
V_T = 1552 FT/SEC
ALTITUDE = 50,000 FT.

A - 85% DETECTION RANGE
B - LOCK-ON RANGE (10 SEC. LOCK-ON
C - SPARROW III MAX. AERODYNAMIC
D - SPARROW III MIN. AERODYNAMIC
E - CONSTANT LOAD FACTOR LOCUS
F - 90% SPARROW III SEEKER LOCK
G - 6.5 N.M. INTERLOCK

FIG 29 - CO-ALTITUDE LEAD PURSUIT ATTACK ZONE OVERLAYS.

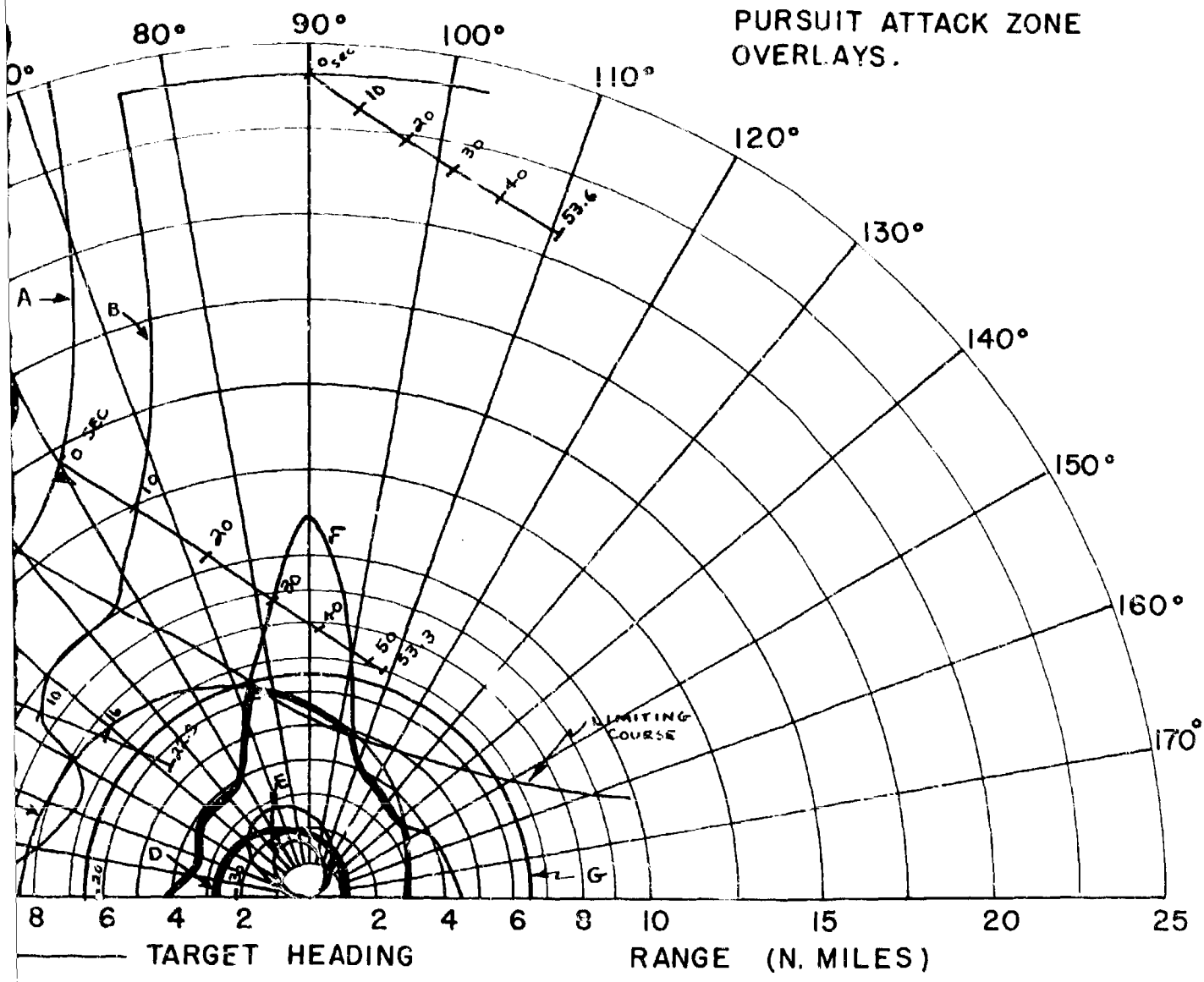

85% DETECTION RANGE
LOCK-ON RANGE (10 SEC. LOCK-ON TIME)
SPARROW III MAX. AERODYNAMIC RANGE
SPARROW III MIN. AERODYNAMIC RANGE
CONSTANT LOAD FACTOR LOCUS (N_Z = 2,3)
90% SPARROW III SEEKER LOCK-ON RANGE
6.5 N.M. INTERLOCK

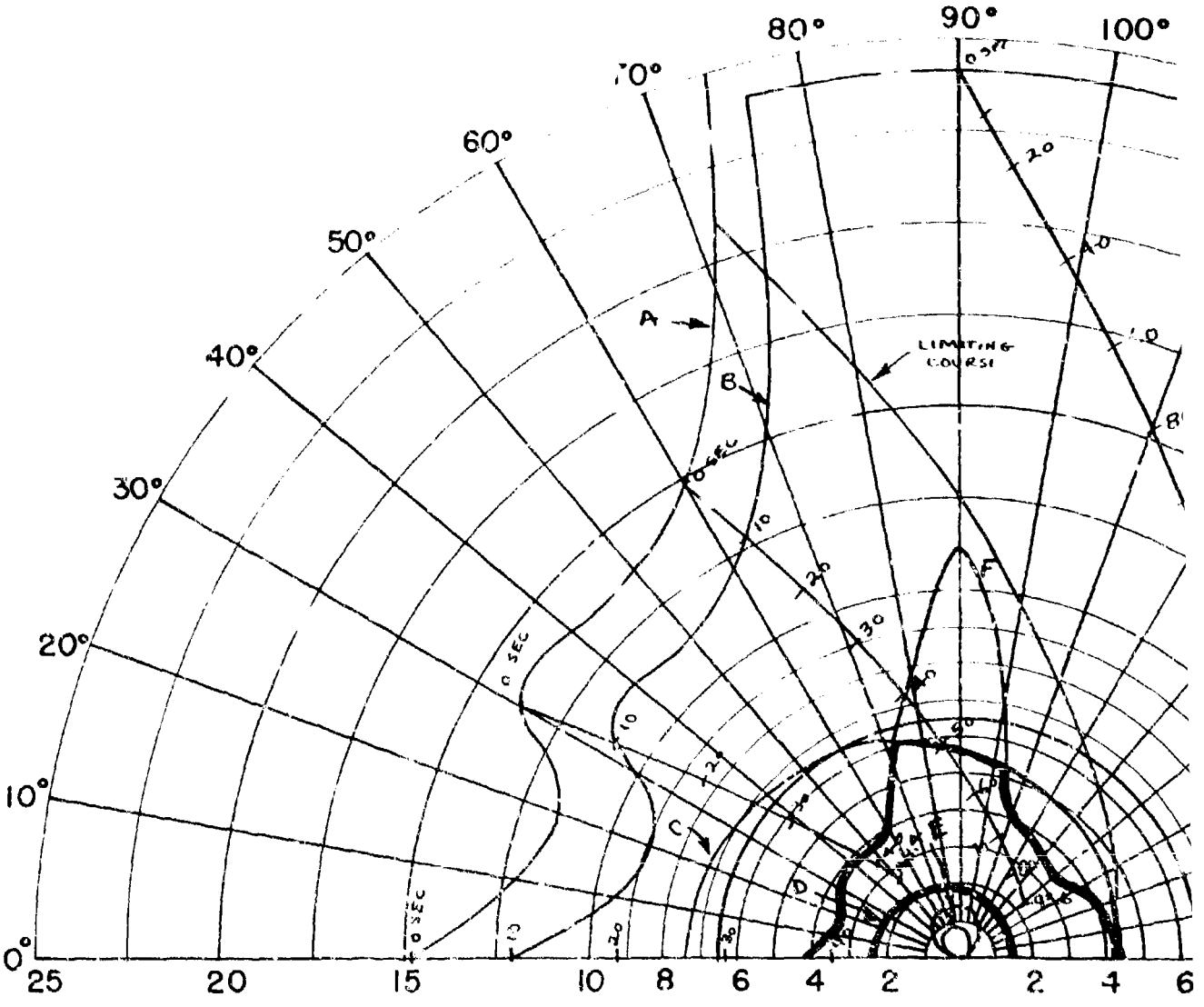

V_F = 873 FT/SEC (F4H-1)
V_T = 873 FT/SEC
ALTITUDE = 50,000 FT.

A - 85% DETECTION RANGE
B - LOCK-ON RANGE (10 SEC. LOCK-O
C - SPARROW III MAX. AERODYNAMIC
D - SPARROW III MIN. AERODYNAMIC
E - CONSTANT LOAD FACTOR LOCUS
F - 90% SPARROW III SEEKER LOCI
G - 6.5 N.M. INTERLOCK

FIG. 30 - CO-ALTITUDE LEAD PURSUIT ATTACK ZONE OVERLAYS.

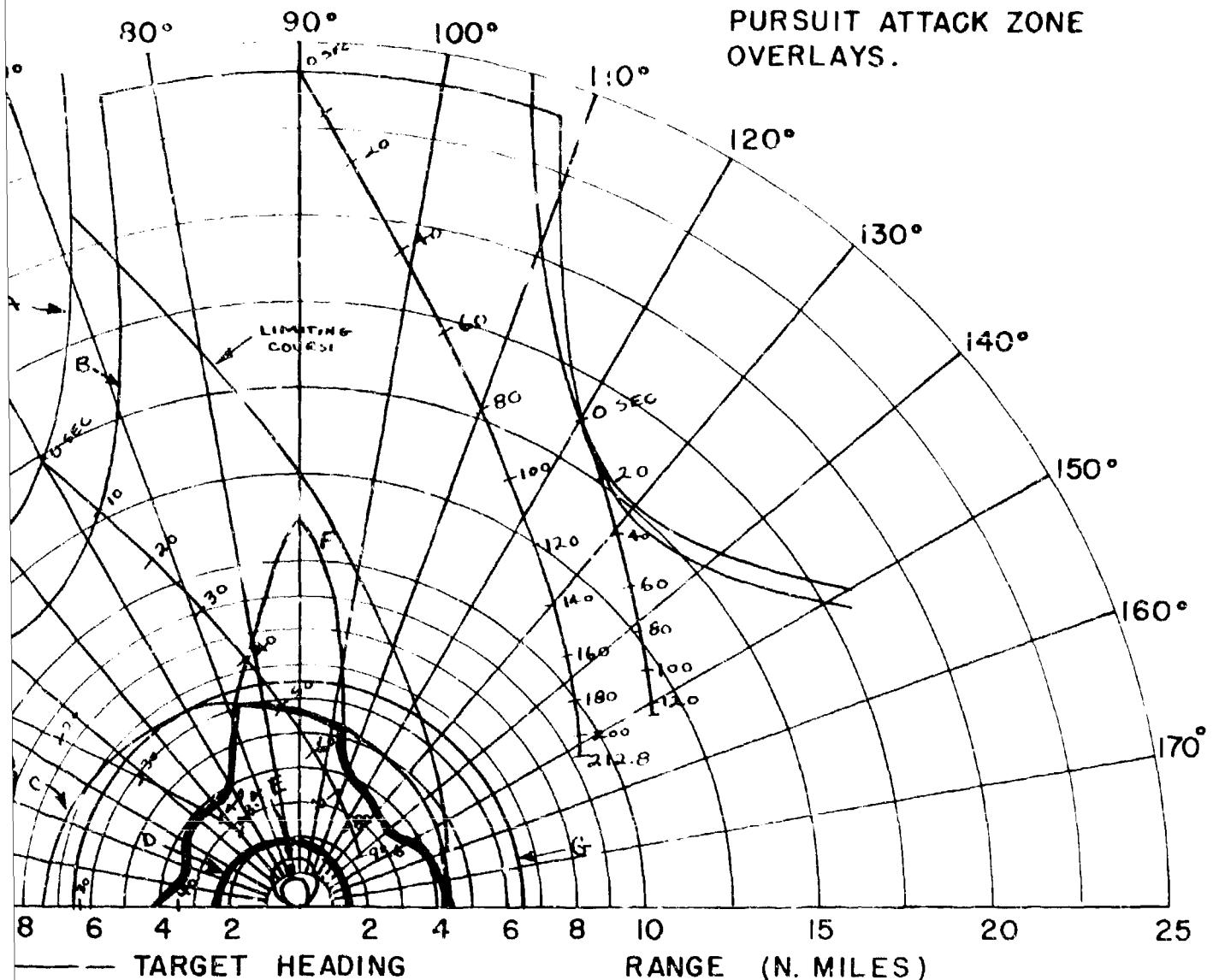

5% DETECTION RANGE
OCK-ON RANGE (10 SEC. LOCK-ON TIME)
PARROW III MAX. AERODYNAMIC RANGE
PARROW III MIN. AERODYNAMIC RANGE
ONSTANT LOAD FACTOR LOCUS (N_Z = 2,3)
0% SPARROW III SEEKER LOCK-ON RANGE
.5 N.M. INTERLOCK

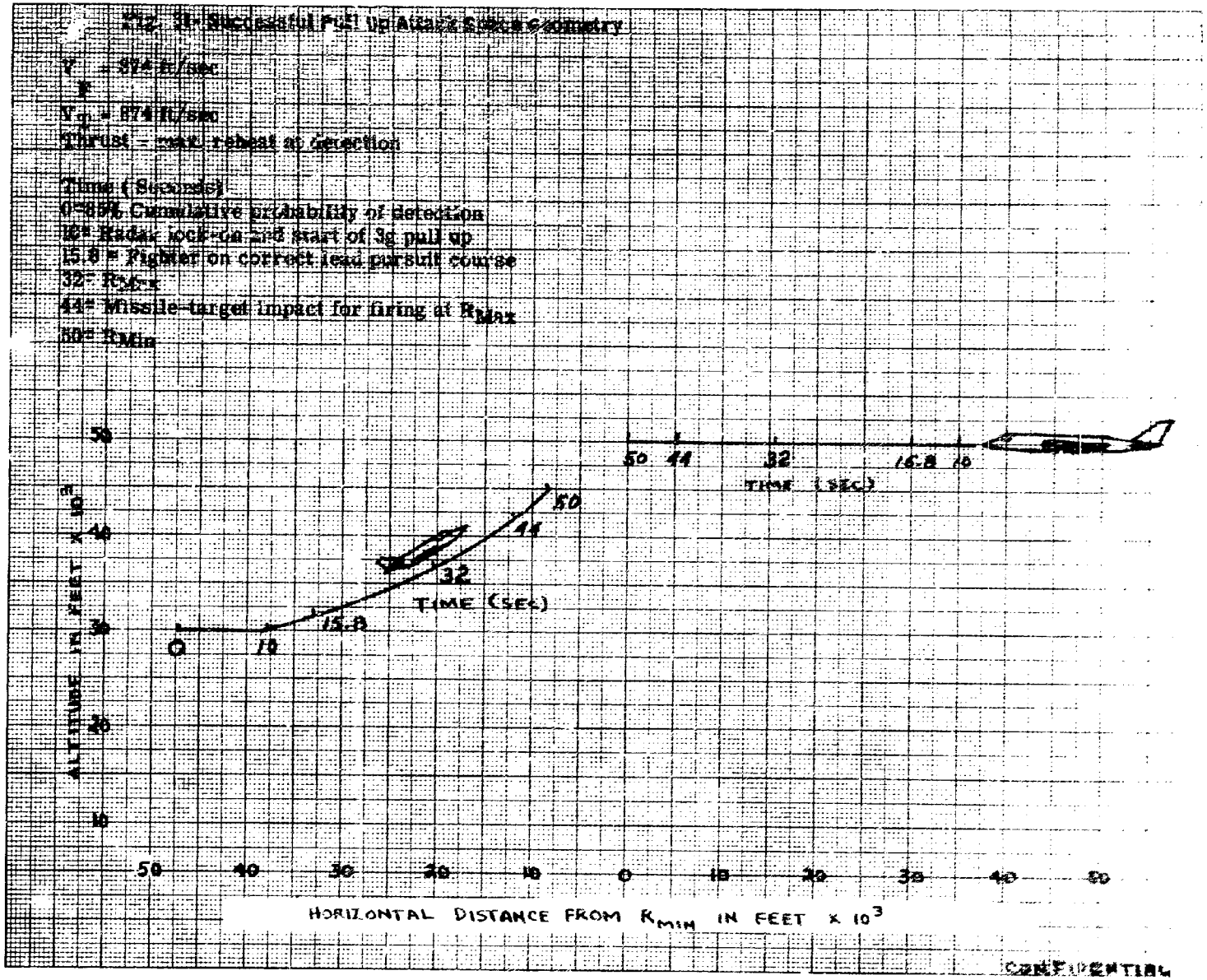
Fig 12. 3- Successful Full up Attack Geometry
V = 874 ft/sec
T
V = 874 ft/sec
T
Thrust - max reheat at detection
Time (Seconds)
0=85% Cumulative probability of detection
10= Radar lock-on and start of 3g pull up
15.8 = Fighter on correct lead pursuit course
32= R
44= Missile-target impact for firing at R
50= R
50
40
30
20
10
ALTITUDE IN FEET
50
44
32
15.8
10
0
TIME (SEC.)
50
44
32
15.8
10
0
TIME (SEC.)
50
40
30
20
10
0
10
20
30
40
50
HORIZONTAL DISTANCE FROM K IN FEET x 10
CONFIDENTIAL

Fig. 32- Space Geometry for One Unsuccessful Pull Up Attack

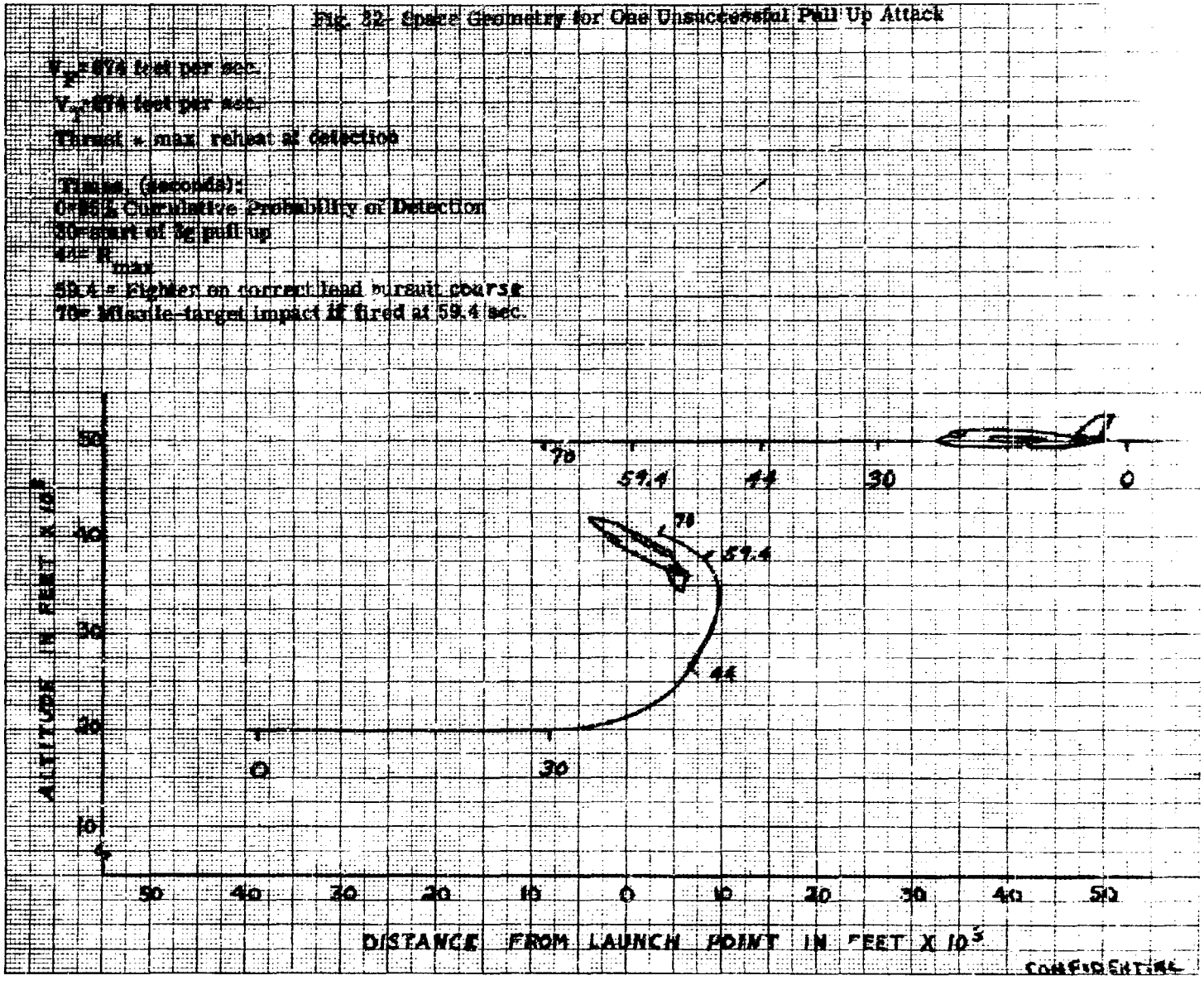

CONFIDENTIAL

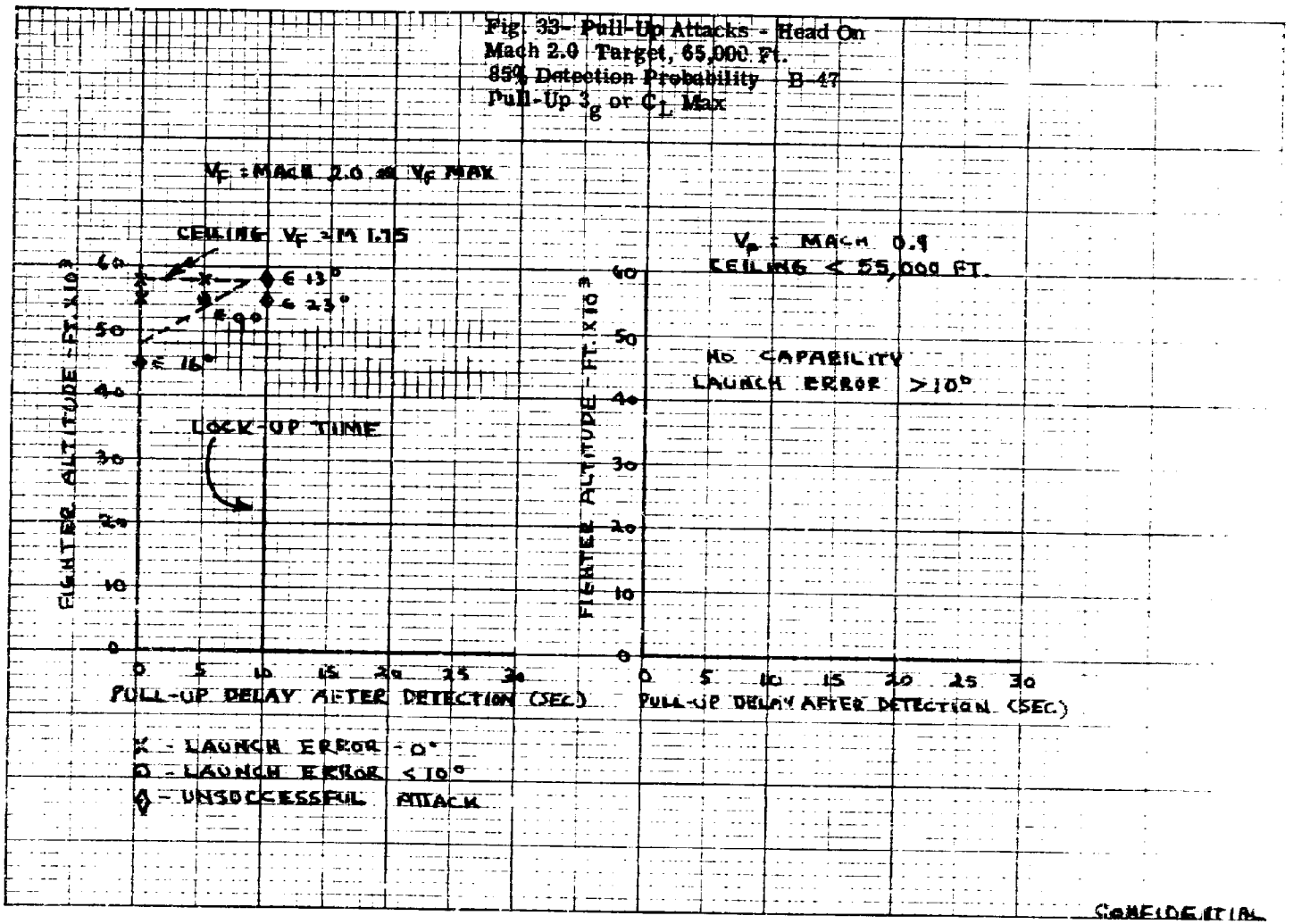

Fig. 33- Pull-Up Attacks - Head On
Mach 2.0 Target, 65,000 Ft.
85% Detection Probability - B-47
Pull-Up 3 g or C_L Max

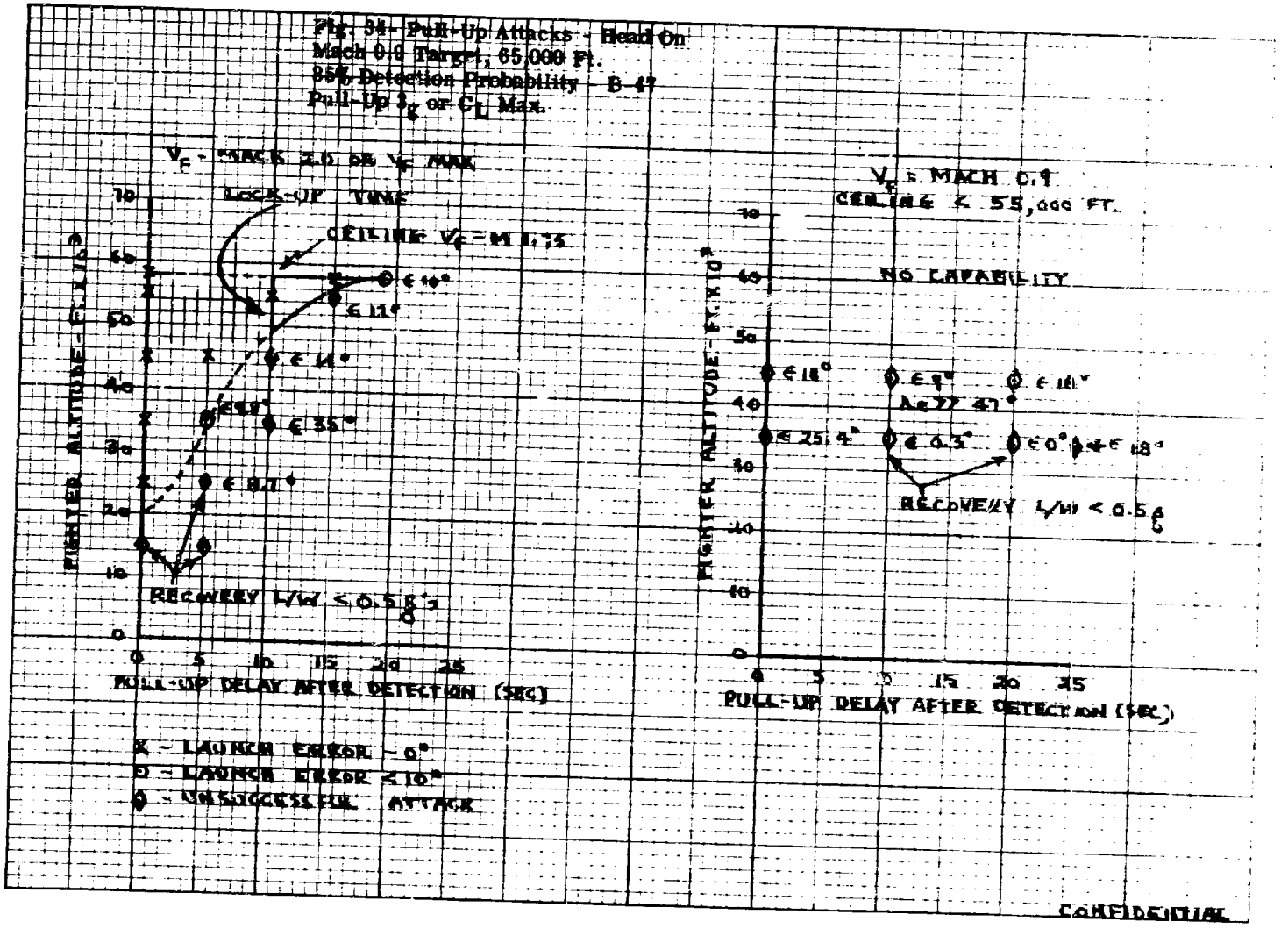
Fig. 34 - Pull-Up Attacks - Head On
Mach 0.8 Target, 65,000 Ft.
85% Detection Probability - B-47
Pull-Up n_g or C_L Max.
V_F = MACH 2.0 OR V_F MAX
LOCK-UP TIME
CEILING V_F = M 1.35
ϵ 10°
ϵ 11°
ϵ 14°
ϵ 35°
ϵ 8.7°
RECOVERY L/W ≤ 0.5 g's
FIGHTER ALTITUDE - FT. X 10³
PULL-UP DELAY AFTER DETECTION (SEC)
X - LAUNCH ERROR = 0°
O - LAUNCH ERROR < 10°
◊ - UNSUCCESSFUL ATTACK
V_F = MACH 0.9
CEILING < 55,000 FT.
NO CAPABILITY
ϵ 18°
ϵ 9°
ϵ 18°
Δε 27.4°
ϵ 25.4°
ϵ 0.3°
ϵ 0°
ϵ 18°
RECOVERY L/W < 0.5 g
FIGHTER ALTITUDE - FT. X 10³
PULL-UP DELAY AFTER DETECTION (SEC)
CONFIDENTIAL

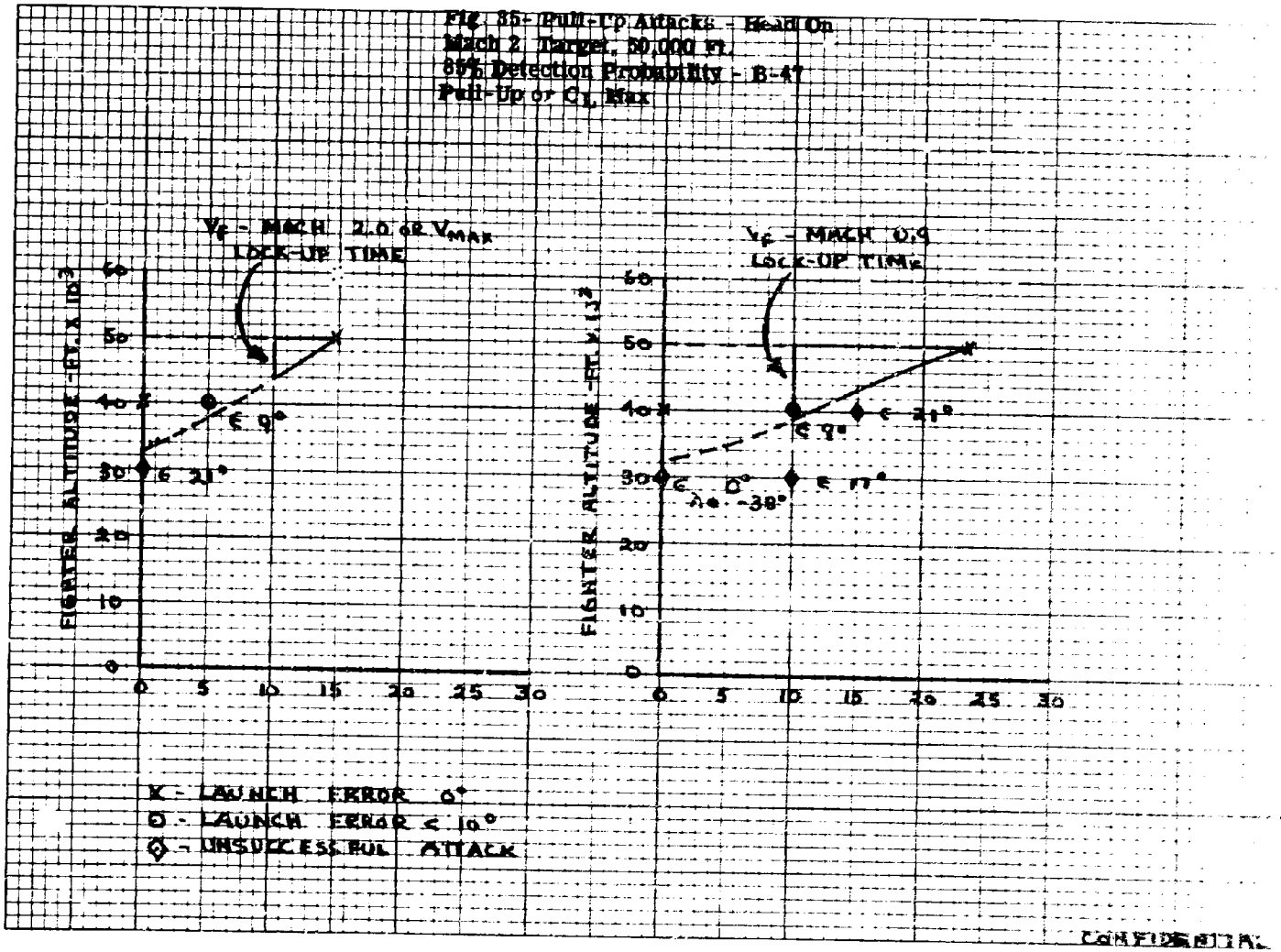
Fig. 35- Pull-Up Attack - Head On
Mach 2 Target, 50,000 Ft.
85% Detection Probability - B-47
Pull-Up or C_L Max
V_F - MACH 2.0 or V_{MAX}
LOCK-UP TIME
V_F - MACH 0.9
LOCK-UP TIME
FIGHTER ALTITUDE - FT. X 10^3
FIGHTER ALTITUDE - FT. X 10^3
60
50
40
30
20
10
0
0 5 10 15 20 25 30
ϵ 9°
ϵ 21°
ϵ 0°
ϵ 11°
λ_e -38°
K - LAUNCH ERROR 0°
O - LAUNCH ERROR < 10°
◇ - UNSUCCESSFUL ATTACK
CONFIDENTIAL

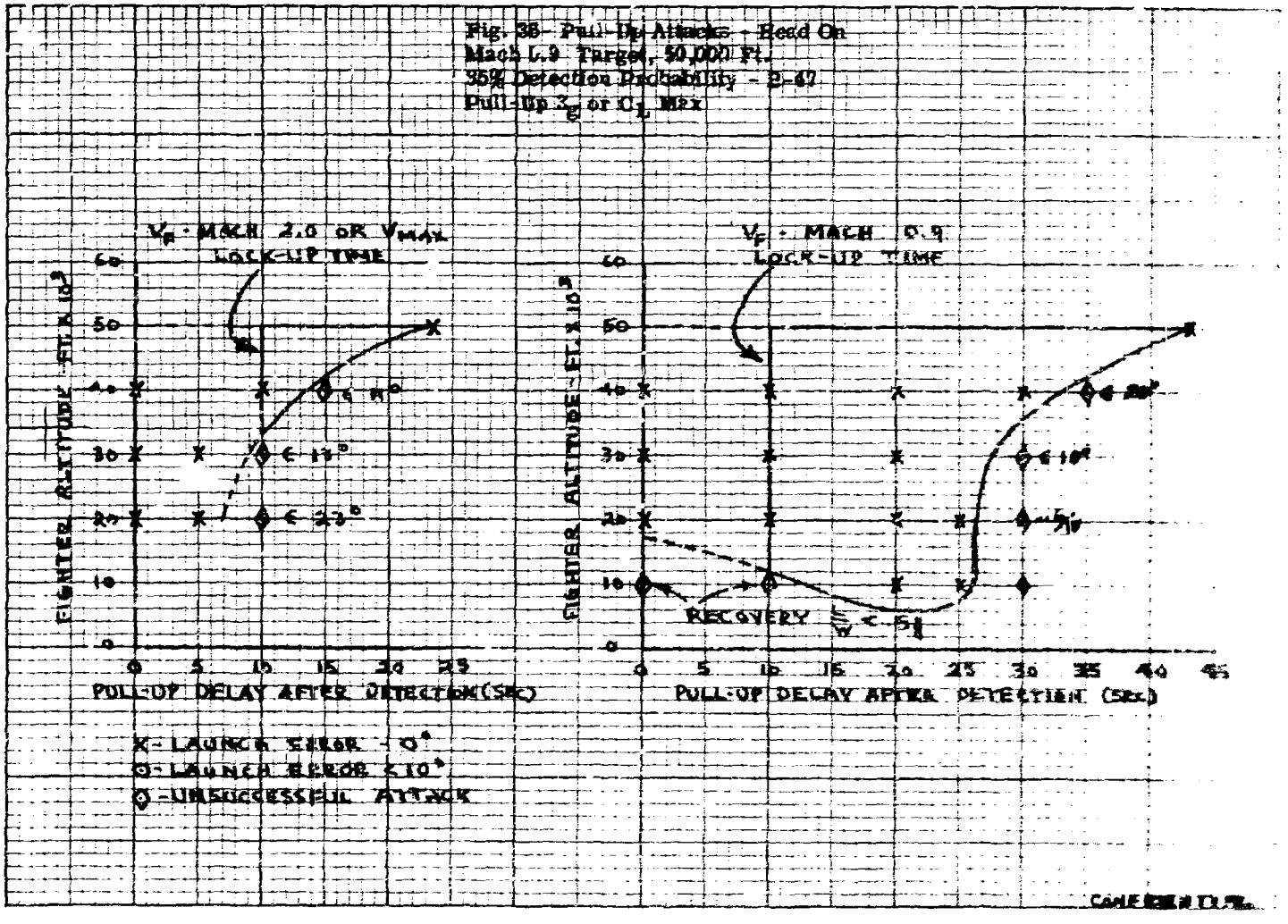
Fig. 38- Pull-Up Attacks - Head On
Mach 1.9 Target, 50,000 Ft.
35% Detection Probability - 2-47
Pull-Up n_z or $C_{L_{MAX}}$
V_F - MACH 2.0 OR V_{MAX}
LOCK-UP TIME
V_F - MACH 0.9
LOCK-UP TIME
FIGHTER ALTITUDE - FT. X 10^3
PULL-UP DELAY AFTER DETECTION (SEC)
RECOVERY $\frac{h}{V} < -5\frac{1}{2}$
X - LAUNCH ERROR = 0°
⊙ - LAUNCH ERROR ≤ 10°
◇ - UNSUCCESSFUL ATTACK

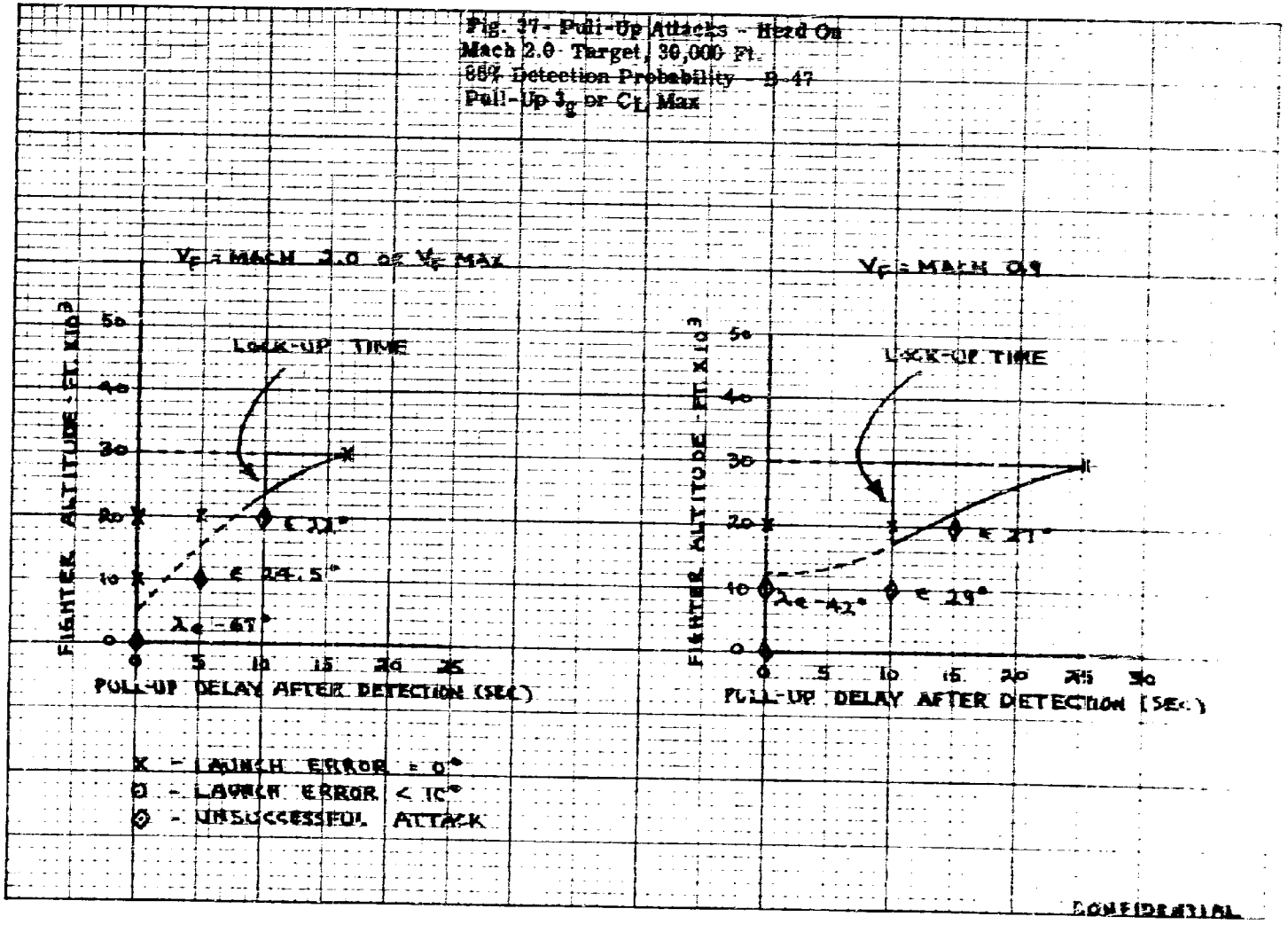
Fig. 37- Pull-Up Attacks - Head On
Mach 2.0 Target, 30,000 Ft.
65% Detection Probability - 9-47
Pull-Up 3_g or C_L Max
V_F = MACH 2.0 or V_F MAX
LOCK-UP TIME
FIGHTER ALTITUDE - FT. X 10^3
50
40
30
20
10
0
ϵ 21°
ϵ 24.5°
λ_e = 67°
0 5 10 15 20 25
PULL-UP DELAY AFTER DETECTION (SEC.)
V_F = MACH 0.9
LOCK-UP TIME
ϵ 21°
λ_e = 42°
ϵ 29°
0 5 10 15 20 25 30
PULL-UP DELAY AFTER DETECTION (SEC.)
X - LAUNCH ERROR = 0°
O - LAUNCH ERROR < 10°
◇ - UNSUCCESSFUL ATTACK
CONFIDENTIAL

Fig. 38 - Pull-Up Attacks - Head On
Mach 0.9 Target, 30,000 Ft.
85% Probability Detection - B-47
Pull-Up 3_g or C_{L_1} Max

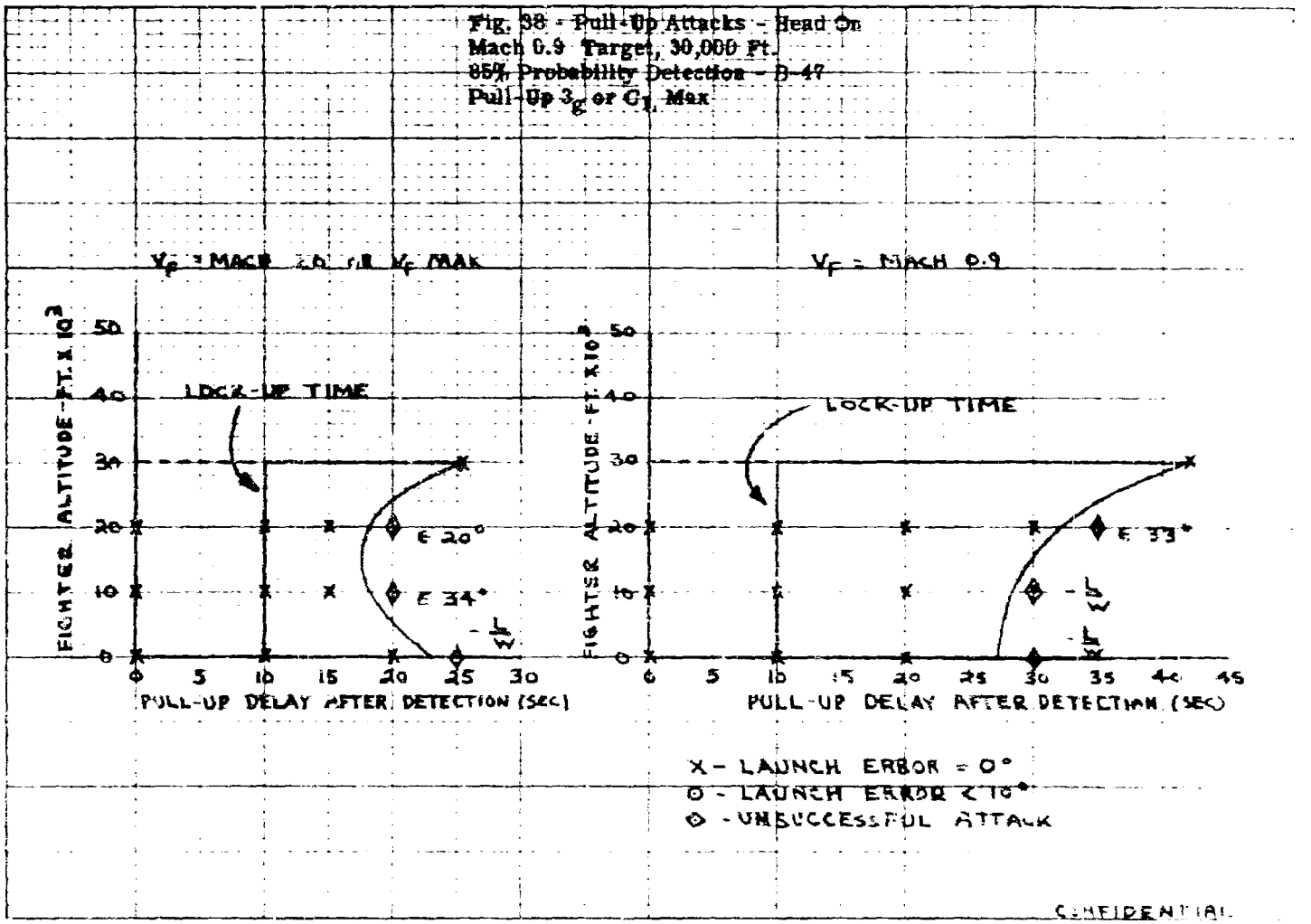

CONFIDENTIAL

F.G. 39 - PULL-UP ATTACK,
F4H-1 - SPARROW III
V_T = 876 FT/SEC, TARGET ALT. 45 000 FT.
V_F = 1935 FT/SEC AT DETECTION
THRUST = MAX REHEAT AT DETECTION
PULL-UP TO LEAD PURSUIT = 3 g OR $C_{L\,MAX}$
INITIAL FIGHTER ALT. 55,000 FT.

TIME FROM DETECTION TO PULL-UP	MAX. GIMBAL ANGLE (+°)	MAX. GIMBAL ANGLE (-°)	AT IMPACT V_F FT/SEC	AT IMPACT FLIGHT PATH ANGLE (°)
0	—	11.1	1119	11.7
10	2.53	14.0	1665	19.5

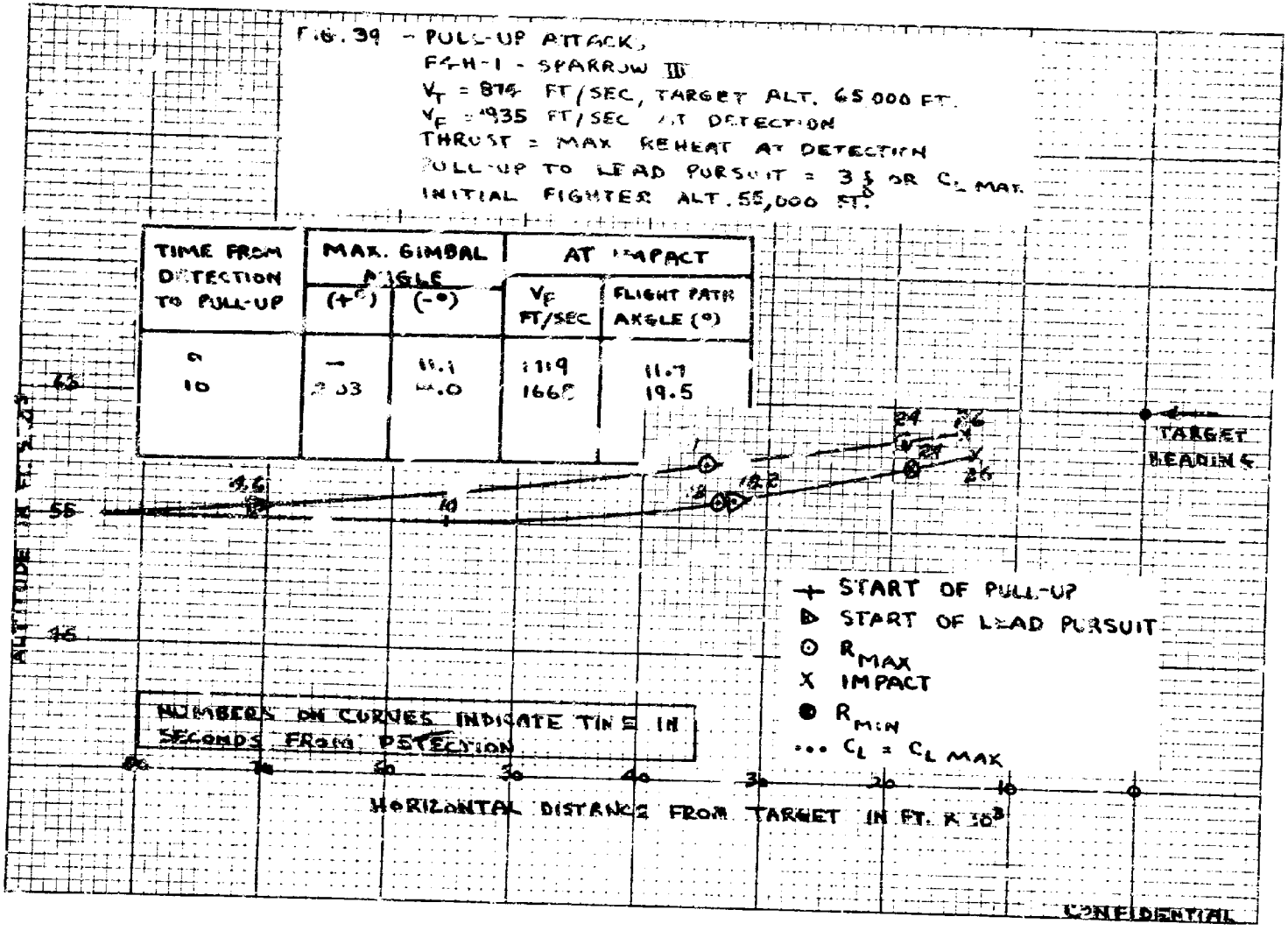

CONFIDENTIAL

FIG. 40 - PULL-UP ATTACKS
F4H-1 - SPARROW III
V_T = 870 FT/SEC, TARGET ALT. 65,000 FT.
V_F = 870 FT/SEC AT DETECTION
THRUST = MAX REHEAT AT DETECTION
PULL-UP TO LEAD PURSUIT = 3 g OR $C_{L\,MAX}$
INITIAL FIGHTER ALT. 35,000 FT.

TIME FROM DETECTION TO PULL-UP	MAX. GIMBAL ANGLE		AT IMPACT	
	(+°)	(−°)	V_F FT/SEC	FLIGHT PATH ANGLE (°)
10	23.77	25.38	266	−1.01
20	24.0	31.38	331	66.8

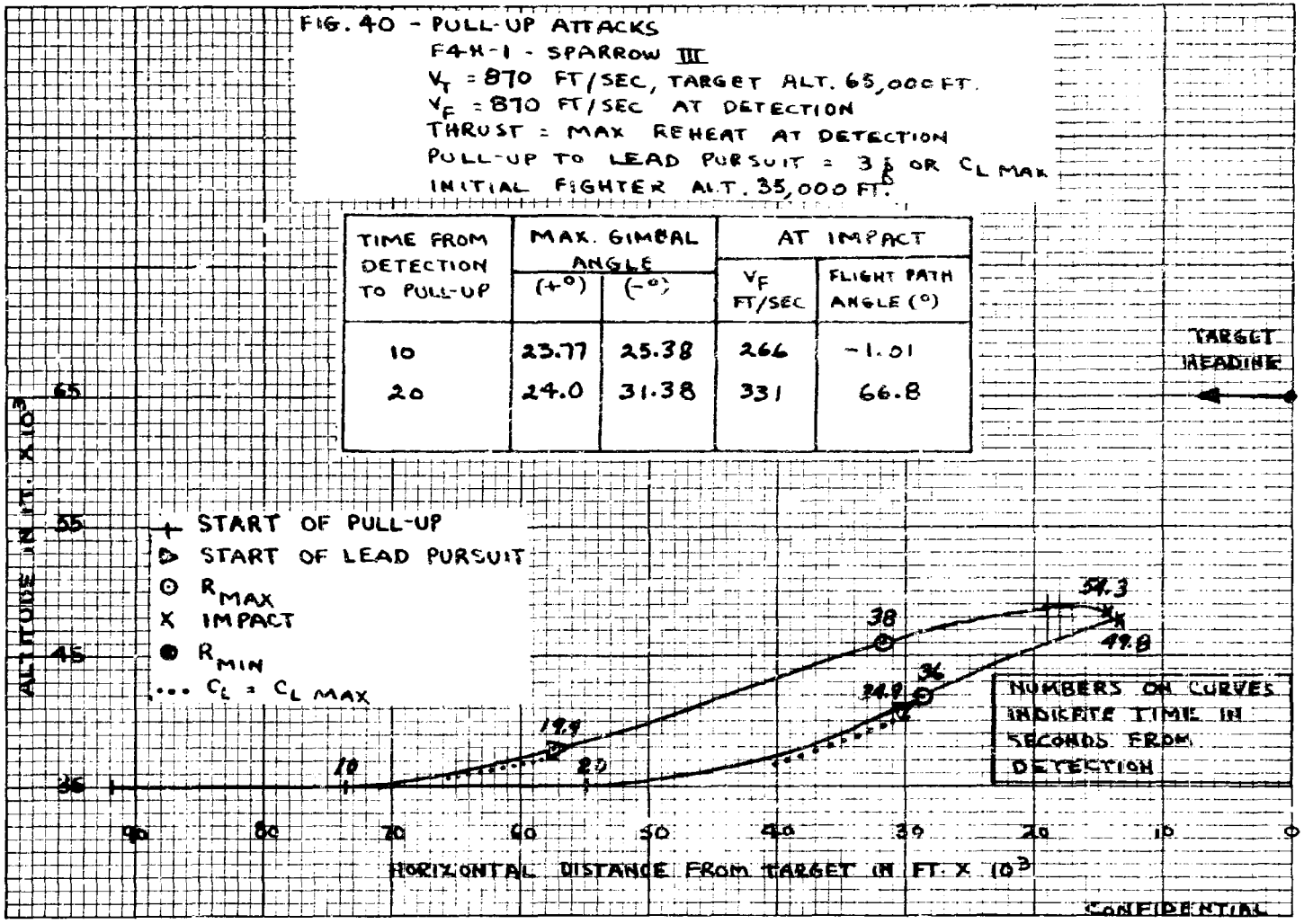

CONFIDENTIAL

FIG. 41 - PULL-UP ATTACKS
F4H-1 - SPARROW III
V_T = 1940 FT/SEC, TARGET ALT. 50,000 FT.
V_F = 873 FT/SEC AT DETECTION
THRUST = MAX REHEAT AT DETECTION
PULL-UP TO LEAD PURSUIT = 3 $\dot{\beta}$ OR $C_{L\,MAX}$
INITIAL FIGHTER ALT. 40,000 FT.

TIME FROM DETECTION TO PULL-UP	MAX. GIMBAL ANGLE		AT IMPACT	
	(+°)	(−°)	V_F FT/SEC	FLIGHT PATH ANGLE (°)
0	.208	21.8	652	27.4

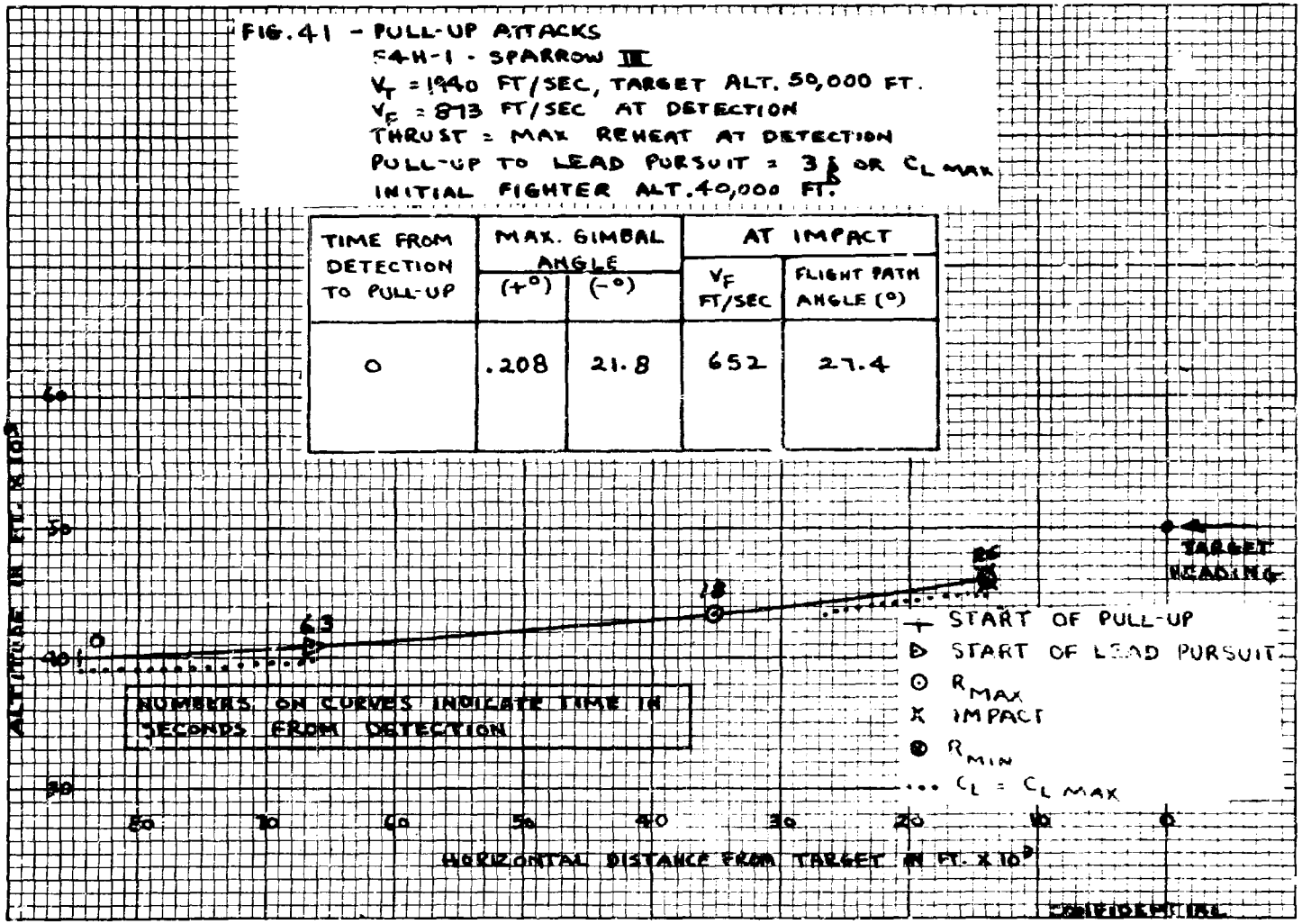

FIG. 42 - PULL-UP ATTACKS
F4H-1 - SPARROW III
V_T = 874 FT/SEC, TARGET ALT. 50,000 FT.
V_F = 874 FT/SEC AT DETECTION
THRUST = MAX REHEAT AT DETECTION
PULL-UP TO LEAD PURSUIT = 3 g OR $C_{L\,MAX}$
INITIAL FIGHTER ALT. 30,000 FT.

TIME FROM DETECTION TO PULL-UP	MAX. GIMBAL ANGLE		AT IMPACT	
	(+°)	(−°)	V_F FT/SEC	FLIGHT PATH ANGLE (°)
10	11.5	17.8	713	36.6
20	17.3	18.7	763	45.8

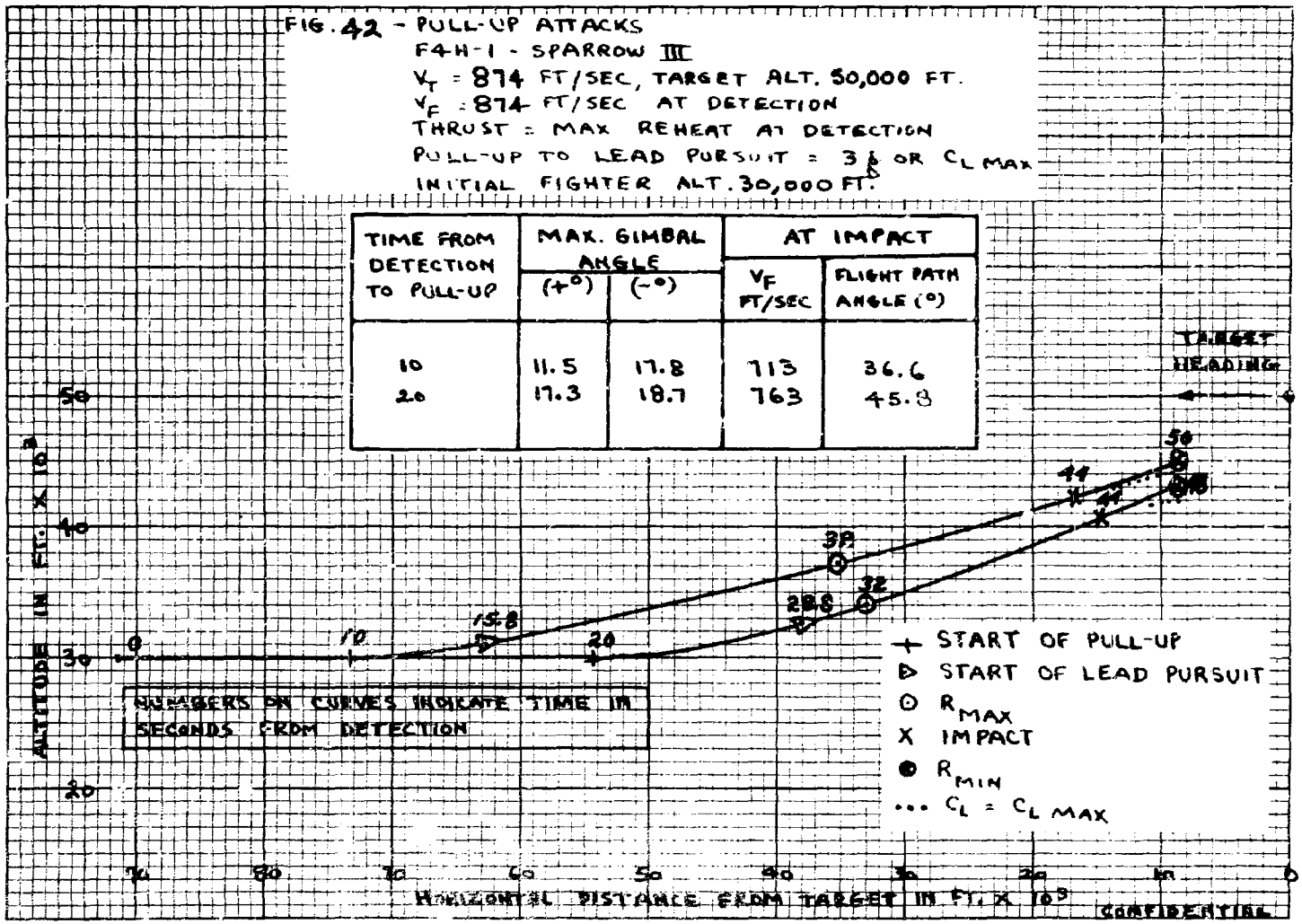

CONFIDENTIAL

FIG. 43 - PULL-UP ATTACKS
F4H-1 - SPARROW III
V_T = 874 FT/SEC, TARGET ALT. 50,000 FT.
V_F = 874 FT/SEC AT DETECTION
THRUST = MAX REHEAT AT DETECTION
PULL-UP TO LEAD PURSUIT = 3 g OR $C_{L\,MAX}$
INITIAL FIGHTER ALT. 20,000 FT.

TIME FROM DETECTION TO PULL-UP	MAX. GIMBAL ANGLE (+°)	MAX. GIMBAL ANGLE (−°)	AT IMPACT V_F FT/SEC	AT IMPACT FLIGHT PATH ANGLE (°)
10	21	25	624	57
20	28	29.6	652	77.7
25	33.8	31.4	623	104.3
30	41.4	36.3	466	157.8

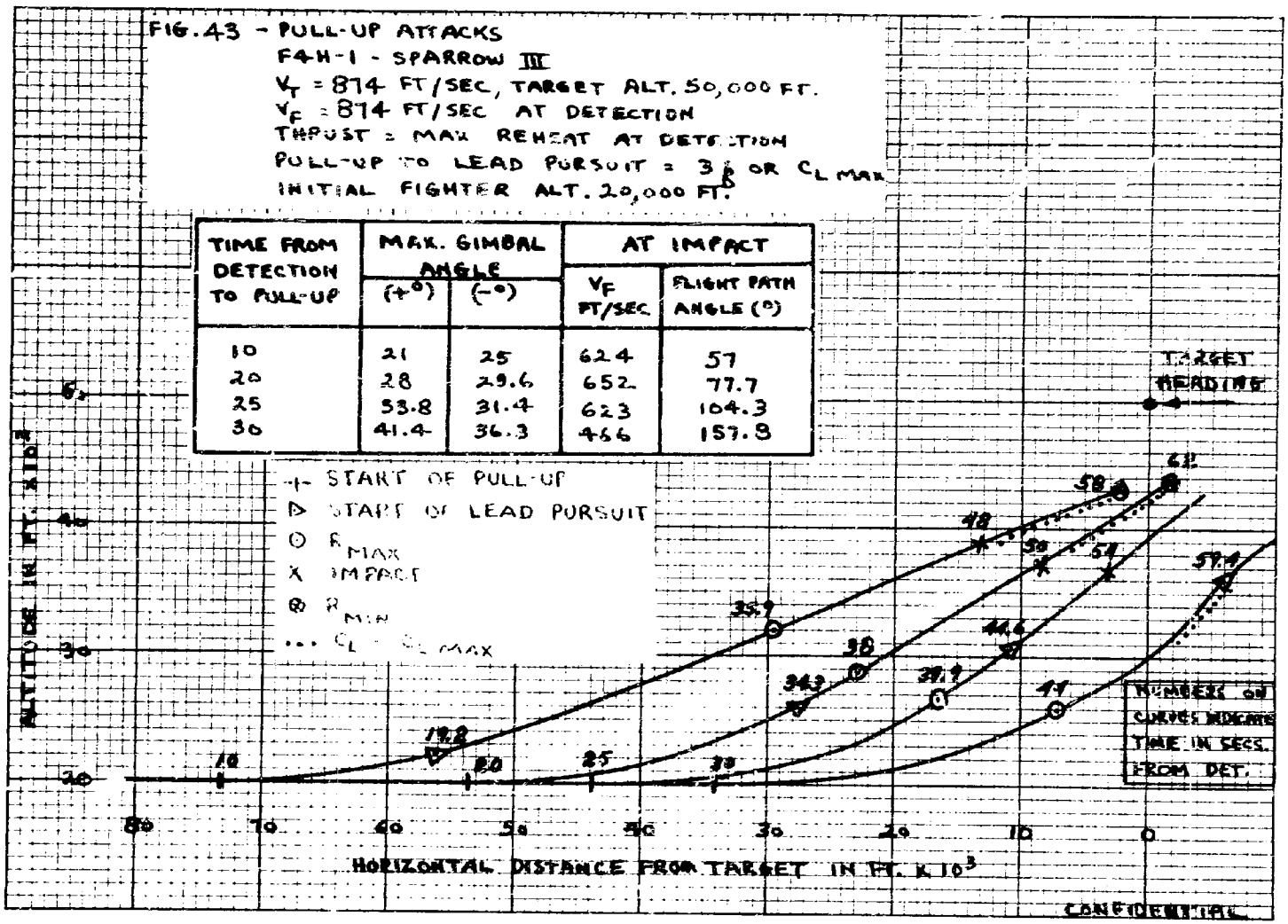

FIG. 44 - PULL-UP ATTACKS
F4H-1 - SPARROW III
V_T = 873 FT/SEC, TARGET ALT. 50,000 FT.
V_F = 873 FT/SEC AT DETECTION
THRUST = MAX REHEAT AT DETECTION
PULL-UP TO LEAD PURSUIT = 3 g OR $C_{L\,MAX}$
INITIAL FIGHTER ALT. 10,000 FT.

TIME FROM DETECTION TO PULL-UP	MAX. GIMBAL ANGLE		AT IMPACT	
	(+°)	(−°)	V_F FT/SEC	FLIGHT PATH ANGLE (°)
0	21.8	35.6	323	72.1
10	28.8	33.04	505	80.8
20	31.4	30.9	543	106.8
25	43.5	25.7	585	128.7

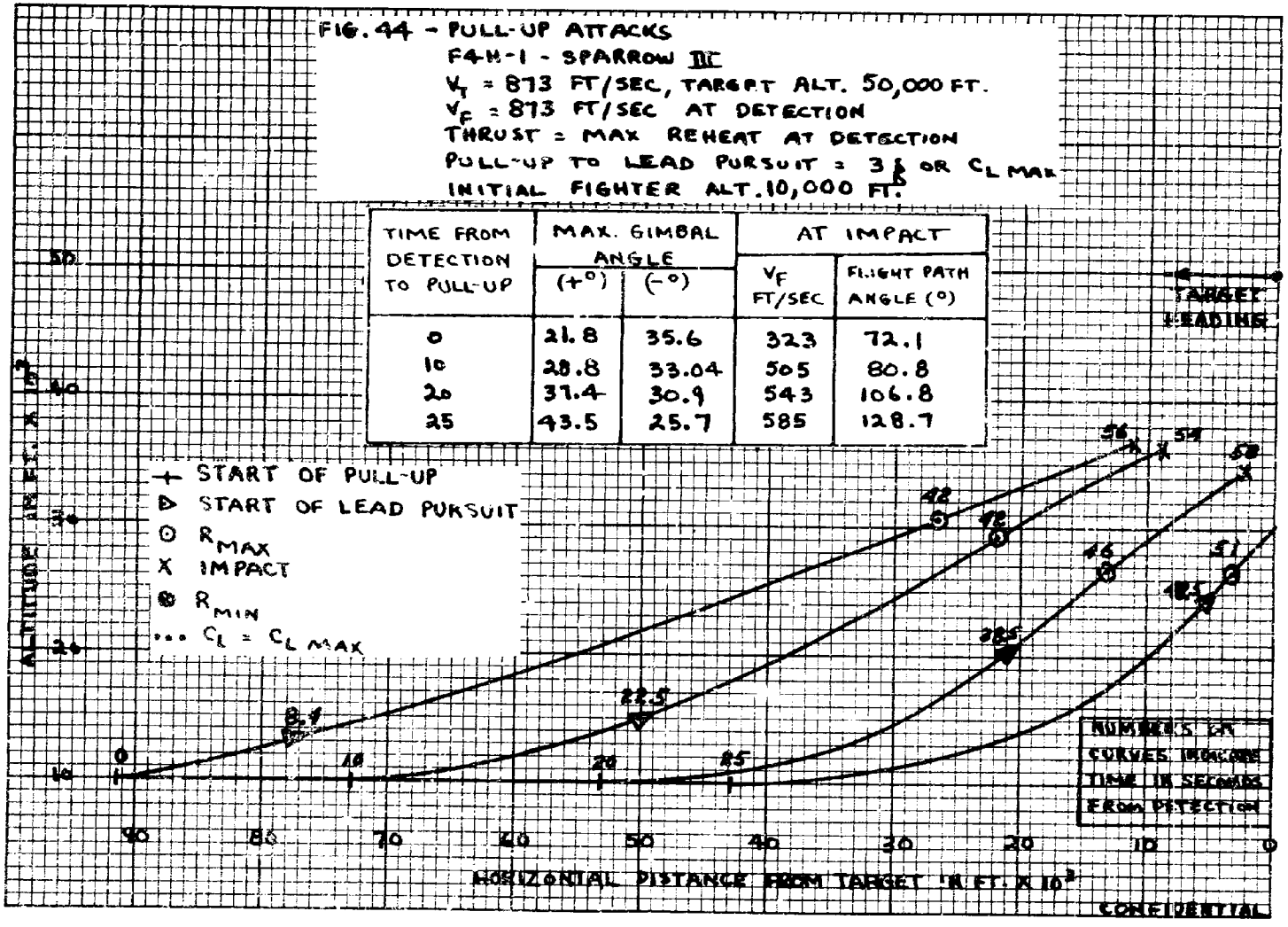

CONFIDENTIAL

FIG. 45 - PULL-UP ATTACKS
F4H-1 - SPARROW III
V_T = 1980 FT/SEC, TARGET ALT. 30,000 FT
V_F = 890 FT/SEC AT DETECTION
THRUST = MAX REHEAT AT DETECTION
PULL-UP TO LEAD PURSUIT = 3 g OR $C_{L\,MAX}$
INITIAL FIGHTER ALT. 20,000 FT.

TIME FROM DETECTION TO PULL-UP	MAX. GIMBAL ANGLE		AT IMPACT	
	(+°)	(-°)	V_F FT/SEC	FLIGHT PATH ANGLE (°)
0	3.61	18	947	67.95
10	9.19	30.9	883	31.3

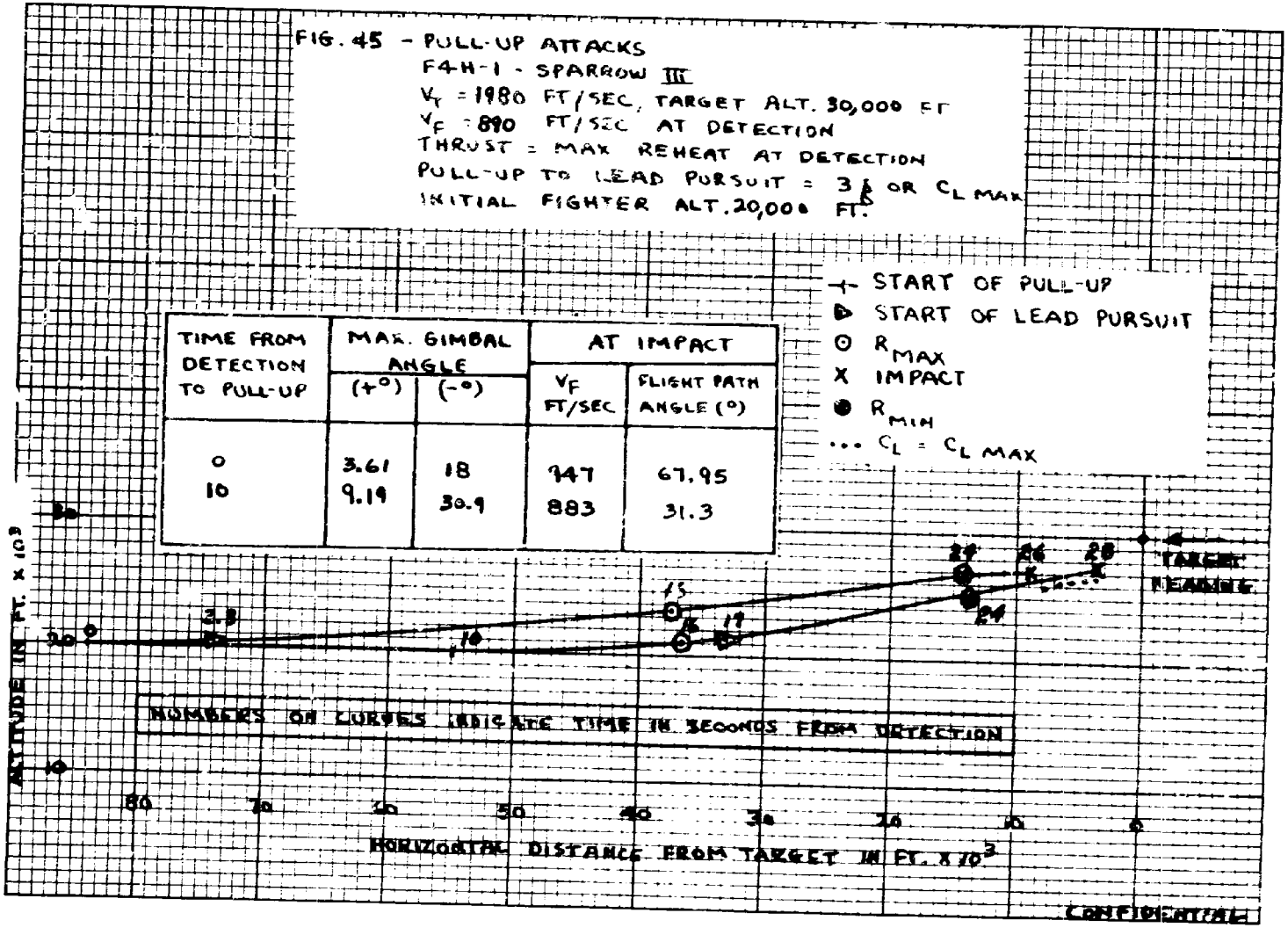

CONFIDENTIAL

FIG. 46 - PULL-UP ATTACKS
F4H-1 - SPARROW III
V_T = 893 FT/SEC, TARGET ALT. 30,000 FT.
V_F = 874 FT/SEC AT DETECTION
THRUST = MAX REHEAT AT DETECTION
PULL-UP TO LEAD PURSUIT = 3 g OR $C_{L\,MAX}$
INITIAL FIGHTER ALT. 10,000 FT.

TIME FROM DETECTION TO PULL-UP	MAX. GIMBAL ANGLE (+°)	MAX. GIMBAL ANGLE (−°)	AT IMPACT V_F FT/SEC	AT IMPACT FLIGHT PATH ANGLE (°)
0	10.76	8.33	4	30.1
10	15.54	10.53	967	37
20	21.30	14.30	956	50.5
30	35.20	13.13	742	178

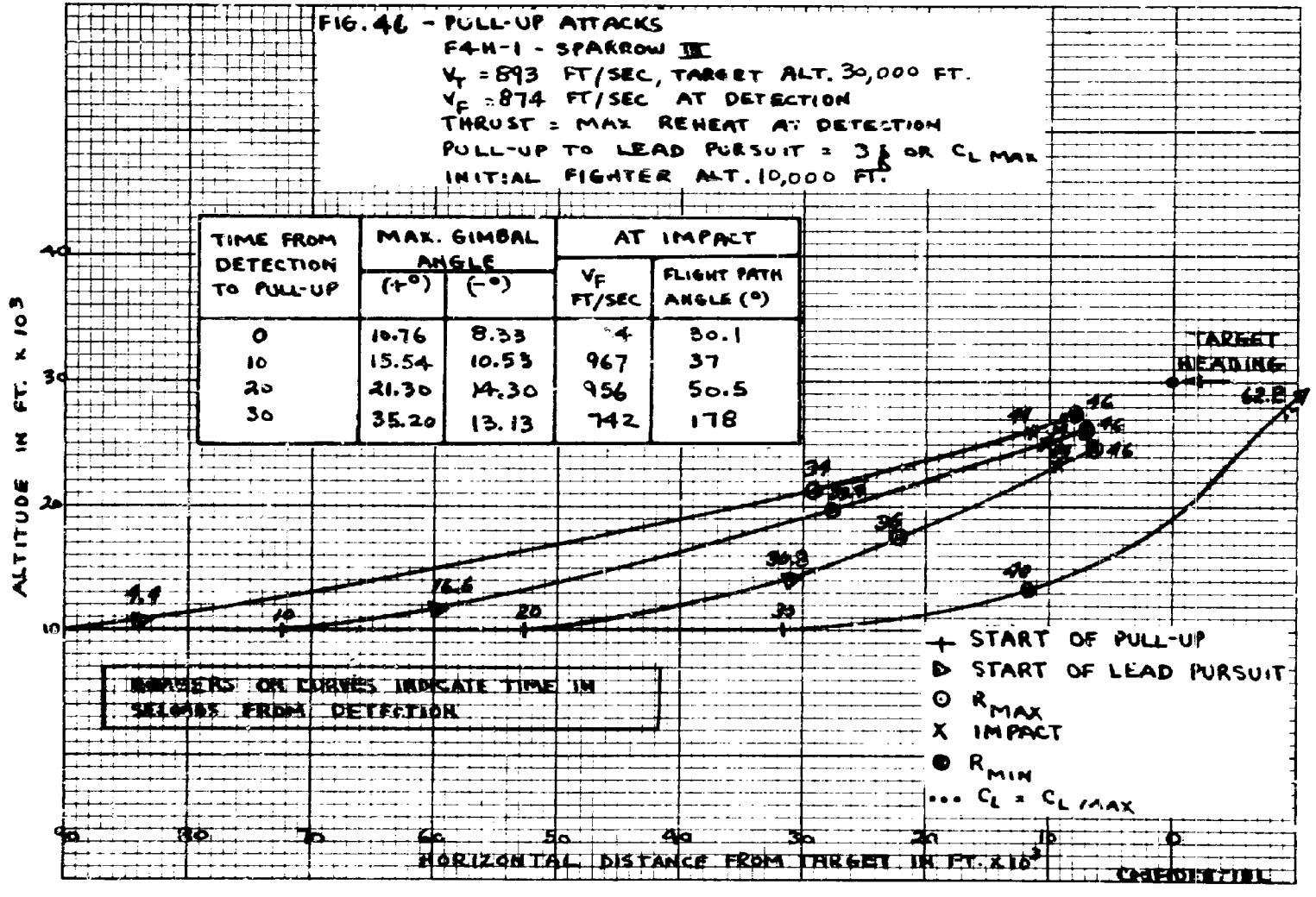

FIG. 47 - PULL-UP ATTACKS
F4H-1 - SPARROW III
V_T = 893 FT/SEC, TARGET ALT. 30,000 FT.
V_F = 890 FT/SEC AT DETECTION
THRUST = MAX REHEAT AT DETECTION
PULL-UP TO LEAD PURSUIT = 3 g OR $C_{L\,MAX}$
INITIAL FIGHTER ALT. SEA LEVEL

TIME FROM DETECTION TO PULL-UP	MAX. GIMBAL ANGLE		AT IMPACT	
	(+°)	(-°)	V_F FT/SEC	FLIGHT PATH ANGLE (°)
20	36.2	21.3	844	84.2
25	37.1	21.3	794	125.9
30	45.3	21.8	835	162

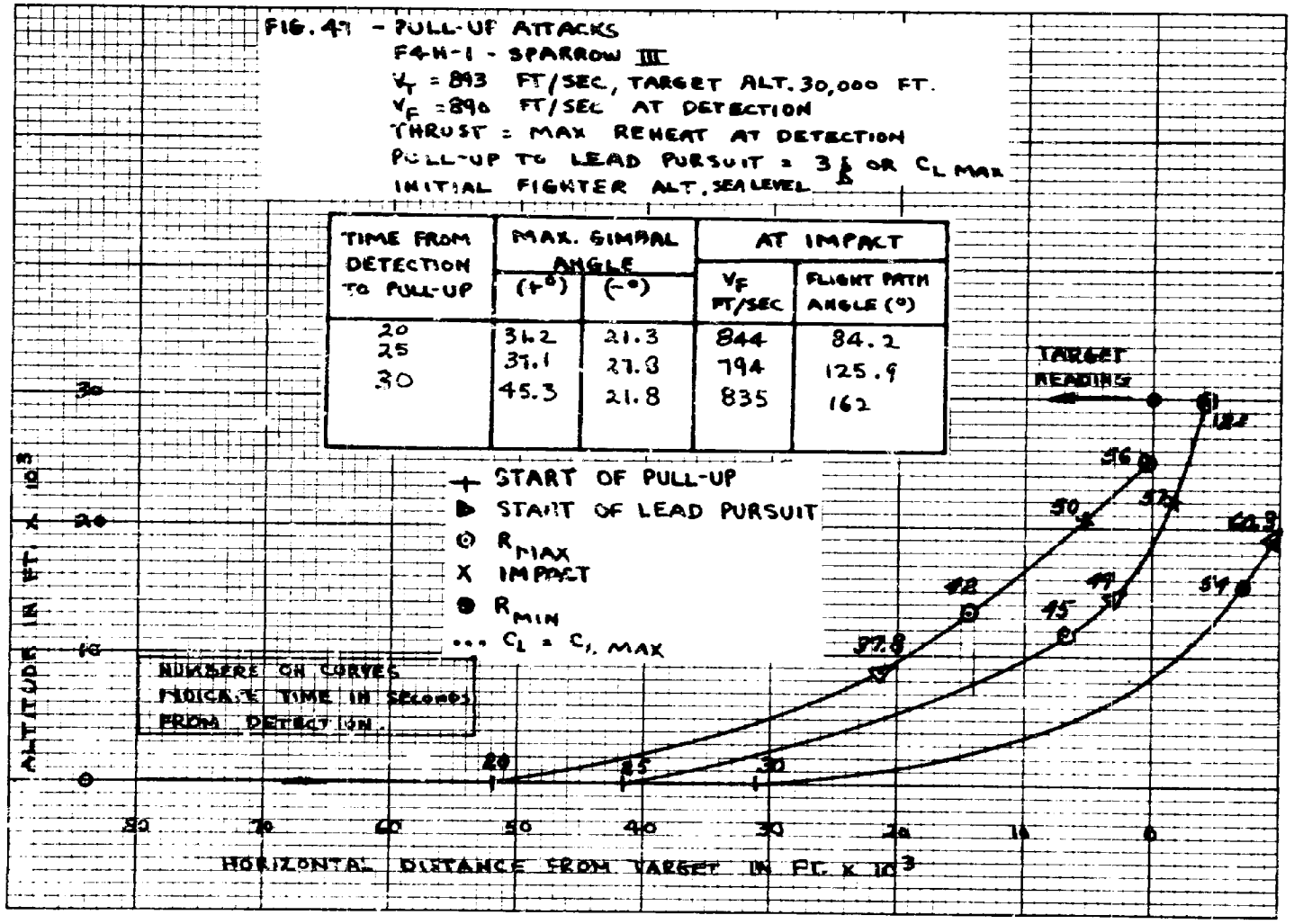

FIG. 48 - PULL-UP ATTACKS
F4H-1 - SPARROW III
V_T = 1480 FT/SEC, TARGET ALT. 30,000 FT.
V_F = 890 FT/SEC AT DETECTION
THRUST = MAX REHEAT AT DETECTION
PULL-UP TO LEAD PURSUIT = 3 g OR $C_{L\,MAX}$
INITIAL FIGHTER ALT. SEA LEVEL

TIME FROM DETECTION TO PULL-UP	MAX. GIMBAL ANGLE		AT IMPACT	
	(+°)	(−°)	V_F FT/SEC	FLIGHT PATH ANGLE (°)
0	19.3	67.3	716	108.7

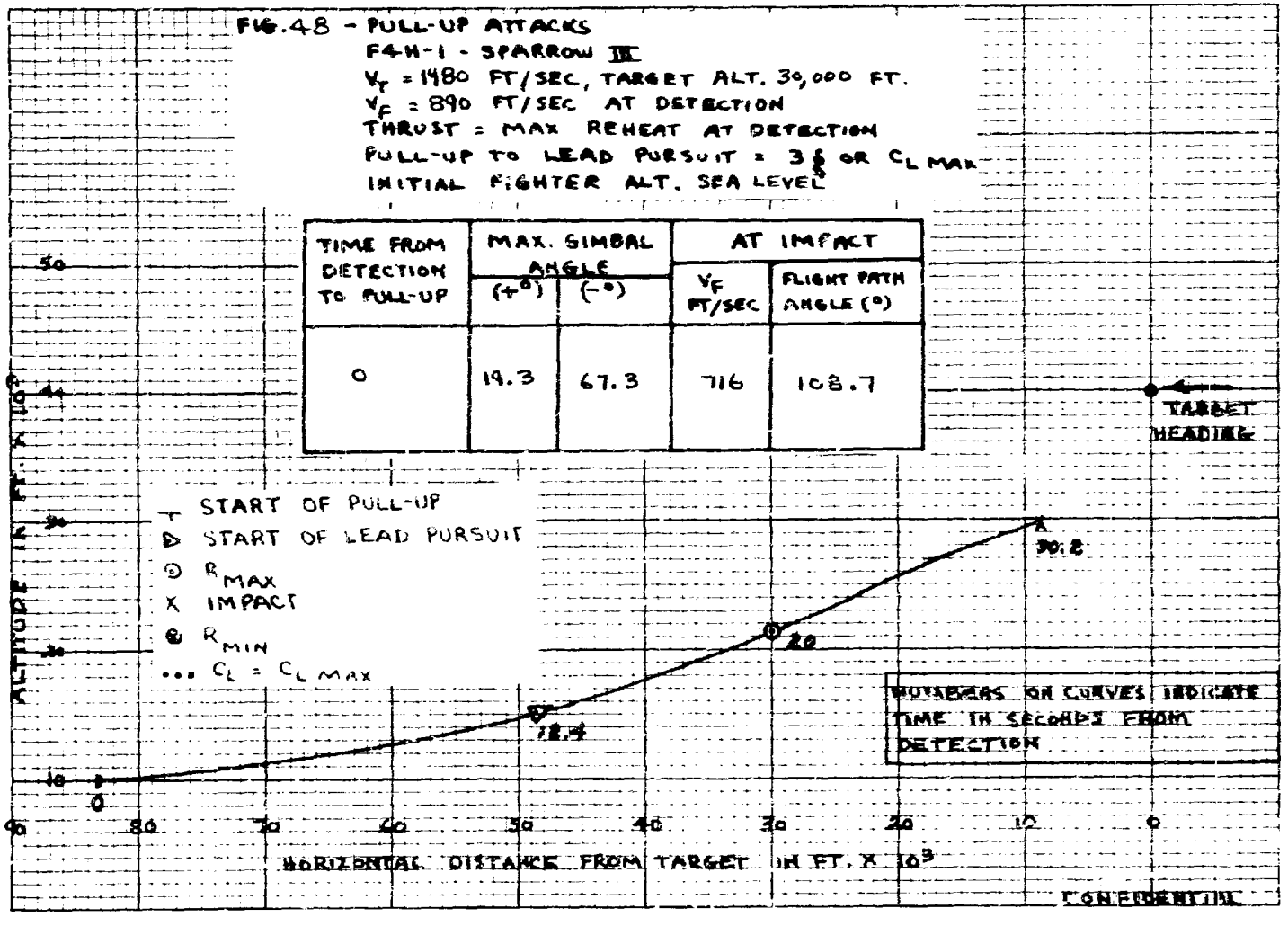

CONFIDENTIAL

FIG. 49 - PULL-UP ATTACKS
F4H-1 - SPARROW III
V_T = 1440 FT/SEC, TARGET ALT. 50,000 FT.
V_F = 873 FT/SEC AT DETECTION
THRUST = MAX REHEAT AT DETECTION
PULL-UP TO LEAD PURSUIT = 3 g OR $C_{L\,MAX}$
INITIAL FIGHTER ALT. 10,000 FT.

TIME FROM DETECTION TO PULL-UP	MAX. GIMBAL ANGLE		AT IMPACT	
	(+°)	(-°)	V_F FT/SEC	FLIGHT PATH ANGLE (°)
0	23.7	139.3	481	217.7

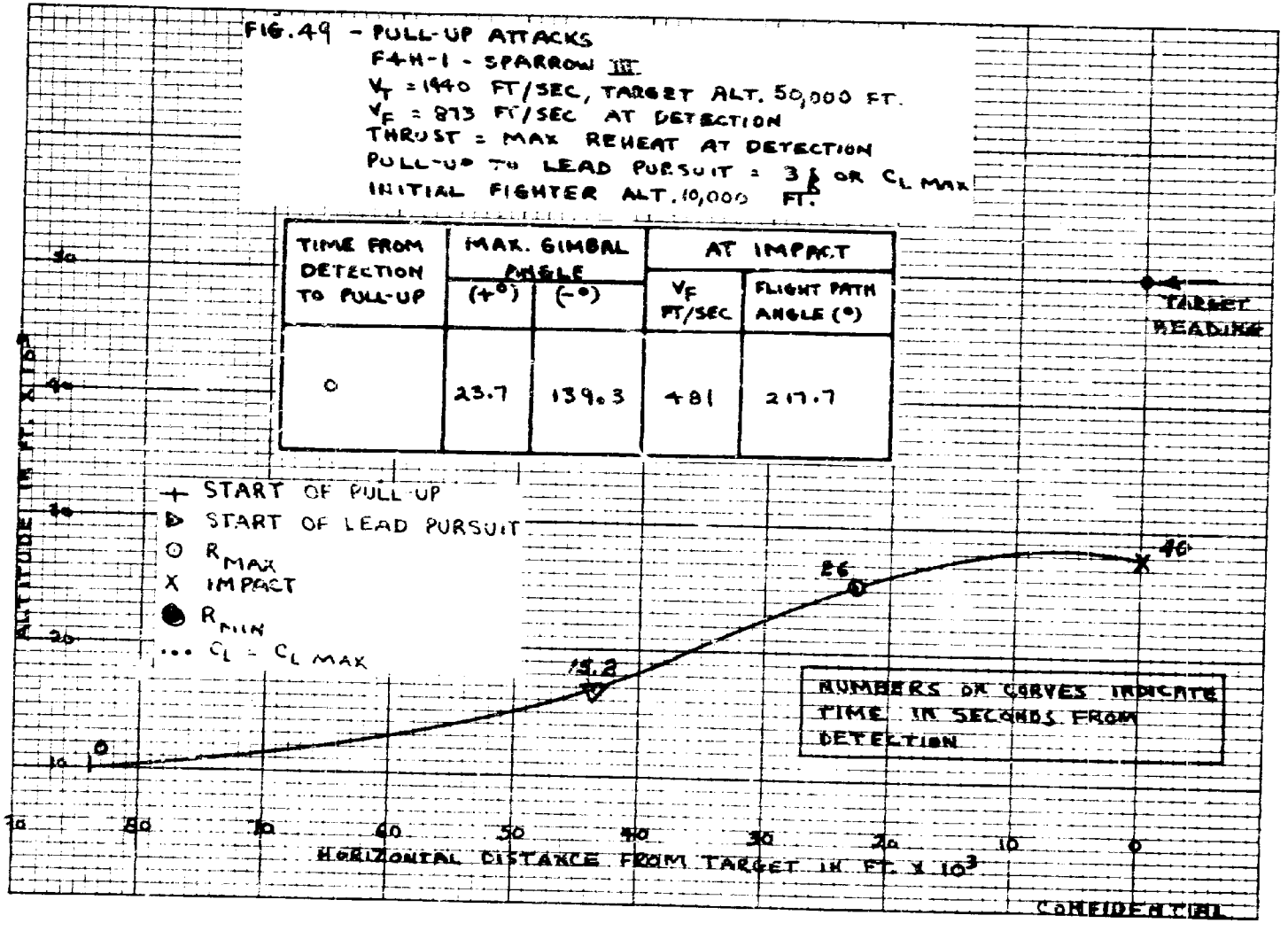

CONFIDENTIAL

Fig. 50- Noise Power Density vs Range - B-47 Target Nose View. Data Computed for Sparrow III Assuming 14 Deg. Beamwidth and 285 cps Tracking Rate

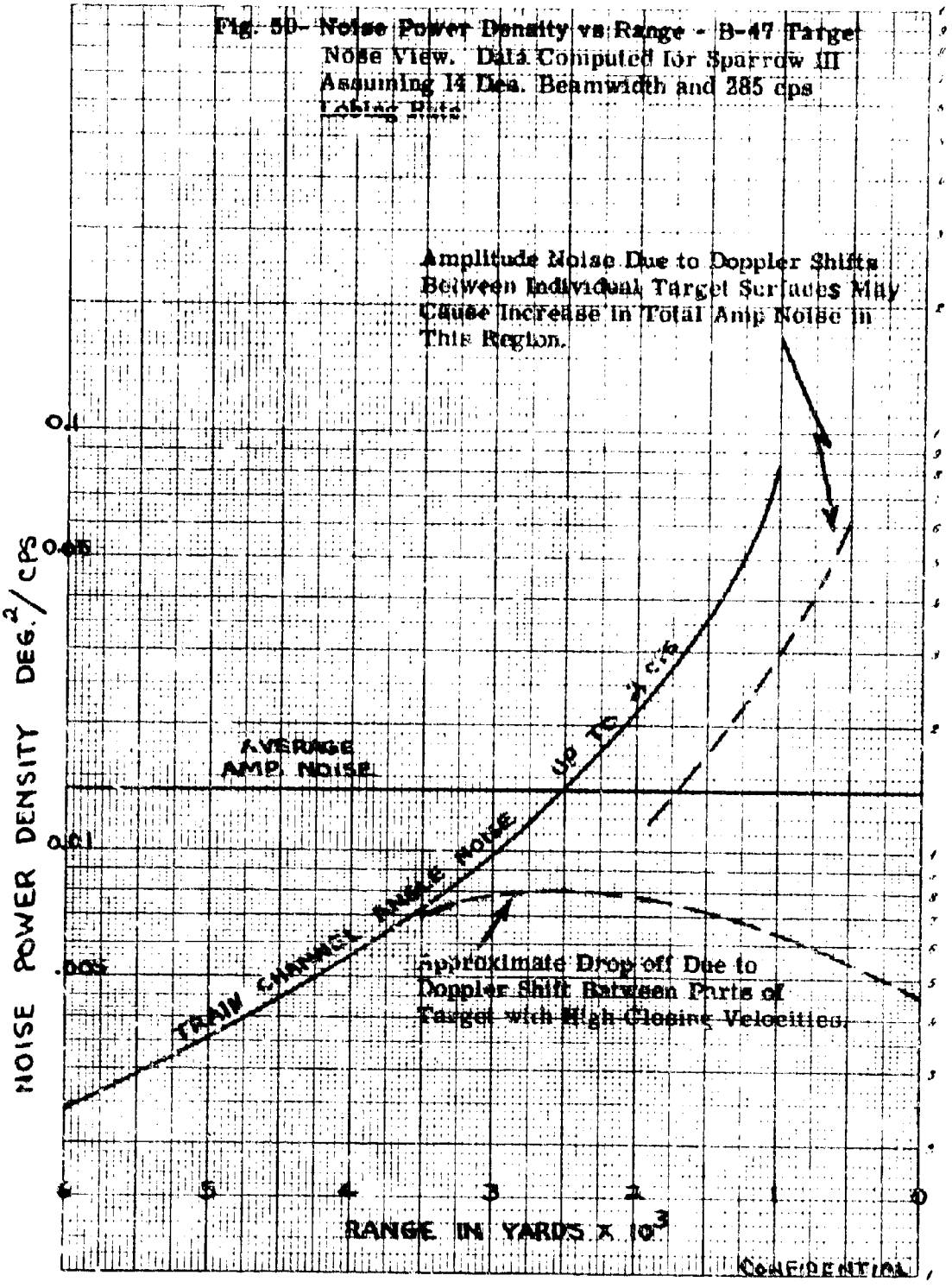

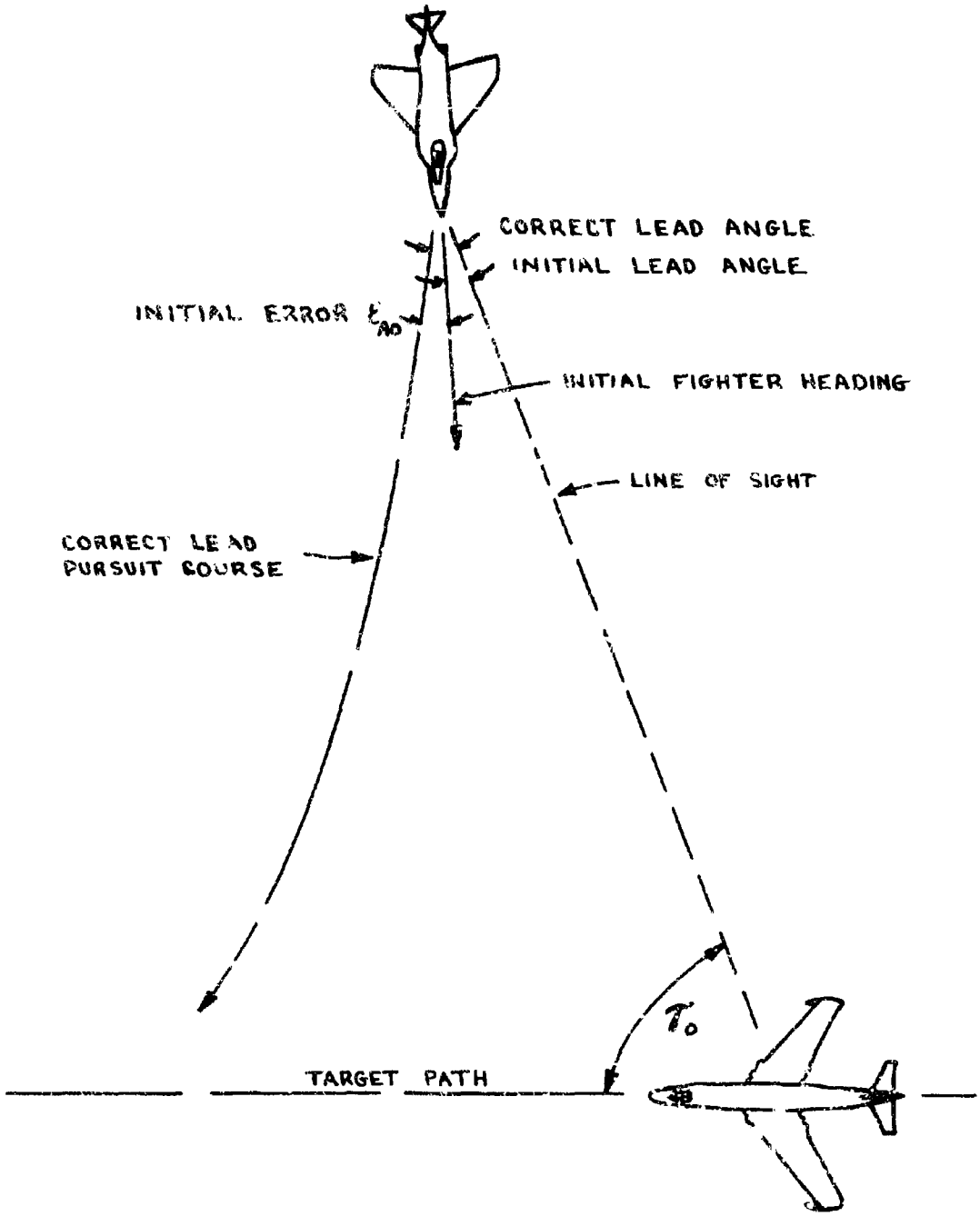

Fig. 51- Initial Conditions for Settling Time Study

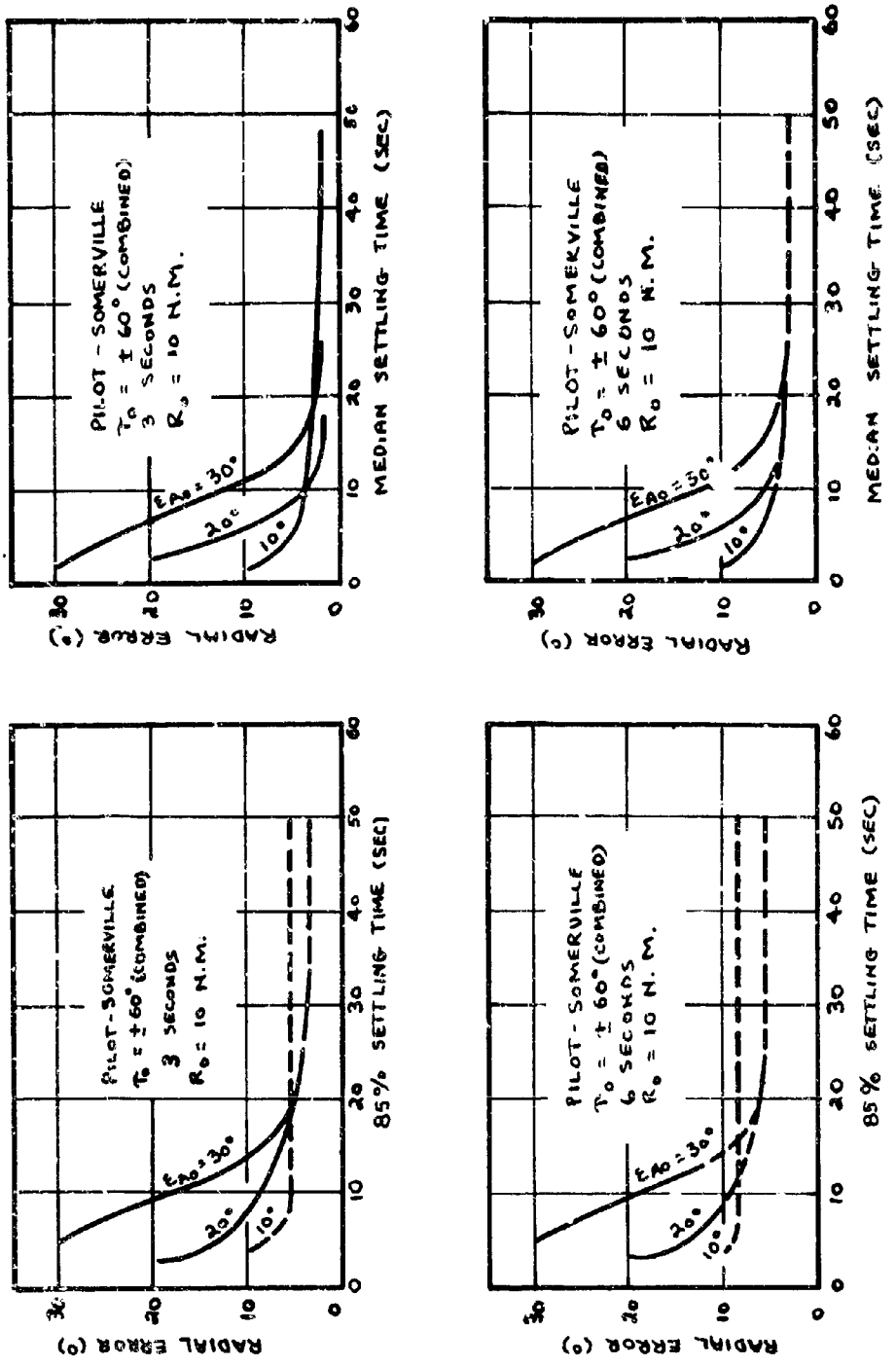

Fig. 52- Error vs Time from Settling Time Study

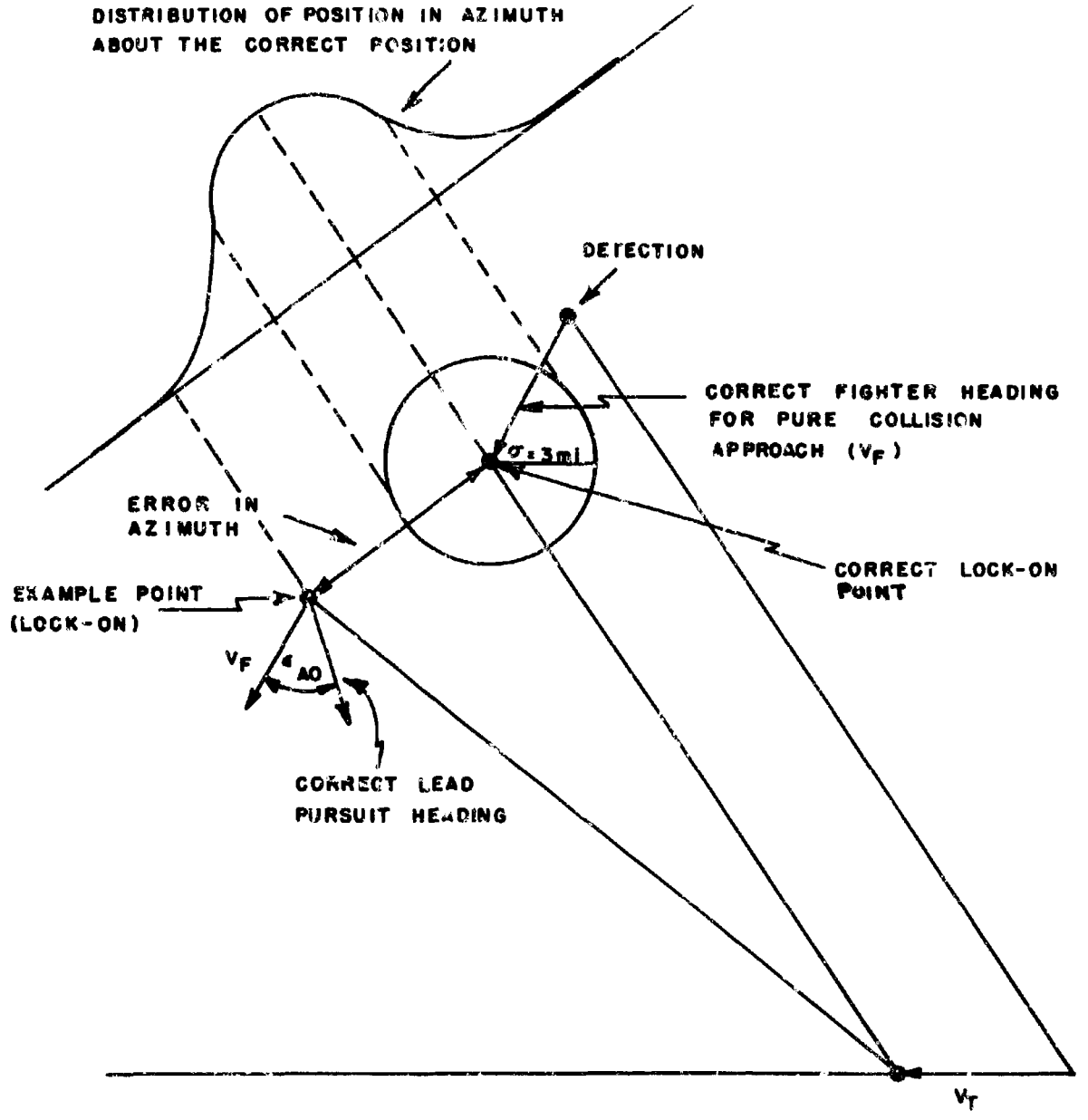

Fig. 53- Conditions Applied to Get Initial Errors

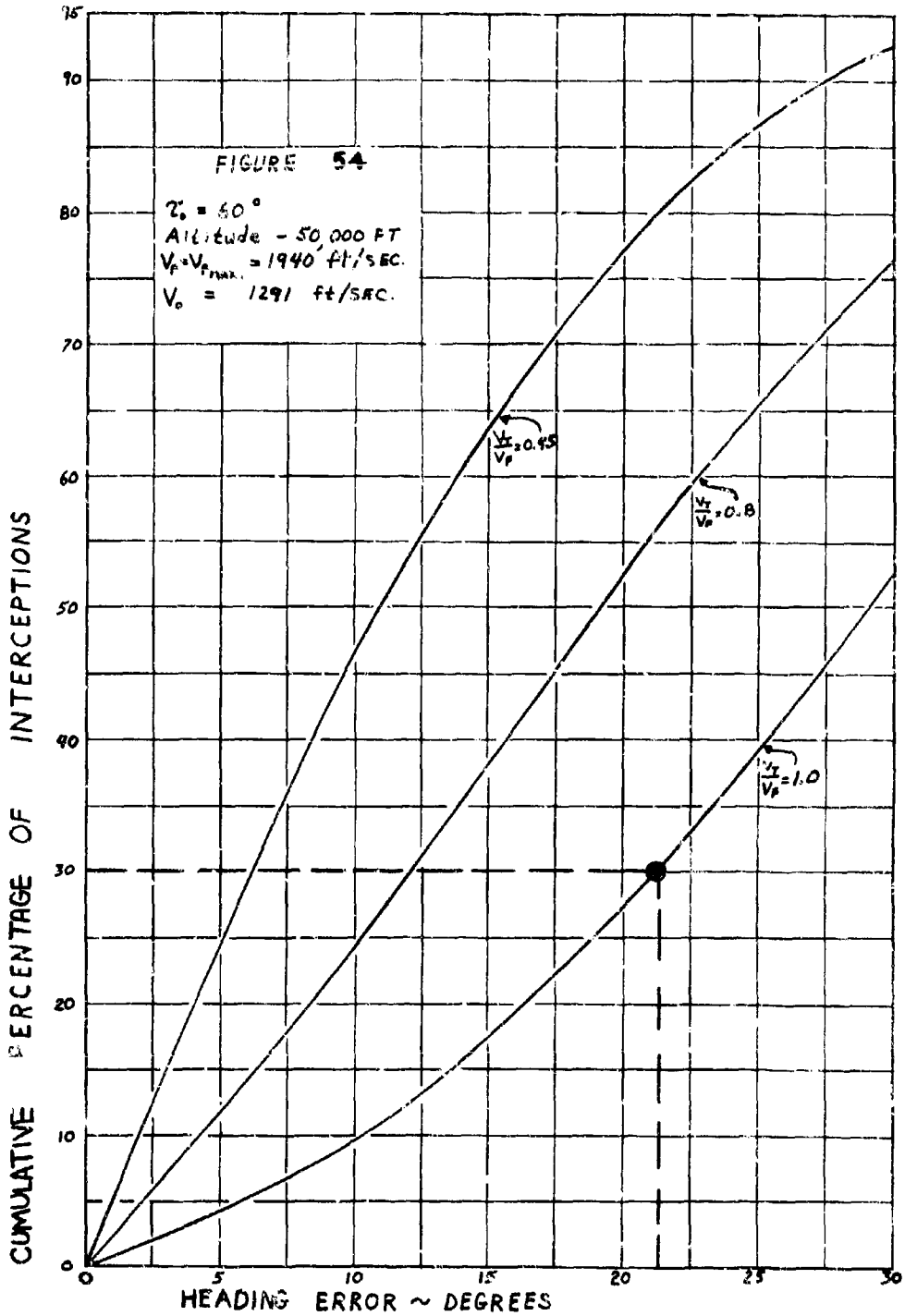

CONFIDENTIAL

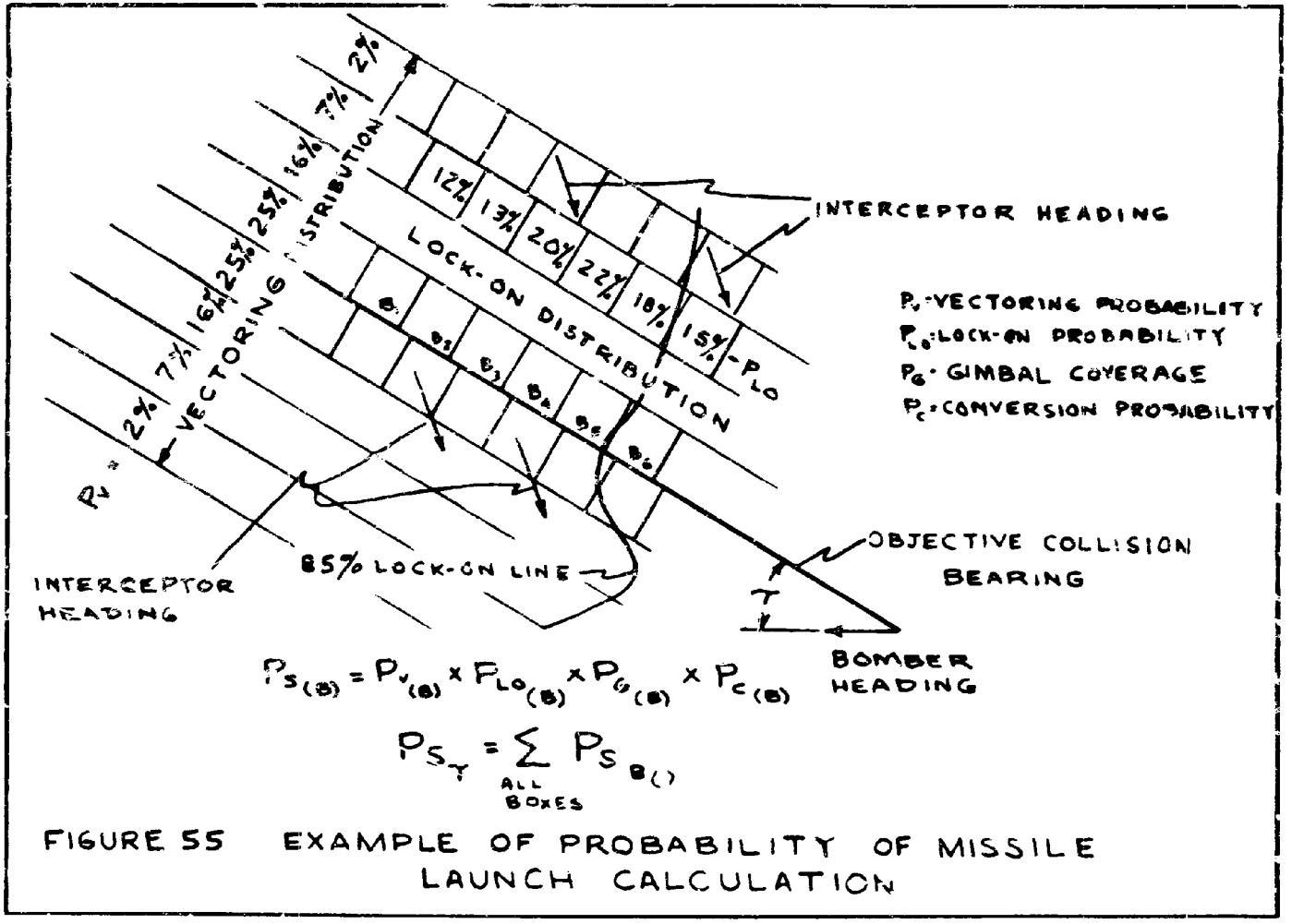

FIGURE 55 EXAMPLE OF PROBABILITY OF MISSILE LAUNCH CALCULATION

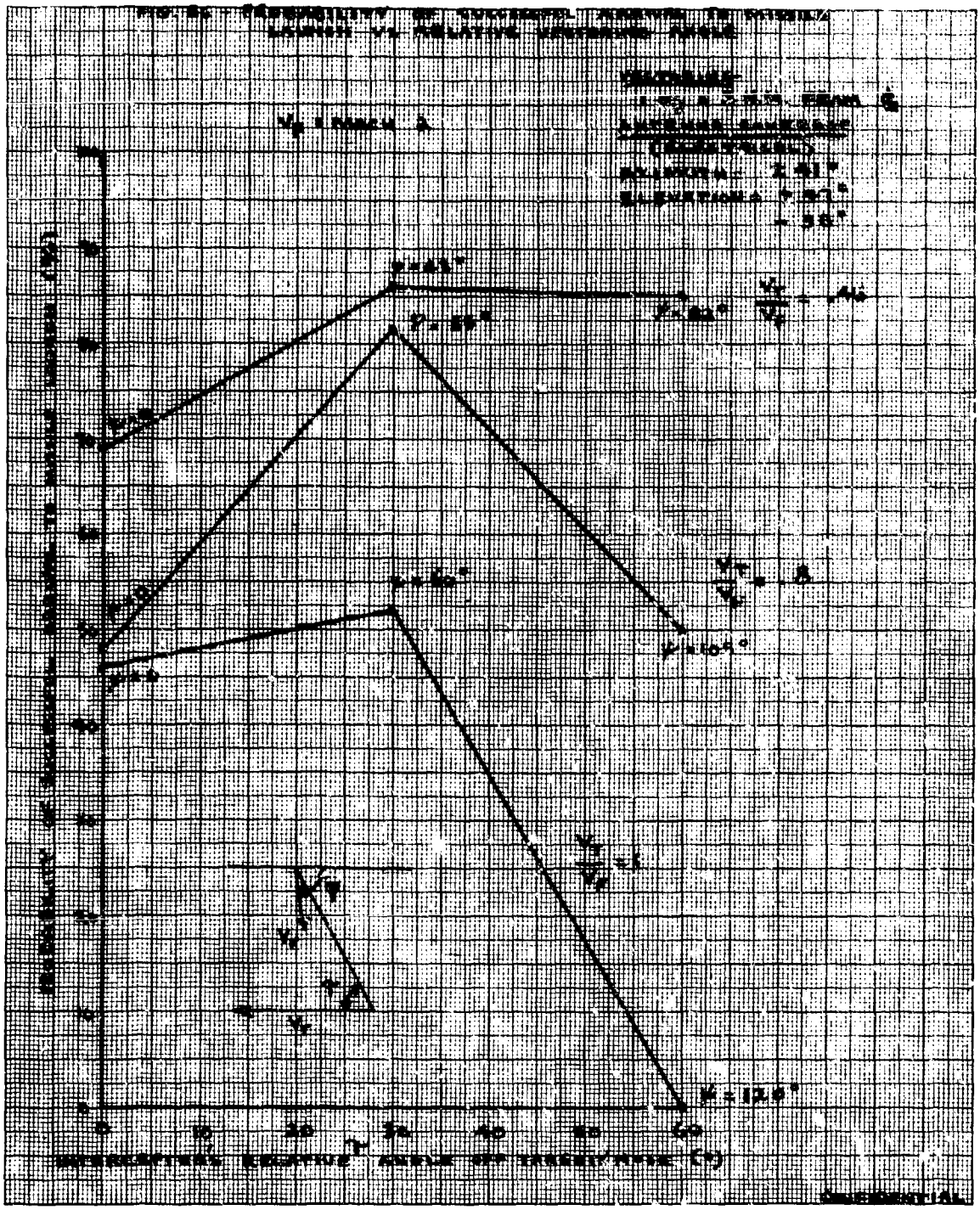

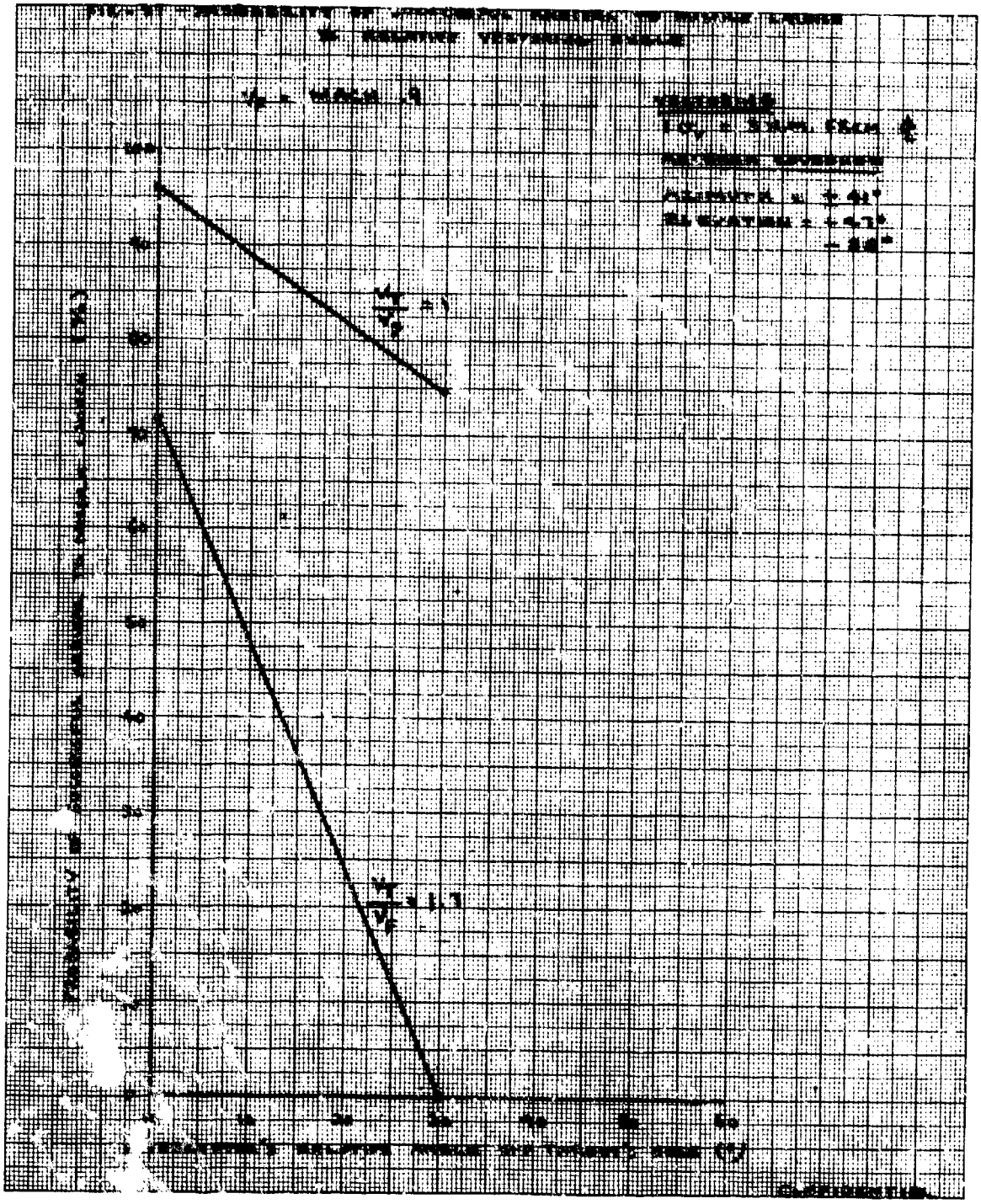

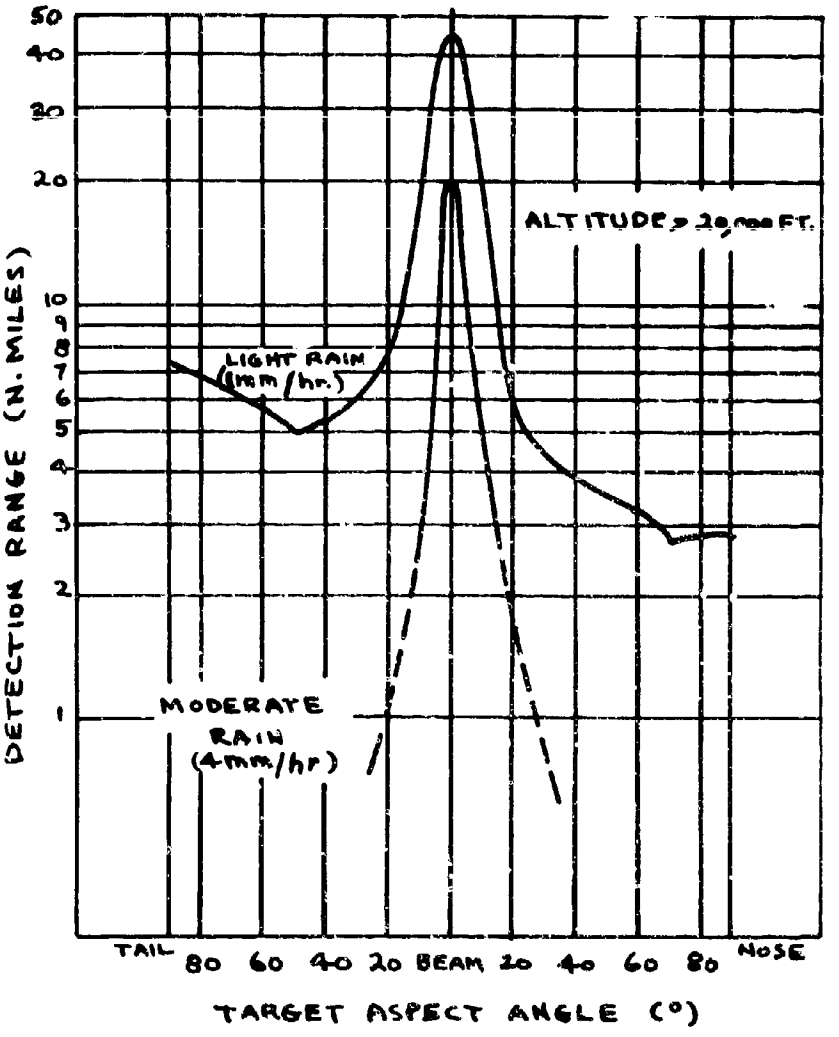

FIG. 58 - DETECTION RANGE FOR RAIN AT THE TARGET WITH VERTICAL POLARIZATION

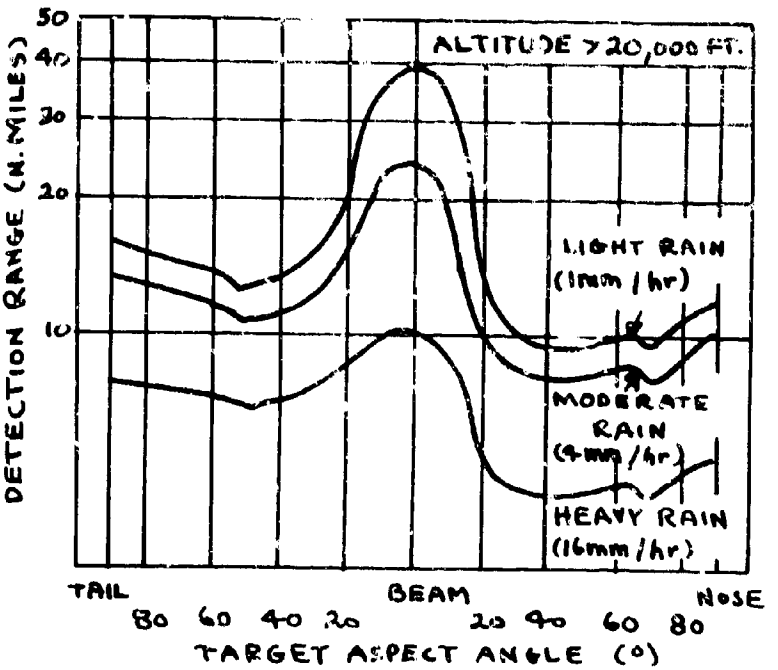

FIG. 59- DETECTION RANGE FOR RAIN BETWEEN RADAR AND TARGET WITH VERTICAL POLARIZATION

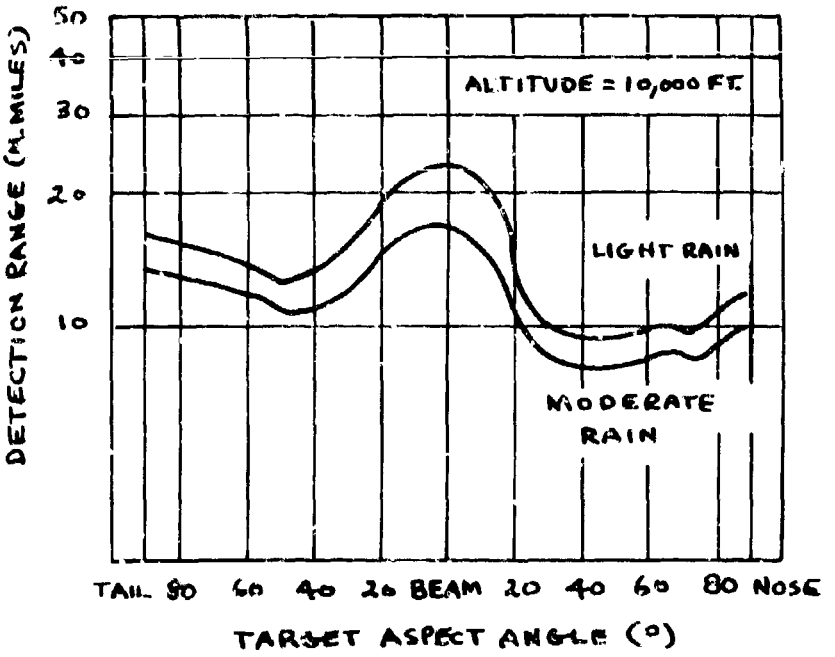

FIG. 60 - DETECTION RANGE FOR RAIN BETWEEN RADAR AND TARGET WITH VERTICAL POLARIZATION.

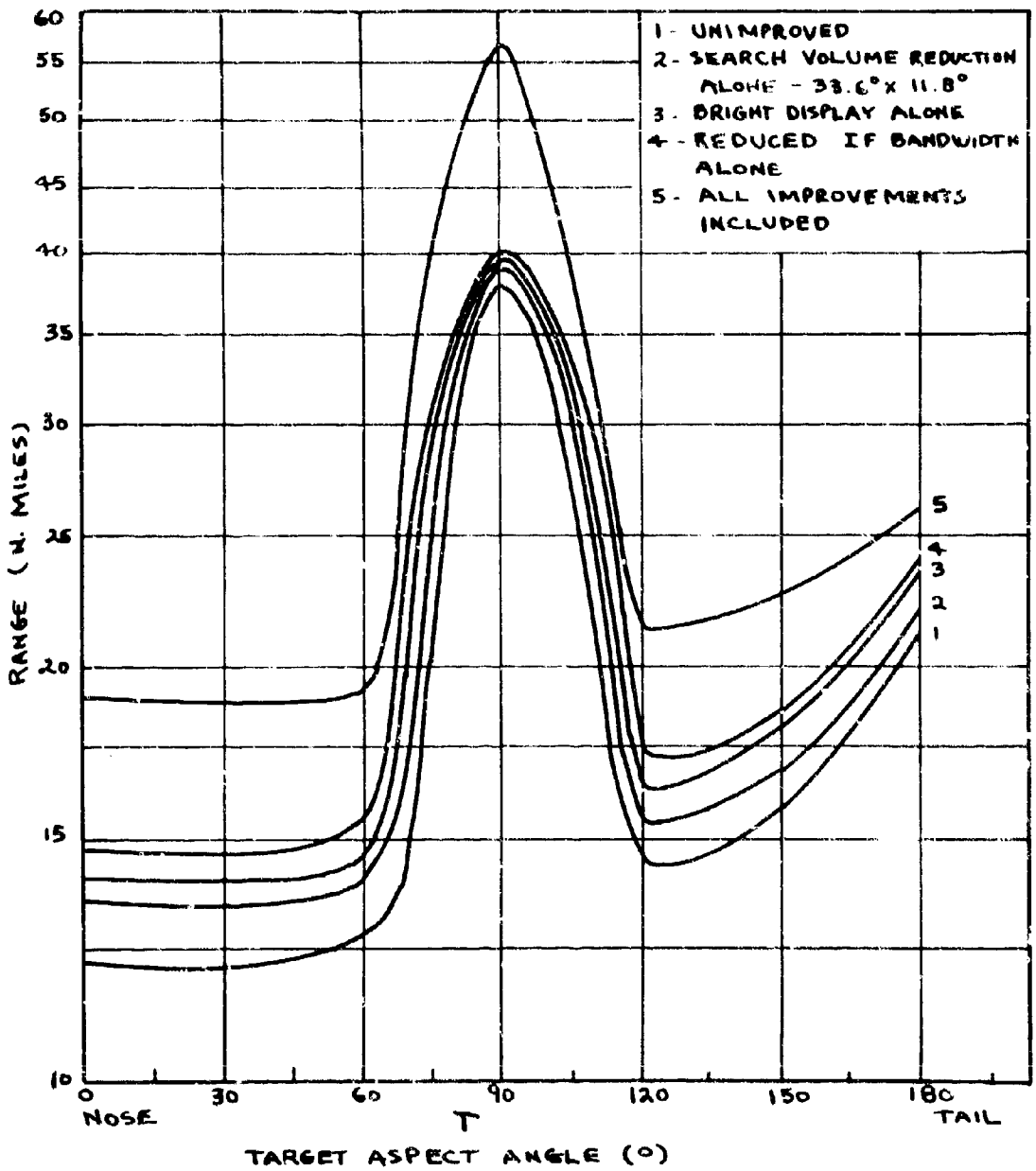

FIG. 61 - IMPROVED AI RADAR RANGE PERFORMANCE (85% PROBABILITY OF DETECTION, FAIR WEATHER, NO CLUTTER, NO ECM)

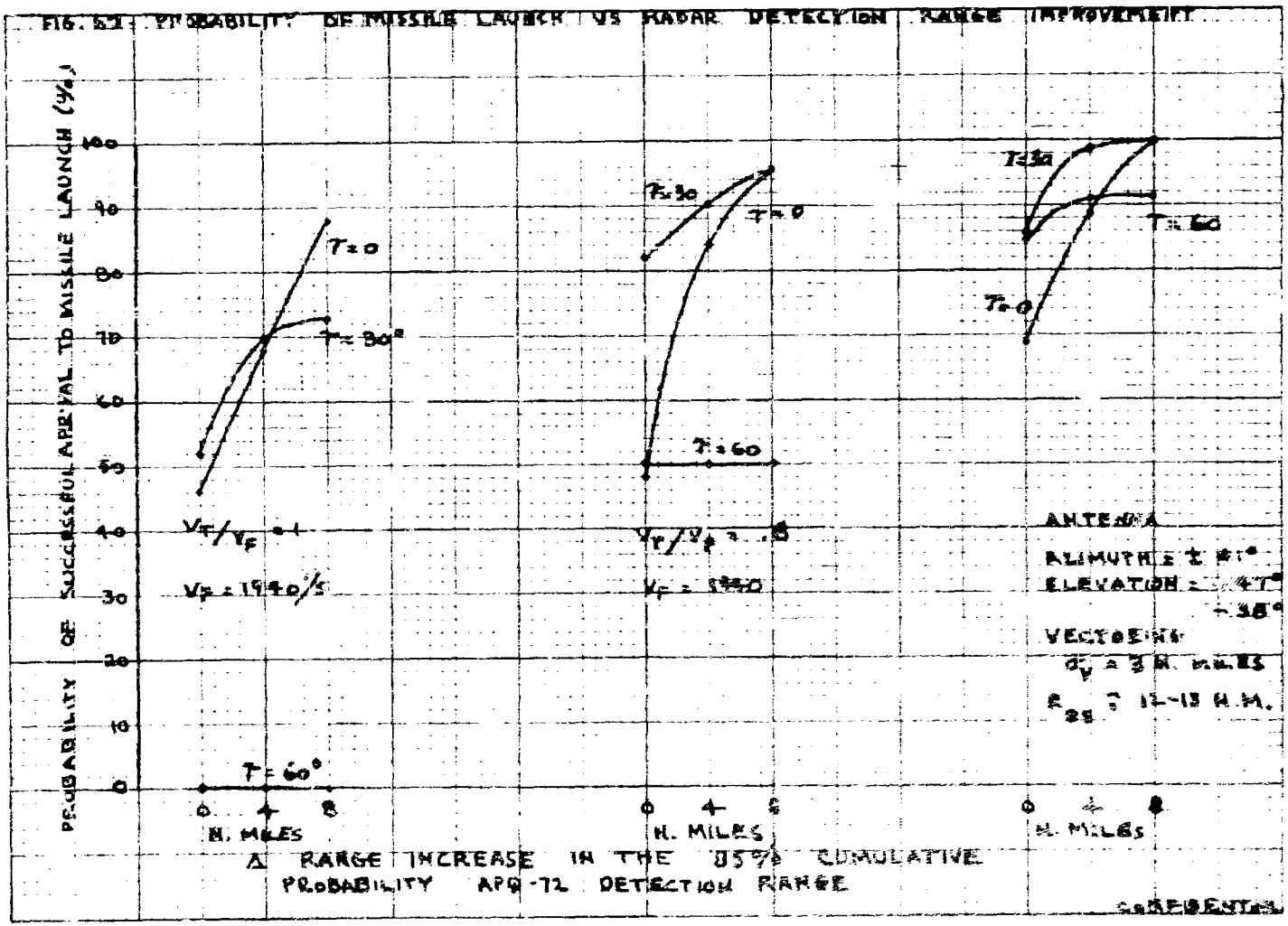

FIG. 52 - PROBABILITY OF MISSILE LAUNCH VS RADAR DETECTION RANGE IMPROVEMENT

Δ RANGE INCREASE IN THE 85% CUMULATIVE PROBABILITY APQ-72 DETECTION RANGE

CONFIDENTIAL

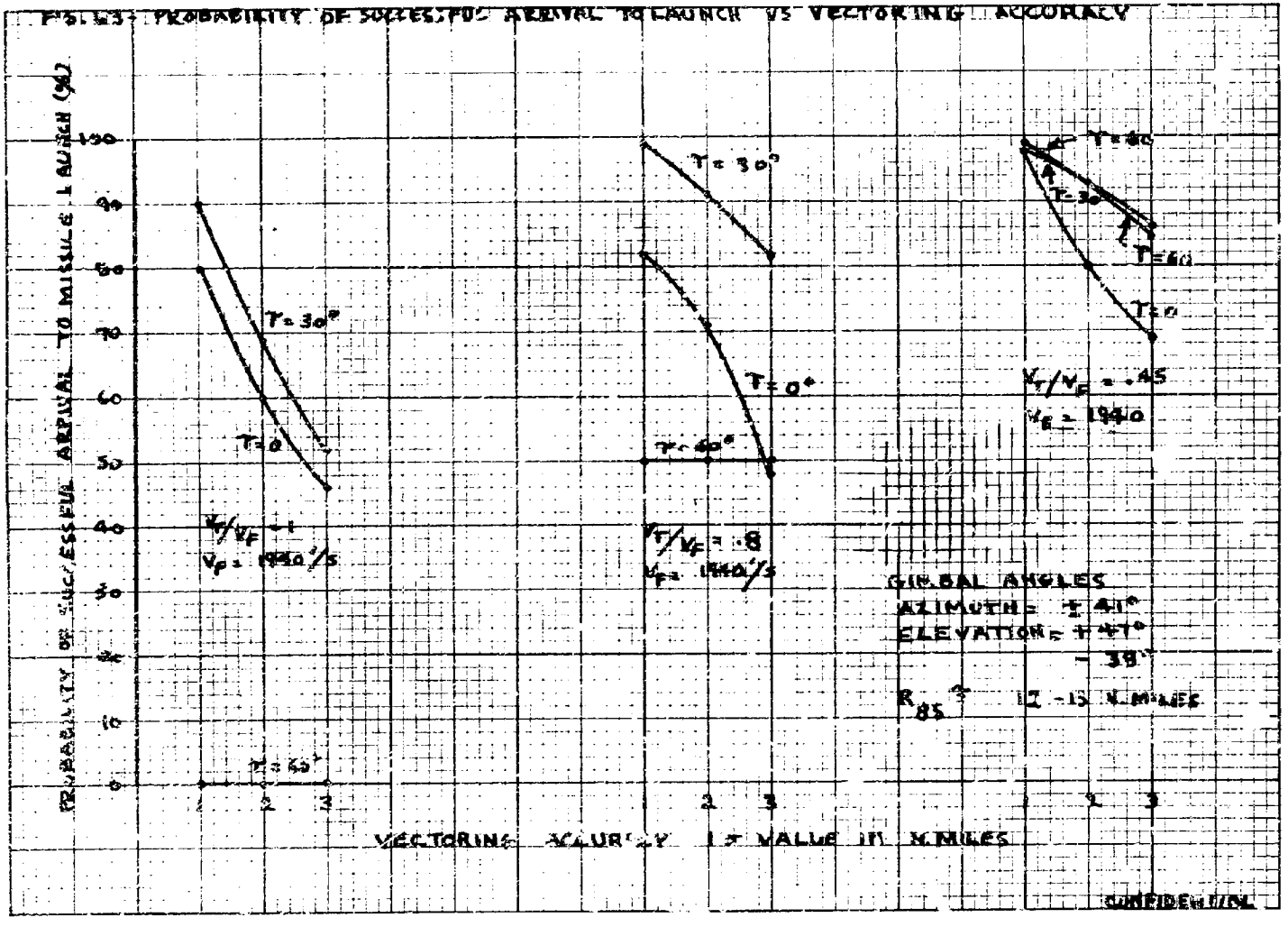
FIG. 3 - PROBABILITY OF SUCCESSFUL ARRIVAL TO LAUNCH VS VECTORING ACCURACY
PROBABILITY OF SUCCESSFUL ARRIVAL TO MISSILE LAUNCH (%)
100
90
80
70
60
50
40
30
20
10
0
T = 30°
T = 0°
T = 60°
V_T/V_F = 1
V_F = 1940'/s
V_T/V_F = .8
V_F = 1940'/s
V_T/V_F = .45
V_F = 1940
GIMBAL ANGLES
AZIMUTH = ± 41°
ELEVATION = + 47°
- 39°
R_{85} = 1.15 N. MILES
1
2
3
VECTORING ACCURACY 1 σ VALUE IN N. MILES
CONFIDENTIAL

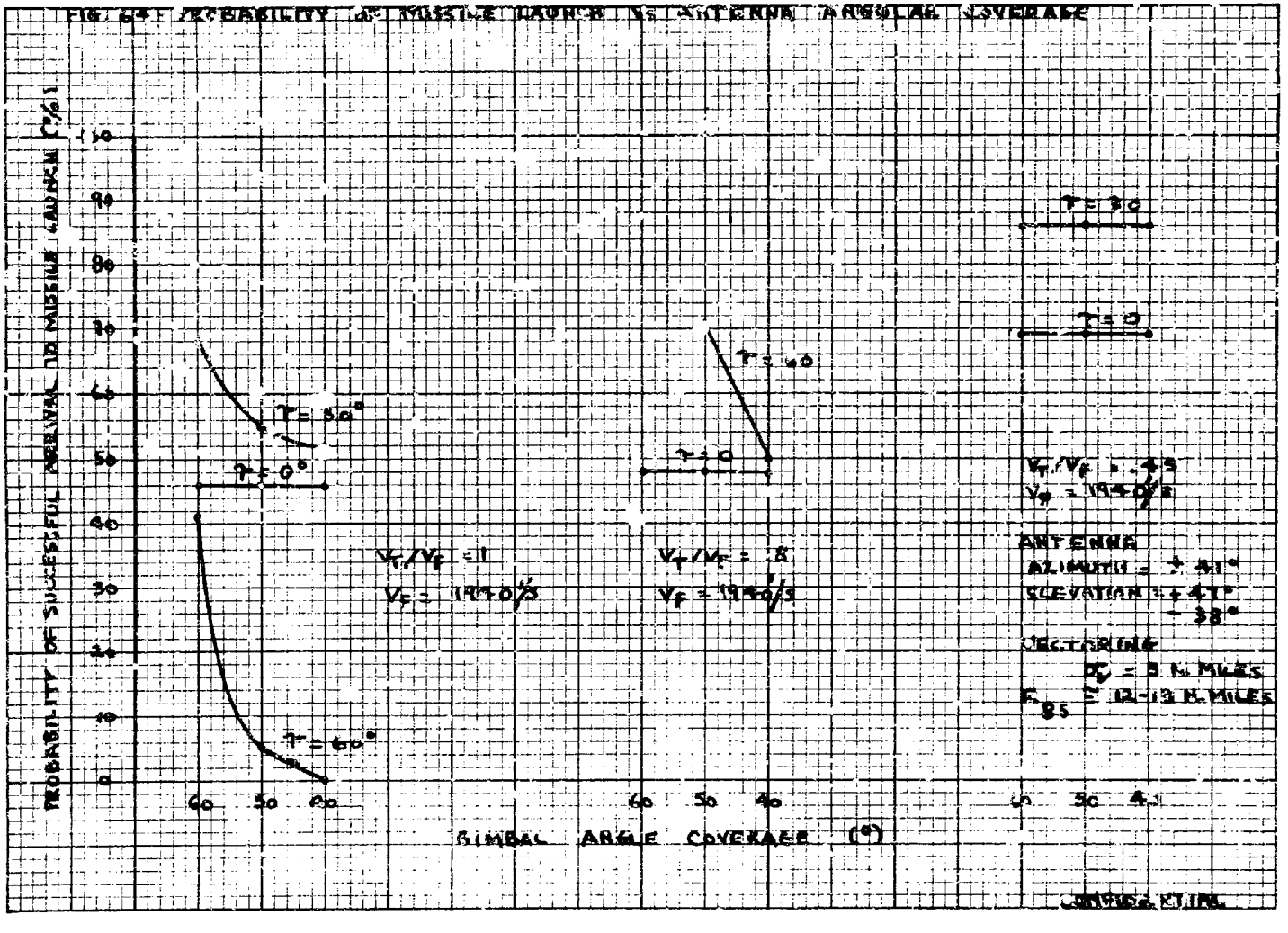
FIG. 64 PROBABILITY OF MISSILE LAUNCH VS. ANTENNA ANGULAR COVERAGE
PROBABILITY OF SUCCESSFUL ARRIVAL OF MISSILE (%)
100
90
80
70
60
50
40
30
20
10
0
γ = 30°
γ = 0°
γ = 60°
γ = 0°
γ = 60°
γ = 0°
V_T/V_F = 1
V_F = (1960)²/s
V_T/V_F = .5
V_F = (1960)²/s
V_T/V_F = .45
V_F = (1960)²/s
ANTENNA
AZIMUTH = ± 41°
ELEVATION = + 41°
− 38°
DETECTING
R_{50} = 9 N. MILES
R_{85} = 12-13 N. MILES
60 50 40
60 50 40
5 30 4
GIMBAL ANGLE COVERAGE (°)

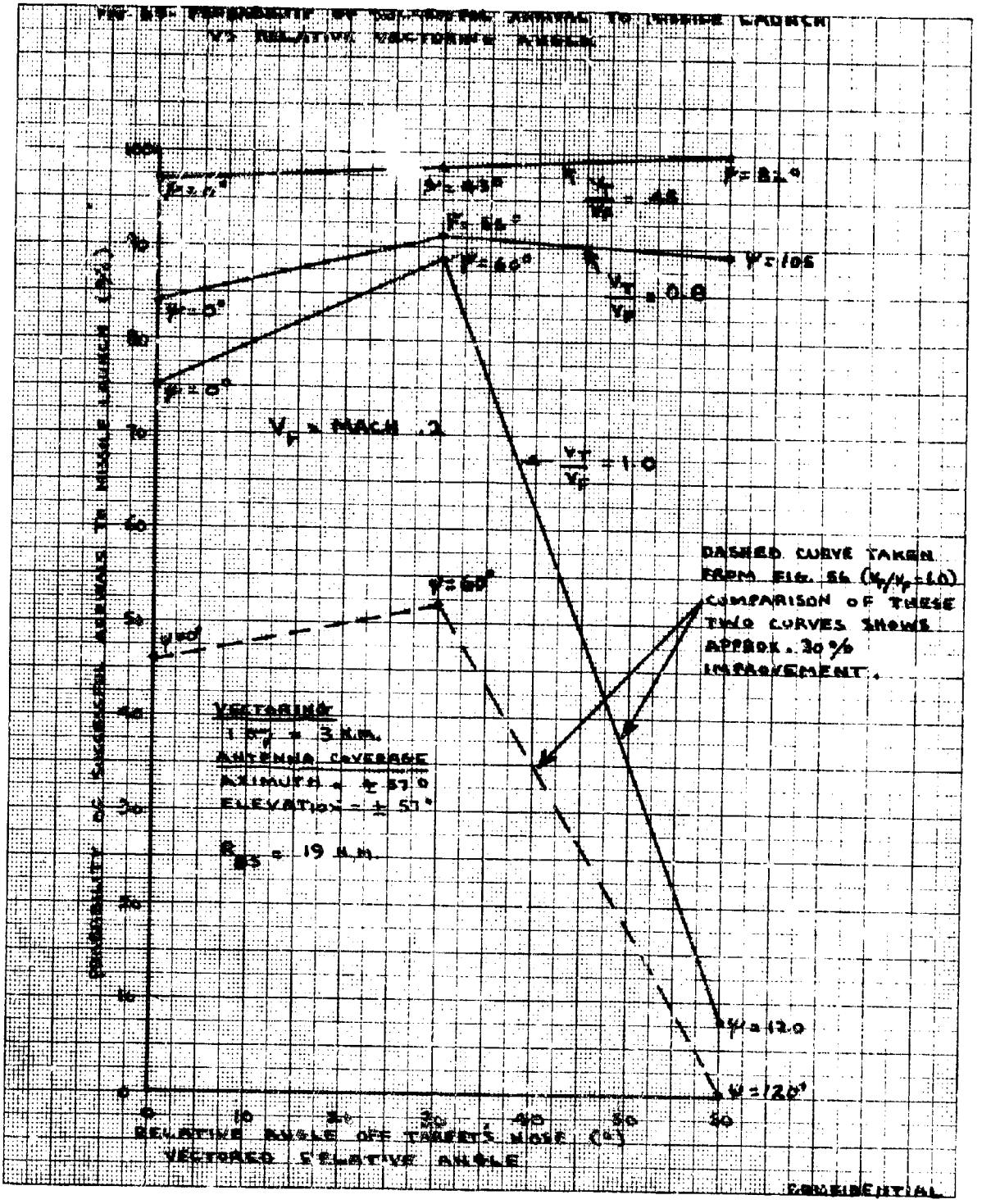
VS RELATIVE VECTORING ANGLE
$\psi = 45°$
$\psi = 90°$
$\psi = 60°$
$\psi = 0°$
$\frac{V_T}{V_P} = 1.0$
$\frac{V_T}{V_P} = 0.8$
V_P = MACH .2
DASHED CURVE TAKEN FROM FIG. 56 ($V_T/V_P = 1.0$)
COMPARISON OF THESE TWO CURVES SHOWS APPROX. 30% IMPROVEMENT.
VECTORING
1 BW = 3 N.M.
ANTENNA COVERAGE
AZIMUTH = ± 57.0
ELEVATION = ± 57°
R_{BS} = 19 N.M.
$\psi = 12.0$
$\psi = 120°$
RELATIVE ANGLE OFF TARGET'S NOSE (°)
VECTORED RELATIVE ANGLE
CONFIDENTIAL

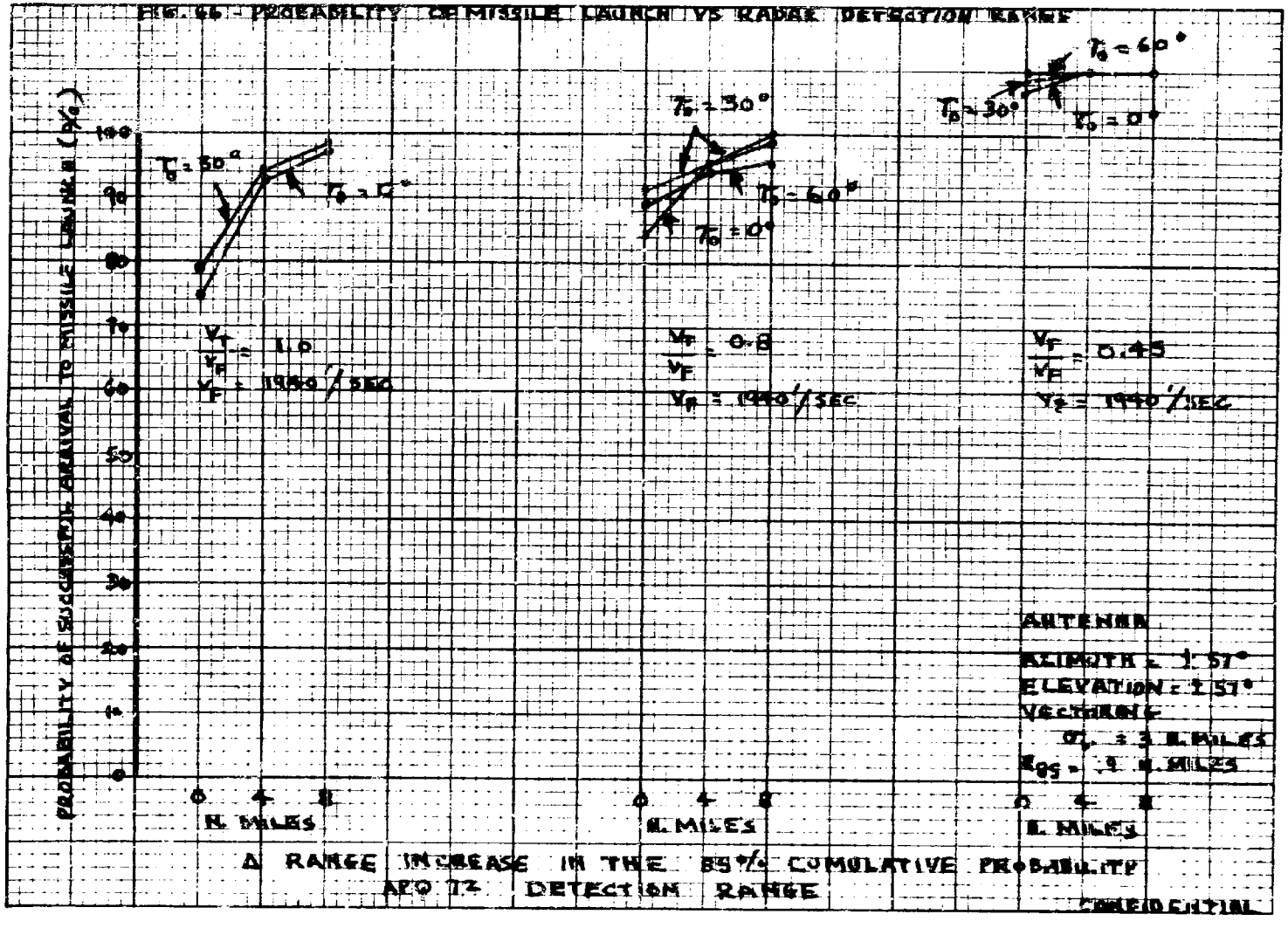
FIG. 46 - PROBABILITY OF MISSILE LAUNCH VS RADAR DETECTION RANGE
PROBABILITY OF SUCCESSFUL ARRIVAL TO MISSILE LAUNCH (%)
100
90
80
70
60
50
40
30
20
10
0
$T_0 = 30°$
$T_0 = 0°$
$\frac{V_T}{V_F} = 1.0$
$V_F = 1980$ / SEC
0 4 8
N. MILES
$T_0 = 30°$
$T_0 = 60°$
$T_0 = 0°$
$\frac{V_F}{V_F} = 0.8$
$V_F = 1980$ / SEC
0 4 8
N. MILES
$T_0 = 60°$
$T_0 = 30°$
$T_0 = 0°$
$\frac{V_F}{V_F} = 0.45$
$V_F = 1980$ / SEC
ANTENNA
AZIMUTH = 1.57°
ELEVATION = 2.57°
VECTRONIC
σ_R = 3 N. MILES
R_{95} = 4 N. MILES
0 4 8
N. MILES
Δ RANGE INCREASE IN THE 85% CUMULATIVE PROBABILITY
APQ 72 DETECTION RANGE
CONFIDENTIAL

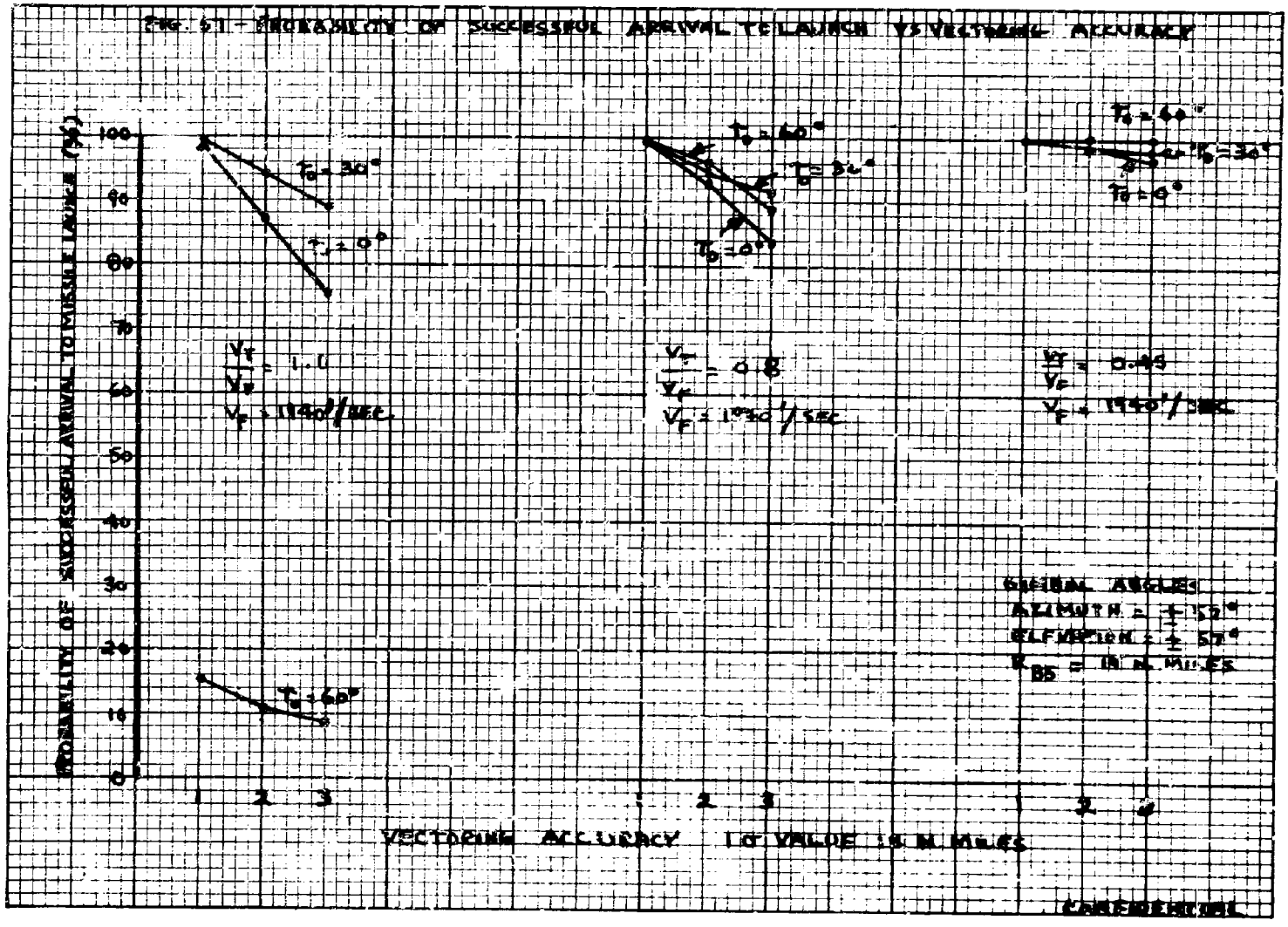
FIG. 51 - PROBABILITY OF SUCCESSFUL ARRIVAL TO LAUNCH VS VECTORING ACCURACY
PROBABILITY OF SUCCESSFUL ARRIVAL TO MISSILE LAUNCH (%)
100
90
80
70
60
50
40
30
20
10
0
1
2
3
$\tau_0 = 30°$
$\tau_0 = 0°$
$\frac{V_T}{V_F} = 1.0$
$V_F = 1140'/sec.$
$\tau_0 = 60°$
$\tau_0 = 30°$
$\tau_0 = 0°$
$\frac{V_T}{V_F} = 0.8$
$V_F = 1140'/sec.$
$\tau_0 = 60°$
$\tau_0 = 30°$
$\tau_0 = 0°$
$\frac{V_T}{V_F} = 0.45$
$V_F = 1140'/sec.$
$\tau_0 = 60°$
GIMBAL ANGLES
AZIMUTH = ± 52°
ELEVATION = ± 57°
R_{BB} = IN N. MILES
VECTORING ACCURACY 1σ VALUE IN N. MILES
CONFIDENTIAL

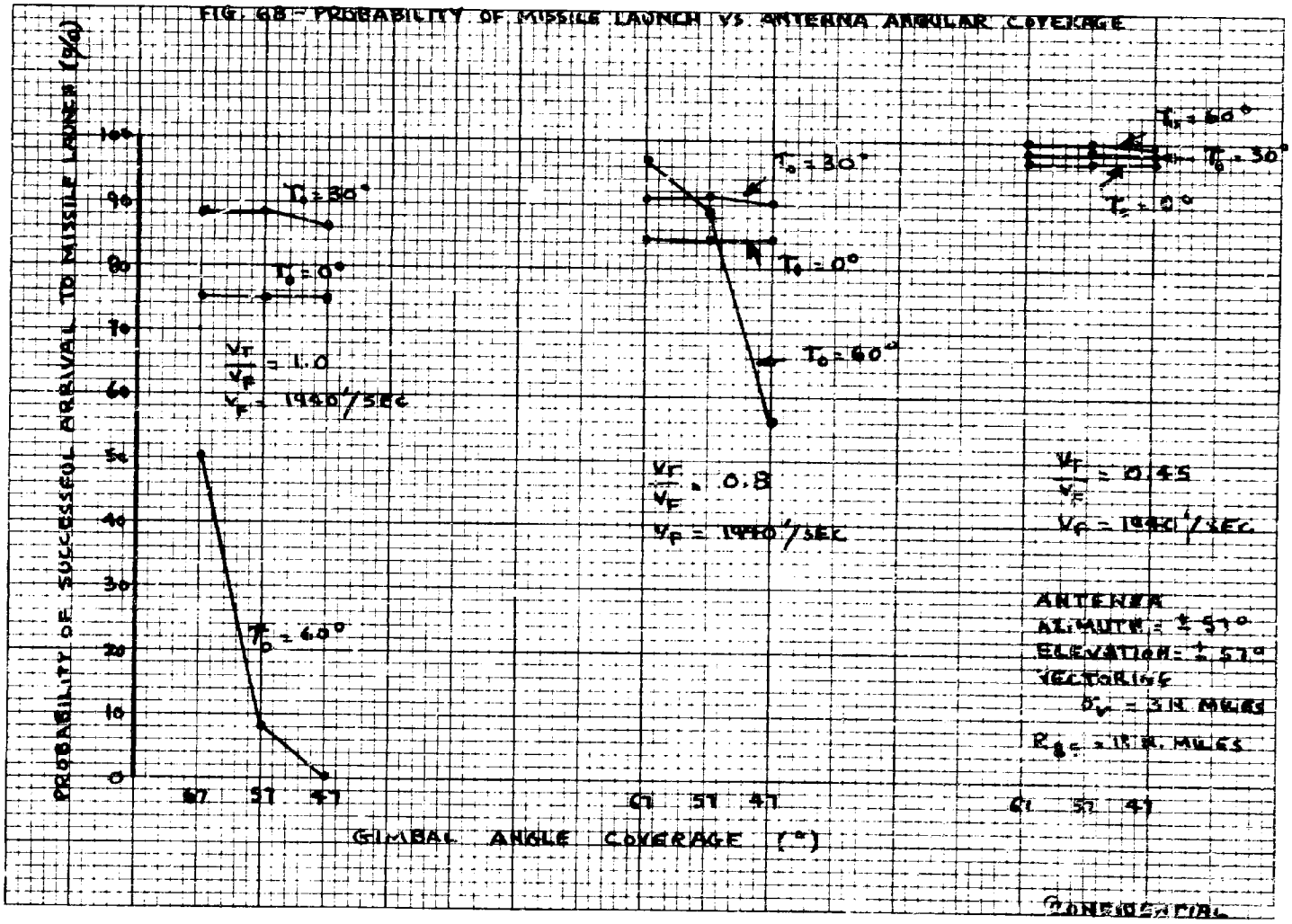
FIG. 68 - PROBABILITY OF MISSILE LAUNCH VS ANTENNA ANGULAR COVERAGE
PROBABILITY OF SUCCESSFUL ARRIVAL TO MISSILE LAUNCH (%)
100
90
80
70
60
50
40
30
20
10
0
$T_0 = 30°$
$T_0 = 0°$
$\frac{V_T}{V_F} = 1.0$
$V_F = 1940'/SEC$
$T_0 = 60°$
87 51 47
$T_0 = 30°$
$T_0 = 0°$
$T_0 = 60°$
$\frac{V_T}{V_F} = 0.8$
$V_F = 1940'/SEC$
87 51 47
$T_0 = 60°$
$T_0 = 30°$
$T_0 = 0°$
$\frac{V_T}{V_F} = 0.45$
$V_F = 1940'/SEC$
87 51 47
ANTENNA
AZIMUTH = ± 51°
ELEVATION = ± 51°
VECTORING
θ_V = 3.13 MILES
R_ϕ = 1.13 R. MILES
GIMBAL ANGLE COVERAGE (°)
CONFIDENTIAL

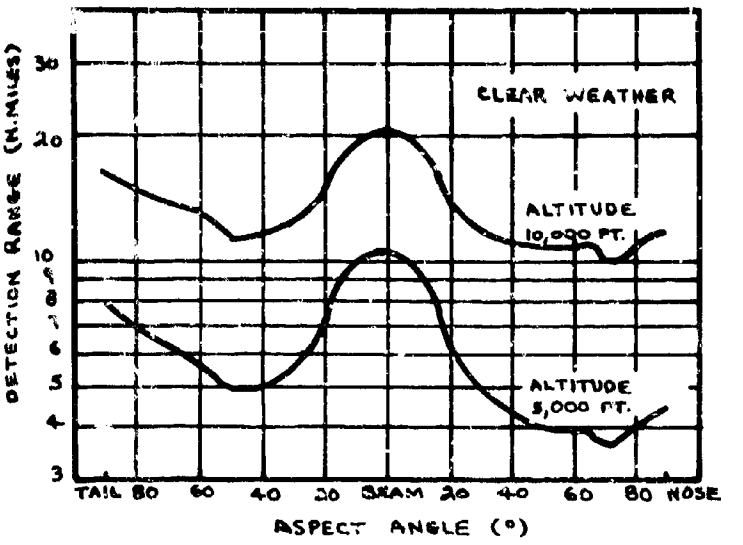

FIG. 69- Detection Range in Clear Weather
Circular Polarization
Low Altitude

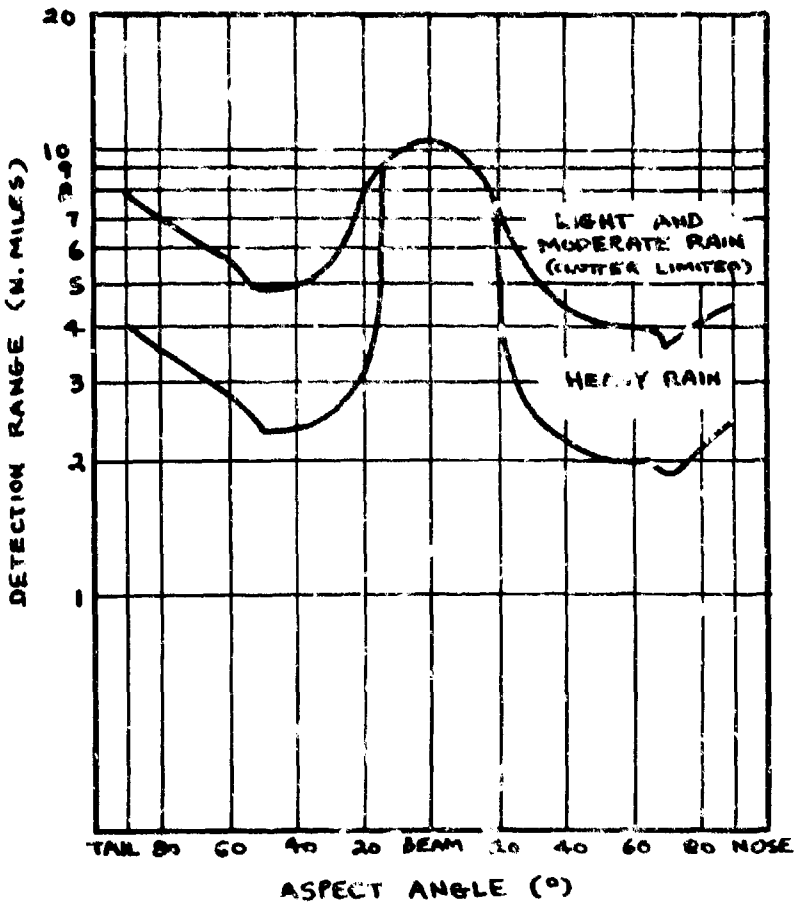

Fig. 70- Detection Range with Rain at the Target
Circular Polarization
Altitude - 5000 ft.

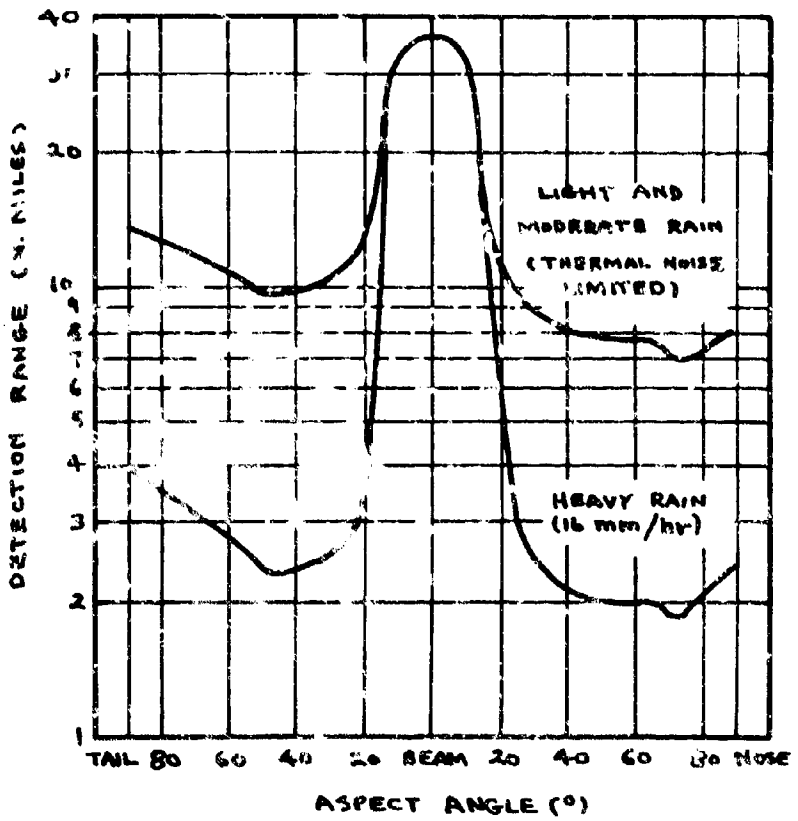

Fig. 71- Detection Range with Rain at the Target
Circular Polarization
Altitude Greater than 20,000 ft.

Naval Research Laboratory
Technical Library
Research Reports Section

DATE: February 26, 2001

FROM: Mary Templeman, Code 5227

TO: **Code 5300 Paul Hughes**

CC: Tina Smallwood, Code 1221.1 ts 3/8/01

SUBJ: Review of NRL Reports

Dear Sir/Madam:

1. Please review NRL Report MR-754 Volumes I, II, III, IV, VII, VIII, IX, X, XI, XII, XIII, XIV, XV, MR-1372 and MR-1289 for:

   ☑ Possible Distribution Statement
   ☐ Possible Change in Classification

Thank you,

Mary Templeman

Mary Templeman
(202)767-3425
maryt@library.nrl.navy.mil

The subject report can be:

☒ Changed to Distribution A (Unlimited)
☐ Changed to Classification _____
☐ Other:

Ben H Cantrell 3-8-01

Signature Date

AN (1) AD- 367 910/XAG
FG (2) 150600
CI (3) (U)
CA (5) NAVAL RESEARCH LAB WASHINGTON D C
TI (6) DESIGN AND DEVELOPMENT PROGRAM FOR F4H-1 AND F8U-3 WEAPON SYSTEMS.
DN (9) Memo. rept.
AU (10) Waterman,Peter
RD (11) 30 Nov 1957
PG (12) 191 Pages
RS (14) NRL-MR-754
RC (20) Unclassified report
AL (22) Distribution: DoD only: others to Director, Naval Research Lab., Attn: Code 1221.1. Washington, DC 20375-5000.
DE (23) (*jet fighters, weapon systems), (*research management, weapon systems) search radar, identification systems, display systems, radar operators, performance(engineering), interception probabilities, detection, aerial warfare (u) air to air missiles, fire control systems, naval aircraft, combat information centers, infrared equipment
DC (24) (U)
ID (25) an/apq-50, an/apq-72, an/apq-74, f-4 aircraft, f-8 aircraft, sidewinder, sparrow
IC (25) (U)
DL (33) 04
CC (35) 251950